RAINFALL-RUNOFF-SEDIMENT YIELD MODELLING OF MOUNTAINOUS WATERSHEDS

A THESIS

Submitted in partial fulfilment of the requirements for the award of the degree of

DOCTOR OF PHILOSOPHY

in

WATER RESOURCES DEVELOPMENT

by

SOBAN SINGH RAWAT

DEPARTMENT OF WATER RESOURCES DEVELOPMENT & MANAGEMENT
INDIAN INSTITUTE OF TECHNOLOGY ROORKEE
ROORKEE-247 667 (INDIA)

DECEMBER, 2011

ABSTRACT

Rainfall-runoff-sediment yield modelling being highly complex, dynamic, and non-linear, exhibits temporal and spatial variability and comprises several physical processes. Varying in complexity from lumped empirical to physically based space and time-distributed, several models are available in literature to model runoff and subsequent soil erosion/sediment yield. Although physically based models have proven very useful as a research tool but are of limited use in field, especially in developing countries like India as they require large amount of data. However, search is still continuing for developing new and simple model. In the present research work, an attempt is therefore made to explore new/modified or improved techniques to model major components of the rainfall-runoff-sediment yield process in a more sound theoretical and mathematical environment. However, in the mean time, simplicity of model structure, practical utility in terms of data requirement as well as easiness in use, and parsimony in data, time, and funds are central to the present study. The present research investigates a few an important components of process of the hydrological cycle, specifically the process of rainfall-runoff-sediment yield including evapotranspiration, runoff, soil erosion, and sediment yield.

Evapotranspiration (ET), a major component of the hydrologic cycle, is important for planning, design, and operation of irrigation systems. Most of the hydrologic, water-management, and crop-growth models also require an accurate estimate of potential evapotranspiration (PET) for its reliable application (Parmele 1972; Skaggs 1982). A common procedure for estimating ET is to first estimate potential evapotranspiration (PET). Further, crop coefficients, which depend on the crop characteristics and local conditions, are used to convert PET to ET. Secondly, runoff is an important component of hydrologic cycle and quantitatively second major component, after evapotranspiration, of the cycle. The runoff is of prime importance for the hydrologist at both field and at large scales. At the field scale, the runoff is used in planning and design of soil conservation practices, irrigation water management, wetland restoration, and water table management. However, at large scale, it is of major concern in flood forecasting, floodplain management, design of hydro-power projects, and water supply studies. Furthermore, soil erosion, normally resulting from rainfall and consequent runoff is a serious problem affecting the soil, land, and water which are essential resources for any civilization. Soil erosion either as on-site erosion or off-site erosion is equally important for the society. On-site erosion (sediment source) is important for the rural population especially the

farmer community in terms of removal of fertile top soil layer which ultimately hampers the agricultural production. However, the off-site erosion (sediment sink areas) is of interest to the society at large i.e. in multi-purpose reservoir preservation, flood protection, and water quality control (Garen et al., 1999).

CN-PET Relationship Derivation

Evapotranspiration is a major component of the catchment water balance and potential evapotranspiration (PET) data therefore forms a key to rainfall-runoff models. As far as concerned to surface water, PET is required for water availability, estimation of daily, weekly, and monthly flows for multipurpose reservoir operation, design (frequency) flows, scheduling of irrigation project, and flood forecasting. Long-term changes in PET can affect the hydrologic processes as well as the performance of agricultural crops. Several PET estimation methods based on temperature, radiation, and their combination have been developed over the last 50 years in different parts of the world but none can be recommended as the best one for any area or any season in terms of its accuracy and profitability. Furthermore, different researchers (Buransh, 1995; Fowler, 2002 Andreassian et al. 2004; Morton, 1994) have criticized the performance of complex PET methods, and raised the question "Is the temporal PET, derived from complex PET methods, suitable in rainfall-runoff modelling?"

In the present research work, nine commonly used PET methods (one based on temperature, two based on radiation, and six combination based) were employed for estimation of duration-dependent long-term mean PET on a large set of hydro-meteorological data from three catchments of Narmada river basin, located in Central India. Significant variations (up to 42%) among the estimated PET values by different methods were observed. Therefore, care should be taken in selection of an appropriate PET estimation method. Furthermore, the performance of different commonly used PET methods was compared with Penman-Monteith method, a standard method recommended by FAO-56. Following the usual statistical criteria, temperature based Hargreeves method was found most suitable (Root Mean Square Error = 0.2) for PET estimation of Narmada river basin. The performance of radiation-based Priestley-Taylor (RMSE=4.71), and Turc methods (RMSE=3.90) was also found to be satisfactory.

The Soil Conservation Service Curve Number (SCS-CN) method, though empirical, has increasingly gained wide recognition as a practical tool for solving wide range of hydrologic problems involving the rainfall-runoff process because of its

overwhelming simplicity. In the present study, interrelationship of CN and PET was also investigated. This interrelationship was derived from the coupling of SCS-CN concept and Mintz and Walker (1993) equations (for the root-zone soil moisture (W) and evapotranspiration (ET)). The water balance equation and proportionality hypothesis of SCS-CN method invoked SCS-CN parameter S to be expressible in terms of the maximum possible evaporable depth or PET, described in power form as: $PET = \alpha S_I^{\beta}$ or more generalized as $ET = \alpha S^{\beta}$. Consequently, long term mean PET values of duration ranges from 1-day to 30-day for seven watersheds of India were correlated with the runoff curve numbers derived for the respective durations from observed rainfall-runoff data, following the Mishra et al. (2008) procedure. The correlation exhibited a strong power relationship with coefficient of determination (R^2) values in the range (0.96, 0.99). Such a relationship invokes determination of PET from the available CN values, and therefore, may be quite useful in field applications.

Probability Distribution-Based SUH derivation

The use of probability distribution functions (pdf) for derivation of synthetic unit hydrograph (SUH) is gaining acceptance among the hydrologists due to similarity in typical shape and unit area enveloped by a pdf curve. The present study explores, first time in hydrology, the potential of two-Parameter Inverse Gamma Distribution (2PIGD) for SUH derivation using geomorphological parmeters i.e., Horton's ratio. The performance of 2PIGD was compared with the most popular flexible and accurate two-Parameter Weibull Distribution (2PWD) and conventional two-Parameter Nash Gamma Model (2PNGM) (Rosso, 1984). When applied to the data from two Himalayan watersheds from India, the performance of 2PIGD found superior to the 2PWD and 2PNGM based on statistical as well as visual criteria. Using 2PIGD and geomorphological parameters of Ramganga watershed, a simple regression model for peak flow rate ($Q_p = 17.149\ v + 0.1361$, R^2=0.99), and time to peak flow ($T_p = 29.535\ v^{-1}$, R^2 =1) for known value of dynamic flow velocity (v) were developed. Such a simple linear relationship can be of importance for the field engineers as well as hydraulic engineers for design of hydraulic structures and development of flood prediction and warning systems.

Lag Time Based GIUH Derivation

Linking of hydrological response of a catchment with the geomorphologic characteristics has been of paramount research interest for last three decades. The Instantaneous Unit Hydrograph (IUH) theory, popularly known as geomorphologic IUH (or GIUH) of Rodriguez-Iturbe et al. (1979) and further refinement by Gupta et al (1980), became more promising for ungauged catchments or data deficient catchments. Consequently, Rosso (1984) derived Nash parameters 'n' and 'k' in terms of Horton's ratio and a dynamic velocity parameter using power regression and derived the complete shape of the unit hydrograph. However, estimation of dynamic velocity itself is an ambiguous task and involves great subjectivity in routine applications. In the present study, using the basic GIUH governing equations (Rodriguez-Iturbe et al., 1979 and Rosso, 1984), a revised GIUH model based on watershed lag time concept has been proposed. The proposed approach is more pragmatic than the older one due to replacement of dynamic velocity by lag time of the watershed. The resulting high value of coefficient of efficiency and low values of relative error in peak estimation of direct runoff hydrograph for eight single-peaked isolated storms of two hilly watersheds indicated the suitability of the proposed lag time-based GIUH approach. The model outcome was better than the result of kinematic-wave based GIUH approach (Kumar & Kumar, 2008). For estimation of Horton's ratio the realistic drainage network was extracted using the Melton concept in GIS environment. Moreover, the proposed approach can be extended for an ungauged watershed, and UHs derived from variable lag time may be helpful to quantify the effect of urbanization and land use changes on water resources, for the lag time is the finger print of the watershed.

Development of RBFANN-Based Runoff Model

Artificial Neural Network (ANN) is a technique which comprises of both linear and non-linear concepts in model building and is capable of handling the problem which is dynamic and even not clearly defined. Radial Basis Function Artificial Neural Network (RBFANN) is a specific type of ANN recently used by a number of researchers in hydrological modelling. The RBFANN network model is motivated by the locally tuned response. Owing to this ability, the networks are easily trained by using a sufficiently large data set. In the present research, an RBFANN model was developed based on k-means clustering algorithm to model the daily rainfall-runoff process. The training of RBFANN network can be split into an unsupervised part and a supervised part.

Unsupervised training techniques are relatively fast. Clustering algorithm k-means is used for unsupervised learning in function layer. Gradient descent algorithm is used for supervised learning part in output layer.

Different network parameters such as learning rate in function layer (ALR), learning rate in output layer (ALRG), and number of iterations are optimized using the data of calibration period for three Himalayan watersheds, Naula, Chaukhutia, and Ramganga. The model network weights are calibrated using five years seasonal (June-September) rainfall-runoff data. Then model performance was evaluated by two unknown data sets, cross-validation and verification. The Nash efficiency of proposed RBFANN was satisfactory and it was 86.28%, 84.91%, and 86.81% in calibration, cross-validation, and verification, respectively. As such, the efficiency was consistent during all three periods in case of Naula watershed. However, the model efficiency was good and consistent in cross-validation and verification with efficiencies of 84.76%, and 84.59%, respectively, and satisfactory in calibration (efficiency = 77.48%) for Chaukhutia watershed. In case of Ramganga watershed, the model performed well in calibration (76%) and cross-validation (77.68%), and it was however reasonable (68.25%) in verification. Overall, the model efficiency was excellent in error convergence due to adopting k-means cluster algorithm, and there was no need to go beyond 1000 iterations. However, the higher network achieves the desired performance within 500 iterations. The model is very sensitive to learning rate in function layer (ALR), but not to learning rate in output layer (ALRG).

Development of a Spatially Distributed Sediment Yield Model

It is well known that onsite erosion reduces the soil quality due to removal of nutrient rich top soil layer and also reduced the water holding capacity of many soils. Therefore, in developing countries like India, where rural population is more than 65% and land is the identity of the people, assessment of erosion focuses mainly on the on-site effects of erosion. To this end, a spatially distributed sediment yield model was developed in GIS environment (ERDAS 8.5 and ArcGIS 9.3) which is capable to identify the sediment source and sink areas within the catchment. Transport capacity and gross soil erosion maps were generated by overlaying different thematic maps according to their equations. In the transport capacity map, the ridges and the flatter areas near the channel, generally cultivated (viz., south-west direction of Chaukhutia gauging site) are the areas possessing low transport capacity. However, transport capacity is high in channels and

steep head water areas especially where the slope plane curvature is convex in nature. Employing transport capacity maps alongwith gross soil erosion (GSE), a programme was developed in Interactive Data Language (IDL) to route the sediment form ridge pixel to the outlet of the watershed by following the hydrological drainage path. The programme compares the gross soil erosion (total soil ready to move out of particular pixel) and transport capacity of the flow in that pixel, if transport capacity is equal or greater than gross soil erosion then entire eroded soil will be transported to the next pixel. However, If the transport capacity of any pixel is less than total soil ready to move out of a particular pixel, the tools will assign the difference between transport capacity and the total soil ready to move out, as amount of sediment deposited in that pixel. Such maps exhibit sediment rate at a particular cell in spatial domain, and the value at the outlet cell indicate the sediment outflow from the entire watershed. Lumped as well as spatial accuracy of the model was checked by comparing the model output with the observed sediment data at the outlet and three upstream gauging sites and theses are found to be within limit. Further, the spatial distribution ability of the model was improved by incorporating the variable rainfall erosivity map. By overlaying the gross soil erosion and deposition maps, net erosion/deposition maps were generated. Theses are of importance in soil erosion inventory and site selection for a multipurpose reservoir.

Keywords: ANN, ArcGIS, GIUH, Horton's ratio, Inverse gamma distribution, Lag time, Penman-Monteith, Potential evapotranspiration, Probability density function, RBFANN, SCS curve number, Soil erosion, SRTM, SUH, Spatially distributed sediment yield model, Transport capacity, USLE, Weibull distribution.

ACKNOWLEDGEMENT

At the outset, the author bows his head with reverence to Him who is omnipresent, omnipotent and omniscient and is the cause behind every effect.

I draw pleasure in expressing my profound indebtedness and heartfelt gratitude and reverence to my supervisors Dr. S. K. Mishra, Associate Professor, Dr. U. C. Chaube, Professor, Department of Water Resources Development and Management, and Dr. M. K. Jain, Assistant Professor, Department of Hydrology, IIT Roorkee for their invaluable guidance, constant encouragement, moral support, and wholehearted co-operation during this research work. Their painstaking efforts in going through the manuscript and personal interest into the research work cannot be described in words.

I wish to express my gratitude to the respected family of my supervisors Dr. S. K. Mishra, Dr. U.C. Chaube, and Dr. M. K. Jain for their extending love, blessings, and moral encouragement during the course of my research work.

The cooperation and help extended by the Professor & Head, all faculty members of Department of Water Resources Development and Management, Indian Institute of Technology Roorkee, is gratefully acknowledged. I also want to thank Chairman SRC and my research committee members for providing me an insight and constructive suggestion. I thankfully acknowledge the financial assistance provided by MHRD under Institute fellowship for the present study. I am also thankful to G. B. Pant University of Agriculture and Technology, Pantnagar for providing study leave during my PhD programme.

I express my sincere thanks to Dr. Avinash Aggarwal, Scientist F, Dr. R. P. Pandey, Scientist E2, National Institute of Hydrology, Roorkee, and Dr. Anil Kumar, Professor, G. B. Pant University of Agriculture & Technology, Pantnagar, for their esteemed help and constant encouragement during this research work.

I am highly grateful and indebted to Er. Bhaskar R. Nikam, Scientist-D, Er. Prasun Kumar Gupta, Scientist-C, Indian Institute of Remote Sensing, Dehradun, and Dr. Pradeep Kumar Sachan, Scientist-B, Western Himalayan Regional Center, Jammu, for their ever valuable help during this research work.

I thankfully acknowledge the help by the fellow friends Mr. Santosh Pingale, Dr. Pushpendra Kumar Singh, Mr. Kasiviswanathan, Dr. D. S. Deshmukh, Er. Praveen Kumar, Dr. Tejwant Singh Brar, Er. L. N. Thakral, Mr. Satynaryan, Dr. Ravi Kale, Mr. Atul Sidola,

Mr. Vaibhav Gossavi, Mr. Shakti, Mr. Kuldeep Sharma, Mr. Hemant Parmar, Mr. Vipin Saklani, Mr. Pradeep Behl, and all other well wishers for their direct and/or indirect help at various stages of this research work.

I am short of words to express my feelings for my family members, who stood beside me during the course of present work. My parents, bhaiya-bhabhi, and their children and my in-laws were always source of inspiration for the completion of this research work in time. I am extremely grateful to my wife Neeru and son Yashvardhan for their persuasive inspiration, love, affection, and patience throughout the study.

(SOBAN SINGH RAWAT)

TABLE OF CONTENTS

LIST OF FIGURES

LIST OF TABLES

LIST OF SYMBOLS AND ABBREVIATIONS

$\beta_{T,S}$	Coefficient of transpiration plus soil evaporation
$\overline{A}_w$	Mean area of basin of order w
$\overline{L}_w$	Mean length of stream of order 'w'
ε	Non-dimensional parameter used for defining time base
α and β	Coefficient and exponent of PET-CN relation
'α' and 'c'	Scale parameter and shape parameter of 2PWD
'a' and 'b'	Distribution parameters of 2PIGD
A_s	Upslope contributing area per unit width of contour (or rill)
C	Runoff factor
C_i	Cover management factor
d	Euclidean distance
D*i*	Deposition in cell *i*
e_a	Actual vapour pressure (kpa)
E_a	Aerodynamic term (mm day^{-1})
E_I	Daily interception loss
EI_{30}	30 minutes rainfall intensity
E_S	Soil evaporation
e_s	Saturation vapour pressure (kpa)
E_T	Daily transpiration
F	Actual infiltration
G	Soil heat flux density ($mjm^{-2}day^{-1}$)
GSE_i	Gross amount of soil erosion in cell *i* (MT ha^{-1} $year^{-1}$)
H	Average catchment slope in meter per meter
I_a	Initial abstraction
i_e	Rainfall-excess rate (ms^{-1})
K_i	Soil erodibility factor in cell *i* (MT ha h ha^{-1} MJ^{-1} mm^{-1})
K_{TC}	Transport capacity coefficient
L	Length of main channel
LS_i	Slope steepness and length factor for cell *i*
n and k	Shape and scale parameters of Nash Model
N_w	Number of streams of order 'w'

P	Total rainfall
P_i	Supporting practice factor for cell *i*
Q	Direct surface runoff
Q_p	Peak discharge (m^3/s) of hydrograph
q_p	Peak discharge of GIUH (hr^{-1})
R_A, R_B, & R_L	Area ratio, bifurcation ratio, and length ratio
RH	Relative humidity (%)
R_n	Net radiation ($mjm^{-2}day^{-1}$)
S	Potential maximum retention
S_I	Maximum potential retention corresponding to AMC-I
t_B	Time base
T_c	Time of concentration
TC	Transport capacity ($kg\ m^{-1}\ a^{-1}$)
T_{ini}	Sediment inflow from upstream cells
t_l	Lag time
T_{mean}	Mean daily air temperature
T_{outi}	Sediment outflow from the cell *i*
T_p	Time to peak of hydrograph (hr)
t_p	Time to peak of GIUH (hr)
u_2	Average wind speed at 2 m height (m/s)
v	Dynamic velocity
W	Root-zone moisture
W^*	Root-zone storage capacity
W_f	Wind function
w_{jk}	Weight coefficient between $(j)^{th}$ hidden unit and $(k)^{th}$ output unit
Y_{mean}	Mean of the observed sediment (tonnes)
Y_{obs}	Observed seasonal sediment (tonnes)
Y_{pred}	Predicted seasonal sediment (tonnes)
β	Non dimensional term of IUH theory
γ	Psychometric constant ($kpa\ ^0C^{-1}$)
Δ	Slope of saturation vapour curve ($kpa\ ^0C^{-1}$)
θ_i	Slope gradient in degrees for cell *i*
λ	Initial abstraction coefficient

σ	Spread

ABBREVIATIOS

2PGD	Two-Parameter Gamma Distribution
2PIGD	Two-Parameter Inverse Gamma Distribution
2PNGM	Two-Parameter Nash Gamma Model
2PWD	Two-PSarameter Weibull Distribution
ALR	learning rate in the function layer
ALRG	learning rate in output layer
AMC-I	Antecedent Moisture Condition for dry condition
AMC-II	Antecedent Moisture Condition for normal condition
AMC-III	Antecedent Moisture Condition for wet conditions
ANN	Artificial Neural Network
BPANN	Back Propagation Artificial Neural Network
CC	Correlation Coefficient
CN	Curve Number
DEM	Digital Elevation Model
DRH	Direct Runoff Hydrograph
ET	Evapotranspiration
EV	Volumetric Error
FAO	Food and Agricultural Organization
GIS	Geographic Information System
GIUH	Geomorphologic Instantaneous Unit Hydrograph
IDL	Interactive Data Language
ILWIS	Integrated Land and Water Information System
IUH	Instantaneous Unit Hydrograph
KW	Kinematic-Wave based method
LAI	Leaf Area Index
LT	Lag Time method
ME	Model Efficiency
MUSLE	Modified Universal Soil Loss Equation
NBSS&LUP	National Bureau of Soil Survey and Land Use Planning
NEH	National Engineering Handbook

NSE	Nash-Sutcliffe Efficiency
Pdf	Probability Distribution Function
PET	Potential Evapotranspiration
RBFANN	Radial Basis Function ANN
REP	Relative Error in Peak
RMAE	Root Mean Absolute Error
RMSE	Root Mean Square Error
RRMSE	Relative Root Mean Square Error
RS	Remote Sensing
RUSLE	Revised Universal Soil Loss Equation
SAC-SMA	Sacramento Soil Moisture Accounting model
SCS-CN	Soil Conservation Service Curve Number
SDR	Sediment Delivery Ratio
SMC	Soil Moisture Condition
SMD	Soil Moisture Deficit
SPR	Sediment Producing Rate
SRTM	Shuttle radar topography Mission
STDER	Standard Error
SUH	Synthetic Unit Hydrograph
TCT	Tassel Cap transformations
UH	Unit Hydrograph
UNO	United Nations Organization
USLE	Universal Soil Loss Equation
UTM	Universal Transverse Mercator
VI	Vegetation Index
WI	Water Index

CHAPTER 1
INTRODUCTION

1.1 GENERAL

The announcement of decade 2005-2015 as the International Decade for "Action – Water for Life" by the United Nations Organization (UNO) has invoked the interest of scientists and researchers around the globe to explore new water sources and conserve the existing ones. The decade will focus on water-related issues at all levels and on the implementation of programmes and projects, and the furtherance of cooperation at all levels, in order to help achieve the internationally agreed water-related goals. Although there is plenty of water available on the earth, however its distribution in time and space is not uniform. The science which deals with water is called Hydrology, and in nutshell, can be described as "the science of water that deals with the space-time-frequency characteristics of the quantity and quality of water of the earth with respect to their occurrence, distribution, movement, storage and development" (Mishra and Singh, 2003a). It plays a fundamental role in addressing a range of issues related to environmental and ecological management and social development. One of theses issues of permanent importance is the process of rainfall-runoff-sediment yield, which interacts with the phenomena like flood, drought, climate change, water availability, reservoir operation and management, environmental impact assessment, soil erosion, and sediment yield etc. This study attempts to investigate a few important components of the hydrological cycle, such as evapotranspiration, runoff, soil erosion, and sediment yield.

1.2 EVAPOTRANSPIRATION

It is well known that rainfall-runoff modelling encompasses several hydrometeorological components which directly and indirectly affect this complex process. Among all the components, evapotranspiration (ET) (commonly used for evaporation plus transpiration) is the second largest after rainfall, component of the catchment water balance, and therefore, forms a key input to rainfall-runoff modelling and long-term hydrologic simulation studies. On an average, 50-80% of the mean annual rainfall is returned to atmosphere as ET (Brutsaert, 1982, 1986; Kustas, 1990; Philip, 2002). Most of the current hydrologic, water-management, and crop growth models require an accurate estimation of potential evapotranspiration (PET) for reliable application. A large number of methods, simple empirical to complex physical (Penman ;

FAO-24 Penman, Busignrer van-Bavel ; Priestley-Taylor; 1982 Kimberley-Penman; Hargreaves-Samani; Turc; Jensen-Haise; FAO 24 Pan; FAO-56 Penman-Monteith, etc.), calculate PET employing weather data and those have been developed and tested for varying geographic and climatic conditions. Since empirical and semi-empirical methods have been developed for particular sets of conditions, their use is restricted to these conditions only (Beven, 2001). The International Commission for Irrigation and Drainage (Allen et al., 1994) and the Food and Agricultural Organization (FAO-56) (Allen et al., 1998) recommend the use of physically based Penman-Monteith (PM) method for computation of reference/potential evapotranspiration using climatic data, if sufficient data are available to ensure their reliability. However, physically based methods are based on physical processes between plant and atmosphere, and therefore, represent only point estimation of PET, thus all the methods must be calibrated and validated with field data before use (Vörösmarty et al., 1998). However, often experienced scarcity of field data invokes the problem of selecting an appropriate method.

Soil moisture condition (SMC) generally represents the moisture contained in the root zone depth of a soil profile (normally 1-2 m top layer) which can potentially evaporate and/or take active part in transpiration. Therefore, ET is directly influenced by SMC. Notably, PET represents the upper limit of ET, when soil is fully saturated. ET as such affects the land surface energy dynamics, climatology, hydrology, and ecology (Vinnikov et al., 1999; Moran et al., 2004). SMC depends on the water holding capacity that depends on the soil type. Furthermore, it is closely related with the potential maximum retention (or curve number), only parameter of the popular Soil Conservation Service Curve Number (SCS-CN) method, for a watershed can be characterized by a particular set of curve numbers with three distinct antecedent moisture conditions (AMC). Since these curve numbers are derived from the real rainfall-runoff data of a watershed (Mishra et al., 2008), they represent both watershed and its hydro-meteorological characteristics. However, the CN parameter of SCS-CN method and PET has not yet been investigated for their interrelationship. The linking of theses two different concepts supported by the argument that the watershed characteristics (land use/treatment, soil type, climate etc.) which affect CN also influence the ET mechanism, albeit differently. Such land-atmospheric relationship evidence in support of the existence of a land–atmosphere feedback comes from numerical as well as observational experiments from analyses of the relationships between computed indices of soil moisture and observed

meteorological condition (Mintz and Walker, 1993; Karl 1986; Georgakakos et al., 1995; Entekhabi et al., 1996; Huang et al., 1996).

1.3 RUNOFF

Runoff is one of the most important hydrologic variables and an indicator of availability of water. Rainfall-runoff models are tools to help in answering the questions like "What happens to the rain" (Penman 1961)? Despite the simplicity of the question, the answer is anything but not simple due to the complexity of the hydrological processes taking place. The rainfall runoff modelling can be broadly categorized into two parts, short duration and long duration.

1.3.1 Short Duration Rainfall-Runoff Modelling

To model the short duration or event-based rainfall-runoff mechanism, the unit hydrograph (UH) concept was introduced by Sherman (1932). Subsequently, synthetic unit hydrograph (SUH) (Bernard 1935) was developed and applied from time to time by several researchers (Synder, 1938; Edson; 1951; Gray 1961; CWC 1983) to predict the peak flow (q_p) and time to peak (t_P) for different duration storm events. Such kinds of studies have immense significance in design applications such as design of dams, spillways, culverts, etc. The major advantage of SUH concept is that its ordinates can be derived from watershed characteristics rather than real rainfall-runoff data. In 1957, Nash derived for the first time the IUH as a two-parameter gamma distribution (2PGD) by simulating the whole catchment as "n" identical conceptual cascade of linear reservoirs. Due to similarity in typical shape, and unit area envelop by a probability distribution function (pdf) were systematically examined by Koutsoyiannis and Xanthopouleos (1989); Croley (1980); Haktanir and Sezen (1990); Singh (2000); Bhuniya et al. (2003, 2004). Nandrajah (2007) suggested eleven different flexible PDFs ranging from one parameter to three parameters for derivation of SUH. However, the applicability of several PDFs in derivation of SUH has yet to be examined.

Furthermore, linking of hydrological response of a catchment with the geomorphologic characteristics has been of interest for last three decades. Proposed by Rodriguez-Iturbe et al. (1979) and further refinedment by Gupta et al (1980), the Instantaneous Unit Hydrograph (IUH) theory, popularly known as geomorphologic IUH (or GIUH) became more promising for ungauged catchments or data deficient catchments. The theory represented some hydrological parameters, viz., peak discharge (q_p) and time to peak (t_p) in terms of geomorphological characteristics of river basin. The

requirement of land use and climatic parameters are obviously omitted and it is one of the major advantages of this theory. Consequently, Rosso (1984) derived the Nash parameters 'n' and 'k' in terms of Horton's ratio and a dynamic velocity parameter using power regression. Nevertheless, the difficulty with the GIUH theory is its dependency on a dynamic parameter namely velocity. Rodriguez-Iturbe & Valdes (1979) advocated to take a constant velocity corresponding to peak discharge, since most of the flows in the watershed occurred at the peak discharge velocity. However, the question of how the velocity at peak flow is calculated was not addressed.

1.3.2 Long-Term Rainfall-Runoff Modelling

The long-term daily hydrologic simulation is useful in augmentation of hydrologic data, water resources planning and watershed management (Mishra and Singh, 2003a, 2004a) and is efficacious in describing the performance of a water resource system under climatic variations of rainfall and other aspects (Kottegoda et al., 2000). These models have been widely applied since they were first introduced in late 1960s and early 1970s.

The existing rainfall-runoff models can be broadly grouped under two main categories, conceptual and black box. The conceptual models attempt to represent the known physical process occurring in the rainfall-runoff transformation in a simplified manner by way of linear or nonlinear mathematical formulations but their implementation and calibration is complicated and time consuming. The Sacramento Soil Moisture Accounting (SAC-SMA) model is defined by 22 parameters in addition to 12 parameters required by the potential evapotranspiration. The number of water balance (Watbel) models can be much larger and can often exceed 50, or even 100, for larger basin with a large number of computational units (Markus and Baker 1994). The simplest conceptual rainfall-runoff model (SCRR) model has seven fitting coefficients and two storage elements (McCuen and Synder 1986). Despite their comprehensive structure, many of these models have not yet become standard tools in hydrological practice in developing countries, such as India, Pakistan, Nepal, and other countries of Asia as well as African countries. The reason is two-fold. First, most basins in these countries are ungauged and there is little hydrometeorological (generally rainfall and runoff) data available. Second, the major problem with the conceptual model is the lack of uniqueness in parameters obtained in calibration from the observed data (Spear, 1995, Wheater et al, 1993) which restrict their use in other catchments. Nevertheless, the black box type models are designed to identify the connection between input and output, without going to analysis of

the internal structure of the physical processes. The Artificial Neural Network (ANN) is one such black box model that has been applied to several diverse hydrological problems and the results in each case have been very encouraging. Furthermore, in conceptual models, precipitation, air temperature, evaporation data and other data of sub-processes of rainfall-runoff are usually employed as input data, which are rarely available in developing countries. However, an ANN model relies on rainfall-runoff series, which is generally available for most of the watersheds. Therefore, they are most efficient tool for runoff simulation and forecasting especially in developing countries.

1.4 SEDIMENT YIELD

Eighty percent of the sediment material delivered to the world's oceans each year comes from Asian rivers, and amongst these, Himalayan rivers are the major contributors (Stoddart 1969). The Himalayan and Tibetan regions cover only about 5% of the earth's land surface but supply about 25% of the dissolved load to the world ocean (Raymo and Ruddiman 1992). The Himalayas is the youngest mountain range on the earth, and it is the origin of world's three major river systems viz. the Indus, the Ganges, and the Bhrahmaputra. In spite of the hydrological importance of the region, a few studies have been reported on rainfall induced soil erosion/sediment yield modelling. Depending on the model algorithms which describe erosion, transportation processes, and the data requirement, several models ranging from simple empirical to complex physically based have been developed. Simple popular empirical models such as USLE and its derivatives perform very well at the plot scale. However, there use at catchment scale is problematic. Therefore various physically based models such as Water Erosion Prediction Project (WEEP) (Nearing at al., 1989), Areal Non-point Source Watershed Environment Response Simulation (ANSWERS) (Beasley and Huggins, 1980), Agricultural Nonpoint SourcePollution Model (AGNPS) (Young et al., 1989), and Soil and Water Assessment Tool (SWAT) (Arnold et al., 1993), and many others have been developed and theses have proved very useful as research tools. Theses are however of limited use in field, especially in developing countries, because they require skill and large amount of data. Ramganga reservoir, an important multi-purpose project of northern India (452 million unit annual power generation, irrigated an additional area of 5.12 lakh hectare), as an example, was designed for (assumed) sediment producing rate (SPR) of 4.25 ha.m per 100 sq. km; however a fairly high SPR of 17.3 was observed. Therefore, an emphasis should be given to develop models that are less complex than the physically based models

but yield precise results compared to those due to USLE or its derivatives (Aksoy et al., 2005).

1.5 RESEARCH OBJECTIVES

Based on the above discussion, the specific objectives set out for the present research work are summarized as follows:

1. To review the literature on rainfall-runoff-sediment yield modelling of mountainous watersheds.
2. To apply various available PET estimation methods and inter-compare their performance on watersheds belonging to different agro-climatic zone of India.
3. To propose an implicit relationship between Soil Conservation Service Curve Number (SCS-CN) parameter CN and potential evapotranspiration (PET).
4. To explore the potential of two-parameter Inverse Gamma Dstribution (2PIGD) for describing the complete shape of SUH using geomorphological parameters of watershed response and compare it with two-parameter Weibull Distribution (2PWD) and two-parameter Nash Gamma Model (2PNGM) for SUH derivation.
5. To propose a simplified GIUH based on time lag concept and check its workability in computation of peak runoff from mountainous watersheds.
6. To investigate the suitability of Melton number concept and GIS in extraction of realistic drainage network and geomorphological parameters of mountainous watersheds.
7. To propose a Radial Basis Artificial Neural Network (RBFANN) model for long term rainfall-runoff analysis of Ramganga river basin.
8. To propose a simple spatially distributed sediment yield model.

1.6 ORGANIZATION OF THESIS

The thesis is arranged in nine chapters as follows:

Chapter One: The first chapter briefly introduces the problems, describes the present state-of-the-art knowledge, and outlines the research objectives.

Chapter Two: This chapter deals with the review of literature on different components of rainfall- runoff-sediment yield modelling related with the present study.

Chapter Three: This chapter describes the study area considered for different studies as well as the data used. The types of data used are lumped, event rainfall-runoff data, daily rainfall-runoff data, unit hydrograph, and seasonal sediment yield data.

Chapter Four: In this chapter, different PET estimation methods and their inter-comparison have been discussed. Furthermore, mathematical and physical consequences which invoke an implicit relationship between parameter CN and long-term mean PET have been discussed in detail. The relationship was tested on seven catchments belonging to different agro-climatic zones of India.

Chapter Five: In this chapter, the potential of two-parameter Inverse Gamma Distribution (2PIGD) for SUH derivation is explored. An analytical approach is used to estimate the distribution parameters and the UH parameters, viz., peak discharge and time to peak are estimated using Horton's ratio given by Rodriguez-Iturbe & Valdes (1979). Finally, the workability of 2PIGD for SUH derivation is compared with two-parameter Weibull Distribution (2PWD) and two-parameter Nash Gamma Model (2PNGM) of Rosso (1984) for two Himalayan watersheds in the limited data condition. Using 2PIGD, a simple regression model is proposed for peak discharge and time to peak with dynamic velocity for an ungauged watershed.

Chapter Six: In this chapter, Nash Gamma IUH shape and scale parameters are redefined in terms of geomorphological parameters and lag time of watershed using the basic concept of IUH (Rodriguez-Iturbe and Valdes, 1979; and Rosso, 1984). The workability of the revised GIUH model is checked using different single peaked isolated runoff events from two Himalayan watersheds. For extraction of a realistic drainage network and geomorphological parameters, a coupling of Melton numbers with GIS is proposed.

Chapter Seven: In this chapter, an RBFANN model is proposed using k-means clustering algorithm to model the rainfall-runoff process. To test its potential, daily data of monsoon period (June-September) of three Himalayan watersheds are used.

Chapter Eight: This chapter deals with the formation of geo-database and finally proposes a simple spatially distributed sediment yield model. Its adequacy is checked using the observed data for four gauging sites located in a Himalayan watershed.

Chapter Nine: This chapter summaries the study and presents its conclusions besides the major research contributions and scope for future work.

CHAPTER 2
REVIEW OF LITERATURE

In correspondence with the major objectives of the present research work, this chapter is divided into five sections. In the first section, different commonly used potential evapotranspiration (PET) methods and their uncertainty in PET estimation in context of rainfall-runoff modelling is discussed. The second section deals with the concept of popular SCS-CN method and its myriad applications in different areas of hydrology. In the third section, different synthetic unit hydrographs and their utility in unit hydrograph derivation is summarized. The fourth section deals with the application and capability of Artificial Neural Network (ANN) in rainfall-runoff modelling. The available different soil erosion and sediment yield methods have been reviewed in the fifth section.

2.1 POTENTIAL EVAPOTRANSPIRATION (PET)

Evapotranspiration (ET), the major component of the hydrologic cycle, is important for planning, design, and operation of irrigation systems. ET depends on several climatological factors, such as temperature, humidity, wind speed, radiation, and type and growth stage of the crop. ET can be either directly measured using lysimeter, catchment water balance, and Pan evaporation approaches or indirectly by using climatological data. Lysimeter, a popular instrument for measuring ET, is often expensive in terms of its construction, and its operation requires skill. It is, however, most accurate if surface cover condition of the catchment perfectly matches the inside cover conditions of the lysimeter. However, exact simulation of prototype field condition in lysimeter is practically not possible and hence the results obtained may not be very accurate. Furthermore, the lysimeter experiment needed extensive care, longer time, high cost and sufficient data, which is normally not practicable.

Nevertheless, the water balance method yields the best estimates of mean long-term evaporation from large (plain) river basin (Gidrometeoizdat, 1967). However, the estimation of ET using water balance method is often limited due to inconvenience and inaccuracy in measurement of ground water inflow and outflow especially at shorter time span. Furthermore, pan evaporation method is one of the simplest and least time consuming methods of irrigation scheduling and has been used successfully in most parts of the world (Prescott, 1986). However, the common problem is the selection of accurate

pan factor which depends on the surrounding of the pan. Therefore, an indirect common procedure for estimating ET is to first estimate PET (Kashyap and Panda, 2001). Further, crop coefficients, which depend on the crop characteristics and local conditions, are used to convert PET to ET. PET is defined as (Allen et al., 1998) "the rate of evapotranspiration from a hypothetical crop with an assumed crop height (0.12 m) and a fixed canopy resistance (70 s/m) and albedo (0.23) which would closely resemble evapotranspiration from an extensive surface of green grass cover of uniform height, actively growing, completely shading the ground and not short of water". A large number of methods varying from simple empirical to complex physically based have been developed for different parts of the world. Theses methods utilize the climatological data and can be grouped into three broad categories i.e. temperature based, radiation based, and combination theory based methods.

Since solar radiation provides the energy required for the phase change of water, several methods (Makkink, 1957; Turc, 1961; Priestley and Taylor, 1972; Doorenbos and Pruitt, 1977) have been developed for PET estimation. The radiation methods show good results in humid climates where the aerodynamic term is relatively small, but the performance in arid condition is erratic and normally underestimates evapotranspiration. Turc (1960) developed a formula based on solar radiation and mean air temperature for 10 days period which was later modified by Turc (1961). Turc radiation method is the best method for ET estimation for humid locations. Priestley and Taylor (1972) method is the approximation of Penman method based on the fact that for very large areas the second term of the Penman equation is approximately thirty percent that of the first. Jensen-Haise (1963) method is often classified as a solar radiation method, however air temperature is also used and the coefficients used in the model are based on other inputs such as elevation and long term mean temperature (Burman *et al.*, 1983).

In temperature based PET method, a relationship has been developed between air temperature and PET. Hargreeves, Thornthwaite, and Blaney-Criddle etc. are the few examples of temperature-based PET methods. However, temperature-based methods are empirical and require local calibration in order to achieve satisfactory results. Thornthwaite (1948) correlated mean monthly temperature with PET for the east-central US and developed an equation which is widely used throughout the world. Thornthwaite method usually underestimates ET. However, simplicity in generating the seasonal distribution of PET is one of the strengths of the method (Jensen et al., 1990). Makkink (1957) published a formula for estimating PET based on solar radiation and air

temperature that is still used in Western Europe. Makkink utilized the energy-weighting term of the Penman equation, solar radiation, and a small negative constant. The Blaney and Criddle (1950) procedure for estimating ET is well known in the western USA and has been used extensively elsewhere (Singh, 1989). The method uses temperature as well as daily sunshine duration, minimum daily relative humidity, and the day-time wind at 2 m height. The model is quite sensitive to the wind speed variable and somewhat insensitive to the estimate of relative humidity. Christiansen (1968) and Christiansen and Hargreaves (1969) reduced weather data requirements up to only air temperature, calculated extraterrestrial radiation, and estimated the difference between maximum and minimum air temperatures to predict the effects of relative humidity and cloudiness. These efforts resulted in a very simple and accurate Hargreaves and Samani (1985) method for PET estimation. This method is most suitable for both arid and humid locations, if only maximum and minimum temperatures are available.

The combination methods were developed by combining the energy balance and mass transfer approaches. These methods combine fundamental physical principles and empirical concepts based on standard meteorological observations and have been widely used for estimation of ET from climatic data. Penman (1948) first derived the combination equation by combining components of energy balance and aerodynamics. Later, many scientists modified the Penman equation by incorporating stomatal resistance, modifying the wind function and vapor pressure deficits (Penman, 1963; Monteith, 1965; Wright and Jensen, 1972; Doorenbos and Pruitt, 1977; Wright, 1982). Penman-Monteith, FAO-24 Penman, 1982 Kimberly-Penman, and FAO-24 corrected Penman are the few examples of combination methods.

An ASCE Committee (Jensen et al., 1990) evaluated the performance of 20 different methods against the measured ET for 11 stations around the world under different climatic conditions. The Penman-Monteith method has ranked as the best method for all climatic conditions. However, the subsequent ranking of other methods varied with climatic condition. A user friendly Decision Support System (DSS) was developed for PET estimation by George et. al. (2002) which helps the user to decide the best PET method following ASCE ranking based on the data availability and the prevailing climatic condition.

2.1.1 Major Uncertainty with PET Methods

As discussed above, several empirical, semi-empirical, and physically based methods are available and theses differ from each other based on input data availability, accuracy and use over the last 50 years in different parts of the world. The applicability of PET methods is well documented in the text books related to hydrology and meteorology. The following text discusses some major uncertainties in PET methods.

The available PET methods have been shown to produce inconsistent results, as much high as 500 mm/yr (Amatya et al., 1995; Federer et al., 1996; Lu et al., 2005). In PET estimation by using remote sensing, an uncertainty of 20-30% in western riparian corridors of cottonwood has been reported (Nagler et al., 2005). Study of Cleugh et al. (2007) revealed that most sophisticated Penman-Monteith method using MODIS remote sensing data and surface meteorology as input also encountered an error between 20 and 25%. However, this uncertainty is due to inaccuracy in measurement of input parameters. It is worth noting here that the methods like Penman-Monteith are high data demanding and are also sensitive to data. Furthermore, the simple methods like Blaney-Criddle (1950) and Thornthwaite (1948) and Hargreeves (1982), employing only temperature data, are not very accurate especially under extreme climatic conditions. These methods underestimated (up to 60%) PET in windy, dry, and sunny areas, while in calm, humid, and cloudy areas, the PET is overestimated (up to 40%). Brutsaert (1982) points out that "...in the case of evaporation besides sampling, there is also the problem of simply determining it at a point location." However, in many situations, a single meteorological station data represents the climate of a large catchment, a poor spatial representation. This problem is frequently encountered in PET calculation using formulae requiring large data input.

Xu and Singh (2002) compared the performance of the five best PET methods from each category, viz., Hargreaves and Blaney-Criddle (temperature-based category), Makkink and Priestley-Taylor (radiation-based category), and Rohwer (mass-transfer-based category) with respect to Penman-Monteith (Allen *et al.*, 1998), and found their acceptable performance when the parameters are locally determined. They also concluded that the differences of performance between these best methods selected from each category are smaller than the differences between the different methods within each category as reported in earlier studies (for example, Xu and Singh, 2000, 2001).

Though the Penman-Monteith method is usually considered as a standard method, it performs well on saturated surfaces, and specifically, when its assumptions are met and

reliable input data are available. However, several researchers raise an important question: Is the Penman model the most relevant PET model for catchment modelling? (Qudin et al., 2005). Morton (1994) critically states on Penman's approach as follows: "The use of the Penman-Monteith equation to estimate evaporation from hydrologically significant areas has no real future, being merely an attempt to force reality to conform to preconceived concept derived from small wet areas".

Andreassian et al. (2004) used a sample of 62 mountainous catchments and two rainfall-runoff models to test the impact of a regionalized Penman PET on the performance of rainfall-runoff models. They found that the use of an average PET for all catchments yields similar results as due to more accurate regionalize PET. Paturel et al. (1995) and Nandakumar and Mein (1997) checked the sensitivity of PET in hydrological modelling and found PET errors to induce much smaller errors than the error in rainfall. Calder (1983) study showed that the use of a simple evaporation formula requiring no direct meteorological measurements other than rainfall gave better results than those due to using more data demanding potential evaporation equations (Priestley-Taylor, 1972; Penman, 1948; Thom-Oliver, 1977) for the prediction of soil-moisture deficit (SMD). This approach improved the performance of SMD prediction at all sites and for all years (including the drought year) over the other sophisticated evaporation equations. Furthermore, Andersson and Harding (1991) reported that the model performance was enhanced by using mean climatological PET, due to a negative feedback mechanism between stomatal resistance and evaporative demand which more sophisticated PET equations do not account for.

The validity of mean monthly PET was investigated and supported by Fowler (2002) in long-term daily water balance studies. The substitution of mean PET estimates into the daily water balance produced a soil water regime very similar to that derived using actual PET, particularly in relatively extreme periods. Using a large sample of 308 catchments of France, Australia, and the United States, Qudin et al. (2005) investigated the validity of 27 PET formulae in stream flow simulation and found that the observed daily PET data were not necessary as input into a rainfall-runoff model, rather a long-term regime (for example, annual) curve was sufficient. Therefore, many studies did not find any difference in the use of PET and mean PET (Burnash, 1995) even in extreme situations (Fowler, 2002).

2.1.2 Remarks

Several empirical, semi-empirical, and physically based methods have been developed over the last 50 years in different parts of the world but none can be recommended as the best one for any area or any season in terms of its accuracy and profitability. Furthermore, application of temporally varying PET (estimated from complex methods) is nothing but to increase the complexity and calculation of the model especially in rainfall-runoff modelling. Thus, the usefulness of more data demanding complex methods in PET estimation appears to be questionable and it, in turn, invokes a need for development of simpler methods to derive mean PET representing the whole catchment and compatible with the available complex methods.

2.2 SCS-CN METHOD

The SCS-CN method is based on the water balance equation along with two fundamental hypotheses. The first hypothesis equates the ratio of actual amount of direct surface runoff (Q) to the total rainfall (P) (or maximum potential surface runoff) to the ratio of actual infiltration (F) to the amount of the potential maximum retention (S). The second hypothesis relates the initial abstraction (I_a) to S and also described as potential post initial abstraction retention (McCuen, 2002). Expressed mathematically:

(a) Water balance equation

$$P = I_a + F + Q \tag{2.1}$$

(b) Proportional equality (First hypothesis)

$$\frac{Q}{P - I_a} = \frac{F}{S} \tag{2.2}$$

(c) I_a-S relationship (Second hypothesis)

$$I_a = \lambda S \tag{2.3}$$

The values of P, Q, and S are in depth dimensions, while the initial abstraction coefficient (λ) is dimensionless. Though the original method was developed in U.S. customary units (inch), an appropriate conversion to SI units (cm) is possible (Ponce, 1989). In a typical case, a certain amount of rainfall is initially abstracted as interception, infiltration, and surface storage before runoff begins. A sum of these three at initiation of surface runoff is usually termed as 'initial abstraction'.

The first hypothesis (Eq. 2.2) is primarily a proportionality concept (Fig. 2.1). This proportionality concept incorporated three major envelopes of interpretation, viz., (i) reconciles the popular concept of partial area contributing with the curve number

(Hawkins, 1979); (ii) undermines the source area concept (Steenhuis et al., 1995), allowing runoff generation only from saturated or wetted fractions of the watersheds; and (iii) ignores the statistical theory (Moore & Clarke, 1981; Moore, 1983; 1985), based on the runoff production from only saturated (independent or interacting) storage element. The parameter S of the SCS-CN method depends on soil type, land use, hydrologic condition, and antecedent moisture condition (AMC). Similarly, the initial abstraction coefficient λ is frequently recognized as a regional parameter depending on geologic and

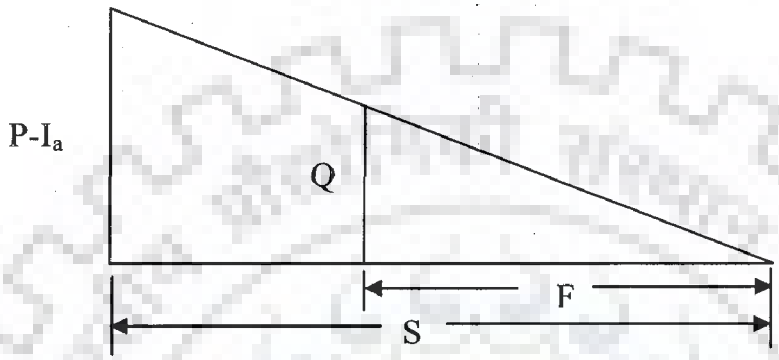

Fig. 2.1: Proportionality concept of the existing SCS-CN method (after Mishra and Singh, 2003a)

climatic factors (Boszany, 1989; Ramasastry and Seth, 1985). The existing SCS-CN method assumes λ to be equal to 0.2 for practical applications which has been frequently questioned for its validity and applicability (Hawkins et al., 2001), invoking many researchers for a critical examination of the I_a–S relationship for pragmatic applications. More recently, Zhi-Hua Shi (2009) examined I_a-S relationship using 6 years of rainfall and runoff event data from three gorges area of China. The results indicated that the I_a/S values, using event rainfall-runoff data, varied from 0.010 to 0.154, with a median value of 0.048. The average initial abstraction ratio of the watershed was equal to 0.053.

The second hypothesis (Eq. 2.3) is a linear relationship between initial abstraction I_a and potential maximum retention S. Coupling Eqs. (2.1) & (2.2), the expression for Q can be written as:

$$Q = \frac{(P - I_a)^2}{P - I_a + S} \tag{2.4}$$

Eq. (2.4) is the general form of the popular SCS-CN method and is valid for $P \geq I_a$; $Q = 0$ otherwise. For $\lambda = 0.2$, the coupling of Eqs. (2.3) & (2.4) results into

$$Q = \frac{(P - 0.2S)^2}{P + 0.8S} \tag{2.5}$$

Eq. (2.5) is well recognized as popular form of the existing SCS-CN method. Thus, the existing SCS-CN method with $\lambda = 0.2$ is a one-parameter model for computing surface runoff from daily storm rainfall, having versatile importance, utility and vast untapped potential.

Since parameter S can vary in the range of $0 \leq S \leq \infty$, it is mapped onto a dimensionless curve number CN, varying in a more appealing range $0 \leq CN \leq 100$, as:

$$S = \frac{25400}{CN} - 254 \qquad (2.6)$$

where S is in mm. The difference between **S** and CN is that the former is a dimensional quantity [L] whereas the latter is non-dimensional. In an ideal situation, the value of CN = 100 represents a condition of zero potential maximum retention (S = 0), that is, an impermeable watershed. Conversely, CN = 0 depicts a theoretical upper bound to potential maximum retention ($S = \infty$) that is an infinitely abstracting watershed. Many researchers attempted towards the practical design values validated by experience lying in realistic range (40, 98) (Van-Mullem, 1989). It is proper and appropriate to explicitly mention here that CN has no intrinsic meaning, it is only a convenient transformation of S to establish a 0-100 scale (Hawkins, 1978).

2.2.1 Application of SCS-CN Method in Hydrology

Since its development, the SCS-CN method has witnessed myriad applications all over the world (Mishra and Singh, 2003a). Rallison (1980) provided detailed information about the origin and evaluation of the methodology and highlighted major concerns to its application to hydrology and water resources problems it was designed to solve and suggested future research areas. A significant amount of literature has been published on the SCS-CN method in the recent past and several recent articles have reviewed the method at length. For example, McCuen (1982) provided guidelines for practical application of the method to hydrologic analysis. Ponce and Hawkins (1996) critically examined this method; discussed its empirical basis; delineated its capabilities, limitation and uses; and identified the areas of research in SCS-CN methodology. Hjelmfelt (1991), Hawkins (1993), Bonta (1997), McCuen (2002), Bhunya et al (2003), and Schneider and McCuen (2005) suggested procedures for determining curve numbers for a watershed using field data. Yu (1998) derived the SCS-CN method analytically assuming the expontial distribution for the spatial and temporal variation of the infiltration capacity and rainfall rate, respectively. Mishra and Singh (1999a, 2002a) derived the method from the

Mockus (1949) method and from linear and non-linear concepts, respectively. Mishra and Singh (2003) presented a state-of-the-art account and mathematical treatment of the SCS-CN methodology, and its application to several areas.

Originally, the method was intended for event based rainfall-runoff modelling but the method has been extended for long-term hydrologic simulation (Williams and LaSeur, 1976; Hawkins, 1978; Knisel, 1980; Pandit and Gopalakrishnan, 1996; Mishra and Singh, 2004a; and Geetha et al., 2007). SCS-CN method is also constructed as an infiltration model (Aron et al., 1977; Mishra and Singh, 2002a, 2004b). Hielmefelt (1980) proposed an SCS-CN based infiltration equation comparable with Holtan and Overton infiltration equations to compute infiltration rate from uniform rainfall intensity. Mishra (1998) and Mishra and Singh (2002a) introduced a term for steady state infiltration rate and proposed an infiltration equation by expressing the SCS-CN method in the form of Horton method assuming constant rainfall intensity.

Mishra and Singh (2002b) developed a modified SCS-CN method to incorporate the antecedent soil moisture in the existing SCS-CN method. Jain et al. (2006) applied existing SCS-CN method, its variant, and the modified Mishra and Singh (2002b) model to a large set of rainfall-runoff data from small to large watersheds and concluded that the existing SCS-CN method was more suitable for high runoff producing agricultural watersheds than to watersheds showing pasture/range land use and sandy soil.

Gaur (1999) extended SCS-CN applicability to derivation of Synthetic Unit Hydrograph (SUH) to predict surface runoff responses from a few catchments assuming them as ungauged. The computed surface runoff responses were quite satisfactory. Gaur and Mathur (2001, 2003) suggested synthetic SCS unit pulse hydrographs for generating overland roughness predictive equations for facilitating their application to kinematic wave modelling in ungauged situations. It indicated SCS-CN potential for hydrological evaluation of ungauged catchments.

Mishra et al., (2004) employed the concept of SCS-CN methodology for partitioning of 12 metals into dissolved and particulate bound forms. Yuan et al. (2001) modified the SCS-CN method to estimate subsurface drainage for five drainage monitoring stations. The method has also been successfully applied to distributed watershed modelling (White, 1988; Moglen, 2000; and Mishra and Singh, 2003a).

Mishra et al. (2006) coupled the SCS-CN method with the universal soil loss equation (USLE) to propose a new model for estimation of the rainstorm-generated lumped sediment yield from a watershed. The coupling is based on three hypotheses: (1)

the runoff coefficient is equal to the degree of saturation, (2) the potential maximum retention can be expressed in terms of the USLE parameters, and (3) the sediment delivery ratio is equal to the runoff coefficient. Furthermore, Tyagi et al. (2008) extended the sediment yield model to estimate the temporal rates of sediment yield from rainfall events on natural watersheds. The model utilizes the SCS-CN based infiltration model for computation of rainfall-excess rate and the SCS-CN-inspired proportionality concept for computation of sediment-excess.

Besides above application, the SCS-CN method has also been used, in association with erosion models for computation of sediment yield. Modified Universal Soil Loss Equation (MUSLE) (Williams, 1975), Agricultural Non-Point Source model (AGNPS) (Young, et al., 1989), Soil and Water Assessment Tool, SWAT (Arnold et al., 1993), Erosion-Productivity Impact Calculator, EPIC (Williams et al., 1983) are but a few examples. Sharda et al. (2002) used SCS-CN method in combination with USLE to compare runoff and soil loss from conservation bench terrace system and the conservation farming system.

2.2.2 Remarks

The SCS-CN method is a well accepted and widely practiced technique in applied hydrology because it is simple, easy to understand and applicable to watersheds with minimum of hydrologic information requirments. Bedside the task for which method originally intended, various advanced applications of the methodology has also been reported, and the existence of potential to extend the method in other areas advocated.

2.3 SYNTHETIC UNIT HYDROGRAPH (SUH)

The unit hydrograph concept proposed by Sherman (1932) for estimating the storm runoff hydrograph at the gauging site in a watershed corresponding to a rainfall hyetograph is still a widely accepted and admired tool in hydrology. This was one of the first tools available to the hydrologic community to determine the complete shape of the hydrograph rather than the peak discharge only (Todini, 1988). As the unit hydrograph concept needed the observed rainfall-runoff data at the gauging site for hydrograph generation, the paucity of these data sparkled the idea of synthetic unit hydrograph (SUH). The beginning of SUH concept can be traced back to the model (distribution graph) proposed by Bernard (1935) to synthesize the UH from watershed characteristics, rather than the rainfall-runoff data (Singh, 1988). The methods used for derivation of unit hydrograph in the catchment where there is a limited amount of data and for catchments

with no data, i.e. ungauged catchments, are discussed here under four sections: (i) Empirical SUH methods; (ii) Conceptual methods of SUH; (iii) Geomorphologic Instantaneous Unit Hydrograph (GIUH) based SUH methods; and (iv) Probability distribution function based SUH methods.

2.3.1 Empirical SUH Methods

The methods of Snyder (1938), Taylor and Schwarz (1952), SCS-CN (SCS, 1957), Gray (1961), and Espey and Wilson (1974) are a few examples among others, which utilize empirical equation to estimate salient points of the hydrograph, such as peak flow (Q_p), lag time (t_l), time base (t_B), and UH widths at $0.5Q_p$ and $0.75Q_p$. After estimation of these selected points, a complete unit hydrograph can be obtained by manual fitting of these points with the constraint that area under the SUH is unity. However, manual fitting of theses points with the simultaneous adjustment for the area under the SUH involves great degree of subjectivity. In addition to this, these methods use some regional constants such as C_T and C_p which vary in a wide range and may not be equally suitable for all the regions.

The SCS-CN methods (SCS, 1957, 1972) uses a specific average dimensionless unit hydrograph derived from the analysis of a large number of natural UHs for the watersheds of varying sizes and geographic locations, to synthesize UH. Assuming the triangular shape of dimensionless unit hydrograph the method computes the time to peak (t_p) and peak discharge (Q_p) in terms of time base (t_B), time lag (t_l), and time to recession (t_r). However, the major drawback of this method was to fix the ratio of time base to time to paek (t_B/t_p) for triangular UH as 2.67 (or 8/3). Note, the ratio other than this may lead to other shapes of the UH. In practice, the larger the ratio implies the greater catchment storage, and vice-versa. Therefore, the use of SCS-CN method should be limited to midsize watershed in the lower end of the spectrum (Ponce, 1989). Furthermore, Gray (1961) used some empirical relation to develop a dimensionless graph based on two parameters gamma distribution function and watershed characteristics to derive an SUH. The applicability of the method is however restricted due to use of empirical relations.

2.3.2 Conceptual SUH Methods

The models proposed by Clark (1945) and Nash (1959) are the most commonly used conceptual models. The Clark IUH model is based on the concept that IUH can be derived by routing unit rainfall-excess in the form of a time-area diagram through a single linear reservoir. For derivation of IUH, the Clark model uses two parameters viz. time of

concentration (T_c) in hours and storage coefficient (k) in hours of single linear reservoir in addition to the time-area diagram. The Clark model is frequently used by the field engineers in developing the regional relations. However, the entire recession of hydrograph represented by a single constant is one of the inconsistencies associated with the Clark model. In this continuation, Nash (1957, 1959, 1960) developed a conceptual model based on the cascade of 'n' equal linear reservoirs with equal storage constant **K** for derivation of IUH for a natural watershed. The analytical form of the model is expressed as:

$$q(t) = \frac{1}{k\Gamma n}\left(\frac{t}{k}\right)^{n-1} \exp\left(-\frac{t}{k}\right) \tag{2.7}$$

where q(t) is the depth of runoff per unit time per unit effective rainfall and K is the storage coefficient of the reservoir in units of hour. The parameters 'n' and 'k' are often termed, respectively, as the shape and scale parameters. The IUH can be extended to a UH for the catchment using existing conventional procedure (Ponce, 1989). It is noteworthy that the Nash model is nothing but the two-parameter gamma distribution (2PGD).

Bhunya et al. (2005) developed a hybrid model for derivation of SUH by splitting Nash single linear reservoir into two serially connected reservoirs of unequal storage coefficients to have a physically realistic response. The hybrid model was found to work significantly better than the widely used methods such as Synder, SCS, and Nash model when tested on the data of Indian and Turkey catchments for partial and no data availability.

2.3.3 GIUH-Based SUH Methods

Several attempts have been made to establish the relationships between parameters of the models for ungauged catchments and the physically measurable watershed characteristics (Bernard, 1935; Snyder, 1938; Taylor and Schwarz, 1952; Gray, 1961; and Boyd et al., 1979). In this regard, the pioneering works of Rodriguez-Iurbe and Valdes (1979) which explicitly integrate the geomorphological details and the climatological characteristics of a basin, in the framework of travel time distribution, are a boon for stream flow synthesis in ungauged basins or partial information on storm data. Gupta et al. (1980) examined the above approach and reformulated, simplified, and generalized it. Rosso (1984) parameterized the Nash model in terms of Horton order ratios of a catchment based on the geomorphologic model of a catchment. Rinaldo and

Rodriguez-Iurbe (1996) and Rodriguez-Iurbe and Rinaldo (1997) expressed the pdf of travel times as a function of the basin forms characterized by the stream networks and other landscape features. Chuthea and Dooge (1990) reformulated the GIUH on a deterministic platform rather than on Markov and statistical approaches. Kirshen and Bras (1983) studied the effect of linear channel on GIUH. Cudennec et al. (2004) provided the geomorphologic explanation of the UH concept based on the statistical reasoning (similar to Maxwell's reasoning) that considers hydraulic lengths of the components and derived the theoretical expressions of probability density functions (pdf) of hydraulic lengths of all components in the form of gamma pdf in terms of geomorphological parameters. Jain et al. (2000), Jain and Sinha (2003), Sahoo et al. (2006), and Kumar et al. (2007) applied geographic information system (GIS) supported GUIH approach for estimation of design flood. Similarly, the works of Berod et al. (1995), Sorman (1995), Bhasker et al. (1997), Yen and Lee(1997), Nasri et al. (2004), and Fleurant et al. (2006) based on GIUH approach for estimation of design flood from gauged as well as ungauged basins are noteworthy. Some of the pertinent works related with GIUH approach are discussed here as follows.

The gemorphological model proposed by Rodriguez-Iturbe & Valdes (1979) was parameterized in terms of the Horton's order laws (Horton, 1945) of drainage network composition and Strahler's stream ordering scheme (Strahler, 1957). The expressions for peak flow (q_p) and time to peak (t_p) of the IUH are given as:

$$q_p = \left(\frac{1.31}{L}\right) R_L^{0.43} v \tag{2.8}$$

and

$$t_p = 0.44\left(\frac{L}{v}\right) R_B^{0.55} R_A^{-0.55} R_L^{-0.38} \tag{2.9}$$

where L is the length of main channel or length of the highest order streams in kilometers, v is the average peak flow velocity and or characteristic velocity in m/s, q_p and t_p are in units of hr^{-1} and hr respectively. Rodriguez-Iturbe and Valdes (1979) defined a non dimensional term β as the product of q_p (Eq. 2.8) and t_p (Eq. 2.9) as:

$$\beta = 0.584\left(\frac{R_B}{R_A}\right)^{0.55} R_L^{0.05} \tag{2.10}$$

It is observed from Eq. (2.10) that beta is independent of velocity v and length of higher order stream or scale variable L, thereby, of the storm characteristics. Therefore it is a

function of only catchment characteristics. Alternatively, Eqs. (2.8) and (2.9) can be expressed as (Rosso, 1984):

$$q_p = 0.364 R_L^{0.43} v L^{-1} \tag{2.11}$$

$$t_p = 1.584 \left(\frac{R_B}{R_A}\right)^{0.55} R_L^{-0.38} v^{-1} L \tag{2.12}$$

where q_p, t_p, L and v must be in coherent units. The difficulty with the GIUH approach is the dependency on the dynamic parameter namely velocity. Rodriguez-Iturbe & Valdes (1979) advocated to take a constant velocity corresponding to peak discharge, since most of the flows in the watershed occurred at the peak discharge velocity. However, the question of how the velocity at peak flow is calculated was not addressed. In this sequence, Rodriguez-Iturbe et al. (1982) rationalized that velocity must be a function of the effective rainfall intensity and duration and proceeded to eliminate velocity from the results. In order to investigate this velocity-rainfall excess functionality, a study was conducted by Moughamian et al. (1987) for computation of GIUH proposed by Rodriguez-Iturbe et al. (1982). They found GIUH model to have performed poorly compared with sample distribution even when rainfall-excess was computed by sophisticated time varying infiltration capacity methods. In this continuation, Sormen (1995) used different flow velocities derived from some selected storms for computation of GIUH using Rodriguez-Iturbe *et al.* (1982) and found reasonable results. However, the subsequent method was not a substitute for other UH simulation methods. Bhaskar et al. (1997) found that the use of rainfall-excess intensity to estimate 'v' can lead to inaccurate estimation of q_p and t_p of the GIUH. They extended that the velocity is overestimated (when derived from rainfall-excess intensity), and hence, giving a smaller value of the Nash parameters k, thereby yielding hydrographs with higher peak flows and corresponding lower time to peaks than the observed.

Practical measurement of dynamic velocity corresponding to peak discharge is a tough task especially in remote areas. In this contest, Kumar et al. (2002) described two approaches to derive the dynamic velocity parameter: (1) when geometric properties of the cross-section of the gauging site are known with an adopted value of Manning's roughness coefficient (Chow 1964). Then a regression equation $v=ai_e^b$ can be drawn between the equilibrium velocity v (m/s) and the rainfall-excess intensity i_e (mm/hr); and (2) a power equation $v=ai_e^b$ can be used when Manning's roughness coefficient is not available but the velocities corresponding to discharge passing through the gauging

section at different depths of water flow are known from the observation. However, Kumar et al. (2002) used the value of v based on experience due to lack of data required for their procedure.

2.3.4 Probability Distribution Function-Based SUH Methods.

Due to similarity in shape and satisfying all UH criteria, pdf supports their applicability to UH derivation. The attempts made in the past for SUH derivation are described in brief as below.

Croly (1980) developed SUH by fitting two-parameter Gamma distribution for different sets of boundary conditions: (t_p, q_p), (t_p, t_1) or (q_p, t_1). These boundary conditions are used to estimate the parameters 'n' and 'K' of the distribution. The methodology provides a line of initiation to work with probability distribution functions for SUH derivation for ungauged catchments. Koutsoyiannis and Xanthopoulos (1989) applied eight different parametric expressions for formation of IUH. The parameter estimation method based on integral square error gave more accurate results than the method of moments.

Haktanir and Sezen (1990) explored the suitability of two-parameter Gamma and three-parameter Beta distributions as SUH for Anatolia catchments in Turkey. The parameters of both the distributions were estimated by using classical Newton iterative algorithm. They found both the distributions to fit reasonably well to observed unit hydrographs. Bhunya et al., (2003) introduced a simplified version of two-parameter gamma distribution to derive an SUH. The parameter 'n' of gamma distribution expressed mathematically in terms of non-dimensional β ($=q_p t_p$) same as did Rosso (1984). The present approach was more convenient and accurate than the popular Snyder and Gray methods. Bhunya et al. (2007) further evaluated the potential of four popular i.e. two-parameter Gamma, three-parameter Beta, two-parameter Weibull, and one-parameter Chi-square distribution to derive SUH. Simple formulae are derived using analytical and numerical schemes to compute the distribution parameters, and their validity is checked with simulation of field data. The Gamma and Chi-square distributions behave analogously, and the beta distribution approximates a gamma distribution in a limiting case. Application to field data shows that the Beta and Weibull distributions are more flexible in hydrograph prediction than the Gamma and Chi-square distribution.

Nadarajah (2007) suggested eleven flexible probability distributions to derive SUH. They are two-parameter Log-normal distribution, two-parameter Gamma

distribution, two-parameter Inverse Gamma distribution, three-parameter Beta distribution, three-parameter Kumaraswamy distribution, three-parameter two-sided Power distribution, two-parameter Pareto distribution, two-parameter Inverse Gaussian distribution, two-parameter F-distribution, two-parameter Weibull distribution, and two-parameter Fre´chet distribution. However, their workability was not evaluated at catchment scale. Bhunya et al. (2008) used two-parameter Weibull distribution (2PWD), and two-parameter gamma distribution (2PGD) similar to an IUH and parameterized in terms of Horton catchment ratios on the basis of a geomorphologic model of catchment response. Expressing parameters of the 2PGD in terms of Horton ratios by the numerical method shows better accuracy than the method due to Rosso (1984). For describing the shape of SUH under limited data conditions, the proposed 2PWD approach is marginally better than the existing 2PGD. Rai et al. (2008) compared the performance of nine popular pdfs, viz., Beta , Exponential (EXP), Gamma (GM), Normal, Lognormal (LN), Weibull (WB), Logistic (LG), Generalized logistic (GLG), and Pearson Type 3 (PT 3) distribution functions were for the derivation of UH. These distributions were tested on 13 watersheds (area ranges from 0.012 km^2 to 4300 km^2) of different characteristics and it was observed that except for the EXP distribution function, most other distribution functions produced UHs in satisfactory agreement with observed UHs. Combining the overall performance of the distributions over 13 watersheds, the order of ranking the suitability of distributions were as: gamma > pearson type 3 > beta ≥ generalize logistic ≥ lognormal > weibull.

2.3.5 Remarks

Employing only two points on the UH e.g. time to peak and peak flow, gamma, beta, weibull, lognormal, Chi-square, Fre´chet etc. probability distribution functions (pdfs) are suitable to describe the shape of unit hydrograph, and they perform better than the existing methods suggested by Snyder (1938), SCS (1957), and Gray (1961). The GIUH approach (Rosso, 1984) has improved substantially the capability of predicting the parameters of the Nash model with respect to the others. However, there is scope to work on dynamic velocity parameter to make more conceivable approach for SUH derivation. Among the pdfs explored by now for SUH derivation, two-parameter Weibull distribution (2PWD) was found to be more flexible and accurate for all types and sizes of the catchments. However, several pdfs are yet to be explored for their utility in SUH

derivation. Analytical solutions for parameter estimations are simple to use and yield satisfactory results.

2.4 ARTIFICIAL NEURAL NETWORK MODELLING

A neural network may be defined as a massively parallel connected network made up of simple processing units called *neurons,* which is capable of extracting features from the environment in which it is embedded and making this information available for use. Neural Networks are also known as *neurocomputers*, connectionist networks, or *parallel-distributed processors* (PDPs). The power of the neural network lies in its massively parallel-distributed structure and its versatility comes from its ability to learn by example and producing reasonable outputs even for inputs not encountered during training. Neural network learns from experience and then perform 'recognition without definition' (Kasko, 1992). ANN models are developed using the measured time series instead of utilizing mathematical expressions describing the physical processes of the catchment. ANN is one such technique in series that provides reliable estimation without considering the physical nature of the process. Since early 1990s, the method has developed largely because of powerful new algorithms and computational tools (Govindajaru, 2000), medicine (Venkatesan and Anitha, 2006), aero-dynamic optimization (Wei et al., 2008); construction cost forecasting (Zhigang and Yajing, 2009), pattern recognition (Miyoung and Cheehang, 2000) etc. ANNs have been successfully applied in handling extraordinary range of problem domains. Following are the advantages of neural network in hydrology:

- Neural networks are useful when the underlying problem is either poorly defined or not clearly understood.
- ANN application does not require knowledge of the underlying process beforehand.
- A small amount of errors in the input does not produce significant change in the output because of distributed processing.
- Neural networks are more suitable for dynamic forecasting problems because the weight involved can be updated when fresh observations are made available.
- They do not require any exogenous input other than a set of input-output vectors for training purpose.

Development of back propagation ANN (BPANN) created great impact in the field of ANN among the researchers. The back propagation algorithm originated from Widrow and Hoff's learning rule and it is popularized by Rumelhart et al. (1986). It is a

systematic method for training multilayer neural networks. As a result of this algorithm, multilayer perceptrons are able to solve many important practical problems. A gradient decent algorithm used in back propagation neural network sometimes gets trapped in local minima instead of global minima. This problem is solved by radial basis function ANN (RBFANN) introduced by Broomhead and Lowe (1988).

2.4.1 Application of ANN in Rainfall-Runoff Modelling

The available literature related to the application of neural network in hydrological modelling is described in brief as follows:

Hsu et al. (1995) demonstrated the applicability of ANN approach to simulation of rainfall-runoff process. The non-linear ANN model approach was shown to provide a better representation of the rainfall-runoff relationship of the medium size Leaf river basin near Collins Mississippi than the linear autoregressive moving average with exogenous input (ARMAX) time serious approach and the conceptual Sacramento Soil Moisture Accounting (SAC-SMA) model. Out of three models used, the first was a nonlinear system theoretical mode. Six consecutive water years (October 1st to September 30th) were selected for model development and testing, only one water year data were used for model development, and rest five years for validation. The improvement was tested on the basis of root-mean-square error, percent error in volume, percent error in peak flow and linear correlation between measured and estimated, a marginal improvement by ANN was seen.

Mason et al. (1996) suggested that RBFANN networks are effective in modelling runoff for a large rainfall data base with radial centers. Fixed by a suitable data, clustering technique will provide good results more rapidly. They discouraged traditional neural network learning procedures such as back propagation because of slow convergence and expensive to carry out.

Minns and Hall (1996) developed a model for which the data were generated from synthetic storm sequences routed through a conceptual hydrological model consisting of a single non-linear reservoir. The application of different standardization factors to both training and verification sequences underlined the importance of such factors to network performance. Trials with both, one and two hidden layers in the ANN showed that, although improved performances were achieved with extra hidden layers, the additional computational effort did not appear to be justified for data sets exhibiting the degree of non-linear behaviour typical of rainfall and flow sequences from many catchment areas.

When the fitted ANNs were verified on storm sequences containing the same range of extremes as the training data, the coefficients of efficiency were comparable. When ANNs were verified on sequences having larger extremes than the training data, coefficients of efficiency reduced. Minns and Hall (1996) however suggested that ANNs were not very good extrapolators and extreme caution should be applied if ANNs were to be employed to predict out of range.

Shamseldin (1997) applied the multi-layer feed forward neural network to rainfall-runoff modelling on the data of six catchments. It was tested under four different external input scenarios using the input information required for the operation of three selected rainfall-runoff models, namely, simple linear model (SLM), the seasonally based linear perturbation model (LPM) and the nearest neighbour linear perturbation model (NNLPM). In each of the first three scenarios, the input information corresponds to that used by one of these models, while in the fourth scenario, it corresponded to both LPM and NNLPM. The comparison of the results of the neural network forms corresponding to each of the four external input scenarios with those of the SLM, the LPM and NNLPM showed that one or other form of neural network has substantially higher correlation coefficient in calibration than these models. However, in verification, one or other form of neural network was better than these models in case of four out of the six catchments.

Fernando and Jayawardena (1998) used RBFANN networks with orthogonal least square (OLS) algorithm for runoff forecast of Kamihonsha catchment in Uratsukuba. They found that OLS algorithm is capable of synthesizing the suitable network architecture, reducing the time consuming trial and error approach. Results showing that RBFANN networks performed accurate results than ANN model that uses the Back-Propagation (BP) algorithm, an ARMAX model.

ASCE (2000a) described an introduction of ANNs, the role of ANNs in hydrology, presented some guideline on their uses, compared ANNs with other modelling philosophies, and described their strengths and limitations along with their similarity with other modelling approaches, such as a physical model. ASCE (2000b) critically examined the role of ANN in various branches of hydrology. It was found that ANNs are tool for modelling many of the non-linear hydrologic processes such as rainfall-runoff, stream flow, groundwater management, water quality simulation, and precipitation. A good physical understanding of the hydrologic process being modelled can help in selecting the input vectors and designing a more efficient neural network. However, ANNs were data intensive, and there appears to be no established methodology for their design and

successful implementation. The merits and limitations of ANN application were discussed and potential research avenues were briefly explored.

Tokar and Markus (2000) compared the ANN model with traditional conceptual model in predicting watershed runoff as a function of rainfall, snow water equivalent and temperature. The models used were water balance (WATBAL) model, SAC-SMA model, and simple conceptual rainfall-runoff (SCRR) model. A standard back-propagation algorithm and the sigmoid transfer function were applied in training of the network. In case of comparison of ANN with SAC-SMA, four different ANN structures (different in input parameter) were trained. The model which was included in the stream flow at (t-1) as an input to the ANN model had reasonable calibration accuracy when compared to that of the conceptual model. The reason may be that the values of Q(t-1) provided information that was not contained in precipitation and temperature. Based an average precipitation, three data sets representing average, wet, and dry years were selected in the comparison of ANNs with SCRR model. The ANN model provided significantly higher training accuracy for the average and wet years than that of the SCRR, whereas SCRR illustrated better training accuracy for the dry years.

Agarwal and Singh (2004) developed a multilayer back-propagation ANN (BPANN) to simulate rainfall-runoff process on three different time scales, viz. weekly, ten daily, and monthly with variable data sets. Based on the performance evaluation criteria, the BPANN models developed using the data of block I having relatively low variability and uncertainly showed an improvement over the Linear Transfer Function (LTF) model but this development was not seen uniformly both in cross validation and verification periods. While the BPANN models developed using the data of block III having relatively high variability and uncertainty of data had a significant effect in the development of generalized BPANN model. The number of iterations required for development of the generalized model reduced with increase in variability of dataset used.

Chang and Chen (2003) applied RBFANN networks for water stage forecasting in a study under high flood and tidal effects in Tanshui River situated near the city of Taipei. In this study, they chose a hybrid unsupervised learning scheme, in which the commonly used k-means clustering method is replaced by fuzzy min-max clustering is proposed for choosing best patterns for cluster representation in an efficient and automatic way and supervised learning scheme which is a multivariate linear regression method to produce a weighted sum of the output from hidden layer was applied. Finally, they concluded that

the advantage of using fuzzy min-max clustering was that the member, centers and 'σ' of the radial basis function could be determined systematically and automatically. Lin and Chen (2004) demonstrated the use of RBFANN to model the rainfall-runoff process in the Fei-Tsui reservoir watershed in northern Taiwan with supervised learning algorithm and hybrid- learning algorithm for setting up the number of hidden layer neurons. Finally, they concluded that fully supervised learning algorithm provides better training and accuracy than the network trained using the hybrid-learning algorithm. Adam et al. (2006) applied RBFANN, Fuzzy, BPANN, Nearest Neighbor approach, linear regression and classical empirical formulae for evaluation of longitudinal dispersion coefficient for a river reach. The results obtained by means of each neural network type were better than those due to empirical formulae, regression method, and Nearest Neighbour approach. Moreover, BPANN networks allowed more precise evaluation of longitudinal dispersion coefficient than RBFANN and fuzzy models.

Sudheer et al. (2008) proposed two hybrid models namely, ANN-based hybrid model (ANNHM) and the linear parametric-based hybrid model (LPHM) for modelling annual stream flows of rivers. The proposed ANN based-hybrid model (ANNHM) was able to reproduce the skewness present in streamflows better than the linear parametric-based hybrid model (LPHM), owing to the effective capturing of the non-linearities. The ANNHM, being a completely data-driven model, reproduced the features of the marginal distribution more closely than the LPHM, but it offered less smoothing and little extrapolation value. Despite a better preservation of the linear dependence structure, the LPHM was not able to predict the variation of critical drought duration effectively with respect to truncation level. In contrast, the ANNHM was able to model the variation of critical drought duration better even though the preservation of linear dependence structure was inferior to the LPHM.

2.4.2 Remarks

ANN has some unique qualities enabling them to model better than the other conventional methods, the complex hydrological processes especially the process of rainfall-runoff generation. In relation to RBFANN networks, BPANN networks are sometimes poorer to converge, better in generalization, and poorer in performance.

2.5 SOIL EROSION AND SEDIMENT YIELD

The process of soil erosion involves the processes of detachment, transportation, and accumulation of soil from land surface due to either impact of raindrop, splash due to

rain impact, shearing force of flowing water, wind, sea waves or moving ice. Erosion due to water is an area of interest to hydrologists and sedimentologists. Various forms of soil erosion due to water are inter-rill, rill, gully and stream channel erosion. Rain drop plus sheet erosion jointly cause inter-rill erosion. The concentrated flow causes rill erosion. Gully erosion is an advanced stage of rill on account of head cutting at the gully head. Apart from rainfall and runoff, the rate of soil erosion from the area is also strongly dependent on its soil, vegetation, and topographic characteristics. During the process of erosion and transportation to downstream side, some part of the eroded material may get opportunity to deposit. The net amount of sediment flowing through the watershed is termed as sediment yield.

Deposition of sediment transported by a river into a reservoir reduces the reservoir capacity, thereby adversely affecting the water availability for power generation, irrigation, domestic and industrial use. Sediment deposition on river bed and banks causes widening of flood plains during floods. Control of upland erosion does not always reduce the sediment yield immediately, because of the increased erosivity of channel flow in the downstream. Soil erosion is a serious problem in lower Himalayas and foothill ecosystem. Sustainable use of mountains depends on conservation and potential use of soil and water resources. High population growth has placed a demand on limited natural resources present in the hills. High rainfall coupled with fragile rocks and high relief conditions in Himalayas are conducive to soil erosion. It is a prime threat to sustained land use for crop production in Himalayan ecosystem. Rapid increase in the developmental activities, mining and deforestation etc. are major factors contributing to soil erosion and thus leading to land degradation.

2.5.1 Popular Soil Erosion and Sediment Yield Models

A multitude of models are available in hydrologic literature for estimation of soil erosion and sediment yield from watersheds. Most of these models can be grouped into three broad categories, viz., (i) empirical models based on empirical equations generally derived from field data, for example, the equation of Musgrave (1947), Universal Soil Loss Equation (USLE) (Wischmeier and Smith, 1978), Modified Universal Soil Loss Equation (MUSLE) (Williams, 1975) or Revised Universal Soil Loss Equation (RUSLE) (Renard et al., 1991); (ii) conceptual soil erosion models, for example, the models of Johnson (1943), Rendon-Herrero (1978), Williams (1978), Kalin et al. (2004); and (iii) physically based model, for example, the models of WEPP (Water Erosion Prediction

Project) (Nearing et al., 1989), European Soil Erosion Model (EUROSEM) (Morgan et al., 1998), sediment component of SHE (SHESED) (Wicks and Bathurst, 1996), Chemicals, Runoff, and Erosion from agricultural Management Systems (CREAMS) (Kinsel, 1980), and Areal Non-point Source Watershed Response Simulation (ANSWERS) (Beasley et al., 1980).

(a) Empirical erosion models

Models based on empirical equations are generally derived from field data and are commonly termed as empirical models. Some of the empirical soil erosion/sediment yield models are as follows:

USLE: Soil erosion is most frequently assessed by using Universal Soil Loss Equation (USLE) since early 1960's. The equation was designed for inter-rill and rill erosion (Wischmeier and Smith, 1978; Renard et al., 1991). Although the equation is described as universal, its database, though extensive, is restricted to slopes (normally) 0 to 17° and to soils with a low content of montmorrilonite. It is also deficient in information on erodibility of sandy soils. In addition to the limitation of its database, there are theoretical problems with the equation. Soil erosion cannot be adequately described merely by multiplying together six factor values (E = RKLSCP). There is considerable interdependence between variables (Morgan, 1995). Despite all, it is most commonly used throughout the globe.

MUSLE: It is the modified version of the USLE. In MUSLE (Williams. 1975), the rainfall erosivity factor was replaced by runoff. The runoff factor includes both total storm runoff volume and peak runoff rate. Compared to USLE, this model is applicable to individual storms and it eliminates the need for sediment delivery ratios, because the runoff factor represents energy used in detaching and transporting sediment. The main limitation is that it does not provide information on time distribution of sediment yield during a runoff event.

RUSLE: It is a revised version of USLE intended to provide more accurate estimates of erosion (Renard et al., 1991). It contains the same factors as USLE, but all equations used to obtain factor values have been revised. It updates the content and incorporates new material that has been available informally or from scattered research reports and professional journals. The major revisions occur in the cover management factor, C, support practice factor, P, and slope length gradient factor, LS, factors. C is now the

product of four sub-factors: prior land use, canopy cover, soil surface cover, and surface roughness.

MMF Model: Morgan-Morgan-Finny (MMF) model (Morgan et al., 1984) was developed to predict annual soil loss from field size areas on hill slopes. The model has the simplicity of the universal soil loss equation and yet it covers the advances in understanding of the erosion process. This model is physically based empirical model and needs less data than the most other erosion predictive models. This model divides soil erosion processes into two phases including a water phase and a sediment phase. Water phase determines the energy of rainfall available to detach soil particles, and in the sediment phase, soil particles detached by the rain are estimated. The MMF model can be easily applied in raster-based geographic information system (GIS) (Shrestha, 2007). It was further refined by adding the erosion by flow (Morgan, 2001). However, the flow component in the model is not very realistic since there is no transfer of flow down slope to other pixels.

SLEMSA Model: The Soil Loss Estimator for Southern Africa (SLEMSA) (Elwell. 1978; Stocking, 1981) was developed largely from the data from Zimbabwe to evaluate the erosion resulting from different farming systems so that appropriate conservation measures could be recommended. Generally, the model looks like USLE and it has the same limitations as USLE.

SEDD: The SEdiment Delivery Distributed (SEDD) model, which is based on the empirical USLE model, was proposed by Ferro and Porto (2000). Monte Carlo technique was used to test the effect of uncertainty in the model parameters on sediment yield computations, similar to the study by Biesemans et al. (2000) on the RUSLE.

(b) Conceptual models

Conceptual models tend to include a general description of catchment processes, without including the specific details of process interactions, which would require detailed catchment information (Sorooshian, 1991). This allows these models to provide an indication of the qualitative and quantitative effects of land use changes, without requiring large amount of spatially and temporally distributed input data. The conceptual models lie somewhere between empirical and physically based models.

Johnson (1943) was perhaps the first to derive a distribution graph for suspended sediment concentration employing the hypothesis analogues to that embodying in the unit hydrograph. Rendon-Herrero (1978) extended the unit hydrograph method to directly

derive a unit sediment graph (USG) for a small watershed. The sediment load considered in the USG is the wash load only. Williams (1978) extended the concept of an instantaneous unit hydrograph (IUH) to instantaneous unit sediment graph (IUSG) to determine the sediment discharge from an agricultural catchment. The concept of USG has also been employed by Singh et al. (1982), Chen and Kuo (1986), Kumar and Rastogi (1987), Raghuwanshi et al., (1994), Banasik and Walling (1996), among others, for the purpose of estimating the temporal variation of sediment yield. Kalin et al. (2004) developed a modified unit sedimentograph approach for identification of sediment source area within the catchment. The catchment was portioned into a number of elements. The sediment flux response of the elements at the basin outlet was computed by characterizing the rainfall event by the pulse of rainfall excess depths. The application of these methods requires considerable input data for their calibration, but the models inherit the limitations of unit hydrograph theory.

Viney and Sivapalan (1999) coupled a continuous (daily time interval) conceptual sediment generation and transport algorithms, to an existing water and salt balance model, LASCAM. LASCAM was originally developed to predict the effect of land use and climate change on the daily trends of water yield and quality in forested catchments in Western Australia. The developed sediment transport algorithm does not discriminate between sediment size classes. It was found that the amount of runoff and sediment produced by the model matched well in monthly and daily time intervals.

(c) Physically based models

The other category of models which use theoretical description of processes involved in the form of mathematical equations are termed as physically based models. These models are intended to represent the essential mechanisms controlling erosion and they incorporate the laws of conservation of mass and energy. Most of them use particular differential equations and generally require more input parameters than empirical models. Numbers of the physically based models are developed in the recent past.

AGNPS: The Agricultural Non-Point Source model (AGNPS) is an event-based model developed by the US Department of Agriculture, Agricultural Research Service (USDA-ARS) in cooperation with the Minnesota Pollution Control Agency and the Soil Conservation Service (SCS) in the USA (Young et al., 1989). AGNPS simulates runoff, sediment, and nutrient transport from agricultural watersheds. The model divides the watershed into square cells uniformly distributed over the watershed. The erosion and

sediment transport components are based on estimating the upland erosion by USLE and routing it by the steady-state continuity equation of sediment. The model produced comparable results for runoff and sediment (Young et al., 1989). Panuska et al. (1991) identified that the grid size selected by the model user was a major factor influencing sediment yield calculations. Consequently, care needs to be taken when applying such a model to ensure that the resolution chosen for modelling is adequate for the task.

ANSWERS: Areal Nonpoint Source Watershed Response Simulation (ANSWERS) model (Beasley et al., 1980) is an event based, distributed parameters watershed model to simulate the runoff and sediment yield from agricultural watershed and to evaluate the effect of various management practices on the runoff and sediment response of the watershed. The recent version of the ANSWERS model, i.e. ANSWERS-2000 (Dillaha et al., 2001), is capable of simulating the runoff and sediment yield on continuous basis. Preparing input data file for ANSWERS is rather complex (Norman, 1989) as it is the case for many physically-based hydrological, erosion and sediment transport models. The applicability of ANSWERS is limited in many catchments by the large spatial and temporal input data requirements of the model. Given the lack of such data in most catchments, parameters may need to be calibrated, raising problems of identifiability and physical interpretability of model parameters.

LISEM: The LImburg Soil Erosion Model (LISEM) (De Roo and Jetten, 1999) is a spatially distributed, physics-based hydrological and soil erosion model developed by the Department of Physical Geography at Utrecht University and the Soil Physics Division at the Winard Staring Centre in Waneningen, the Netherlands, for planning and conservation purposes. LISEM (De Roo et al., 1996) is one of the first models that use GIS. In the soil erosion part, the model accounts also for roads, wheel tracks and channels. Approximately 25 maps are required for simulation, including maps describing catchment morphology, leaf area index, random roughness of the soil, and the fraction of the soil with crop cover. LISEM does not simulate concentrated erosion in rills and gullies, rather it simulates sediment detachment by flows in the ponded area only. Additionally, regardless of how well constructed or sophisticated a model is, the performance of a model such as LISEM ultimately is constrained by the resolution and quality of these GIS inputs.

CREAMS: Chemicals, Runoff, and Erosion from Agricultural Management Systems (CREAMS), a physically based daily simulation model, maintain the elements of USLE, but include the sediment transport capacity of flow. The sediment transport component of

CREAMS analyzes the inter-rill area and rill separately. Detachment on both rill and inter-rill area is determined by the modified USLE. The procedure allows parameters to change along the overland flow profile and along waterways to describe spatial variability (Foster et al., 1981). An advantage of CREAMS is that it accounts for gully erosion and deposition, in addition to overland erosion sources, erodability factor to be updated from one runoff event to the next (Govers and Loch, 1993). The model applies to field-sized catchments of approximately 40 ha, although it can be used on scales up to 400 ha (Lane et al., 1992).

WEPP: Water Erosion Prediction Project (WEPP) (Nearing et al., 1989) is a continuous simulation (field or watershed) scale model that incorporates new erosion prediction technology developed by USDA. The model requires input data of rainfall amount and intensity, soil texture, plant growth, residue decomposition, effect of tillage implements on soil properties, slope shape, steepness, and orientation, and soil erodability parameters. The watershed version of WEEP routes runoff and sediment from fields and incorporates channel scour based on the work of Foster and Meyer (1972), and Knisel (1980). The model was found reliable (Zhang et al., 1996) in predicting long term averages of soil loss under cropped conditions. The ability of WEPP to accurately predict where detachment and deposition will occur will be useful in establishing appropriate conservation or management practices. Despite the process-based nature of the model, WEPP still contains a degree of empiricism and care should be taken when applying the model to new sites.

EUROSEM: The EUROpean Soil Erosion Model (EUROSEM) (Morgan et al., 1998) is a model for predicting soil erosion by water from fields and small catchments. The model was designed as an event-based model, for it was assumed that erosion was dominated by only a few events per year. EUROSEM is a dynamic erosion model and is able to simulate sediment transport, erosion and deposition by rill and inter-rill processes over the hillslope. The model provides total runoff, total soil loss, storm hydrograph and storm sediment graph.

KINEROS: KINematic EROsion Simulation (KINEROS) (Smith, 1981; Woolhiser et al., 1990) is composed of elements of a network, such as planes, channels or conduits, and ponds or detention storages, connected to each other. KINEROS is an extension of KINGEN, a model developed by Rovey et al. (1977), with incorporation of erosion and sediment transport components. The sediment component of the model is based on the

one dimensional unsteady state continuity equation. Erosion/deposition rate is the combination of raindrop splash erosion and hydraulic erosion/deposition rates.

2.5.2 Remarks

Based on the processes considered, involvement of complexity, accuracy, scale (space and time), and ultimately input data requirement, a wide range of models exist for modelling sediment yield and soil erosion. However, the use of physically based models is limited to research only due to their complexity and non-availability of data required for field use. The major problem with the conceptual model is lack of uniqueness in parameters obtained in calibration from the observed data. Therefore, empirical models are more commonly used in field application in data scarce regions. However, these are based on inductive logic and generally applicable only to those conditions for which the parameters have been calibrated. Overall, there is not a single model valid for all applications. Thus there exists a need to develop such models that describe the complex physical process of sediment erosion/deposition in a simple manner as USLE and, at the same time, the output is close to reality, as far as possible, in space and time.

Based on the literature review, some of the model has been proposed/modified in the study and some have been investigated for their applicability to a large set of data collected from mountainous watersheds, where sufficient research/application potential exists. The following chapter describes the study areas and availability of data for their use in the forthcoming chapters.

CHAPTER 3
STUDY AREA AND DATA PREPARATION

Four types of data are used in the present study:

(i) Daily hydrological and meteorological data for CN-PET relationship

(ii) Short-term time-distributed data of rainfall-runoff for SUH derivation

(iii) Long-term rainfall-runoff data for ANN modelling

(iv) Seasonal rainfall-sediment yield data for distributed sediment yield modelling.

3.1 DAILY HYDROLOGICAL AND METEOROLOGICAL DATA

In the present study, daily hydrological and meteorological data from seven watersheds belonging to different agro-climatic regions of India were used to test the workability of relationship between the CN parameter of Soil Conservation Service Curve Number (SCS-CN) model and potential evapotranspiration (PET). Study watersheds are described below.

3.1.1 Ramganga Watershed

The Ramganga river is a major tributary of Ganga and drains a catchment area of 3,134 km^2 (Fig. 3.1). Its catchment lies in the Sivalik ranges of Himalayas and the valley is known as Patlei Dun. River Ramganga originates at Diwali Khel. It emerges out of the hills at Kalagarh (District Almora) where a major multipurpose Ramganga dam is situated. Its catchments lies between elevation 338 m and 3088 m above mean sea level, and it is considerably below the perpetual snow line of the Himalayas. The river traverses approximately 158 km before it meets the reservoir and then continues its journey in the downstream plains for 370 km before joining River Ganga at Farrukhabad. During its travel up to Ramganga dam, the river is joined by main tributaries: Gagas, Bino, Khatraun, Nair, Badangad, Mandal, Helgad, and Sona Nadi. About 50% of the drainage basin is covered with forest, 30% is under cultivation on terraced fields, and the remaining 20% is urban/barren land. At the outlet of the Upper Ramganga watershed, i.e. Kalagarh, there exists a multi-purpose Ramganga dam. The dam is 127.5 m height earth and rock-fill type designed for the estimated sediment rate of 4.25 ha-m/100 sq. km per year.

The climatic condition of the river basin is largely influenced by the orographic effect. The area receive majority of precipitation in the form of rainfall. Ramganga valley experiences approximately an mean annual precipitation of 1,550 mm. The raingauge

network consists of Ranikhet, Chaukhatia, Naula, Marchulla, Lansdowne and Kalagarh besides the other existing stations. Stream flow records of the Ramganga River, including river stages, instantaneous as well as monthly, are available at Kalagarh.

3.1.2 Hemavati Watershed

River Hemavati (Fig. 3.2a) is a tributary of River Cauvery, originating in Ballaiarayanadurga in the Western Ghats in Mundgiri taluk of Chikmanglur district in Karnataka State (Mishra and Singh, 2003a). It passes through a region of heavy rainfall in its early reaches, in the vicinity of Kotigere and Mudigere. It has Yagachi and Algur tributaries and drains an area of 600 sq. km up to Sakleshpur. The watershed of Hemavati lies between 12°55′ and 13°11′ north latitudes and 75°20′ and 75°51′ east longitudes. It is a hilly watershed with steep to moderate slopes. Agriculture and plantation are the major industries of the basin. Its land use can be characterized by forests (12%), coffee plantations (29%), and agricultural lands (59%). The principal soil types are red loamy soil (67%) and red sandy soil (33%). Soils in the forest area and coffee plantations are greyish due to high humus content.

3.1.3 Kalu Watershed

River Kalu is a tributary of Ulhas River in the Thane District of Konkan Region in Maharashtra (Fig. 3.2b). It originates near Harichandragad in Murbad Taluka of Thane District at an elevation of 1,200 m above mean sea level and extends between East Longitude 73° 36′ to 73° 49′ and North Latitude 19° 17′ to 19° 26′. The steep terrain watershed (area=224 sq. km) experiences an average annual rainfall of 2,450 mm. The watershed is covered with 50% thickly wooded forest, and 50% is the cultivable area. Existing crop pattern of the cultivation covers 46% of paddy, 16% of nanchani vari, 3% of pulses, and 35% of grass.

3.1.4 Narmada Watershed

River Narmada is one of the major rivers with 41 tributaries flowing through central parts of India. It rises from Amarkantak plateau of Maikala range in Shahdol district in Madhya Pradesh at an elevation of about 1,059 m above mean sea level. The river travels a distance of 1,312 km before it joins the Gulf of Cambay in the Arabian Sea near Bharuch in Gujarat. The streamflow data used in the study belong to River Narmada at Manot, Banjar at Hridaynagar, and Burhner at Mohegoan, as shown in Fig. 3.3 and described in brief as below.

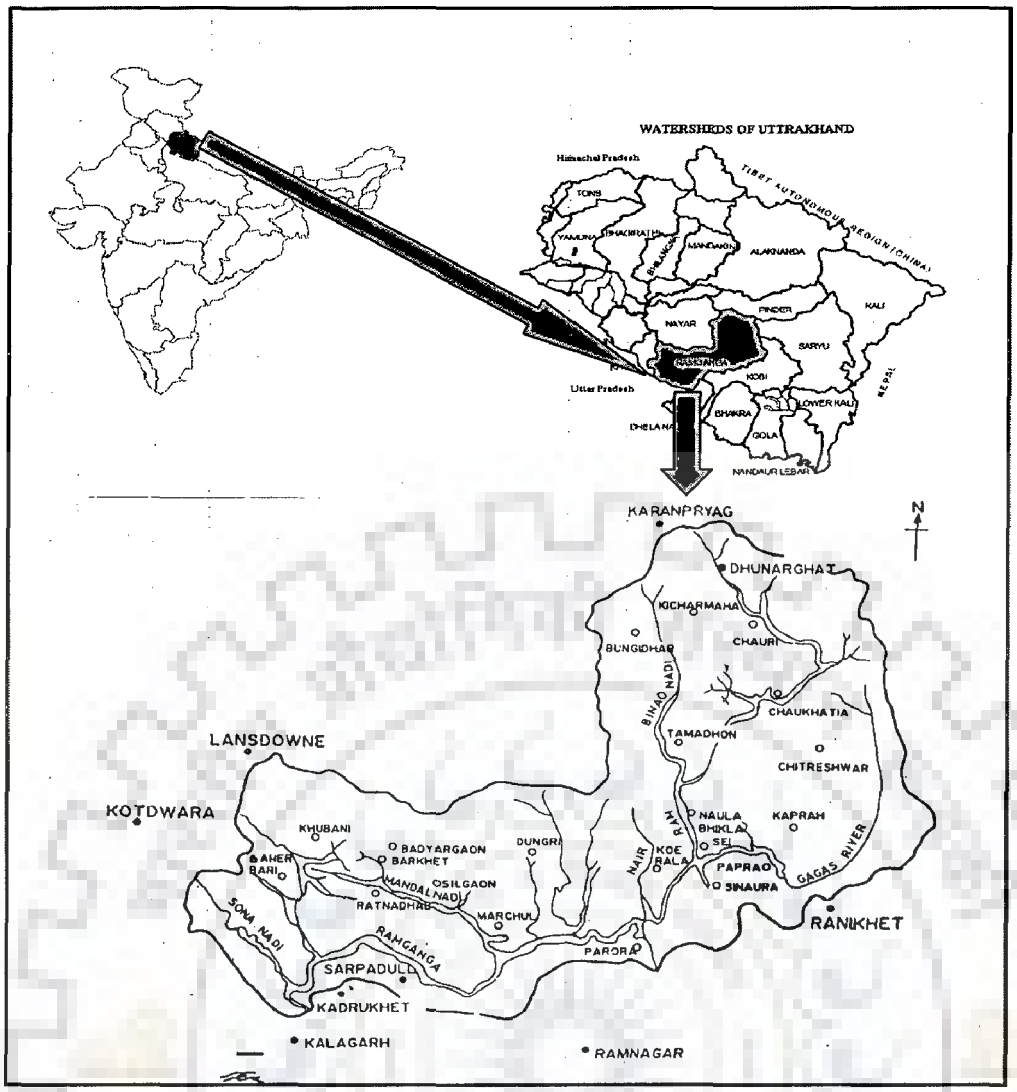

Fig. 3.1: Index map of Ramganga watershed showing the location and major drainage network of watershed.

(a) Narmada upto Manot

The Narmada catchment up to Manot lies between north latitudes 22° 26′ and 23° 18′ and east longitudes 80° 24′ and 81° 47′. The length of the river Narmada from its origin up to Manot is about 269 km with the drainage area of 5,032 sq. km. The watershed is covered by forest and its topography is hilly. Its elevation ranges from 450 m near Manot site to 1,110 m in the upper part of the watershed. It has continental type of climate classified as sub-tropical and sub-humid with average annual rainfall of 1,596 mm. It is very hot in summer and cold in winter. In the major part of the watershed, soils are red, yellow, and medium black with shallow to very shallow depth. In some small pockets of plain land, soils are moderately deep dark grayish clay. Approximately 52% of watershed area is under cultivation, about 35% under forest, and 13% under wasteland.

(b) Burhner up to Mohegaon

The Burhner river rises in the Maikala range, south–east of Gwara village in the Mandla district of Madhya Pradesh at an elevation of about 900 m at north latitude 22° 32′ and east longitude 81° 22′. It flows in westerly direction for a total length of 177 km to join the Narmada near Manot. The Burhner drains a total area of about 4,661 sq. km and its watershed area up to Mohegoan is about 4,103 sq km (Fig. 3.3). The elevation at Mohegoan gauging site drops to 509 m. Climate of the basin can be classified as sub-tropical and sub-humid with average annual rainfall of 1,547 mm. The catchment area comprises both flat and undulating lands covered with forest and cultivated lands. Soils are mainly red and yellow silty loam and silty clay loam. Forest and agricultural lands share nearly 58 and 42% of the watershed area, respectively.

(c) Banjar upto Hridaynagar

The Banjar river, a tributary of Narmada in its upper reaches, rises from the Satpura range in Durg district of Madhya Pradesh near Rampur village at an elevation of 600 m at north latitude 21° 42′ and east longitude 80° 50′. Its catchment area up to Hridaynagar is about 3,370 sq. km (Fig. 3.3) and the elevation drops from 600 to 372 m at Hridaynagar gauging site. Climate of the basin can be classified as sub-tropical sub-humid with average annual rainfall of 1,178 mm. About 90% of the annual rainfall is received during monsoon season (June–October). The area comprises of both flat and undulating lands covered with timber, grasses, and cultivated land. Soils vary from black to mixed red soils. Nearly 65% of the watershed area is covered with forest. Agricultural crops are grown in 29% area, and the remaining area comes under degraded lands and water bodies.

3.1.5 Ghodahado Watershed

Rushikulya is one of the major rivers in Orissa and originates from Rushamala hills of the eastern Ghats in Phullabani district (Fig. 3.4). It is 165 km long with 8900 sq. km of catchment area. Ghodahado is a tributary of Rushikulya in Ganjam district near Degapahandi block. It extends between east longitude 84° 27' to 84° 40' and north latitude 19° 17' to 19° 28'. The watershed having area of 138 sq. km experiences an average annual rainfall of 1,476 mm having mean maximum summer temperature of 37°C and 10.3°C in winter. Most of the rainfall occurs during June to October. The watershed is situated in the East and South Eastern coastal plain with hot and moist sub-humid climatic condition. The broad soil group of this area is red soils, has blocky structures of either

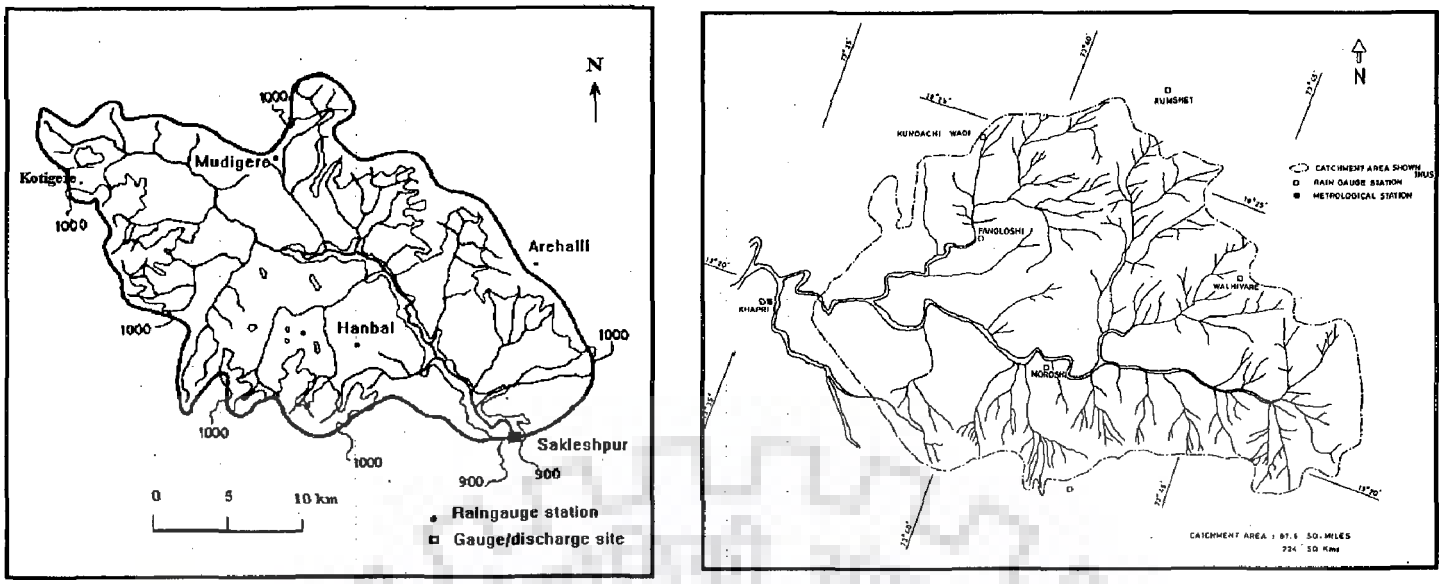

(a) (b)

Fig. 3.2: Watershed map of (a) Hemavati; and (b) Kalu

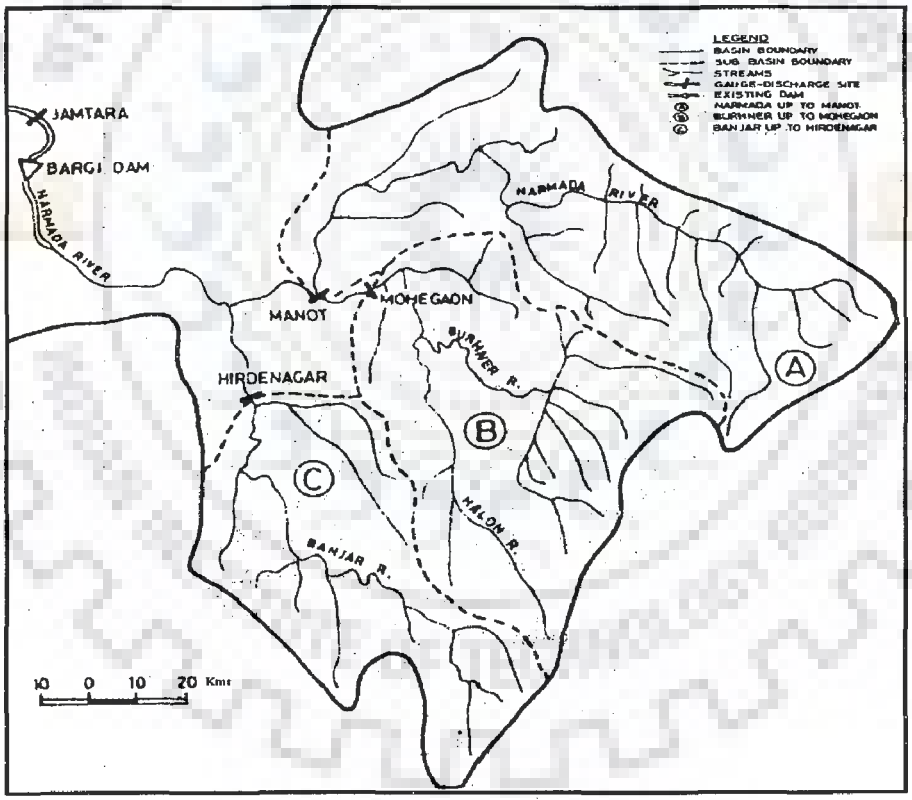

Fig. 3.3: Map of Narmada river basin upto (A) Manot; (B) Mohegaon; and (C) Hridaynagar.

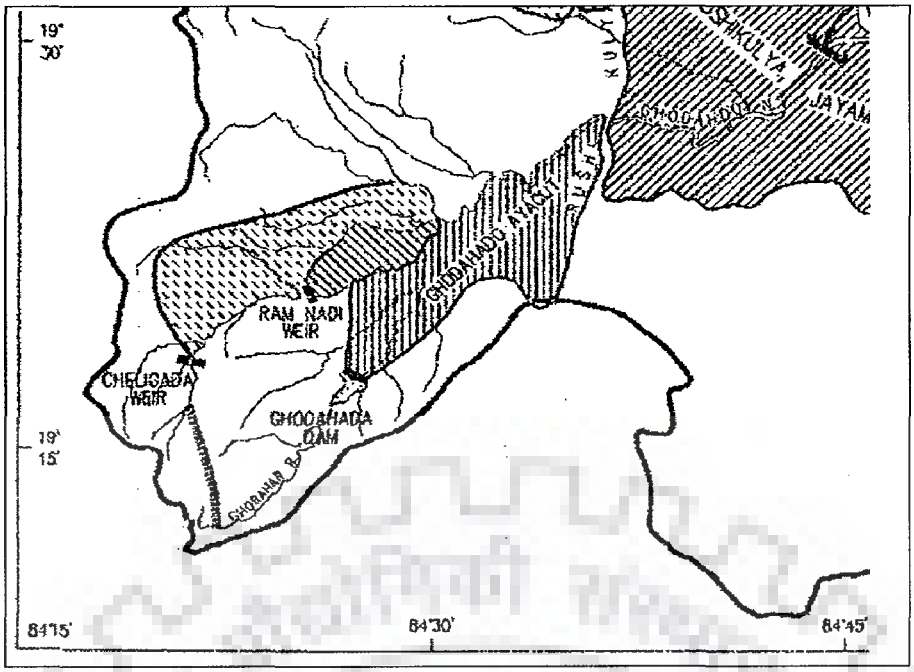

Fig. 3.4: Ghodahado watershed.

granular or sub granular geometry, and it is dominated by Kaolinites and illites. The land use pattern of the watershed is 40% of forest area, permanent pasture is 3%, culturable waste is about 2%, non-agril land use is 5% and 50% of area is under net sown area.

3.1.6 Data Availability

For Ramganga watershed, daily rainfall-runoff data from June 1978 to May 1993 were used for estimation of curve number. However, the corresponding duration meteorological data (minimum-maximum temperature, minimum-maximum relative humidity, wind velocity, and sun-shine hour) taken from Pantnagar observatory (latitude $29^0$1'55" N and longitude $79^0$28'25" E) near Kalagarh were used for estimation of PET. For Hemavati watershed, hydro-meteorological data of five years (June 1974 to May 1979) were used in the study. For Narmada basin, nine year rainfall-runoff data (June 1981 to May 1990) and corresponding meteorological data were taken at three different gauging sites, viz. Manot, Mohegaon, and Haridaynagar. For Kalu watershed, daily hydro-meterorlogical data of 4 years (1990-1993) were used. For Ghodahado, the data available for June 1987–May 1989 and June 1993–May 1996 were used in the study.

3.2 TIME-DISTRIBUTED EVENT DATA OF RAINFALL-RUNOFF

The time-distributed (event) data of rainfall-runoff of three Himalayan watersheds were used to check the suitability of the proposed synthetic unit hydrograph (SUH) method derived from probability distribution function and geomorphologic parameters.

Time-distributed data of rainfall-runoff were also used in the development of lag time based geomorphological instantaneous unit hydrograph (GIUH).

3.2.1 Gagas Watershed

The Gagas watershed is one of the sub-watersheds of the Ramganga catchment located in the Himalayan region of India having an area of 506 km^2 and lies between latitudes 29^0 35' 20" N and 29^0 51'N and longitudes 79^0 15'E and 79^0 35' 30"E as shown in Fig. 3.5. The catchment is approximately rectangular in shape with a minimum elevation of 772 m at the outlet e.g., Bhikiasen and a maximum of 2744 m above mean sea level at the upstream end of the catchment. The watershed area in general has a hilly terrain with undulating and irregular slopes ranging from relatively flat in narrow river valley to steep towards ridge. The mean annual rainfall varies from 903 mm to 1281 mm with a mean value of 1067 mm (Kumar and Kumar, 2008). The soils of the watershed are highly coarse textured, varying from coarse sand to gritty sandy loam, and slightly acidic to neutral in nature. The hydrologic data regarding runoff hydrograph, effective rainfall for six isolated storms were obtained from the Divisional Forest Office, Ranikhet, Uttarakhand.

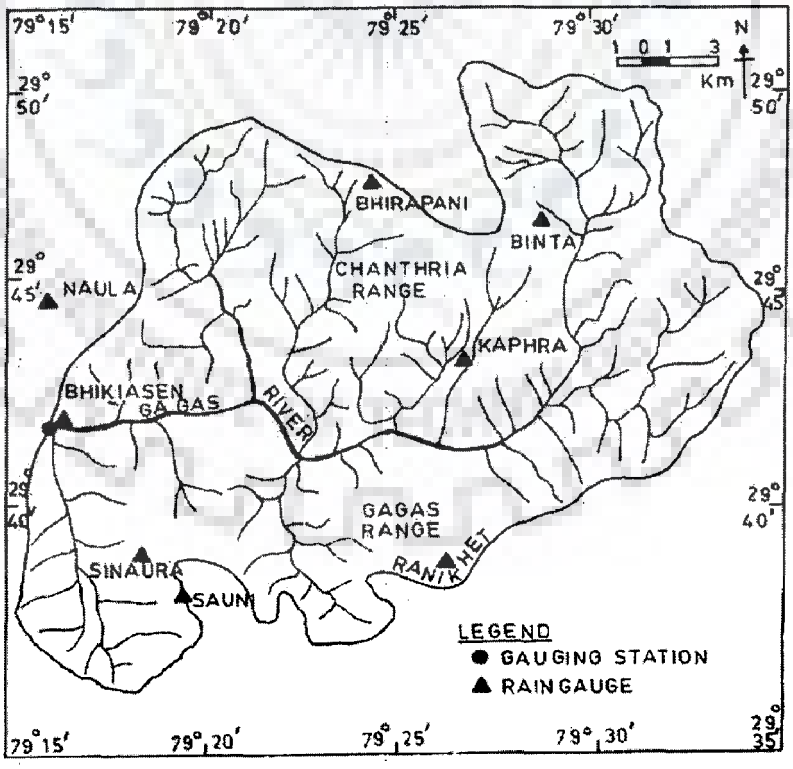

Fig 3.5: Gagas watershed.

3.2.2 Myantdu-Leska Watershed

The Myantdu-Leska River watershed (Fig. 3.6) in the Jaintia Hills, District of Meghalaya, in northeastern India, extends between 92°15′–92°30′E and 25°10′–25°17′N. It is the sixth order watershed comprised of about 350 km^2 area. The watershed area is 350 km^2 and elevation ranges from 565 m to 1372 m above mean sea level.

3.2.3 Chaukhutia Watershed

This watershed is the most upstream sub-watershed of Ramganga reservoir catchment (Fig. 3.7). Ramganga River is a tributary of Holy River Ganges. It originates from sub Himalayan region in the district of Chamoli. The Chaukhutia watershed is the upper watershed of Ramganga River comprising of an area of 572 sq. km. Geographically, the entire boundary of Chaukhutia watershed is situated between latitudes of 29°46'35" and 30°06'11" North and longitudes of 79°11'23" and 79°31'21"East. The variation in altitude influences the climate of the watershed. The climate of this watershed varies from sub-tropical in the lower region to sub-temperate and temperate in upper region with a mean annual temperature of 24.5°C and a mean minimum temperature of 17.3°C. Most of the rainfalls are received during July and August. Winter rainfall occurs during the month of December to February. The maximum and minimum elevations within this watershed are 3088 m and 939 m above mean sea level, respectively. This watershed consists mostly of rolling and undulating topography having very steep irregular slopes. The significant portion of total precipitation in the form of rainfall in the watershed occurs mainly during the four months of the monsoon i. e. from June to September with a mean annual total precipitation of 1388.7 mm. In fact, the monsoon contributes about 74% of the total annual rainfall. The entire hydro-meteorological characteristics of the watershed are characterized by the high precipitation generating peak monsoon flows and low precipitation during the dry season resulting in low flows.

3.2.4 Data Availability

For short term rainfall-runoff modelling, the storm runoff data of three Himalayan watersheds were used. The storm data of Gagas and Chaukhutia were obtained from the Divisional Forest Office, Ranikhet. Direct runoff hydrograph (DRH) characteristics of eight storms of Gagas and Chaukhutia are presented in Table 3.1. The Gagas data have

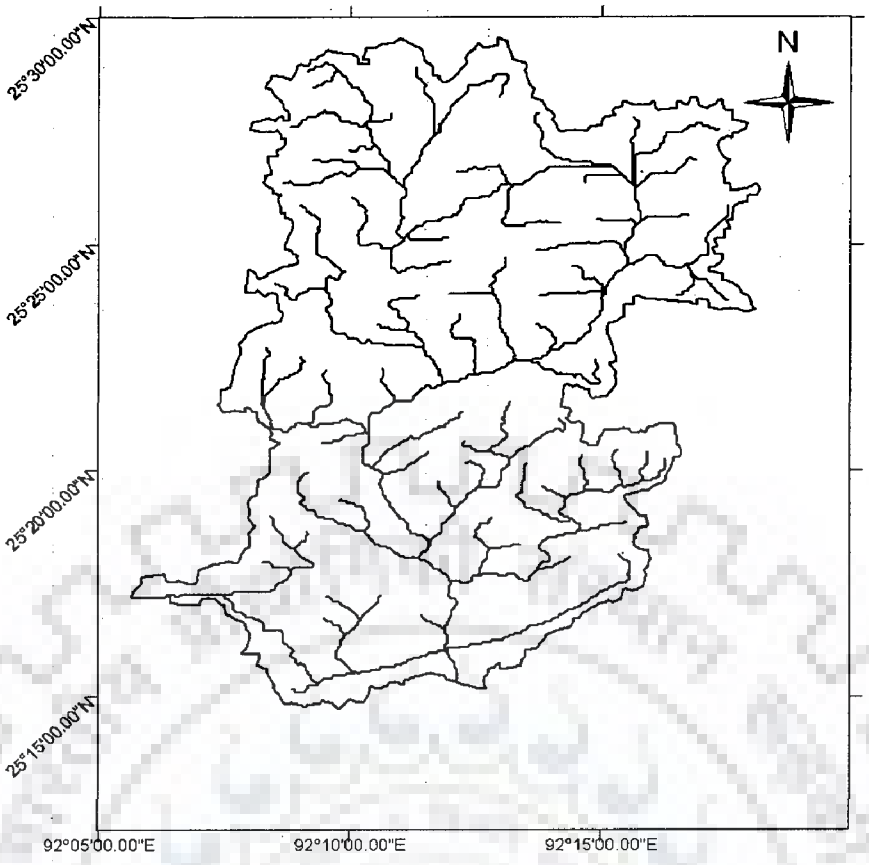

Fig. 3.6: Watershed and river network of Myantdu-Leska.

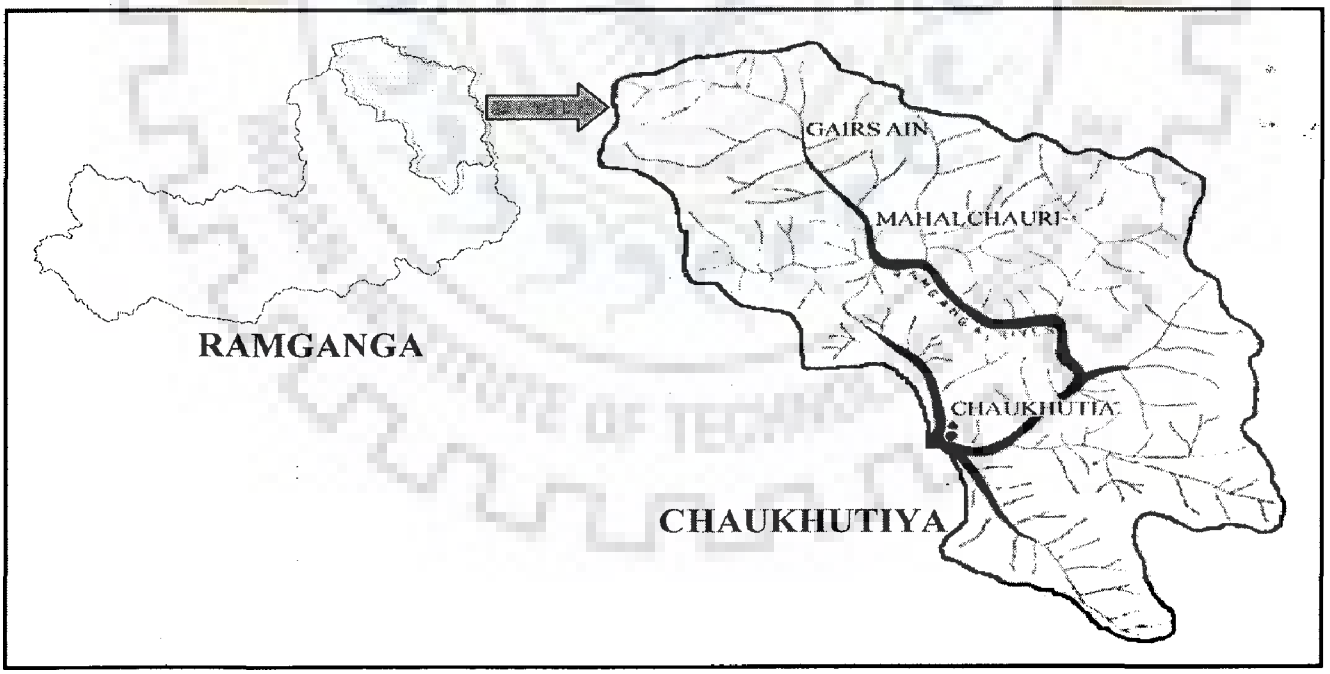

Fig. 3.7: Map showing the location of Chaukhutia in Ramganaga watershed, and drainage network of watershed.

already published by Kumar and Kumar (2008). However the data of Myantdu-Leska was taken from Bhuniya (2005) and used in the study. Length of maximum order stream of Myantdu-Leska watershed is 52 km, whereas Horton ratio, viz., area ratio (R_A), bifurcation ratio (R_B), length ratio (R_L) are 4.61, 4.27, 2.12, respectively. Peak discharge (q_p) of hydrograph is found to be 11.80 m^3/s whereas time to peak (t_p) is 5 hour. The velocity corresponding to peak discharge was calculated from the aforementioned method and was 3.29 m/s for the Myantdu-Leska watershed.

3.3 LONG-TERM RAINFALL-RUNOFF DATA

Three watersheds namely Naula, Chaukhutia, and Ramganga were used in modelling of long-term rainfall-runoff using Artificial Neural Network. The watersheds Chaukhutia and Ramganga have been described above. The hydro-meteorological data used in this study are described below.

3.3.1 Naula Watershed

Naula watershed is a sub-watershed of famous 127.5 meter height Ramganga reservoir catchment (3134 sq. km area) (Fig. 3.8). Ramganga reservoir, built in year 1974, produces approximately 452 million units of electricity annually and also facilitated irrigation for an additional area of about 5.12 lakh ha during non-monsoon period.

Table 3.1: Summary of Direct runoff Hydrographs (DRHs) of different storms from Gagas and Chaukhutia watershed.

Gagas watershed				Chaukhutia watershed			
Date of Storm	Rainfall Excess (cm/hr)	DRH characteristics		Date of Storm	Rainfall Excess (cm/hr)	DRH characteristics	
		Qp (m^3/s)	tp (h)			Qp (m^3/s)	tp (h)
4-Jun-77	0.208	109	2	23-Aug-76	0.116	55	2
25-Jun-78	0.257	122	2	21-Jun-79	0.146	72	2
20-Jun-81	0.136	72.3	2	31-Aug-80	0.213	102	2
31-Jul-82	0.111	59.2	2	2-Aug-81	0.264	124	2
11-Aug-83	0.127	70.3	2	23-Jul-82	0.165	80	2
30-Aug-84	0.168	80	2	5-Sep-83	0.188	85	2
10-Aug-85	0.178	85.5	2	25-Jun-84	0.219	106	2
15-Aug-85	0.169	86	2	22-23-Aug-84	0.484	226	2

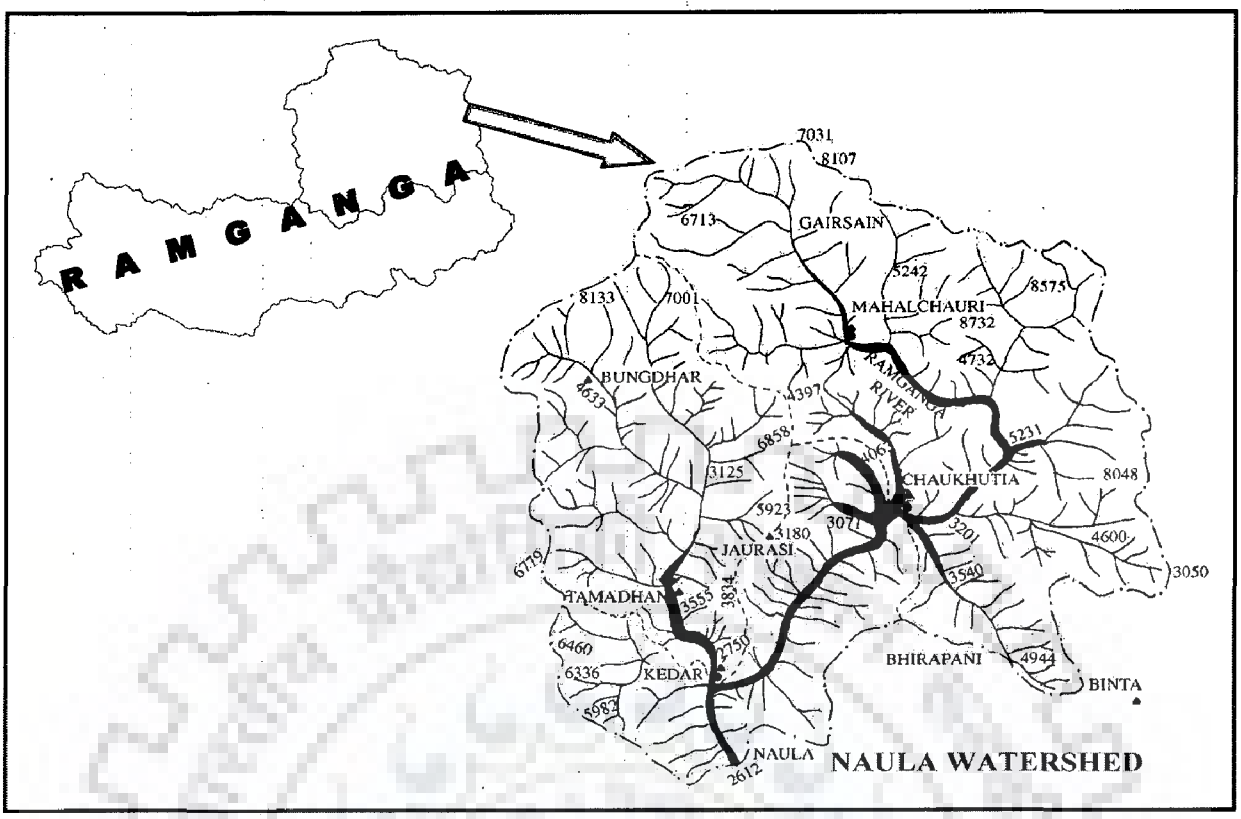

Fig. 3.8: Map showing the location of Naula in Ramganaga watershed and drainage network of watershed.

Notably, the study watershed comprises one third portion of Ramganga reservoir catchment, upper hilly portion of the catchment and hence it is a major sediment contributor in the reservoir among all the sub-catchments. The area of the Naula watershed is about 1084 km^2 which drains from north to south into the Bino tributary and the main Ramganga river. The Naula watershed is geographically located between 29°44'N and 30°6'20"N latitudes and 79°6'15"E and 79°31'15"E longitudes in the Ranikhet Forest Sub-Division of Ramganga river catchment. The topography of the watershed is undulating and irregular with slope varying from moderate to steep. The minimum and maximum elevations of the watershed are 790 m and 3088 m, respectively, above the mean sea level. The watershed is located in a Himalayan sub-tropical area and has a climate with a mean annual temperature of 30.3 °C and a mean minimum temperature of 18.3 °C. The precipitation in the watershed mainly occurs in the form of rainfall from the middle of June to the end of September, with a mean annual rainfall of 1015 mm. The soil of the watershed is acidic in nature with pH in between 5.0 to 6.5.

3.3.2 Data Availability

The hydro-meteorological data of Naula and Chaukhutia watersheds were collected from the Divisional Forest Office (Soil Conservation) Ranikhet, Government of Uttarakhand. However, the Ramganga data was collected from the Ramganga dam

authority at Kalagarh. The rainfall is measured in the units of mm/day, and runoff recorded in the unit of hectare-meter (ha-m). However, runoff data is converted into m^3/s and used for the development of Artificial Neural Network model.

Fourteen years daily rainfall-runoff data for monsoon season (June-September) vary from 1974 to 1987, 1974 to 1988 (except 1984), and 1979 to 1992 were collected for Chaukhutia, Naula, and Ramganga watershed, respectively. Year 1984 could not be included in case of Naula watershed due to non-availability of daily runoff of months June-July. Weighted rainfall for the study area was estimated using thiessen polygons. Six raingauge stations located at Gairsen, Mehalchauri, Vungidhar, Chaukhutia, Bhirapani, and Binta installed in/outside of Chaukhutia watershed were used to calculate the weighted rainfall of Chaukhutia watershed. For naula watershed, ten station data (Naula, Kedar, Tamadhanu, Jourasi, and six stations of Chaukhutia watershed) were used for estimation of weighted rainfall. However, in addition to Naula watershed raingauge stations, four more stations installed at Ranikhet, Bhikiasen, Marchulla, and Kalagrah station rainfall were used for estimation of weighted rainfall of Ramganaga watershed. With the help of weighted average rainfall and runoff, runoff coefficients were calculated for each year of monsoon period and reported in Tables 3.2, 3.3 and 3.4 for Chaukhutia, Naula, and Ramganga watersheds, respectively. It can be seen from Tables 3.2 and 3.3 that Naula and Chaukhutia are the high runoff producing watersheds whereas entire Ramganga is low runoff producing watershed. It is notable here that Chaukhutia and Naula are typical hilly watersheds and hence very sensitive to runoff and sediment production. The runoff coefficients vary from 0.49 to 0.75 for Naula (Table 3.2), 0.52 to 0.79 for Chaukhutia (Table 3.3), and 0.19 to 0.40 for Ramganga watershed (Table 3.4).

3.4 SEASONAL RAINFALL SEDIMENT YIELD DATA

For the development of distributed sediment yield model, rainfall and sediment yield data of Naula watershed was used. The details of Naula watershed have been discussed above.

3.4.1 Data Availability

The availability of rainfall for Naula watershed has been discussed above. Information on sediment yield rates (ha-m) was also collected from the Divisional Forest Office (Soil Conservation) Ranikhet, Government of Uttarakhand. In general, bed load contribution to the total sediment yield is usually small and hence suspended sediment yield can be considered as watershed sediment yield (Chow, 1964; Graf, 1971).

According to Kusre (1995), in the watersheds from similar geographical region, 75% to 80% sediment flow of the season is confined to only two monsoon months, July and August. Therefore, the direct sediment flow (i.e., mobilized sediment) during active period (i.e. most sediment producing ten weeks of the study area) of years 1979-1987 from Naula watershed was modeled. The rainfall and sediment yield data for year 1984 were not available. The data of Naula watershed was published by Pyasi and Singh (2004) on weekly basis. However, in the present study, it was aggregated on seasonal basis. The sediment yield at Chaukhutia, Mehalchauri, and Budakedar used in this study were published in the report Soil Conservation Scheme, River Valley Projects, Ramganga (UP), and Sullaj (HP) published by Ministry of Agriculture and Co-operation, New Delhi, 1991.

In the next chapter, an attempt has been made to develop a relationship between the evapotranspiration (ET), a major component of rainfall-runoff process, and curve number (CN), a single parameter of the most widely used Soil Conservation Service Curve Number (SCS-CN) methodology.

Table 3.2: Summary of rainfall-runoff data of Naula watershed

Year	1974	1975	1976	1977	1978	1979	1980	1981	1982	1983	1985	1986	1987	1988
Annual Rainfall (mm)	834.4	1105.4	1006.6	1145.6	1440.3	716.6	1098.0	603.3	959.2	1102.4	799.2	931.5	581.8	1052.3
Annual Runoff (m^3/s)	4859	7335	7329	10048	12562	5048	7425	4029	5931	7989	5755	8008	3346	6845
Runoff Coefficient	0.50	0.57	0.62	0.75	0.75	0.60	0.58	0.57	0.53	0.62	0.62	0.74	0.49	0.56

Table 3.3: Summary of rainfall-runoff data of Chaukhutia watershed

Year	1974	1975	1976	1977	1978	1979	1980	1981	1982	1983	1984	1985	1986	1987
Annual Rainfall (mm)	843.3	1068.5	1073.4	1295.0	1444.2	826.0	1329.5	680.5	1156.8	1302.4	1175.1	1009.7	1138.6	719.9
Annual Runoff (m^3/s)	2735	3682	3584	4044	5269	2396	4922	1836	3935	5038	4170	3147	4688	2004
Runoff Coefficient	0.62	0.66	0.64	0.60	0.70	0.55	0.71	0.52	0.65	0.74	0.68	0.60	0.79	0.53

Table 3.4: Summary of rainfall-runoff data of Ramganga watershed

Year	1979	1980	1981	1982	1983	1984	1985	1986	1987	1988	1989	1990	1991	1992
Annual Rainfall (mm)	781.3	1072.0	862.0	937.9	1111.4	1022.7	1182.7	1084.4	846.8	1385.8	1067.1	1425.6	942.5	1080.5
Annual Runoff (m^3/s)	9230	13749	10524	10211	13662	13146	13546	13215	5947	15691	10023	20514	9386	10427
Runoff Coefficient	0.33	0.35	0.34	0.30	0.34	0.35	0.32	0.34	0.19	0.31	0.26	0.40	0.27	0.27

CHAPTER 4
CN-BASED LONG-TERM PET ESTIMATION

4.1 INTRODUCTION

Thornthwaite (1948) first used the concept of PET and described it as the maximum rate of evapotranspiration (ET) from the large area covered completely and uniformly by vegetation growing with unlimited water supply. PET can be estimated using energy balance, mass transfer, combination of energy balance and mass transfer based empirical and semi-empirical approaches (Brutsaert, 1982; Allen et al. 1989; Jenson et al., 1990; Morton 1994; Xu and Singh, 2002). The combination approach (Penman, 1948) is however considered as the most physically satisfying approach (Jenson et al., 1990; Smith et al., 1991; Shuttleworth, 1993; Beven, 2001). Though the Penman-Monteith method has been recommended as the sole standard method by Food and Agricultural Oraganization (Allen et al., 1998), the Penman equation yields the most accurate estimates of evaporation from saturated surfaces, if model assumptions are met and adequate input data are available.

The Calder (1983) study showed that a simple evaporation formula requiring no direct meteorological measurements other than rainfall performed better than the more data demanding PET equations, such as those of Priestley-Taylor (1972), Penman (1948), and Thom-Oliver (1977), widely used for predicting soil-moisture deficit (SMD). SMD prediction improves with use of mean climatological PET (Andersson and Harding, 1991), perhaps due to a negative feedback mechanism between stomatal resistance and evaporative demand, not accounted for by the more sophisticated PET equations. The validity of mean monthly PET was investigated and supported by Fowler (2002) in long-term daily water balance studies. The substitution of mean PET estimates into daily water balance produced a soil water regime very similar to that derived using actual PET, particularly in relatively extreme periods. Using a large sample of 308 catchments of France, Australia, and the United States, Qudin et al. (2005) investigated the validity of 27 PET formulae in streamflow simulation and found that the observed daily PET data were not necessary as input to a rainfall-runoff model, rather a long- term regime (for example, annual) curve is sufficient. Therefore, many studies did not find any difference in the use of PET and mean PET (Burnash, 1995), even in extreme situations (Fowler, 2002).

The water balance method yields the best estimates of mean long-term evaporation from large (plain) river basin (Gidrometeoizdat, 1967). The estimation of ET using soil water balance method is however often limited due to inconvenience and inaccuracy in measurement of ground water inflow and outflow. Nevertheless, for the reasons of computational simplicity, stability, ease in understanding and grasping, the soil-water balance method is still frequently used in rainfall-runoff modeling. However, in PET estimation using remote sensing, an uncertainty of 20-30% in western riparian corridors of cottonwood has been reported (Nagler et al., 2005). According to Cleugh et al. (2007), the most sophisticated Penman-Monteith method using MODIS remote sensing data and surface meteorology as input yielded errors between 20 and 25%, attributed to inaccuracy in measurement of input parameters. It is worth noting here that the methods like Penman-Monteith are high data demanding and are also sensitive to data. Furthermore, the simple methods like Blaney-Criddle (1950) and Thornthwaite (1948) and Hargreaves (1982), employing only temperature data, are not very accurate especially under extreme climatic conditions. These methods underestimated (up to 60%) PET in windy, dry, and sunny areas, while in calm, humid, and cloudy areas, PET is overestimated (up to 40%). Brutsaert (1982) points out that "...in the case of evaporation besides sampling, there is also the problem of simply determining it at a point location." However, in many situations, a single meteorological station data represents the climate of a large catchment, a poor spatial representation. This problem is frequently encountered in PET calculation using formulae requiring large data input.

Thus, the usefulness of more data demanding complex methods in PET estimation appears to be questionable and it, in turn, invokes a need for development of simpler methods to derive mean PET representing the whole catchment and compatible with the available complex methods. In this paper, the proportionality concept of the popular SCS-CN method (SCS, 1971) is employed in the simple water balance equation to derive mean PET from the usually available long-term daily rainfall-runoff data and it forms one of the major objectives of this study.

4.2 DEVELOPMENT OF CN-PET RELATIONSHIP

4.2.1 SCS-CN Method

As described in chapter 2, the SCS-CN method (SCS, 1956) employs the water balance equation and two fundamental hypotheses. The resulting equation is given as:

$$Q = \frac{(P - I_a)^2}{P - I_a + S} = \frac{(P - \lambda S)^2}{P + (1 - \lambda)S} \quad (2.4)$$

Here, $P \geq I_a$, $Q = 0$ otherwise. This event-based SCS-CN methodology was developed for small ungauged agricultural watersheds. Ponce and Hawkins (1996) suggested the methodology to be suitable for areas less than 250 km^2. Eq. 2.4 however does not restrict its applicability based on watershed size. Its capabilities, limitations, uses, and its revisions are reported elsewhere (Chen, 1982; McCuen, 1982; Steenhuis et al., 1995; Ponce and Hawkins, 1996; Bonta, 1997; Yu, 1998; Mishra and Singh, 1999b, 2002a,b ,2003a,b, 2004a,b, 2006; Michel et al., 2005, and Singh et al., 2010). Williams and LaSeur (1976), Hawkins (1978), Soni and Mishra (1985), Mishra and Singh (2004b), Eldho et al. (2007), Geetha et al. (2008), Mishra et al. (2008) and several others have employed the SCS-CN methodology for long-term hydrologic simulation in catchments of a few thousand sq. kms.

4.2.2 Proposed SCS-CN Based PET Model

The estimation of PET utilizes the water balance equation (Eq. 2.1) and the proportionality hypothesis (Eq. 2.2) of the SCS-CN methodology. From the former, the maximum amount of moisture available in the form of (source) rainfall (P) can be lost only when the direct surface runoff (Q) is equal to zero. In other words, $P = I_a + S$. Here, the maximum infiltration losses F will equal S (in magnitude) which includes the initial moisture (Mishra and Singh, 2002). From Eq. 2.2, as $Q \rightarrow (P-I_a)$, $F \rightarrow S$. Since $I_a = 0.2S$, the maximum water loss = 1.2S. In terms of Antecedent Moisture Content (AMC), it is equal to $1.2S_I$, where the subscript I refers to AMC I (fully dry condition); or S_I corresponds to the capacity of the fully saturated store. Since, by definition, PET corresponds to unlimited amount of moisture supply to vegetation, as described above, the assumption in the proposed PET computation is that the rainfall (P) is always greater than or equal to $1.2S_I$ during the storm duration. Here, it is worth emphasizing that I_a accounts for all those initial water losses, such as interception, evaporation, surface detention, and infiltration, describable in terms of evaporation and not available for either plant use or runoff generation (Mishra and Singh, 2003a). The water that can transpire through vegetation during the storm duration can be equal to S_I, if the moisture is fully available. Thus, the sum of I_a and S for AMC I describes the potential amount of evapotranspiration that can occur in a watershed during the storm period. Thus, there

appears to be a relation existing between PET and S_I, which can be described in power form as follows:

$$PET = \alpha S_I^{\beta} \tag{4.1a}$$

Eq. 4.1a can be more generalized as

$$ET = \alpha S^{\beta} \tag{4.1b}$$

where α and β are the coefficient and exponent, respectively. Assuming α and β to be nonnegative, it can be seen from Eqs. 4.1b that as $S \rightarrow 0$, $ET \rightarrow 0$. Physically if the soil is completely impervious, moisture storage would be zero and therefore ET would be zero. On the other hand, if $S \rightarrow \infty$, $ET \rightarrow \infty$, since ET is largely governed by climatic conditions, it has an upper limit and so does S. Thus both the extreme conditions are reasonably described by Eq. 4.1. Since there exists an inverse relationship between S and CN (Eq. 2.6), Eq. 4.1 ($\beta > 0$) suggests ET to be high for the watersheds of low CN, and vice versa. The following text endeavors to support this logic.

4.2.3 ET-CN Rationale

(A) Mathematical treatment

The governing equations for the root-zone soil moisture W and evapotranspiration E (Mintz and Walker, 1993) are given as follows:

$$E_T + E_S = \beta_{T,S}\left(E^* - E_I\right) \tag{4.2a}$$

$$\beta_{T,S} = \frac{W}{W^*} \tag{4.2b}$$

$$E = E_I + E_T + E_S \tag{4.2c}$$

where E_T is the daily transpiration (moisture transferred from the soil to the atmosphere through the root-stem-leaf system of vegetation); E_S is the daily soil evaporation (moisture transferred from the soil to the atmosphere by hydraulic diffusion through the pores of the soil); E_I is the daily interception loss (water evaporated from the wet surface of the vegetation and wet surface of the soil) during rain storm; $\beta_{T,S}$ is the coefficient of transpiration plus soil evaporation, taken as a function of soil wetness; E^* is the daily potential evapotranspiration; W is the root-zone moisture at the end of the day; and W^* is the root-zone storage capacity.

From Eq. (4.2a) and Eq. (4.2c),

$$\beta_{T,S} = \frac{E - E_I}{E^* - E_I} \tag{4.3}$$

Coupling of Eq. (4.2b) and Eq. (4.3) leads to

$$\frac{E - E_I}{E^* - E_I} = \frac{W}{W^*} \tag{4.4}$$

The right hand term of Eq. (4.4) represents, by above definition, the ratio of F (= W) to S (= W^*). Thus, Eq. (4.4) states that, similar to the SCS-CN proportionality hypothesis (Eq. 2.2), the ratio of actual evapotranspiration to the potential evapotranspiration is equal to the ratio of actual infiltration (or moisture retention) to the potential maximum retention. A substitution of Eq. (2.2) into Eq. (4.4) yields

$$\frac{E - E_I}{E^* - E_I} = \frac{F}{S} = \frac{Q}{P - I_a} \tag{4.5}$$

Eq. (4.5) when further coupled with Eq. (2.4) yields the following

$$E = E_I + \frac{(P - I_a)(E^* - E_I)}{P - I_a + S} \tag{4.6}$$

Here, E_I, by definition, represents the daily interception loss (water evaporated from the wet surface of the vegetation and wet surface of the soil) during the rain storm. It is however a representation of the above described SCS-CN initial abstraction (I_a) that includes not only interception losses but also surface detention, initial infiltration, and evaporation. This is the water loss abstracted initially and not contributing to either direct runoff or infiltration. On the other hand, E_T and E_S are the water losses occurring during the whole period of rain storm. Thus, within the frame-work of SCS-CN terminology, E_I can be taken as to represent I_a. Therefore, Eq. (4.6) can be recast as:

$$E = I_a + \frac{(P - I_a)(E^* - I_a)}{P - I_a + S} \tag{4.7}$$

Here, Eqs. (4.6) & (4.7) hold for the condition $P > I_a$, a primary condition of the SCS-CN methodology. Taking $I_a = 0.2S$, it is thus possible to derive from Eq. (4.7) the actual evapotranspiration using known values of P, E*, and S (or CN). Eq. (4.7) also exhibits an implicit relationship between E and I_a and, in turn, CN via Eqs. (2.3) & (2.6). Proposed Eqs. (4.1a) & (4.1b) are the versatile form of a non-linear relationship. Further, when E =

P, an analogy between the above described $P = I_a + S$ relation and Eq. (4.2c) (with $E_I = I_a$) yields S to be analogous to $E_T + E_S$, frequently used in long-term simulation, suggesting a link between S (or CN) and ET.

(B) Physical Description

To show the existence of a relationship between CN and ET, it is in order to consider all the factors governing CN and evaluate the impact of their variation on ET (Table 4.1). Here, it is worth emphasizing that, since PET represents the maximum rate at which water is transferred to atmosphere, all the factors responsible to ET also affect PET of a watershed.

(a) Land use

Landuse characterizes the uppermost surface of the soil system and has a definite bearing on infiltration and ET. It describes the watershed cover and includes every kind of vegetation, litter and mulch, and fallow as well as nonagricultural uses, such as water surfaces, roads, roofs, etc. SCS (1956) broadly classified the land use into three categories, urban, agricultural, and woods & forest.

i). Urban Lands

Urban lands are relatively impervious in nature. These include residential, paved parking lots, streets, roads, commercial and industrial areas etc. Larger the impervious area, lesser will be transpiration and opportunity time for evaporation, and hence, lesser will be evapotranspiration and, in turn, larger will be the direct runoff or CN. Therefore, curve number increases and ET decreases with increasing relative imperviousness of the area.

ii). Agricultural land

Agricultural lands can be classified as cultivated and uncultivated lands. Cultivated land comprises fallow, row crops, small grain crops, close seeded legumes or rotation meadow, whereas uncultivated refers to pasture or range, and meadow. Cultivated lands are employed by different tillage and intercropping operations in different times of the year. Tillage generally destroys soil structure and breaks down the capillaries. Consequently, tilled layer dries out quickly, and retards liquid movement of water from the underlying untilled layer (Hillel, 1982), and in turn, significant reduction in ET. However, in uncultivated land like pastures and meadows, capillaries are well developed and water continuously transfers from root zone to atmosphere. NEH-4 table

(SCS, 1956) also describes cultivated lands to exhibit higher CN values than uncultivated lands do, supporting ET to be high in low CN watersheds.

However, a significant variation in ET and CN values can be seen among species, growth stage, canopy cover, and plant height of the crops/vegetation. Evapotranspiration from any crop/vegetation surface depends on the surface and aerodynamic resistance of specific crop/vegetation. Surface resistance depends on active leaf area index (LAI_{active}) and stomatal resistance of the leaf. LAI_{active} is an index of leaf area that actively contributes to transfer of surface heat and vapour. Since biological processes are carried out by the leaves, LAI is fully responsible for energy, water, and gas exchange between the soil/plant to the atmosphere. Normally, LAI increases with growing period and it reaches maximum before harvesting or at flowering (Allen et al, 1998). LAI varies greatly among species and within species due to differences in site, age, stand composition, density, and season (Chang, 2005). Species growing in cool and arid climates usually have small LAI and reach maximum LAI at later stage than those growing in warm and wet environments. Since surface resistance and LAI are inversely related, all the factors governing LAI affect surface resistance, and hence, ET.

Auerswald and Haider (1996) determined CN-values for different ground covers, stages of crop growth and seasons by conducting experiments in 70 small plots at 8 sites for different small grain crops in Germany. The measured CN values ranged from 45 to 99 for AMC II. Between seedbed preparation and harvest, CN values decreased with increasing percentage of ground cover and this was described by relationship CN = 87 – 0.49 x Cover. The existing SCS-CN methodology expressed ground cover by only three different CN values corresponding to three hydrologic conditions, poor, fair, and good. CN, however, changes gradually with ground cover. Seasonal values of CN varied from 44 (July) to 86 (October) for wheat, from 44 (July) to 86 (September) for Barley, from 41 (July) to 86 (October) for Rye, and 39 (July) to 81 (September) for average cover development. It is worth noting here that July is considered as the driest month of the year in Germany. The study reveals that like ET, CN also gets affected by ground cover, crop growth stage, plant height, and type of crop. Furthermore, SCS (1972) reported a CN of 83 and 84 for small grain at AMC II and the hydrologic soil group C for good and poor hydrologic conditions, respectively. Thus, there exists a need to derive CN values for different crops, species, growth stage, and seasons.

Normally, aerodynamic resistance depends on plant height. It decreases with increasing plant height, and therefore, the aerodynamic resistance for short crops, such as

grass is larger than that for taller vegetation like forest (Shuttleworth, 1993). It means that taller vegetation (generally woods and forests) are accomplished with higher evapotranspiration values than low growing grasses or brush. According to NEH-4 table, CN values for woods and forest lands are less than those for pasture, grassland or range, and herbaceous (mixture of grass, weeds and low growing brush).

iii). Wood and Forest

Similar to cultivated land, the evapotranspiration from forest is more pronounced by transpiration from the vegetative surface. Since forest comprises greater LAI, taller plant and soils are rich in organic matters, ET from forest is more than the cultivated/agricultural field. LAI for forest stand can be 5 – 50 times greater than the ground area covered by the forest canopies. Chang et al. (1983) studied the depletion rate of soil water (or evapotranspiration) for six forest conditions based on forest coverage on the wood-tell soil by season and depths. The values indicated that depletion rate of soil water (or evapotranspiration) increases with increasing forest coverage. It takes about 35 days for the undisturbed forest, but 62 days for the cultivated plot to deplete initial soil moisture content of 0.45 g cm^{-3} in the 30 cm surface profile to 0.20 g cm^{-3} during growing season. Furthermore, SCS (1985) has briefly described the forest hydrologic condition on the scale of 1 to 6; the forest coverage decreases from 6 to 1 and runoff potential (or CN) increases from 6 to 1. It shows that ET decreases with decreasing forest coverage (6 to1), and vice versa.

(b) Soil Type

Evaporation from soil depends on atmospheric evaporative power and supply of water to the evaporating surface (Hillel, 1971). Supply of water depends on the water retention and transmission properties namely porosity and hydraulic conductivity of the soil, respectively. The finely structured clay soil has a higher water retention capacity owing to higher porosity, but sandy soil will release more water from its large pores due to small or moderate soil water tension (Shaw, 1988). Clay soil pores exhibit higher suction in comparison to most contrasting sandy soil for same water content (Hillel, 1980). Therefore, it would be easier to extract water (for evaporation) from sandy soil compared to clay. SCS (1956) classifies soils as hydrologic soil groups (HSG) A, B, C, and D based on minimum infiltration and transmission capacity. Group A refers to sandy soils (lowest CN), D to clayey soils (highest CN), and the others lie in between. Consequently, the CN value increases from sandy (soil group A) to clayey (soil group D)

while evaporation (or evapotranspiration) decrease from sandy (soil group A) to clayey (soil group D).

(c) Initial abstraction

The term initial abstraction I_a in the SCS-CN methodology consists of interception, surface detention, evaporation, and infiltration (before the time to ponding after which runoff begins). The water that contributes to interception and surface detention and storage is evaporated back to the atmosphere and contributes neither to runoff nor to infiltration. The infiltrated water before the time to ponding may be interpreted as to have satisfied the atmospheric demand of water absorption (molecular adsorption in particular) of the soil, air column, similar to evaporation. Therefore, the water held by interception, surface detention, and infiltration at the beginning of a storm finally goes back to atmosphere through evapotranspiration. Thus, I_a depends on ET. As I_a increases, direct runoff Q decreases or, in turn, S increases or CN decreases. Thus, ET and CN are inversely related.

(d) Hydrologic condition

The hydrologic condition of an agricultural watershed is defined in terms of grass cover. Three types of hydrologic conditions are prevailed in the NEH table i.e. larger grass cover as good, fair for average cover, and poor for lesser acreage of grass cover. The larger the area of grass cover in a watershed, the lesser will be the runoff potential of the watershed and more will be infiltration. Therefore, the curve number will be highest for poor, average for fair, and the lowest for good condition. However, it is well understood that ET will be high for good or complete grass cover due to high transpiration rate. Furthermore, heavy grazing in dry soil reduces the infiltration rates due to compaction of the soil by hooves, which turns in high value of CN. ET from such a compacted soil will be low due to ceasing of top soil pores and absence of good vegetation. Therefore, it can be concluded that good hydrologic condition accompanies low value of CN, and high ET value, and vice-versa.

(e) Agricultural Management practices

Agricultural management systems involve different types of tillage, vegetation and surface cover. Brakensiek and Rawls (1988) reported that ploughing increases soil porosity and, in turn, increases infiltration rates over non-tilled soil. Rawls and Brakensiek (1983) found that an increase in organic matter in the soil lowers bulk density or increases porosity, and hence, increases infiltration and, in turn, decreases the runoff

potential or curve number. However, soil is loosened and exposed more after tillage operation which, in turns, leads to more evaporation losses. Therefore, now days, no tillage or minimum tillage is preferable to conserve the soil moisture.

(f) Rainfall Intensity

A greater intensity rainfall will render lesser time for rain water to stay over the land surface, leading to a lesser amount of infiltration, and consequently, a greater amount of direct runoff. The reverse will also hold. In reality, a high intensity rainfall or raindrop breaks down the soil structure to make soil fines move into the soil surface or near surface pores, leading to the formation of crust that impedes infiltration and thus increases CN. However, on the other hand, larger the rainfall intensity, evaporation will be lower due to lesser opportunity time available for evaporation, and vice versa.

(g) Antecedent Moisture Conditions (AMC)

ET is more pronounced in growing season than it is in dormant season (SCS, 1956). According to AMC criteria, CN is low in growing season than in dormant season for the same antecedent moisture, supporting the existence of an inverse ET-CN relationship. It is worth emphasizing here that the concept of soil-moisture-index (SMI) is generally used to identify the AMC condition in long-term hydrologic simulation. This concept incorporates climatic factors such as daily temperature, solar radiation etc., and thus, the SCS-CN method also accounts for the climatic factors.

(h) Salt concentration

Use of contaminated water to irrigation or other purposes forms the salt crust at the surface of soil which alters the evaporation and infiltration characteristics of the soil. Fujimaki et al. (2006) found considerable reduction of evaporation with time from a bare saline soil under constant meteorological conditions. The decrease in osmotic potential was not the only one factor responsible for reduction in evaporation since the soil surface was kept wet during the experiment, and therefore, suggested to include one more resistance to water vapor diffusion caused by salt crust in bulk transfer equation. The salt however affects soil structure and clogs the soil pores resulting in reduction of hydraulic conductivity and, in turn, infiltration. Alternatively, CN increases and ET reduces with increase in salt content.

Overall, the variation of CN and ET with respect to the CN governing factors is summarized in Table 4.1.

Table 4.1: Dependence of ET on the factors governing CN

Factor	Variation in CN	Variation in ET
Land use		
(a) Urban	CN increases as imperviousness /urbanization increases.	ET reduces as imperviousness increases, and vice versa.
(b) Agricultural	Cultivated land exhibits lower CN than does uncultivated land.	Cultivated lands are more susceptible to evapotranspiration than uncultivated lands.
	CN decreases with increasing ground cover or leaf area index (LAI).	LAI increases in growing season till the time of flowering. Since LAI and surface resistance are inversely proportional, ET increases with increasing ground covers.
(c) Wood and Forest	Increase in forest cover decreases the runoff potential, and, in turn decreases CN.	ET increases with increasing forest cover (Chang et al. 1983).
	From NEH-4 table, CN values for woods and forest lands are less than those for pasture, grassland or range, and herbaceous (mixture of grass, weeds and low growing brush).	Since aerodynamic resistance decreases with increasing plant height, taller vegetation (generally woods and forests) yields higher ET than low growing grasses or brush (Shuttleworth, 1993).
Soil type	CN value increases from sandy (soil group A) to clayey (soil group D).	Evaporation (or ET) decreases from sandy (soil group A) to clayey (soil group D) soils due to decreasing hydraulic conductivity (Shaw, 1988).
Management practices	All management practices aims to in- crease in-situ moisture or infiltration, and in turn, reduces the runoff potential and CN	All management practices support more ET due to availability of more moisture.
Hydrologic Condition	The larger the grass covers, the lower the CN, and vice versa.	The larger the grass covers, the larger the ET, and vice versa.
AMC	CN increases from AMC I (dry) to AMC III (wet)	ET also increases from AMC I (dry) to AMC III (wet) due to more soil moisture available in AMC III condition.
Initial abstraction (I_a)	As I_a increases, direct runoff Q decreases or, in turn, CN decreases.	In long-term simulation, the greater the I_a, the more the evapotranspiration, and vice versa.
Rainfall intensity	The larger the rainfall intensity, the larger the CN, and vice versa.	The larger the rainfall intensity, the lower the evaporation, and vice versa, due to lesser opportunity time available for evaporation.
Salt concentration	Salt reduces the hydraulic conductivity and, in turn, infiltration and thus CN increases.	Evaporation reduces considerably from a bare saline soil under given meteorological conditions due to inclusion of one more resistance caused by salt crust (Fujimaki et al. 2006)

4.2.4 PET Estimation Methods

Nine commonly used potential evapotranspiration methods ranging from relatively simple temperature-based equations to complex physically based combinations approaches were used for PET estimation. According to the input parameters, PET methods used in this study can be categorized into (i) empirical equation based on temperature (Hargreaves, 1985); (ii) empirical equations based on solar radiation (Turc, 1961; Priestley–Taylor, 1972); and (iii) combination methods (Penman, 1963; Busignrer-van-Bavel, 1966; FAO-24 Penman corrected 1977; FAO PPP-17 Penman, 1979; Kimberly-Penman, 1982; FAO-56 Penman-Monteith, 1998). The Priestley-Taylor and the Hargreaves-Samani (named as Hargreaves) methods, developed for 10-day PET, have been widely used in daily estimation (Jenson et al., 1990; Parmele and McGuinness, 1974; Hargreeaves and Samani, 1985). It is worth emphasizing here that only grass reference evapotranspiration estimated from different methods is being used as PET.

In this study, the watershed characteristics including its location (latitude, longitude) and elevation and hydrometeorology records, viz., daily maximum temperature (T_{max}), daily minimum temperature (T_{min}), daily maximum relative humidity (RH_{max}), daily minimum relative humidity (RH_{min}), wind daily speed (U), and sunshine hours (Ssh) were used. Here, the symbols originally used in description of the PET methods are retained in this study. For the sack of completeness, different PET methods used in this study are described below.

(a) FAO-56 Penman-Monteith (Allen et al., 1998)

Penman-Monteith method describes PET as follows:

$$PET = \frac{0.408\Delta(R_n - G) + \gamma \frac{900}{(T_{mean} + 273)} u_2 (e_s - e_a)}{\Delta + \gamma(1 + 0.34u_2)} \quad (4.8)$$

where Δ = slope of saturation vapour curve at mean air temperature (kPa $^0C^{-1}$), R_n = net radiation ($MJm^{-2}day^{-1}$), G = soil heat flux density ($MJm^{-2}day^{-1}$), γ = psychometric constant (kPa $^0C^{-1}$), T_{mean} = mean daily air temperature computed as the average of maximum and minimum temperatures (^0C), u_2 = average wind speed at 2 m height (m/s), e_s = saturation vapour pressure (kPa), and e_a = actual vapour pressure (kPa).

(b) Hargreaves (Hargreaves and Samani, 1985)

PET is determined as:

$$PET = 0.0023 R_A \sqrt{TD}\,(T_{mean} + 17.8) \quad (4.9)$$

where TD = difference between mean daily maximum and mean daily minimum temperatures (^{0}C) and R_A = extraterrestrial solar radiation (MJ m^{-2} day^{-1})

(c) Kimberley-Penman (Wright, 1982) PET is estimated as:

$$PET = \frac{1}{\lambda}\frac{\Delta}{(\Delta+\gamma)}(R_n - G) + \frac{1}{\lambda}\frac{\gamma}{(\Delta+\gamma)} 6.43 W_f (e_s - e_a) \quad (4.10)$$

where λ = latent heat of vaporization (2.45 MJ kg^{-1}), and W_f = wind function.

(d) FAO PPP-17 Penman (Frere and Popov, 1979)

PET is derived as:

$$PET = \frac{\frac{p_0}{p}\frac{\Delta}{\gamma} R_n + 0.26(e_s - e_a)(1 + 0.54u_2)}{\frac{p_0}{p}\frac{\Delta}{\gamma} + 1} \quad (4.11)$$

where p_0 and p are sea level and site surface pressure, respectively.

(e) FAO-24 corrected (c=1) Penman (Doorenbos and Pruitt, 1977)

This method estimates PET as:

$$PET = c\left[\frac{\Delta}{\Delta+\gamma}(R_n - G) + \frac{\gamma}{\Delta+\gamma} 2.7 W_f (e_s - e_a)\right] \quad (4.12)$$

where c = adjustment factor for FAO-24 penman method.

(f) Priestley-Taylor (Priestley and Taylor, 1972)

PET equation follows:

$$PET = \frac{\alpha}{\lambda}\frac{\Delta}{(\Delta+\gamma)}(R_n - G) \quad (4.13)$$

where α = constant (generally 1.26, but varies with vegetation type, soil moisture condition, and strength of advection.

(g) Businger van-Bevel (van Beval, 1966)

This method estimates PET as:

$$PET = \frac{\Delta}{\Delta+\gamma}(R_n - G) + \frac{\Delta}{\Delta+\gamma}\frac{0.622\lambda\rho k^2}{P}\frac{u_z}{[\ln(Z-d)/z_0]^2}(e_s - e_a) \quad (4.14)$$

where ρ = air density, k = von Karman's constant, u_z = wind speed at the height of Z cm (Km/day), generally taken as 200 cm, P = atmospheric pressure (mb), z_0 = roughness length estimated from reference grass height.

(h) Penman 1963 (Penman, 1963)

The Penman equation is expressed as:

$$PET = 0.8\left[0.408\frac{\Delta}{\Delta+\gamma}R_n + 7.5\frac{\gamma}{\Delta+\gamma}E_a\right] \quad (4.15)$$

where E_a is aerodynamic term (mm day^{-1}):

$$E_a = 0.35(1+0.00438u_2)(e_s - e_a) \quad (4.16)$$

(i) Turc method (Turc, 1961)

It estimates PET for two conditions as follows:

$$PET = 0.013\frac{T_{mean}}{(T_{mean}+15)}(R_S' + 50) \text{ if RH>50\%} \quad (4.17)$$

$$PET = 0.013\frac{T_{mean}}{(T_{mean}+15)}(R_S' + 50)\left(1+\frac{(50-RH_{mean})}{70}\right) \text{ if RH <50\%} \quad (4.18)$$

where R_S' = solar radiation (cal cm^{-2} day^{-1}) and RH_{mean} = average relative humidity (%).

4.2.5 Derivation of Curve Numbers

In the present study, following Mishra et al. (2008) procedure, curve numbers were derived from Eqs. (2.5) and (2.6) utilizing the available long-term daily rainfall-runoff data, covering a wide range of variation in rainfall/runoff and catchment characteristics, geography, and climatic change with time. Thus, the three levels of antecedent moisture condition (AMC) are not limited by the seasonal rainfall and, due to use of observed field data, the derived curve number values represent the actual watershed conditions not covered in the NEH-4 table.

Here, it is assumed that the available daily rainfall-runoff data of all seven catchments meet the requirements of Eq. (2.4), implying that the rainfall of duration greater than or equal to the time of concentration (T_c) of the respective watershed contributes fully to the surface runoff at its outlet. Since the SCS-CN method ignores the base flow contribution, making the runoff factor C (=Q/P) even greater than 1, only those daily (or any other duration) rainfall-runoff events were considered for the derivation of curve numbers which yielded runoff coefficient less than or equal to 1 ($C \leq 1$). The data point can be bounded by two upper and lower envelope curves which are taken to correspond to wet (AMC III) and dry (AMC I) conditions, respectively. Fig. 4.1 represents the upper and lower envelopes corresponding to CN = 98 and CN = 62 (1-day duration), respectively, for Hemavati catchmneht. The best fit, which falls in the middle of the two upper and lower envelopes, represents the average AMC of the watershed, taken as to correspond to

AMC II, for which CN = 88. Employing this procedure, curve numbers were derived for different rain durations using the rainfall-runoff data summed/averaged for the desired duration. Fig. 4.2 represents the variation of curve number with rain duration, for example, for the Hemavati watershed. Curve numbers variation with rain durations for rest of six watersheds are presented in Appendix A (Figs. A1&A2).

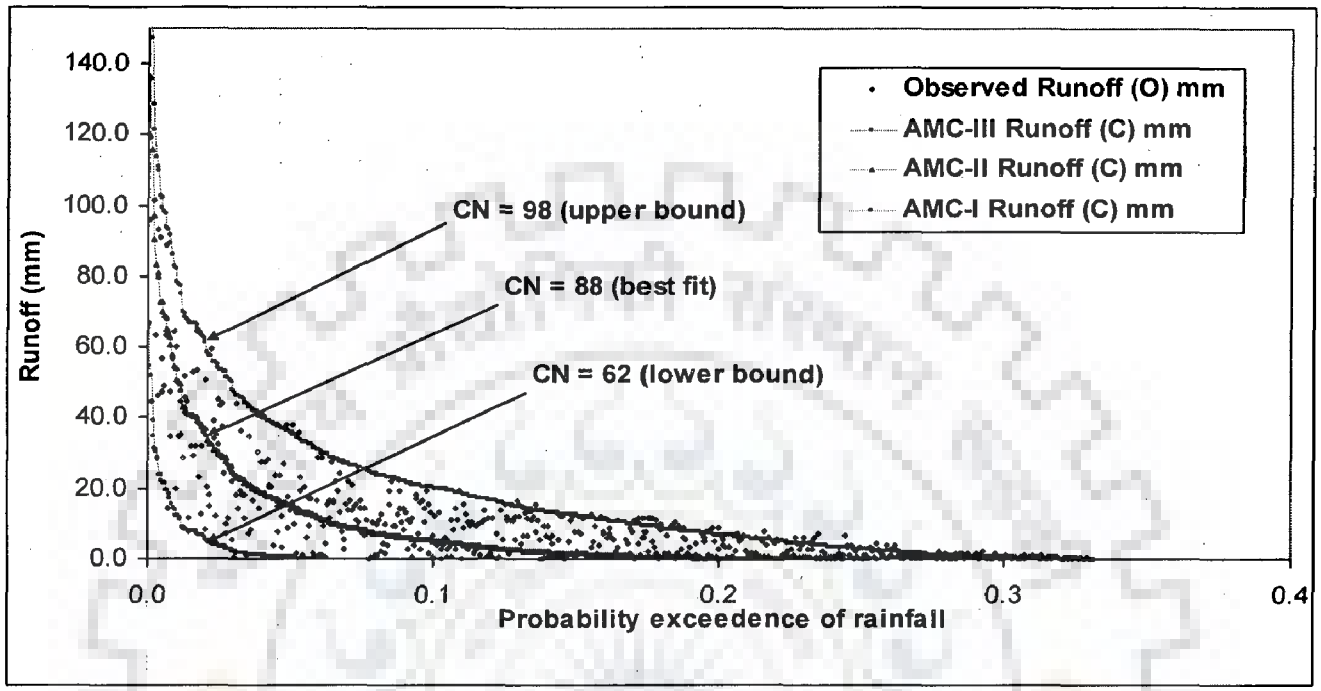

Fig. 4.1: Ordered daily runoff data of Hemavati watershed for determination of CN for three AMCs. Upper and lower bound curve numbers refer to AMC III and AMC I, respectively; and best-ft to AMC II. Runoff (O) & Runoff (C) refers to observed and computed runoff, respectively.

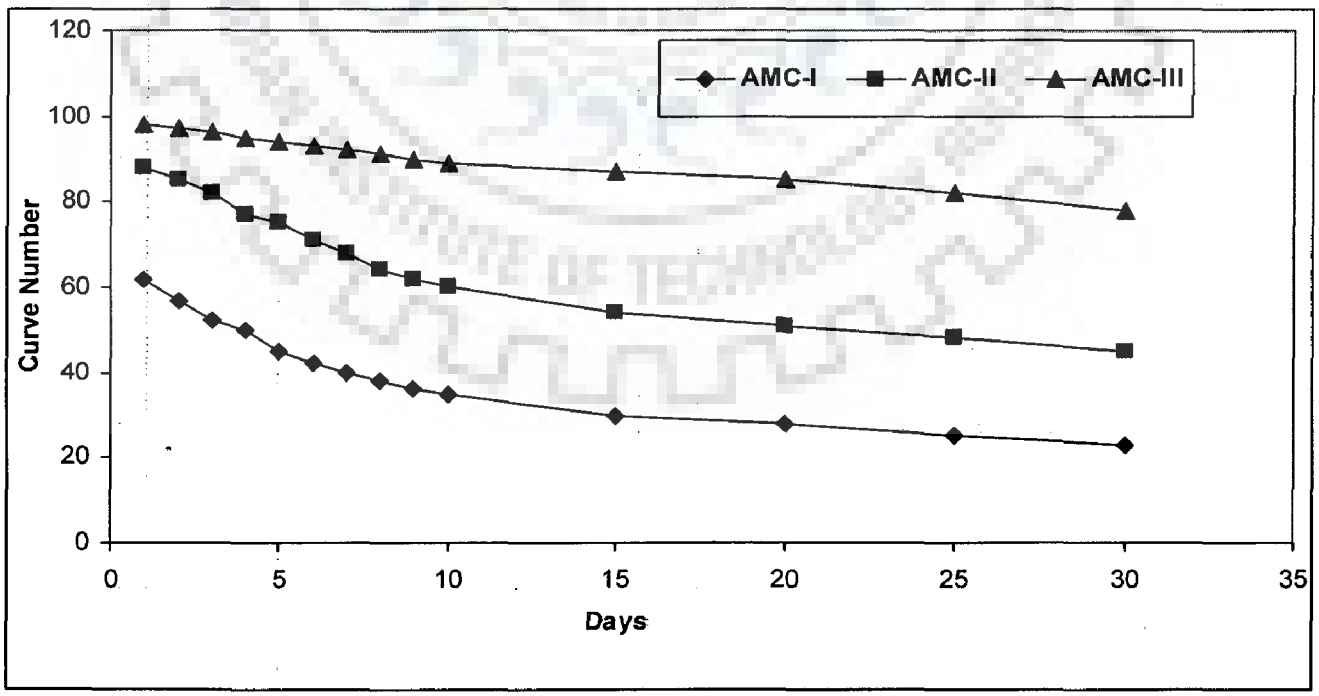

Fig. 4.2: CN Variation with rainfall duration (> 1 day) for Hemavati watershed.

4.3 FIELD VERIFICATION

The above proposed concept is applied to seven watersheds (Chapter 3) falling under different climatic and geographic settings of India. Daily hydro-meteorological data of study watersheds, Hemavati (Mishra and Singh, 2004b) (Fig. 3.2a), a tributary of River Cauvery in Karnataka State, Manot, Hridaynagar, and Mohegaon catchments (Geetha et al., 2008) (Fig. 3.3), tributaries of River Narmada in Madhya Pradesh, Kalu catchment (Geetha et al., 2008) (Fig. 3.2b), a tributary of River Ulhas in Maharashtra, Ghodahado catchment (Jain et al., 2007) (Fig. 3.4), a tributary of Rushikulya river in Orissa, and Ramganga catchment (Mishra and Singh, 2003a) (Fig. 3.1), a tributary of Ganga river in Uttarakhand State of India, were used in this study. However, different characteristics of the study watersheds are compared in Table 4.2. This table indicates that a wide range of catchments varying from an area of 124 sq. km (Ghodahado) to 5032 sq. km (Manot), and flat terrain (altitude ranges 372 m to 600 m from msl for Hridaynagar) to severely undulating (altitude ranges from 338 m to 3088 m from msl for Ramganga) were used to verify the proposed concept. It can be seen from Table 4.2 that most of the watersheds are forest and agriculture dominated.

4.3.1 Inter-Comparison of Different PET Methods

PET values for a watershed for different durations were derived using the above described nine conventional methods, utilizing the daily meteorological data available for the period 1981 - 1989. Before verifying the PET-CN relationship, a comparative study has been conducted to evaluate the performance of different PET methods for three watersheds of Narmada river basin, viz., Mohegoan, Hirdenagar, and Manot (Fig. 3.3). Notably, all three watersheds combinely comprise the area more than 13000 sq. km of central part of India. The statistics of the estimated long-term mean PET values by all nine methods separately for each storm duration for selected study watersheds are given in Tables 4.3a,b&c. It is evident from these tables that maximum variation between the average PET estimated by different methods was up to 42% for 1 day duration in case of Hridaynagar; however this is minimum 33% in case of Manot watershed for 30-day duration. On an average, 35% to 40% variation was reported in average PET value for all study watersheds. Figs 4.3a,b&c represent the deviation of estimated PET values with the average PET for different storm durations. Since such variation in long-term mean PET can significantly affect hydrological modeling results, the selection of an appropriate PET method demands proper care. In general, positive skewed values for all three watersheds

for different storm durations show that few methods predicted relatively high value of PET, which can be clearly seen from Tables 4.3a,b&c. However, the PET values for three watersheds predicted by a particular method and duration is more or less similar for the reason that all the watersheds are close to each other and belong to similar meteorological setting to a large extent.

The radiation-based Turc method estimated lowest PET values. However, the combination-based method Businger-van-Bevel estimated the highest values for all three catchments for most durations. Both the radiation-based Priestley-Taylor and Turc consistently underestimated PET compared to Penman-Monteith method in all the cases. Such an inference supports the conclusion of Whitehead (1986) that, in combination-based Penman-Monteith method, the aerodynamic term contributes 20% of PET for short grass. It is worth emphasizing here that all the combination methods, except the Penman-Monteith method, predicted high values of PET. Minimum standard deviation among PET values due to different methods was 0.71 and 20.39 mm for Manot (Table 4.3c) for 1-day and 30-day storm durations, respectively. However, these are maximum (0.76 and 21.23 mm) for Hridaynagar (Table 4.3b) for the same durations.

Several, more or less empirical, methods have been developed over the last 50 years by numerous researchers worldwide for estimation of PET but none can be recommended as the best one for any area or any season in terms of its accuracy and profitability. However, PET data are frequently needed at short notice for project planning or irrigation scheduling design. To select an appropriate method in the short notice is a tough task especially with the fact that to test the accuracy of any PET method for a new set of climatic condition is painstaking and time consuming task. In this endeavor, FAO (Allen *et al.*, 1994, 1998) recommended the Penman-Monteith equation as the sole standard method. Therefore, considering the Penman-Monteith PET method as a standard method (FAO-56), all remaining eight PET methods were compared based on root mean square error (RMSE). The results are shown in Table 4.4. Here it is worth emphasizing that in computation of RMSE, the PET values computed for different durations by a particular method are taken as a single series. However, RMSE values for each method were compared with respect to series of PET computed by standard Penman-Monteith method. The minimum value of RMSE (0.19 mm) was due to Hargreaves method. It was however maximum (18.84 mm) due to Businger ven-Bevel method for Hridaynagar watershed (Table 4.4).

Table 4.2: Characteristics of study watersheds.

Description	Watersheds						
	Hemavati	Manot	Hridaynagar	Mohegaon	Kalu	Ghodahado	Ramganga
River	Cauvery	Narmada	Narmada	Narmada	Ulhas	Ghodahado	Ramganaga
State	Karnataka	Madhya Pradesh	Madhya Pradesh	Madhya Pradesh	Maharashtra	Orissa	Uttarakhand
Area (sq. km)	600	5,032	3,370	4,661	224	138	3,134
Latitude	12°55′ to 13°11′ N	22°26′ to 23°18′ N	21° 42′ N	22° 32′ N	19° 17′ to 19° 26′ N	19° 17' to 19° 28' N	29°30' to 30°6'N
Longitude	75°29′ to 75°51′ E	80°24′ to 81°47′ E	80° 50′ E	81° 22′ E	73°36′ to 73° 49′ E	84° 27' to 84° 40' E	78°36' to 79°34'E
Topography	Low land, semi hilly and hilly	Hilly	both flat and undulating lands	Both flat and undulating lands	hilly	both flat and undulating lands	hilly with undulating and irregular slope
Land Use (% area)	Forests (12%), Agricultural (59%) Coffee plantation (29%)	Agricultural (52%), forest (35%), Barren (13%)	Forest (65%), Agricultural (29%), Degraded lands (6%)	Forest (58%), agricultural (42%)	Forest (50%), Agricultural (50%)	Forest area (40%), Permanent pasture (3%), Cultivated (50%), Barren land (10%)	Forest (50%), Cultivated (30%), Urban/Barren (20%)
Soil	Red loamy soil and red sandy soil	Red, yellow, and medium black soil	Black to mixed red soil	Red and yellow silty loam and silty clay loam	Silty loam and sandy loam	Red soils with blocky structures dominated by Kaolinites and illites	Loamy sand to silt loam
Elevation (in m, above msl)	890-1,240	450–1,110	372-600	509-900	1,200	305-610	338 - 3088
Av. Annual rainfall (mm)	2,972	1,596	1,178	1,547	2,450	1,476	1,550
Climate	hot, seasonally dry tropical savana	sub-tropical and sub-humid	sub-tropical and sub-humid	sub-tropical and sub-humid	hot and humid	hot and moist sub-humid	sub-tropical to sub-temperate

Table 4.3a: Long-term mean PET estimated from conventional methods for different durations and their statistic for Mohegoan.

SD	PET Methods									Statistics					
	PM	HR	KP	TR	PT	FAO-17	FAO-24	BvB	PM-63	Mean	Max	Min	StD	SKE	VAR (%)
1	4.04	4.02	5.42	3.74	3.95	4.88	5.48	5.66	4.79	4.66	5.66	3.74	0.75	0.12	41.19
2	8.22	8.18	10.87	7.61	7.94	9.88	11.06	11.36	9.67	9.42	11.36	7.61	1.47	0.10	39.85
3	12.53	12.48	16.43	11.60	11.98	15.02	16.79	17.18	14.68	14.30	17.18	11.60	2.20	0.09	39.06
4	16.68	16.65	21.74	15.48	15.90	19.96	22.27	22.72	19.50	18.99	22.72	15.48	2.87	0.08	38.08
5	21.26	21.17	27.53	19.58	19.99	25.38	28.30	28.84	24.74	24.09	28.84	19.58	3.67	0.06	38.45
6	25.52	25.41	33.15	23.52	24.12	30.49	33.99	34.67	29.73	28.96	34.67	23.52	4.41	0.06	38.51
7	30.24	30.13	38.91	27.78	28.30	36.02	40.08	40.73	35.06	34.14	40.73	27.78	5.14	0.04	37.92
8	34.29	34.26	44.14	31.51	32.07	40.81	45.46	46.19	39.77	38.72	46.19	31.51	5.83	0.04	37.90
9	38.83	38.76	49.77	35.83	36.23	46.26	51.44	52.14	45.01	43.81	52.14	35.83	6.54	0.03	37.24
10	42.88	43.01	54.84	39.69	40.00	51.01	56.71	57.36	49.67	48.35	57.36	39.69	7.12	0.03	36.55
15	66.04	65.80	83.48	61.00	60.64	78.41	86.93	87.69	76.04	74.00	87.69	60.64	10.87	0.00	36.55
20	87.19	87.66	109.65	80.44	79.64	103.44	114.52	115.03	100.26	97.54	115.03	79.64	14.15	-0.03	36.28
30	134.92	135.35	166.65	125.76	121.74	159.64	175.90	175.37	154.19	149.95	175.90	121.74	21.01	-0.06	36.12

Table 4.3b: Long-term mean PET estimated from conventional methods for different durations and their statistic for Hridaynagar.

SD	PET Methods									Statistics					
	PM	HR	KP	TR	PT	FAO-17	FAO-24	BvB	PM-63	Mean	Max	Min	StD	SKE	VAR (%)
1	4.03	3.92	5.40	3.71	3.92	4.83	5.44	5.65	4.75	4.63	5.65	3.71	0.76	0.14	41.99
2	8.28	8.07	10.94	7.60	7.95	9.88	11.09	11.45	9.69	9.44	11.45	7.60	1.50	0.12	40.78
3	12.62	12.38	16.50	11.58	12.07	15.03	16.82	17.26	14.71	14.33	17.26	11.58	2.22	0.10	39.64
4	17.05	16.76	22.13	15.71	16.26	20.27	22.64	23.15	19.83	19.31	23.15	15.71	2.93	0.09	38.53
5	21.41	21.13	27.67	19.66	20.33	25.42	28.37	28.98	24.85	24.20	28.98	19.66	3.66	0.08	38.51
6	25.76	25.49	33.17	23.81	24.56	30.59	34.07	34.69	29.89	29.12	34.69	23.81	4.30	0.07	37.39
7	30.63	30.31	39.10	28.20	28.93	36.27	40.32	40.95	35.38	34.46	40.95	28.20	5.05	0.05	37.01
8	35.02	34.68	44.66	32.30	33.07	41.45	46.12	46.83	40.46	39.40	46.83	32.30	5.76	0.06	36.88
9	39.87	39.37	50.67	36.64	37.44	47.09	52.35	53.11	45.92	44.72	53.11	36.64	6.54	0.05	36.85
10	43.90	43.93	55.61	40.62	41.38	51.89	57.58	58.14	50.62	49.30	58.14	40.62	6.99	0.03	35.54
15	67.82	67.31	85.29	62.45	63.24	79.94	88.50	89.31	77.75	75.74	89.31	62.45	10.76	0.02	35.47
20	91.27	91.29	113.81	84.15	84.46	107.55	118.74	119.23	104.37	101.65	119.23	84.15	14.18	-0.01	34.51
30	142.61	141.74	175.03	133.04	131.02	167.68	184.21	183.78	162.22	157.93	184.21	131.02	21.23	-0.02	33.68

Table 4.3c: Long-term mean PET estimated from conventional methods for different durations and their statistic for Manot.

SD	PET Methods									Statistics					
	PM	HR	KP	TR	PT	FAO-17	FAO-24	BvB	PM-63	Mean	Max	Min	StD	SKE	VAR (%)
1	4.04	3.97	5.35	3.74	3.98	4.82	5.41	5.58	4.74	4.63	5.58	3.74	0.71	0.13	39.79
2	8.18	8.07	10.75	7.55	7.99	9.73	10.89	11.21	9.56	9.33	11.21	7.55	1.42	0.12	39.26
3	12.45	12.23	16.30	11.53	12.12	14.81	16.57	17.02	14.54	14.17	17.02	11.53	2.15	0.11	38.71
4	16.77	16.57	21.80	15.45	16.22	19.87	22.21	22.76	19.50	19.02	22.76	15.45	2.84	0.10	38.42
5	21.25	20.89	27.46	19.64	20.50	25.17	28.08	28.71	24.67	24.04	28.71	19.64	3.56	0.10	37.73
6	25.66	25.12	33.17	23.78	24.79	30.40	33.87	34.65	29.76	29.02	34.65	23.78	4.28	0.10	37.48
7	29.83	29.57	38.37	27.62	28.86	35.25	39.24	39.95	34.56	33.69	39.95	27.62	4.83	0.08	36.59
8	34.55	34.21	44.21	31.75	32.99	40.76	45.39	46.16	39.90	38.88	46.16	31.75	5.64	0.06	37.05
9	39.15	38.56	50.11	36.02	37.39	46.24	51.42	52.37	45.19	44.05	52.37	36.02	6.42	0.07	37.11
10	43.58	43.21	55.54	40.17	41.61	51.38	57.13	57.98	50.27	48.99	57.98	40.17	7.00	0.06	36.35
15	67.17	66.17	84.67	61.57	63.27	78.98	87.59	88.78	76.99	75.02	88.78	61.57	10.72	0.04	36.27
20	89.80	89.67	112.31	82.62	84.16	105.58	116.69	117.51	102.74	100.12	117.51	82.62	13.87	0.01	34.86
30	138.05	138.28	170.09	127.95	128.61	161.95	178.24	178.21	157.26	153.18	178.24	127.95	20.39	-0.01	32.83

** All PET values are in mm.*

SD: Storm duration (days); PM: Penman-Monteith; HR: Hargreaves; KP: 1982 Kimberley-Penman; TR: Turc; PT: Prisetley-Taylor; FAO-17: FAO PPP-17 Penman; FAO-24: FAO-24 corrected Penman; BvB: Businger van-Bevel; PM-63: Penman-1963; Max: maximum; Min: Minimum; StD: standard deviation; SKE: skewness; and VAR: variability.

Table 4.4: Root Mean Square Error (RMSE) with reference to standard Penman-Monteith method in estimation of all durations PET from different methods

PET Methods	Hargreaves	1982 Kimberly-Penman	FAO PPP-17 Penman	FAO-24 corrected Penman (c=1)	Priestley-Taylor	Businger-van-Bavel	Turc	Penman 1963
Mohegaon Watershed	0.20	13.58	9.95	16.68	4.71	16.94	3.90	7.97
Hridaynagar watershed	0.19	15.09	11.08	18.60	4.65	18.84	4.53	8.88
Manot watershed	0.42	13.62	9.59	16.33	3.38	16.81	4.19	7.88

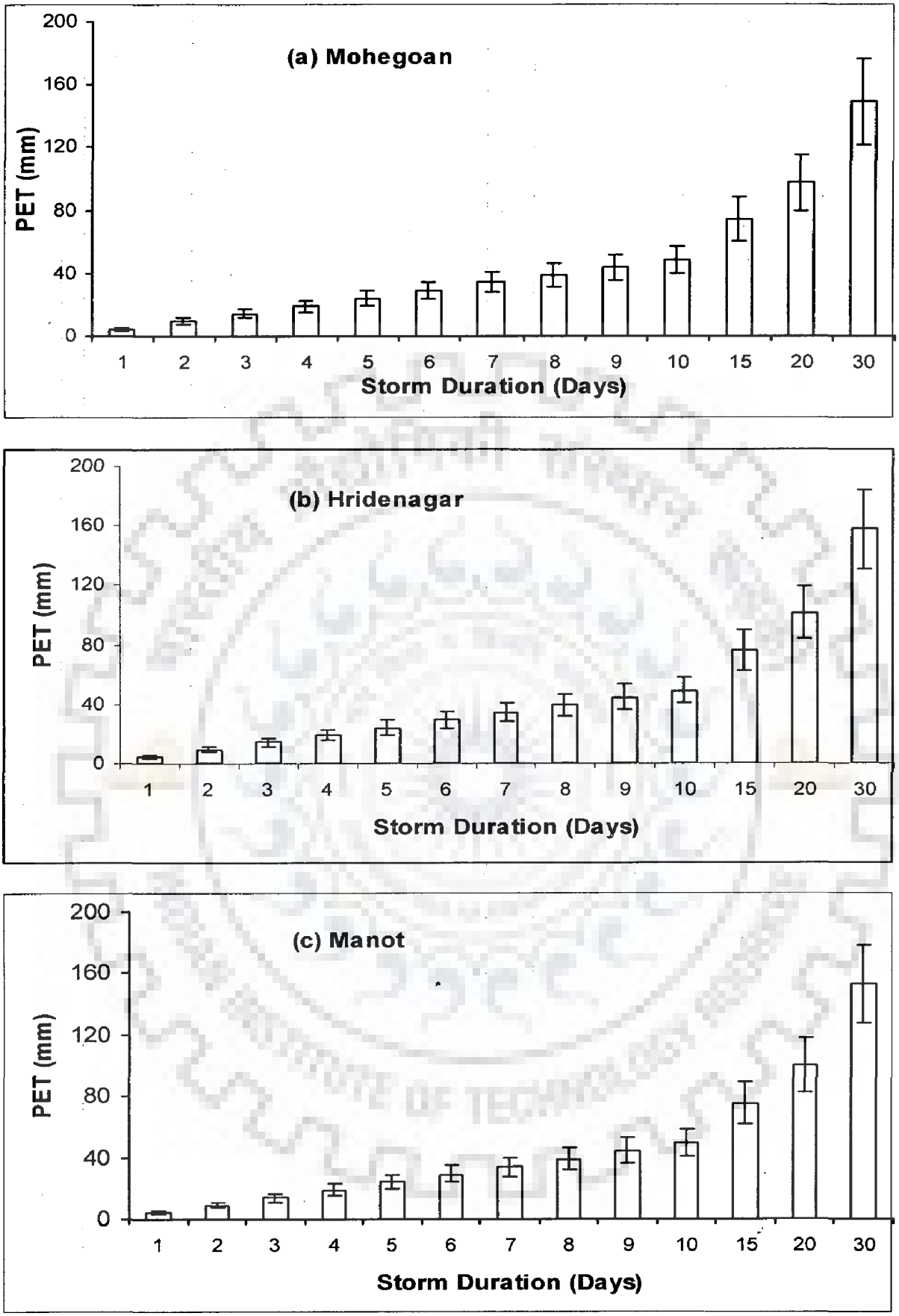

Figs. 4.3a,b,&c: Variation of long-term mean PET estimates with duration for three watersheds. Error bars represent the deviation from the mean of the values derived using conventional methods.

Apart from Penman-Monteith method, based on RMSE values computed for different methods, the Hargreaves, Priestley-Taylor, and Turc methods can be considered for application to Narmada catchments or can be extended for the central part of India. However, Hargreaves method is recommended to be the best of all due to its good agreement with Penman-Monteith for all the three catchments and for all durations. Employing a set of climatic data from various sites, the study of Center Commun de Recherche of the European Economic Community (Choisnel et al., 1992) compared the Penman-Monteith equation with nine other simpler PET relationships requiring less data and the results due to Hargreaves formula were more close to the Penman-Monteith equation than others. The Pristeley-Taylor and Turc methods performed equally well. However, the Priestley-Taylor method performed better for all the durations, except 15, 20, and 30 day durations. Nevertheless, this method can be useful if the parameter α, surrogate of aerodynamic term, is calibrated properly. It is worth emphasizing here that, in this study, all the methods utilized their original values of constants/parameters in PET estimation.

Finally, based on the relative performance of the above eight methods in their application to the three catchments and input data requirement, the Hargreaves method can be recommended for field application, consistent with the work of Martinez-Cob and Tejero-Juste (2004), which describes the method to perform well in windy and semi-arid conditions of northeastern Spain, and others (Schenider et al., 2007; Lopez-Urrea et al., 2006; Shuttleworth, 1993; Allen et al., 1989). It is worth noting that in Hargreeves method only, two-parameter, viz., maximum and minimum temperatures are required for PET estimation. This method was originally developed for the dry climate of California. Moreover, the study suggests that increasing the number of parameters in input domain does not guarantee more accurate results, especially in case of complex phenomenon like PET.

4.3.2 CN-PET Relation

The above concept is validated using the large set of data collected from 7 watersheds belonging to different agro-climatic regions of India (Table 4.2) and area ranging from 138 sq. km (Ghodahado) to 5032 sq. km (Manot). The potential evapotranspiration (PET) was calculated by standard Penman-Monteith method for different watersheds. However, due to non-availability of climatic data of Ramganga catchment, neighboring station (Pantnagar, located at a latitude of $29^0 1'55''$ N and longitude

$79^0$28'25" E) data were used for PET estimation. CN values for different rain durations were derived from rainfall-runoff data described above and these were transformed to potential maximum retention for AMC I (S_I) using Eq. 2.6. These values when plotted (Fig. 4.4 & Appendix B) against the corresponding Penman-Monteith PET exhibited a power relation for all 7 watersheds selected for the study. The coefficient of determination (R^2) was 0.99 for Hemavati and Mohegoan; 0.98 for Haridanagar and Kalu; 0.96 for Manoth, Ghodahadho, and Ramganga applications; indicating the existence of an inverse PET-CN relationship and it, in turn, supports the general applicability of the concept.

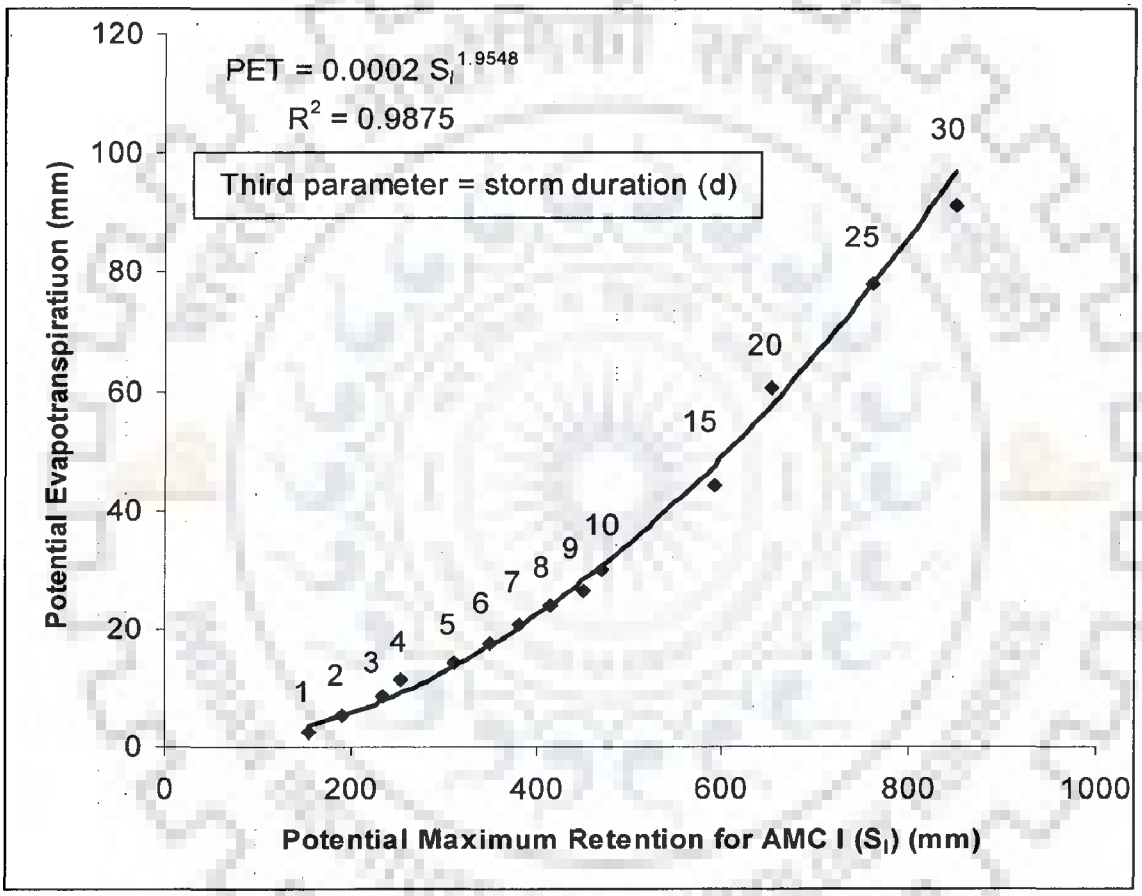

Fig. 4.4: Penman-Monteith PET and potential maximum retention for AMC I (S_I) relationship for Hemavati watershed.

Such a relationship may also lead to describing the SCS-CN parameter S in terms of the maximum possible evaporable depth and determining PET using SCS (1956) CN-values as follows:

(a) Determine the AMC II CN value for a watershed from the NEH-4 table.

(b) Convert the AMC II CN value to AMC I using the NEH-4 table.

(c) Compute S_I using Eq. (2.6) and determine the long-term mean PET from Eq. (4.1).

Here, it is noted that curve numbers derived for different durations from the above described procedure be used for estimation of PET of corresponding duration from the proposed method. Curve Numbers derived from historical rainfall-runoff data accounts for all watersheds' climatic, physical, and geographical characteristics. Consequently, the chances of error incurred in estimation of curve number, which may otherwise occur if NEH-4 table is used, does not outweigh the advantage one would derive from the use of the proposed method. The SCS-CN methodology ignores the base flow contribution to runoff and, therefore, different durations CN-values are derived from only those P-Q data sets following Q/P<1 condition. Consequently, the proposed method can be adequately applied to humid regions. CN (or S)-PET relationship for Kalu watershed (R^2=0.98) shown in Appendix B also supports the applicability of the proposed concept to humid conditions.

4.4 ADVANTAGES AND LIMITATIONS OF THE PROPOSED STUDY

The encouraging results of this study suggest the methodology may be a substitute for the complex PET estimation methods, especially in developing countries where establishment of new meteorological stations are not ever possible due to their high installation and operational costs. In addition, the proposed concept eliminates the need of costly measurements of groundwater inflow and outflow. However, the proposed concept helps derive a long-term mean of potential evapotranspiration, and therefore, is not time/duration/season specific. Notably, the data finally used for CN derivation may not be continuous because of exclusion of those events exhibiting runoff coefficient (C)>1. In addition, since parameter λ is a regional parameter that depends on geological and climatic factors and hence an important parameter in PET estimation, results may be improved with the use of a value other than the standard value of 0.2. Furthermore, it is possible to quantitatively examine the impact of climate change on hydrologic system employing CN-PET relationship. The watersheds used in this study are mostly dominant in forest and agriculture (Table 4.2) with little or no disturbance in land use, and therefore, the accuracy of the proposed concept needs to be investigated on urban watersheds where the SCS-CN concept works fairly well (Ponce and Hawkins, 1996).

4.5 SUMMARY

In the present study, an attempt has been made to develop a power relationship between PET and Soil Conservation Service Curve Number parameter i.e. potential

maximum retention. Mathematical and physical justification of PET-CN rationale invokes the existence of a relationship between the duration dependent PET and runoff curve numbers (or potential maximum retention). The relationship/methodology was verified by employing a large set of hydro-meteorological data belonging to seven different agro-climatic river basins of India. Subsequently, the curve numbers derived from rainfall-runoff data of seven different agro-climatic river basins in India exhibit a strong correlation (of power form) with PET derived using standard Penman-Monteith method. High R^2 values ranging from 0.96 to 0.99 support the general applicability of the proposed concept. Such a relationship invokes to describe the SCS-CN parameter S in terms of the maximum possible evaporable depth and determine PET from the available NEH-4 CN values and very useful especially for field engineers. Furthermore, the nine commonly used conventional potential evapotranspiration methods (six combination methods, two based on radiation, and one temperature-based) were inter-compared for three watersheds falling in the Narmada river basin. Significant variability among the PET estimation methods was observed. Considering the Penman-Monteith method as a standard method, the Hargreaves method performed equally well (low value of RMSE). However, radiation-based Priestley-Taylor and Turc methods can be applied for the same region with reasonable accuracy.

In accordance with the objective of the study, the next chapter deals with the development of synthetic unit hydrograph (SUH) using a probability distribution function and employing the geomorphological parameters extracted in GIS environment.

CHAPTER 5

SUH DERIVATION USING PDF AND GEOMORPHOLOGICAL PARAMETERS

5.1 INTRODUCTION

The unit hydrograph (UH) method was introduced by Sherman (1932). It is widely used for runoff estimation and has immense significance due to its basic simplicity of the definition, i.e. the direct runoff resulting from unit depth of rainfall-excess produced by storm of uniform intensity and specified duration. To exploit the simplicity and less data requirement of UH approach, McCarthy (1938) and Snyder (1938) developed synthetic unit hydrograph (SUH) for ungauged catchments using some empirical equations to derive the salient points of the hydrograph. Similar expressions were later given by Edson (1951), Gray (1961), and Haan et al. (1994). All these methods estimate the salient points of UH, and a smooth curve is fitted through these points to obtain SUH. Thus, a large degree of subjectivity is involved in manual fittings, as simultaneous adjustments are also required for the area under UH to represent unit runoff volume. Furthermore, UH approach is duration-dependent for a number of UHs of different durations are possible for the same catchment.

Clark (1945) was probably the first to propose the Instantaneous Unit Hydrograph (IUH) theory. The main advantage of IUH is that it is independent of the duration of effective rainfall, and thus, has one parameter less than unit hydrograph. Nash (1957) was the first to derive IUH as a two-parameter gamma distribution (2PGD) by simulating the whole catchment by "n" identical conceptual cascaded linear reservoirs. Due to similarity in typical shape and unit area of a probability distribution function (pdf) curve, various suitable distributions have been explored by Gray (1961), Croley (1980), Aron and White (1982), Koutsoyiannis and Xanthopoulos (1989), Haktanir and Sezen (1990), Singh (2000), and Bhunya et al. (2004, 2007, 2009) for SUH derivation. Nandrajah (2007) suggested eleven different flexible pdfs ranging from one-parameter to three parameters for UH derivation. One of the major advantages of the application of pdfs is the subjectivity that existed in manual fitting of UH in earlier methods was eliminated. With the coupling of Horton's geomorphic parameters and hydrological parameters by Rodriguez-Iturbe & Valdes (1979) and further refinement by Gupta et al. (1980), the IUH theory (called GIUH) became more promising for ungauged catchments. Since the theory represented hydrological parameters in terms of geomorphological characteristics of river

basin, and thus, requirement of land use and climatic parameters (like in Clarks, 1945 and Nash, 1957) are obviously omitted.

This chapter presents an extension of the earlier work as follows. It explores the applicability of parametric expression of two-parameter Inverse Gamma distribution (2PIGD), which has not yet been attempted for SUH derivation employing a geomorphological model of the catchment response. Its performance is compared with two-parameter Weibull distribution (2PWD) based on geomorphological model of a catchment response and popular two-parameter Nash gamma model (2PNGM) (Rosso, 1984). Simple analytical procedures are proposed for estimation of distribution parameters. The workability of the proposed procedures is tested on two hilly watersheds located in different regions of India. Finally, a simple regression model is derived for peak discharge and time to peak with dynamic velocity as a third parameter for an ungauged watershed.

5.2 PROBABILITY DISTRIBUTION FUNCTION

5.2.1 Two-Parameter Inverse Gamma Distribution (2PIGD)

The probability density function (pdf) of this distribution is given by (Fig. 5.1):

$$f(x) = \frac{a^b}{\Gamma b} x^{-b-1} \exp\left(-\frac{a}{x}\right); \qquad \text{for } x > 0,\ a > 0, \text{ and } b > 0 \tag{5.1}$$

where 'a' and 'b' are the distribution parameters which define the shape of the function. The cumulative distribution function (cdf) is given by:

$$F(x) = \frac{\Gamma(b, a/x)}{\Gamma b} \tag{5.2}$$

The mean (μ) and variance (σ^2) for the distribution, respectively, are given by:

$$\mu_x = \frac{a}{b-1};\ \text{for } b > 1; \qquad \sigma_x^{\,2} = \frac{a^2}{(b-1)^2(b-2)};\ \text{for } b > 2 \tag{5.3a,b}$$

Now, taking the inverse gamma density function as the discharge ordinates q(t) of UH and x as time t, Eq. (5.1) can be expressed as:

$$q(t) = \frac{a^b}{\Gamma b} t^{-b-1} \exp\left(-\frac{a}{t}\right); \qquad \text{for } t > 0 \tag{5.4}$$

Applying the condition at time to peak (i.e. $t = t_p$), the slope, i.e. dq(t)/dt of the UH is zero, and hence, Eq. (5.4) reduces to:

$$\frac{a^b}{\Gamma b} t_p^{-b-1} \exp\left(-\frac{a}{t_p}\right)\left(\frac{a}{t_p^2}\right) + \frac{a^b}{\Gamma b} t_p^{(-b-2)}(-b-1)\exp\left(-\frac{a}{t}\right) = 0 \qquad (5.5)$$

Simplification of Eq. (5.5) results into

$$\frac{a^b}{\Gamma b} t_p^{(-b-2)} \exp\left(-\frac{a}{t_p}\right)\left[\frac{a}{t_p} + (-b-1)\right] = 0 \qquad (5.6)$$

Now, two conditions can be observed from Eq. (5.6) as: (i) either $[(a/t_p) + (-b-1)] = 0$ or

(ii) $\frac{a^b}{\Gamma b} t_p^{(-b-2)} \exp\left(-\frac{a}{t_p}\right) = 0$; and from condition (i) and (ii):

$t_p = a/(b+1)$ or $t_p = a$ (5.7a,b)

Substitution of $t_p = a/(b+1)$ in Eq. (5.4) gives the expression for peak flow rate (q_p) as:

$$q_p = \frac{1}{a\Gamma b}(b+1)^{-b-1}\exp(-b-1) \qquad (5.8)$$

5.2.2 Two-Parameter Weibull Distribution (2PWD)

The probability density function (pdf) of two-parameter Weibull distribution (2PWD) (Fig. 5.1) is given by Weibull (1939) as:

$$f(x) = \frac{c}{\alpha}\left(\frac{x}{\alpha}\right)^{c-1} \exp\left[-\left(\frac{x}{\alpha}\right)^c\right]; \text{ for } \alpha > 0, c > 1, t > 0 \qquad (5.9)$$

where 'α' is the scale parameter and 'c' is the shape parameter. For c = 1, Eq. (5.9) is an exponential pdf. Thus, the exponential distribution is a special case of the Weibull distribution (Singh, 1987).

The cumulative distribution function (cdf) is given by:

$$F(x) = 1 - \exp\left[-\left(\frac{t}{\alpha}\right)^c\right] \qquad (5.10)$$

The mean (μ) and variance (σ^2) of the pdf are given as:

$$\mu = \alpha\Gamma\left(1+\frac{1}{c}\right) \qquad \sigma^2 = \alpha^2\Gamma\left(1+\frac{2}{k}\right) - \alpha^2\left[\Gamma\left(1+\frac{1}{c}\right)\right]^2 \qquad (5.11a,b)$$

Considering UH similar to the Weibull distribution with discharge ordinate q(t) on the y axis and x axis as time (t), Eq. (5.9) can be used to describe a UH as:

$$q(t) = \frac{c}{\alpha}\left(\frac{t}{\alpha}\right)^{c-1} \exp\left[-\left(\frac{t}{\alpha}\right)^c\right] \qquad (5.12)$$

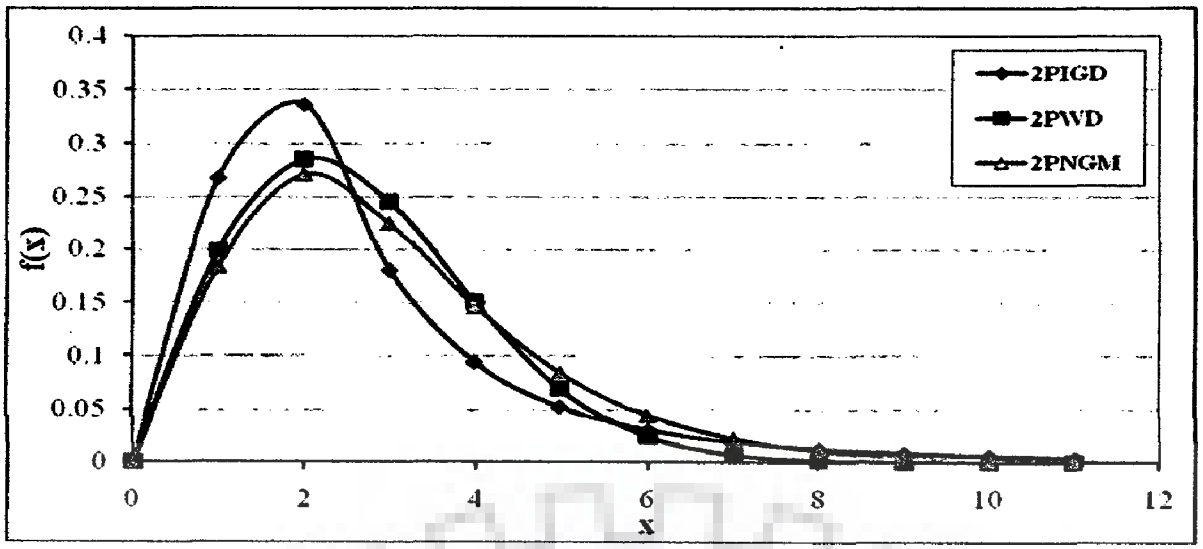

Fig. 5.1: The pdf shapes of two-Parameter Inverse Gamma distribution (2PIGD) (a = 6, b = 3), two Parameter-Weibull distribution (2PWD) (α =3, c = 2) and two-parameter Nash Gamma Model (2PNGM, Rosso, 1984) (n = 3, k = 2).

Applying the condition that at time to peak (i.e. $t = t_p$), the slope, i.e. dq(t)/dt of the UH is zero and hence Eq. (5.12) reduces to

$$\frac{c}{\alpha^2}\left(\frac{t}{\alpha}\right)^{c-1}\exp\left\{-\left(\frac{t}{\alpha}\right)^{c}\right\}\left[(-c)\left(\frac{t}{\alpha}\right)^{c-1}+(c-1)\left(\frac{t}{\alpha}\right)^{-1}\right]=0 \qquad (5.13)$$

Now, two conditions can be observed from Eq. (5.13) as:

$$\text{either } \left[(-c)\left(\frac{t}{\alpha}\right)^{c-1}+(c-1)\left(\frac{t}{\alpha}\right)^{-1}\right]=0 \text{ or } \frac{c}{\alpha^2}\left(\frac{t}{\alpha}\right)^{c-1}\exp\left\{-\left(\frac{t}{\alpha}\right)^{c}\right\}=0$$

Thus, $t_p=\alpha\left(1-\frac{1}{c}\right)^{\frac{1}{c}}$; or $t_p=\alpha$ (5.14a, b)

Substitution of $t_p=\alpha\left(1-\frac{1}{c}\right)^{\frac{1}{c}}$ in Eq. (5.12) gives the expression for peak flow rate (q_p) as:

$$q_p=\frac{c}{\alpha}\left(1-\frac{1}{c}\right)^{1-\frac{1}{c}}\exp\left[1-\left(1-\frac{1}{c}\right)\right] \qquad (5.15)$$

5.3 PARAMETER ESTIMATION

5.3.1 Two-Parameter Inverse Gamma Distribution (2PIGD)

Defining shape factor β (= product of peak discharge and time to peak discharge) (Bhunya et al., 2003; 2009) results into:

$$\beta=q_p t_p=\frac{(b+1)^b}{\Gamma b}\exp-(b+1) \qquad (5.16)$$

A substitution of (b+1) = m; Eq. (5.16) reduces to

$$\beta = \frac{m^{m-1}}{\Gamma(m-1)} \exp(-m) \tag{5.17}$$

Using $\Gamma m = (m\text{-}1)\,\Gamma\,(m\text{-}1)$ Eq. (5.17) reduces to

$$\beta = \frac{(m-1)m^{m-1}}{\Gamma(m)} \exp(-m) \tag{5.18}$$

Now, using Stirling's formula (Abramowitz & Stegun, 1964), gamma function can be expanded as:

$$\Gamma m = \sqrt{2\pi m}\left[m^{m-1}\exp(-m)\right]\left\{1+\frac{1}{12m}+\frac{1}{288m^2}-\frac{139}{51840m^3}-\frac{571}{2488320m^4}\ldots\right\} \tag{5.19}$$

Considering first two terms of Eq. (5.19) in the denominator, Eq. (5.18) reduces to

$$\beta = \frac{m-1}{\sqrt{2\pi m}\left(1+\frac{1}{12m}\right)} \tag{5.20}$$

A further simplification of Eq. (5.20) results into

$$\beta^2 = \frac{(m-1)^2}{\left(2\pi m+\frac{\pi}{3}\right)} \tag{5.21}$$

Replacing m by (b+1), Eq. (5.21) takes the form

$$\beta^2 = \frac{b^2}{\left(2\pi(b+1)+\frac{\pi}{3}\right)} \tag{5.22}$$

A further simplification of Eq. (5.22) results into

$$3b^2 - 6\pi\beta^2 b - 7\pi\beta^2 = 0 \tag{5.23}$$

Using Eq. (5.23) parameter 'b' can be expressed as:

$$b = \pi\beta^2 \pm \beta\sqrt{\pi^2\beta^2 + 7\pi/3} \tag{5.24}$$

Hence, for the known values of the shape factor β, the scale parameter 'b' can be obtained from Eq. (5.24). Once "b" is obtained, the shape parameter 'a' can be estimated using Eq. (5.7a), and the complete shape of UH derived using Eq. (5.4).

5.3.2 Two-Parameter Weibull Distribution (2PWD)

Defining shape factor β, a dimensionless quantity (= product of q_p and t_p) can be expressed as:

$$\beta = q_p t_p = (c-1)\exp\left[-\left(1-\frac{1}{c}\right)\right] \tag{5.25}$$

A further simplification and expansion of the exponential term up to third term results into

$$c^3 - (e\beta)c^2 - (1/2)c - (1/2) = 0 \quad (5.26)$$

The solution of the above equation can be expressed as (Abramowitz and Stegun, 1964):

$$c = (S_1 + S_2) - a_2/3 \quad (5.27)$$

where $S_1 = \left[B + (A^3 + B^2)^{1/2}\right]^{1/3}$ and $S_2 = \left[B - (A^3 + B^2)^{1/2}\right]^{1/3}$; $a_2 = (-e\beta)$ (5.28)

in which $A = a_1/3 - a_2^2/9$; $B = (a_2a_1 - 3a_0)/6$; $a_1 = (-1/2)$; $a_0 = (-1/2)$. Thus, the shape parameter 'c' of the 2PWD can be estimated using Eq. (5.27), and scale parameter 'α' from Eq. (5.14a).

5.4 TWO-PARAMETER NASH GAMMA MODEL (2PNGM)

The possibility of preserving the form of SUH through a two-parameter gamma distribution (2PGD) was analysed by Rosso (1984), where the Nash model parameters were related to Horton ratios as discussed here. The gamma probability density function (Fig. 5.1) is given as:

$$q(t) = \frac{1}{k\Gamma(n)}\left(\frac{t}{k}\right)^{n-1} e^{-\frac{t}{k}} \quad (5.29)$$

where k is the scale parameter [T], n is the shape parameter equal to m_2^{-1}, where m_2 is the second dimensionless moment about the centre of area of the IUH, and $\Gamma(\ )$ is the gamma function. The mean (μ), variance (σ^2), and skewness (γ) of the 2PGD are described as:

$$\mu = n\,k;\ \sigma^2 = n\,k^2;\ \gamma = 2/\sqrt{n} \quad (5.30)$$

For the condition at time-to-peak ($t = t_p$), $dq(t)/dt = 0$, Eq. (5.30) yields the following expression relating n and k:

$$k = t_p/(n-1) \quad (5.31)$$

The expression for the dimensionless product $\beta = q_p t_p$ can be obtained in the simpler form:

$$\beta = q_p t_p = \frac{(n-1)^{n-1} e^{-(n-1)}}{\Gamma(n-1)} \quad (5.32)$$

Rosso (1984) equated both the expressions of $q_p t_p$, Eq. (2.10) and Eq. (5.32) and used an iterative computing scheme to develop expressions for 'n' and 'k' as:

$$n = 3.29(R_B/R_A)^{0.78} R_L^{0.07} \quad (5.33)$$

$$k_* = 0.70[R_A/(R_B R_L)]^{0.48} \quad (5.34)$$

where $k_* = kvL^{-1}$ is a dimensionless scale parameter. Thus, for an observed v, the parameters of the 2PGD and the UH shape can be computed from the geomorphological parameters of the catchment.

5.5 VALIDATION OF PROPOSED METHODS

The workability of the proposed methods i.e. 2PIGD, 2PWD for deriving SUH under limited data condition is checked and compared with the 2PNGM (Rosso, 1984) using real data.

5.5.1 Gagas Watershed

Direct Runoff Hydrographs (DRHs) of six isolated storm events of Gagas watershed were obtained from the Divisional Forest Office Ranikhet, Uttarakhand, the state of India, and described in Table 3.1. Corresponding Unit hydrographs (UHs) were obtained using Singh (1988) method and their characteristics are described in Table 5.1. The geomorphologic parameters (Horton's ratios) of Gagas watershed were taken from Kumar and Kumar (2008). The values of bifurcation ratio (R_B), length ratio (R_L), and area ratio (R_A) for Gagas watershed are 4.82, 2.39, and 5.37, respectively. Detail information of Gagas watershed has been given in Chapter 3.

Following are the steps involved in derivation of SUHs for different storms of Gagas watershed:

(i) Let the storm event be of June 25, 1978, when Q_p is considered to be known. Therefore, $q_p = Q_p/(A_w) = (47.93 \times 1000 \times 3600)/(506 \times 10^6) = 0.34$ mm/hr/mm $= 0.364(2.39)^{0.43}\ vL^{-1}$ (Eq. 2.11). Hence $vL^{-1} = 0.34/[0.364(2.39)^{0.43}] = 0.642$ hr^{-1}

(ii) Now substituting the value of vL^{-1} (Step i) and values of R_A, R_B, and R_L into Eq. (2.12) to get t_p as:
$t_p = 1.584(4.82/5.37)^{0.55} 2.39^{-0.38} (0.642)^{-1} = 1.669$ hr

(iii) Get the dimensionless product $\beta = q_p t_p = 0.34 \times 1.667 = 0.567$.

(iv) Taking these values (at Steps i-iii), estimate parameters of 2PIGD and 2PWD, and 2PNGM. For 2PIGD, use Eq. (5.24) for 'b', and Eq. (5.7a) for 'a'; Eq. (5.27) for 'c' and Eq. (5.14a) for 'α' for 2PWD; and Eq. (5.33) for 'n' and Eq. (5.34) for '**k**' for 2PNGM. The estimated parameters values are given in Table 5.1.

(v) Finally, derive SUHs using the above three methods, viz., Eq. (5.4) for 2PIGD, Eq, (5.12) for 2PWD, and Eq. (5.29) for 2PNGM. The derived SUHs are shown in Fig. 5.2a.

(vi) Similar procedure was followed for estimation of parameters of the distributions for the other storm events and the values are given in Table 5.1. Using the above parameters, SUHs were derived using 2PIGD, 2PWD and 2PNGM methods and depicted in Figs. 5.2b-f.

Table 5.1: Storm characteristics and parameters of the three models for partial data availability condition for the study area.

Storm Event	UH Characteristics		Parameters of:					
			2PIGD		2PWD		2PNGM	
	Q_p (m^3/s)	t_p (h)	a	b	α	c	n	K
Gagas Watershed								
June 25, 1978	47.93	2.0	6.416	2.850	2.428	1.935	3.21	0.759
June 20, 1981	48.35	2.0	6.372	2.850	2.410	1.935	3.21	0.749
July 31, 1982	50.40	2.0	6.070	2.850	2.296	1.935	3.21	0.714
August 30, 1984	46.03	2.0	6.68	2.850	2.527	1.935	3.21	0.785
August 10, 1985	49.09	2.0	6.25	2.850	2.364	1.935	3.21	0.735
August 15, 1985	50.90	2.0	6.035	2.850	2.283	1.935	3.21	0.710
Myndtu-Leska Watershed								
Bhunya *et al.* (2005)	11.80	5	19.840	2.959	7.198	1.964	3.266	2.211

5.5.2 Myantdu-Leska Watershed

The Myantdu-Leska River watershed is described in Chapter 3. Its data were derived from Mani amd Panigrahey (1998) and Bhunya et al. (2005). The geomorphological parameters of the watershed were taken from Mani and Panigrahey (1998) and given in Chapter 3. Following the same procedure, as above, the steps involved in SUH derivation for Myantdu-Leska are given below:

i. At the first step, use Eq. (2.11), and substitute the value of q_p and R_L (Chapter 3) to get the value of vL^{-1}. $q_p = Q_p/(A_w) = (11.8x1000x3600)/(350x10^6) = 0.122$ mm/hr/mm $=0.364(2.12)^{0.43}$ vL^{-1}. Hence $vL^{-1} = 0.122/ [0.364(2.12)^{0.43}] = 0.243hr^{-1}$

ii. Now substituting the value of vL^{-1} (step i) and R_A, R_B, and R_L (Chapter 3) into Eq. (2.12) to get t_p as; $t_p = 1.584(4.27/4.61)2.12^{-0.38}(0.243)^{-1} = 4.72$ hr

iii. Get the dimensionless product $\beta = q_p t_p = 0.122 \times 4.72 = 0.574$.

iv. Taking these values (at Steps i-iii), estimate parameters of 2PIGD and 2PWD, and 2PNGM. For 2PIGD, use Eq. (5.24) for 'b', and Eq. (5.7a) for 'a'; Eq. (5.27) for

'c' and Eq. (5.14a) for 'α' for 2PWD; and Eq. (5.33) for 'n' and Eq. (5.34) for 'k' for 2PNGM. The estimated parameter values are given in Table 5.1.

v. Finally, derive SUHs using the above three methods, viz., Eq. (5.4) for 2PIGD, Eq, (5.12) for 2PWD, and Eq. (5.29) for 2PNGM. The derived SUHs are shown in Fig. 5.3.

5.6 MODEL PERFORMANCE EVALUATION

The qualitative performance of the model was evaluated by visual observation of the shape of the predicted and the observed UHs in respect of peak rate, time to peak, time base, and overall shape of the UHs for different storm events. A quantitative evaluation was also made for the predicted and observed UHs for given storm events, employing the following statistical indices: (i) Standard Error (STDER); (ii) Root Mean Square Error (RMSE); (iii) Relative Error in Peak (REP); (iv) Nash-Sutcliff Coefficient of Efficiency (NSE).

5.6.1 Statistical Indices

(i) Standard Error (STDER): It represents the absolute sum of the mismatching areas to the total hydrograph area, mathematically expressed as:

$$STDER = \left[\left(\sum_{i=1}^{N}(U_{oi} - U_{ci})^2 W_i\right)/N\right]^{1/2} ; W_i = (U_{oi} - U_{av})/2U_{av} \qquad (5.35)$$

where U_{oi} is the i^{th} ordinate of observed hydrograph, U_{ci} is the i^{th} ordinate of the computed hydrograph, W_i is the weighted value of i^{th} hydrograph ordinate, U_{av} is the average of the observed hydrograph ordinates, and N is the total number of hydrograph ordinates.

(ii) Root Mean Square Error (RMSE): It is described as:

$$RMSE = \left[\frac{\sum_{t=1}^{N}\{U_{oi} - Uci\}^2}{N}\right]^{0.5} \qquad (5.36)$$

(iii) Relative Error in Peak (REP): it represents the percentage relative error in peak flow rate of the observed and computed hydrographs, expressed as:

$$REP\ (\%) = \frac{(U_{op} - U_{cp})}{(U_{op})} \times 100 \qquad (5.37)$$

where U_{op} is the peak of observed hydrograph and U_{cp} is the peak of computed hydrograph.

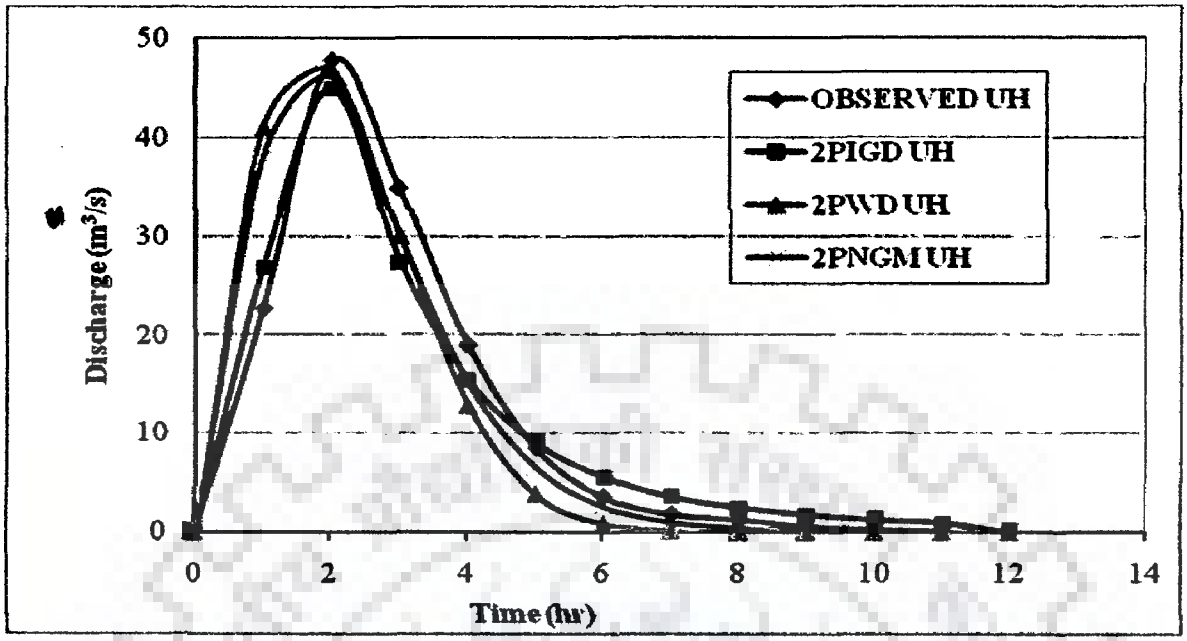

Fig. 5.2a: Comparison between Observed and Computed UHs for Gagas Watershed for the storm of June 25, 1978.

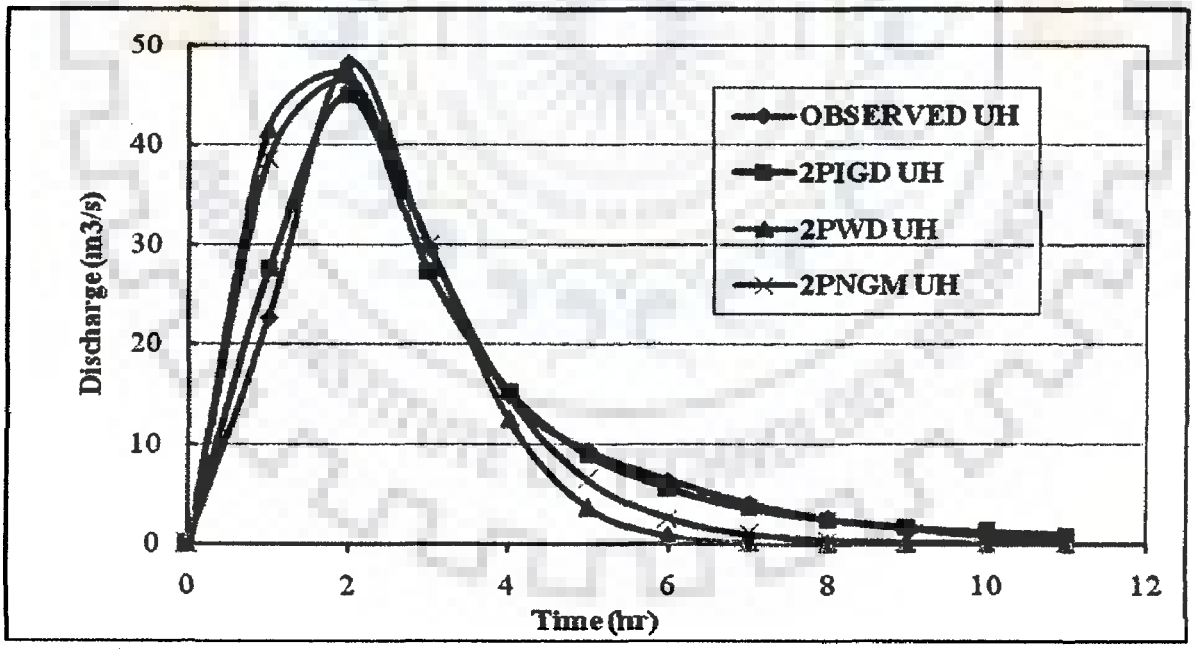

Fig. 5.2b: Comparison between Observed and Computed UHs for Gagas watershed for the storm of June 20, 1981.

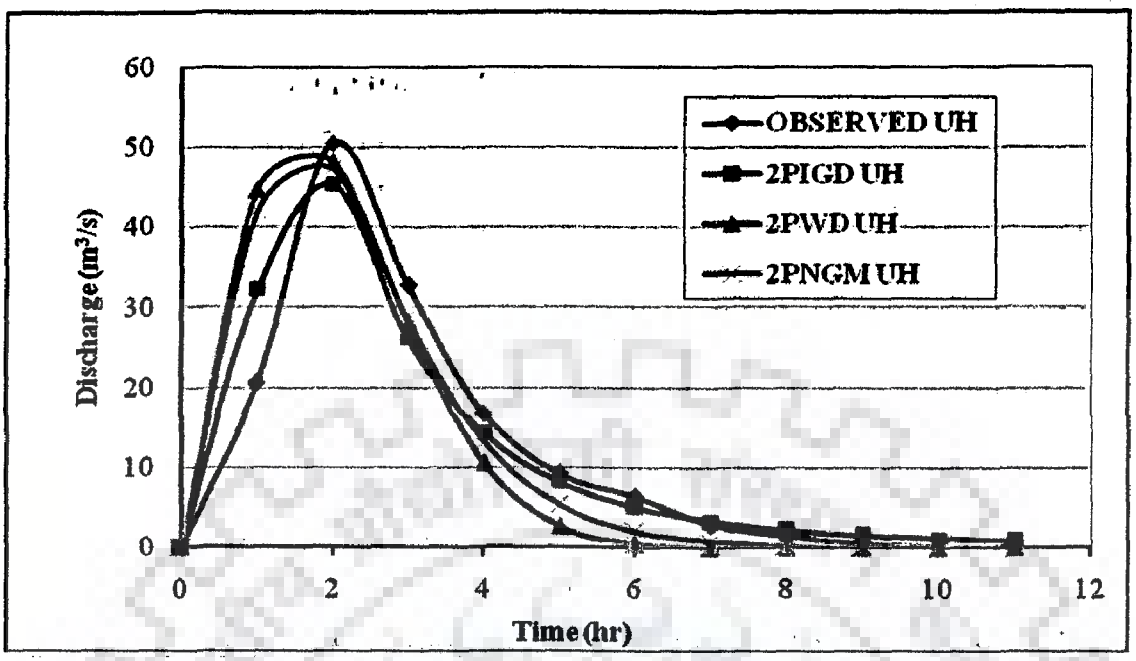

Fig. 5.2c: Comparison between Observed and Computed UHs for Gagas watershed for the storm of June 31, 1982.

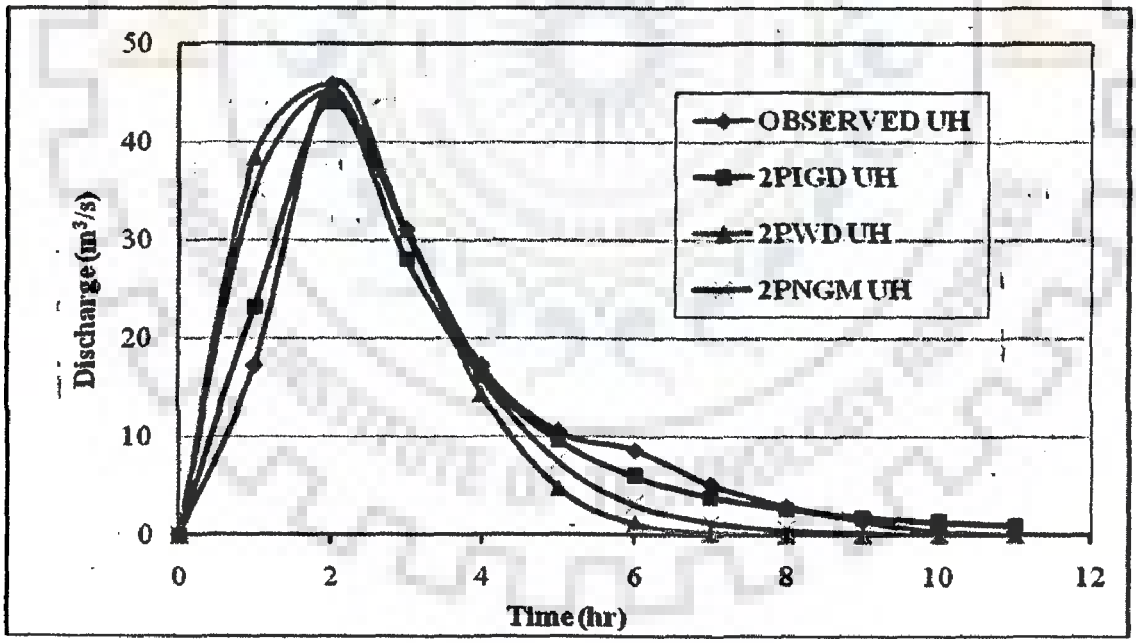

Fig. 5.2d: Comparison between Observed and Computed UHs for Gagas watershed for the storm of August 30, 1984.

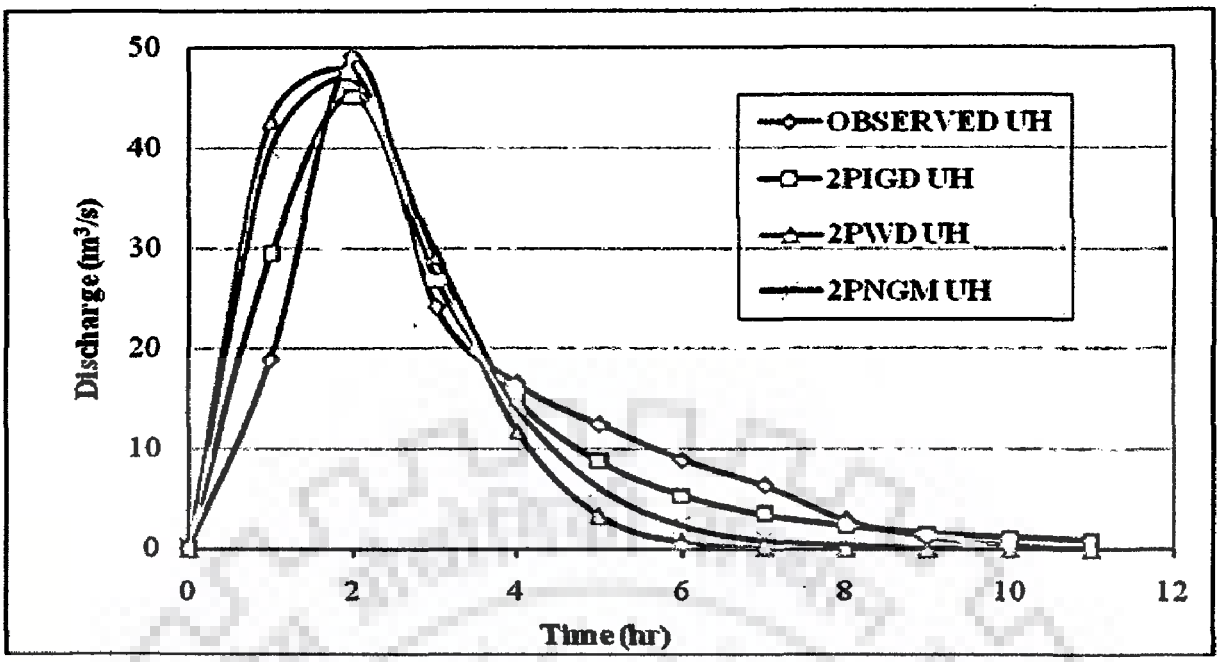

Fig. 5.2e: Comparison between Observed and Computed UHs for Gagas watershed for the storm of August 10, 1985.

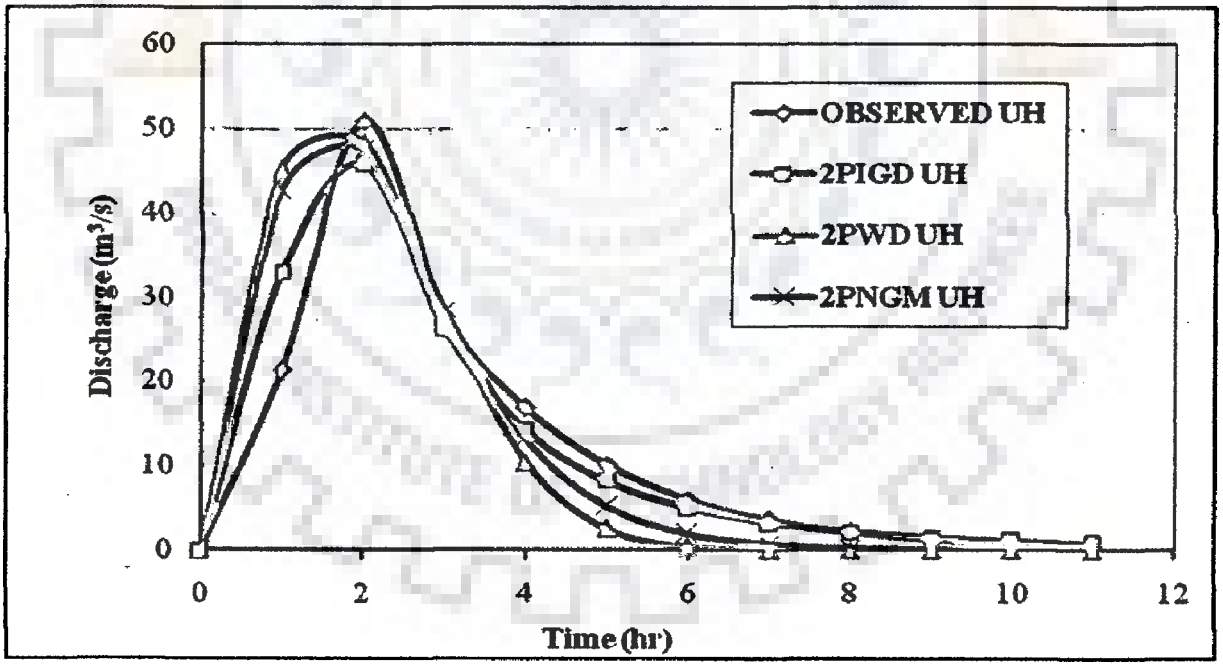

Fig. 5.2f: Comparison between Observed and Computed UHs for Gagas watershed for the storm of August 15, 1985.

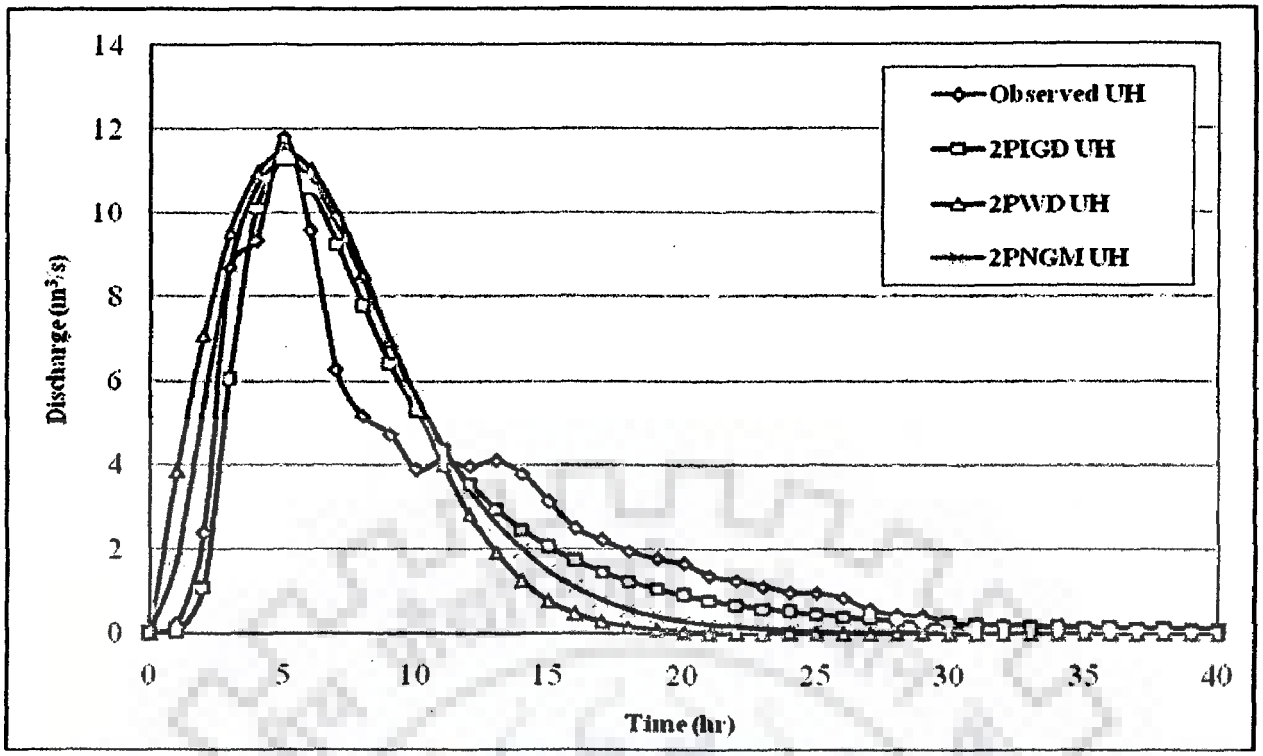

Fig. 5.3: Comparison of observed and computed UHs using three pdfs for Myntdu-Leska watershed.

(iii) Nash-Sutcliffe Coefficient of Efficiency (NSE): It was given by Nash and Sutcliffe (1970) and is given as:

$$NSE(\%) = 1 - \left[\sum_{i=1}^{N} (U_{oi} - U_{ci})^2 \Big/ \sum_{i=1}^{N} (U_{oi} - U_{av})^2 \right] x100 \qquad (5.38)$$

A perfect agreement between observed and estimated values yields the coefficient of efficiency as 100 percent. For a zero agreement, all the estimated values must be equal to the observed mean. A negative efficiency represents that the estimated values are less than the observed mean.

5.6.2 Discussion of Results

The results for the above three goodness-of-fit criteria are given in Table 5.2 for Gagas and Myntdu-Leska watersheds, and depicted in figs. 5.2a-f & 5.3, respectively. It can be observed from Figs. 5.2a-f and Fig. 5.3 that the computed UHs for Gagas and Myntdu-Leska watersheds are well matched, in all three pdfs, with the observed one with respect to peak flow rate, time to peak, time to base, and overall shape of all the storm events. However, the hydrographs predicted by 2PWD and 2PNGM are slightly right skewed in comparison to corresponding observed hydrogrphs for both study watersheds. It can be observed from Table 5.2 that 2PIGD method produces consistently lesser values of STDER than the rest of the two methods for all storm events. Notably, the low value of STDER represents a good fit, and vice versa; and STDER equal to zero represents a

perfect fit. The STDER values are found to vary from 6.31 to 13.75 with an average value of 10.00, from 18.07 to 23.29 with an average value of 20.77, and from 14.87 to 20.09 with an average value of 17.61, respectively for 2PIGD, 2PWD, and 2PNGM methods for Gagas watershed. RMSE value in case of 2PIGD was found considerably low (5.384) in comparison to 2PWD (12.221). The NSE values are found to vary from 92.3% to 98.3% with an average value of 95%, and from 63.7% to 84.8% with an average value of 75%, and from 73.5% to 90.1% with an average value of 82.5%, respectively for 2PIGD, 2PWD, and 2PNGM methods. Low values of REP have been observed due to all three pdfs, however it is interesting that REP slightly better in case of 2PWD than those due to the other two methods. However, RMSE and NSE of 2PWD are high and low, respectively, in comparison to the rest of two pfds. The reason is that the 2PWD is slightly right skewed and therefore over-predicted the ordinates of rising limb and under-predicted the ordinates of recession limb side. Similarly, in case of Myantdu-Leska watershed, 2PIGD yielded the highest efficiency (NSE = 88.9%). However, all three pdfs closely simulate the peak. Moreover, values of all statistical indices (Table 5.2) and visual observation from Figs. 5.2a-f and Fig. 5.3 clearly indicate that the prediction of unit hydrograph by 2PIGD was excellent for both the hilly watersheds. The performance of 2PWD and 2PNGM was however satisfactory.

5.7 APPLICATION TO UNGAUGED WATERSHED

With the encouraging performance of 2PIGD in computation of unit hydrographs for two hilly watersheds, it is further applied to the data of Ramganga watershed considering it to be an ungauged watershed.

5.7.1 Extraction of Geomorphologic Characteristics

To extract the geomorphologic features of the Ramganga watershed, a PC-based GIS and Remote Sensing Software, Integrated Land and Water Information System (ILWIS 3.31) has been used. The DEM of the watershed was extracted form Shuttel Radar Topography Mission (SRTM) data of resolution 3-arc second ($\approx$ 90 m) downloaded from website Global Land Cover Facility (GLCF, 2008) and imported into ILWIS through "import via Geo-gateway". The extracted DEM of the Ramganga watershed is presented in Fig. 5.4. High variability in the elevation, from 338 m to 3088 m (Fig. 5.4), indicated that the Ramganga watershed is a hilly terrain with high steep slopes. Drainage network and subsequent calculation of Horton's ratios (R_A, R_B, and R_L) of Ramganga

Table 5.2: Statistical indices for 2PIGD, 2PWD, and 2PNGM for different in prediction of UH for Gagas and Myntdu-Leska watershed.

Storm Event	2PIGD				2PWD				2PNGM			
	STDER	RMSE	REP (%)	NSE (%)	STDER	RMSE	REP (%)	NSE (%)	STDER	RMSE	REP (%)	NSE (%)
Gagas Watershed												
25-Jun-78	9.89	7.563	6.0	96.3	18.31	15.287	2.0	84.8	15.14	12.347	3.4	90.1
20-Jun-81	6.31	2.797	6.7	98.3	18.07	9.193	2.3	81.6	14.87	7.433	3.8	88.0
31-Jul-82	13.75	4.980	10.1	92.3	23.01	9.172	4.6	73.8	20.06	7.865	6.2	80.7
30-Aug-84	6.53	3.906	4.0	97.3	19.13	12.156	0.6	74.0	15.70	9.899	1.9	82.7
10-Aug-85	11.13	6.558	8.0	92.5	23.29	14.390	3.1	63.7	20.09	12.299	4.7	73.5
15-Aug-85	12.36	6.503	10.3	93.2	22.81	13.128	4.9	72.3	19.82	11.220	6.6	79.7
Average	**9.996**	**5.384**	**7.5**	**95.0**	**20.768**	**12.221**	**2.9**	**75.0**	**17.612**	**10.177**	**4.4**	**82.5**
Myantdu-Leska Watershed												
Bhunya et al. (2005)	**2.34**	**1.01**	**4.7**	**88.9**	**3.43**	**1.71**	**3.2**	**67.8**	**2.79**	**1.33**	**5.0**	**80.4**

watershed is extracted using the module "DEM HYDRPROCESSING" of ILWIS 3.31. However, the user familiarity with the study area is necessary to obtain the realistic drainage network.

Fig. 5.5 represents the drainage network, extracted from SRTM data, of different Strahler order. Consequently, Ramganaga was assigned as fifth order watershed. Maximum length of the river was found 172 km up to outlet of the watershed. The number of streams of different orders, length, corresponding area, and the extracted geomorphologic parameters such as drainage area, perimeter of the basin, length of the basin, maximum and minimum elevations, watershed relief, relief ratio, elongation ratio, mean slope, drainage density, stream frequency, circulatory ratio, farm factor, Horton's bifurcation ratio, length ratio, stream-area ratio, etc. are summarized in Table 5.3.

5.7.2 Derivation of UH Using 2PIGD and Geomorphological Parameters

Unit hydrograph for Ramganag watershed using 2PIGD and geomorphological parameters was computed according to the procedure described above for Gagas or Myntdu-Leska. However, in this case, Ramganga watershed is treated as completely ungauged, unlike Gagas and Myantdu-Leska, for which neither q_p nor t_p were known. Hence q_p and t_p are calculated for various values of dynamic velocities. Using Horton's parameters (R_A, R_B, and R_L), length of the highest order stream L, and dynamic velocity, q_p and t_p can be estimated from Eq. (2.11) and Eq. (2.12), respectively, proposed by Rodriguez-Iturbe & Valdes (1979). However, dynamic velocity can be easily estimated with the help of geometric properties and adopted value of Manning's roughness coefficient of water course. Detail procedure for computation of dynamic velocity is described in the Kumar et al. (2002). Alternatively, this can be taken as the velocity of storms most frequently occurred in the catchment area based on the experience of field engineers. The estimated values of parameters 'a' and 'b' at various flow velocities are given in Table 5.4. Finally, using the estimated values of 'a' and 'b' at different flow velocities 'v', the ordinates of UHs for different velocities were computed using Eq. 5.4 and theses are shown in Fig. 5.6.

5.7.3 Relationship Among Dynamic Velocity, Peak Discharge, and Time to Peak

Using the results obtained from the analysis, simple regression models for q_p and t_p were developed using the GIUH governing equations given by Rodriguez-Iturbe and Valdes (1979) for direct field applications, where only flow velocities are available. Corresponding to different assumed flow velocities, q_p and t_p were calculated using the

Table 5.3: Extracted geomorphological parameters for Ramganga watershed.

Parameters	Value		
Area (km^2)	3134		
Perimeter (km)	379.65		
Length of Basin (km)	173		
Maximum Elevation (m)	3088		
Minimum Elavation (m)	356		
Stream Characteristics			
Order of Stream	**Number**	**Mean length (km)**	**Mean area (km^2)**
1	681	2.17	2.89
2	135	3.45	18.67
3	33	7.28	85.29
4	6	24.13	500.57
5	1	101.15	3134.66
Ratios			
Bifurcation ratio	5.04		
Area ratio	5.45		
Length ratio	2.65		
Drainage density	0.774		
Stream Frequency (km^{-2})	0.273		
Elongation Ratio	0.365		
Circulatory Ratio	0.273		
Farm Factor	0.105		
Shape Factor	9.550		
Compactness Factor	1.913		
Relief ratio (m/km)	15.792		
Drainage texture	2.255		
Length overland flow	0.646		

Table 5.4: Estimated values of 2PIGD parameters at different velocity for Ramganga watershed.

v (m/s)	a (hr)	b	v (m/s)	a (hr)	b
2	59.0499	2.9987	4.5	26.2444	2.9987
2.5	47.2399	2.9987	5	23.6200	2.9987
3	39.3666	2.9987	5.5	21.4727	2.9987
3.5	33.7428	2.9987	6	19.6833	2.9987
4	29.5250	2.9987	6.5	18.1692	2.9987

GIUH governing equations as shown in Figure 5.7. Finally, a linear regression model was fitted to get simple models relating q_p and t_p with dynamic flow velocity, as follows:

$$Q_p = 17.149\ v + 0.1361\ (R^2 = 0.99) \quad (5.39)$$

$$T_p = 29.535\ v^{-1}\ (R^2 = 1) \quad (5.40)$$

where Q_p is the peak flow rate ($m^3/s/mm$), v is the dynamic velocity of flows (m/s), and T_p is time to peak (hours). Based on the velocities, the peak flow and time to peak can be directly obtained. Eqs. (5.39) and (5.40) can be used as a ready reference to field engineers for design of hydraulic structures and flood protection measures.

The practical utility of the above models can be understood as one can directly compute the magnitudes of Q_p and T_p, and hence, the complete shape of UH can be derived utilizing only the dynamic flow velocity of a given channel section at basin outlet. Hence, these linear models can be of immense importance for the field engineers as well as hydraulic engineers for design of hydraulic structures and development of flood prediction and warning systems, particularly for Ramganga watershed.

5.8 SUMMARY

In the present study, the potential of the parametric expressions of two-parameter Inverse Gamma Distribution (2PIGD) was explored for computation of SUH under limited data availability or ungauged conditions. A PC-based GIS and Remote Sensing Software Integrated Land and Water Information System (ILWIS 3.31, 2007) was used for extraction of geomorphological parameters (DEM, drainage network, and Horton's ratios) from easily available and most updated SRTM data. For limited data conditions, UH parameters, e.g. peak discharge or time-to-peak, were determined using Horton ratios through the relationships given by Rodriguez-Iturbe & Valdes (1979). A Simple analytical procedure was suggested for estimation of the distribution parameters of 2PIGD, 2PWD, and 2PNGM, the calculations for which can be performed on simple spread-sheet calculator.

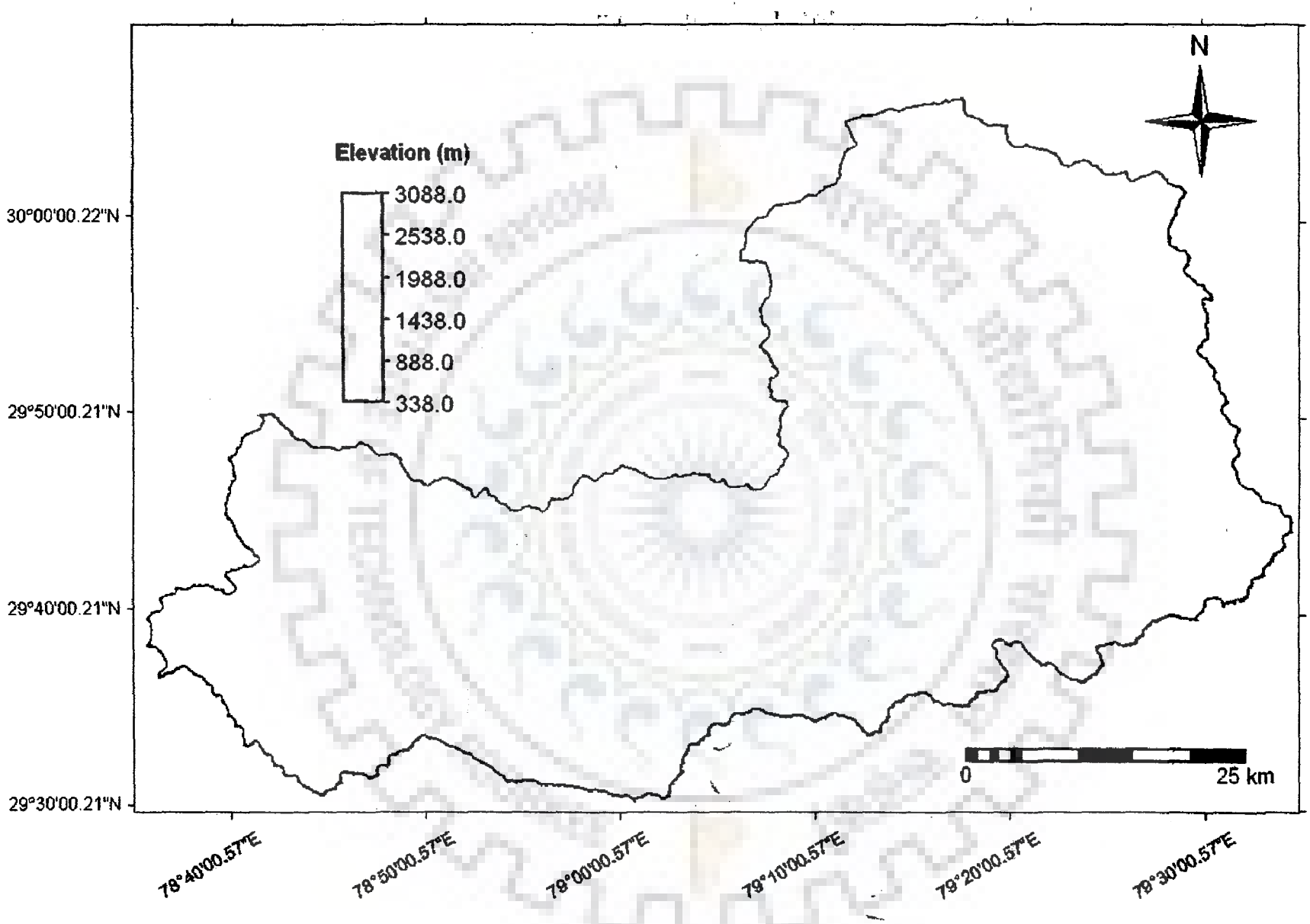

Fig. 5.4: Digital Elevation Model (DEM) of Ramganga watershed extracted from SRTM data.

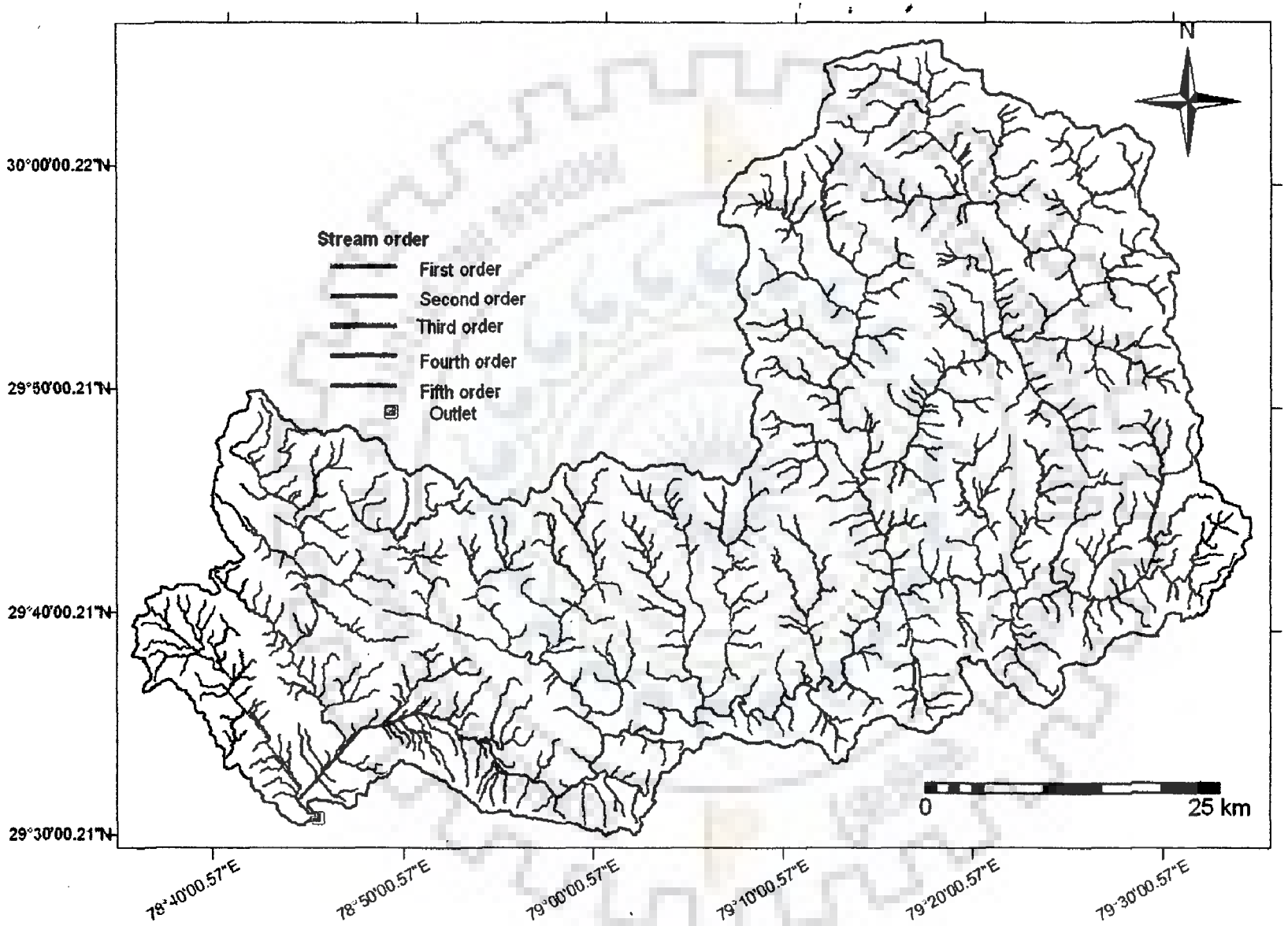

Fig. 5.5: Map showing the drainage line of different Strahler order of Ramganga watershed extracted from SRTM DEM using ILWIS 3.31

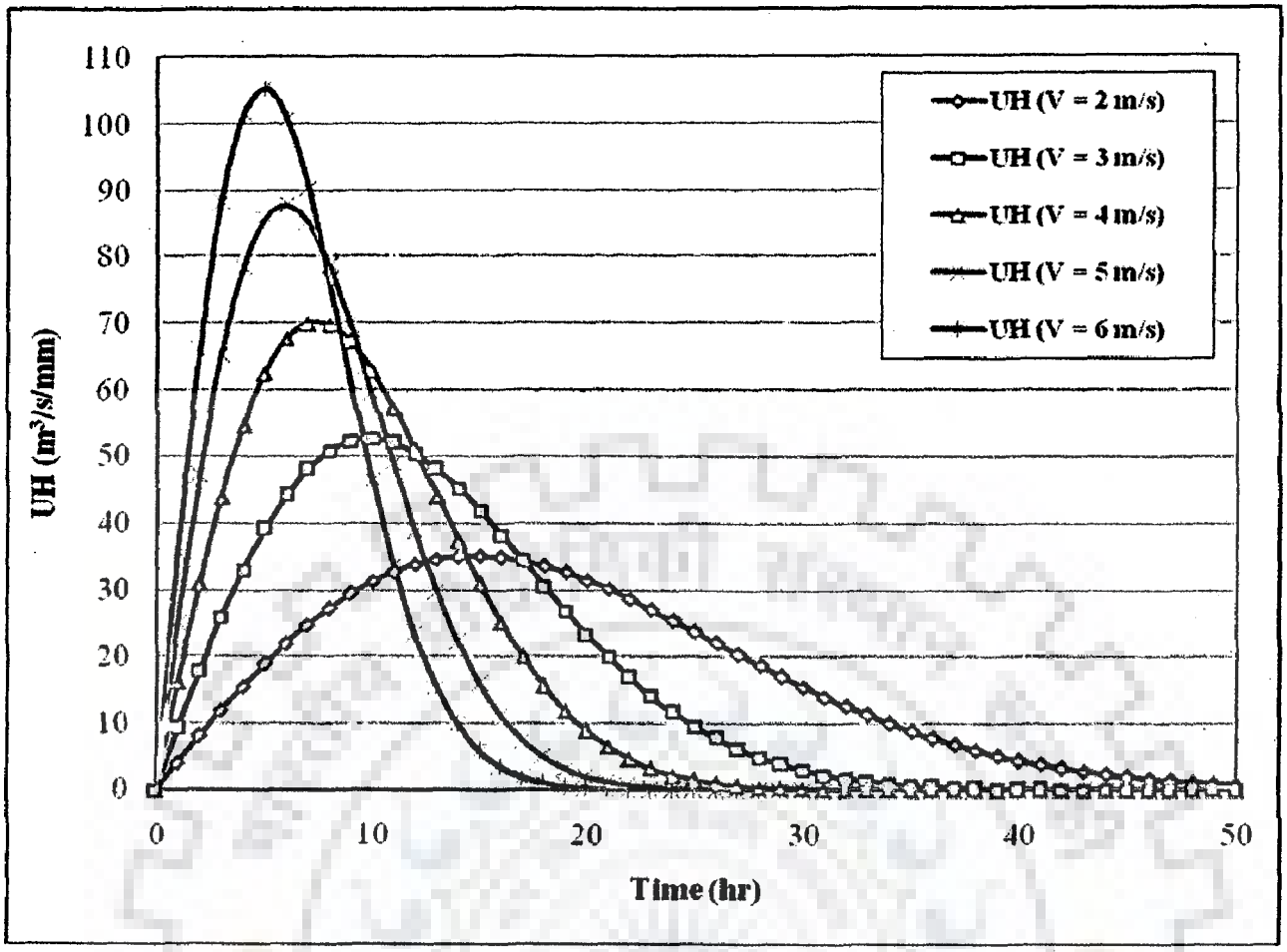

Fig. 5.6: Derived UHs using inverse gamma distribution and geomorphologic parameters for Ramganga watershed corresponding to different flow velocities.

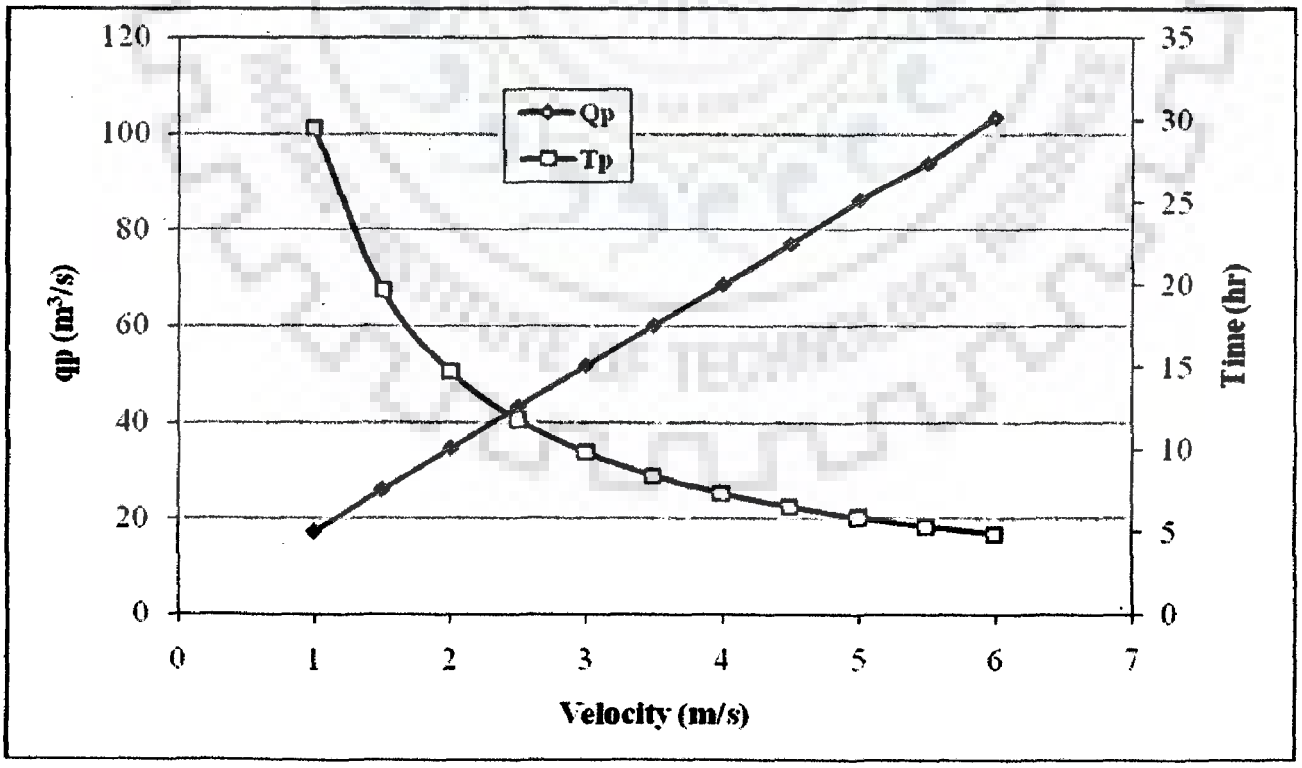

Fig. 5.7: Relation between UH peak q_p, and time to peak t_p with flow velocity v of Ramganga watershed using Inverse Gamma distribution.

Once the parameters are estimated, complete UH shape can be obtained. Finally, the performance of 2PIGD was compared with two parameters Weibull probability distribution (2PWD) and Nash gamma model (2PNGM). Following the visual observation and different statistical error criteria, 2PIGD was found most suitable for two hilly watersheds. However, the performance of 2PWD and 2PNGM was also satisfactory. Inspired from the results of 2PIGD for two hilly watersheds, the proposed methodology was extended for its application to the Ramganga watersheds considering it as an ungagued watershed. Consequently, UHs for various velocities were derived for Ramganga watershed. Based on this analysis, simple regression models for peak flow rate and time to peak flow for a known value of dynamic flow velocity were developed. Such relations can be of immense importance in field for design of hydraulic structures and development of flood prediction and warning systems.

In the next chapter, storm hydrographs for two mountainous watersheds are derived by redefining the Nash Gamma IUH's shape and scale parameters in terms of geomorphological parameters and lag time of watershed using the basic concepts of IUH (Rodriguez-Iturbe and Valdes, 1979, and Rosso, 1984). The developed approach omits the requirement of dynamic velocity parameter which otherwise involves subjectivity.

CHAPTER 6
COMPUTATION OF STORM HYDROGRAPH USING LAG TIME

6.1 INTRODUCTION

To derive the complete shape of the unit hydrogrph a probability distribution can be expressed in terms of its parameters, which can be described by catchmnet morphological parameters. For example, Rosso (1984) derived the Nash parameters 'n' and 'k' in terms of Horton's ratio and a dynamic velocity parameters using power regression. However, the difficulty with the GIUH theory lies in its dependency on a dynamic parameter, velocity. Rodriguez-Iturbe et al. (1982) opined that velocity must be a function of the effective rainfall intensity and duration and proceeded to eliminate velocity from the results. In order to investigate this velocity-rainfall-excess functionality, a study was conducted by Moughamian et al. (1987) for computation of GIUH proposed by Rodriguez-Iturbe et al. (1982). This approach performed poorly compared with the sample distribution even when the rainfall-excess was computed by sophisticated time varying infiltration capacity methods. For estimation of q_p and t_p of GIUH, Sormen (1995) used flow velocities computed by hydraulic approach (Troutman and Karlinger, 1985) and rational approach (flow velocity expressed in terms of effective rainfall intensity and duration (Rodriguez-Iturbe et al., 1982). Sorman (1995) found it to yield reasonable results when applied to the selected storms of Saudi Arabia. According to him, the flow velocity approach is yet to be developed and tested on other experimental basins. Furthermore, Bhaskar et. al. (1997) found that the use of rainfall-excess intensity to estimate flow velocity may lead to inaccurate estimation of peak flow rate (q_p) and time to peak (t_p) of the GIUH. Generally, the flow velocity is overestimated by the rainfall-excess intensity approach which computes smaller value of the Nash parameters 'k' and finally tends to yield higher peaks of hydrographs and corresponding lower times to peak than the observed ones.

Furthermore, manual estimation of geomorphologic parameters is a tedious and cumbersome process and often discourages the field engineers for developing regional methodologies for solving various hydrological problems of the ungauged catchments or in limited data situations. With the advancement in the field of geo-spatial technologies like Geographical Information System (GIS) and Remote Sensing (RS), the automated watershed delineation and drainage network extraction from Digital Elevation Model

(DEM) has gained momentum since last two decades (Tarboton et al., 1991; Moore et al., 1992; Maathuis, 2005; Hengl et al., 2006). Readily available and probably cost free Shuttle Radar Topographic Mission (SRTM) data plays a vital role to extract the catchment's geomorphological parameters for various hydrological applications. Haase and Frotscher (2005) found the SRTM data to be of major relevance for providing terrain information in large and trans-boundary river basins for handling the regional environmental problems and can be applied to meso/macro-scale river network and terrain analysis.

Thus, the present study was carried out to (i) revise and propose a simplified and more versatile GIUH model; (ii) extract more efficient drainage network from SRTM DEM using a raster based GIS software incorporating Melton number concept; (iii) examine the sensitivity of Horton's ratio on stream threshold; and (iv) check the adequacy of proposed model by comparing observed and estimated DRHs for two mountainous watersheds of India, viz., Gagas and Chaukhutia. The results are also compared with the kinematic wave based GIUH model (Kumar and Kumar, 2008) for the Gagas watershed.

6.2 PROPOSED GIUH MODEL

Nash (1957) formulated an IUH in the form of most commonly used two-parameter gamma distribution. The catchment was assumed to be made up of a series of 'n' identical linear reservoirs having the same storage coefficient 'k'. The first reservoir receives a unit volume of effective rainfall instantaneously and it is routed through the first reservoir to the outlet by assuming that the outflow from a reservoir acts as inflow for the next. The Nash IUH can be expressed as:

$$q(t)=\frac{1}{k\Gamma n}\left(\frac{t}{k}\right)^{n-1}\exp\left(-\frac{t}{k}\right) \tag{6.1}$$

where t is in hours and q(t) has the dimensions of hour^{-1}. For estimation of parameters 'n' and 'k', Nash used the first and second order moments of rainfall hyetograph and direct runoff hydrograph, i.e., fully gauged conditions.

The following relationships for 't_p' (or mode of gamma function) and lag time 't_l' (or first moment of gamma function) are valid for the Gamma IUH:

$$t_p = (n-1)k \tag{6.2}$$

$$t_l = nk \tag{6.3}$$

Eqs. (6.2) & (6.3) yield $t_p = t_l (n-1)/n$, indicating that $t_p < t_l$, which is one of the essential conditions of IUH (Subramanya, 1984).

Substituting the value of 't_p' from Eq. (6.2) into Eq. (6.1) results into

$$q_p = \frac{1}{k\Gamma n}(n-1)^{(n-1)} e^{-(n-1)} \tag{6.4}$$

Now, defining a dimensionless term β (= $q_p t_p$) that can obtained by multiplication of Eqs. (6.2) & (6.4) as:

$$\beta = q_p t_p = \frac{(n-1)^{n-1} e^{-(n-1)}}{\Gamma(n-1)} \tag{6.5}$$

Further, in order to link the IUH's peak discharge 'q_p' and time to peak 't_p' with the geomorphological parameters of a catchment, Rodriguez-Iturbe and Valdes (1979) developed functional relationships with dynamic velocity 'v' expressed as:

$$q_p = i * v \tag{6.6}$$

$$t_p = k_1 / v \tag{6.7}$$

where 'i' and 'k_1' depends on R_A, R_B, R_L, and L, expressed as (Rodriguez-Iturbe and Valdes, 1979):

$$i = \left(\frac{1.31}{L}\right) R_L^{0.43} \tag{6.8}$$

$$k_1 = 0.44 * L * R_B^{0.55} R_A^{-0.55} R_L^{-0.38} \tag{6.9}$$

where 'L' is the length of main channel or length of highest order stream in kilometres, 'v' is the average peak flow velocity or characteristic velocity in m/s, 'q_p', and 't_p' are in units of hr^{-1} and hr, respectively. 'R_B', 'R_A', and 'R_L' represent the bifurcation ratio, area ratio, and length ratio, expressed as: $N_w / N_{w+1} = R_B$; $\overline{A}_w / \overline{A}_{w-1} = R_A$; and $\overline{L}_w / \overline{L}_{w-1} = R_L$. N_w is the number of streams of order 'w'; $\overline{A}_w$ is the mean area of basin of order w; and $\overline{L}_w$ is the mean length of stream of order 'w'.

Substitution of i and k_1 from Eqs. (6.8) & (6.9) into (6.6) and (6.7), respectively, yields:

$$q_p = \left(\frac{1.31}{L}\right) R_L^{0.43} v \tag{6.10}$$

$$t_p = 0.44 \left(\frac{L}{v}\right) R_B^{0.55} R_A^{-0.55} R_L^{-0.38} \tag{6.11}$$

Eq. (6.10) and Eq. (6.11) were further re-arranged by Rosso (1984), in which 'q_p', 't_P', 'L', and 'v' are to be measured in coherent units, expressed as:

$$q_p = 0.364 R_L^{0.43} v L^{-1} \quad (6.12)$$

$$t_p = 1.584 \left(\frac{R_B}{R_A}\right)^{0.55} R_L^{-0.38} v^{-1} L \quad (6.13)$$

Further, the multiplication of Eqs. (6.12) & (6.13) results into non-dimensional term β, expressed as:

$$\beta = 0.584 \left(\frac{R_B}{R_A}\right)^{0.55} R_L^{0.05} \quad (6.14)$$

Notably, the expressions derived by Rodriguez-Iturbe and Valdes (1979) assume a triangular IUH and only specify the expressions for the peak value (Eq. 6.10) and time to peak (Eq. 6.11). The major drawback of foregoing method is that it is very difficult and subjective to draw complete shape of IUH, if anybody interested for any reason, using only two salient points, i.e., q_p and t_p.

To overcome the above subjectivity, Rosso (1984) equated both the expression of non-dimensional term β of GIUH (Eq. 6.14) and Gamma IUH (Eq. 6.5) and used an iterative computing scheme to derive the Nash parameters as:

$$n = 3.29 (R_B/R_A)^{0.78} R_L^{0.07} \quad (6.15)$$

$$k = 0.70 [R_A/(R_B R_L)]^{0.48} v^{-1} L \quad (6.16)$$

Remarkably, the dynamic velocity 'v' can vary from storm to storm and even within a storm (Rodriguez-Iturbe and Valdes, 1979). The computation of 'v' involved several parameters like channel slope, Manning roughness coefficient, velocity at different depths, geometric properties of cross-section at gauging site. Hence, the observed value of 'v' is rarely available and an approximate value is taken, in general, based on the experience of field engineers, which often leads to severe error.

On equating Eq. (6.5) with Eq. (6.14) one gets

$$\frac{(n-1)^{n-1} e^{-(n-1)}}{\Gamma(n-1)} = 0.584 \left(\frac{R_B}{R_A}\right)^{0.55} R_L^{0.05} \quad (6.17)$$

All the terms in the right hand side of Eq. (6.17) are known. The only unknown term is the Nash model parameter 'n', which can be obtained by solving it using any suitable optimization scheme such as Newton-Raphson method of non-linear optimization.

Now coupling Eqs. (6.2) & (6.3) and equating the value of t_p with Eq. (6.13) one gets

$$\left(\frac{n-1}{n}\right)t_l = 1.584\left(\frac{R_B}{R_A}\right)^{0.55} R_L^{-0.38} v^{-1} L \qquad (6.18)$$

From Eq. (18), the expression for velocity 'v' can be easily expressed as:

$$v = 1.584\left(\frac{R_B}{R_A}\right)^{0.55} R_L^{-0.38}\left(\frac{n}{n-1}\right)\frac{L}{t_l} \qquad (6.19)$$

Finally, substituting the expression of 'v' (Eq. 19) into Eq. (16) one gets a new expression for k as:

$$k = 0.442\left(\frac{R_A}{R_B}\right)^{1.03} (R_L)^{-0.10}\left(\frac{n-1}{n}\right)t_l \qquad (6.20)$$

Notably, the above expression does not contain any velocity term. Therefore, for the known values of R_A, R_B, R_L, and t_l, the parameters 'n' and 'k' can be computed using Eqs. (6.17) & (6.20), respectively, without knowing the velocity and so forth the complete shape of GIUH for ungauged conditions.

6.3 COMPUTATION OF LAG TIME (t_l)

The concept of lag time, basin lag, and catchment lag is central to rainfall-runoff modelling particularly in context of unit hydrograph concept. Normally, it is a measure of the time elapsed between the occurrence of unit rainfall and the occurrence of unit runoff. Hall (1984) suggested several definition of the time lag, as it can be measured from the beginning of the rainfall, beginning of the runoff, centroid of the total rainfall, centroid of the effective rainfall, or the end of the rain storm to the time to peak discharge, time to centroid of the runoff or time to second point of inflection of the runoff hydrograph.

6.3.1 Limitations of the Lag Time Concept

Various relationships have been developed for computation of lag time by embodying hydraulic length, catchment gradient, drainage pattern, drainage density and other related factors, in overall measures of the response time (Singh, 1990). On the other hand, lag time can be computed analyzing the observed rainfall-runoff data from the catchment. Furthermore, National Resource Conservation Service (previously Soil Conservation Service, SCS, 1972) has suggested different empirical relationships between lag time t_l, time of base t_B, time of concentration t_c, time to peak t_p of a hydrograph. However, in context of GIUH, Singh (2009) emphasized that due care should be taken in computation of lag time using different empirical relationships. SCS (1972) suggested an empirical relationship to compute lag time t_l from time of base t_B of a hydrograph expressed as:

$$t_l = \frac{t_B}{1.667} \tag{6.21}$$

Singh (2009) developed an analytical but an approximate invertible equation to examine the parameters of Gamma IUH in terms of t_l and t_B, expressed as:

$$n = \frac{\ln(1/\varepsilon) - 1}{(t_B/t_l - 1)} \tag{6.22}$$

where $\varepsilon = q/q_p$ is a non-dimensional parameter used for defining time base and generally taken as 0.01, implying that the end of gamma UH is assumed when its ordinates become 0.01 times its peak. Since coupling of Eqs. (6.21) & (6.22) yields a value of n = 5.41 and hence Eq. (6.21) can be used only for those catchments having n=5.41. Similarly, using Eq. (6.22), the empirical relationship $t_l = t_B/3$ as suggested by Nash can be adjudged for the watersheds having n=1.80. Thus, from the above discussions, it can be summarized that the adequacy of the empirical equation, used for computation of lag time by other hydrograph parameters should be tested in mathematical sense so that these equations can be applied for all catchments (i.e. valid for all possible values of 'n').

6.3.2 Lag Time Method

Computation of lag time using storm runoff data can be more realistic owing to the fact that they inherently consist catchment as well as storm characteristics and hence applicable to all values of n (or all catchments). Therefore, in the present study, the distribution hydrograph (Benard, 1935) approach has been used for t_l computation by assuming that runoff hydrograph of at least one event is available. The distribution graph is basically a unit hydrograph whose ordinates are expressed in percentage of the surface runoff occurring in successive periods of equal time interval. Distribution hydrographs were developed using available only storm runoff events for Gagas and Chaukhutia watersheds. The distribution graphs for all storm events for both the watersheds were analyzed and the average cumulative percentage distribution graphs are plotted. Finally, to evaluate t_l, a time value of corresponding 50% runoff volume from cumulative distribution graph was selected and used in this study (Raghuwanshi, 1986).

6.4 DERIVATION OF DIRECT RUNOFF HYDROGRAPH

Once 'n' and 'k' are estimated, the complete shape of GIUH can be estimated using Eq. (6.1), and subsequently, the D-hour UH can be computed from the equation:

$$(D-\text{hour UH}) = \frac{1}{2}\left[(IUH)_t + (IUH)_{t-D}\right] \tag{6.23}$$

If two IUH are lagged by D-hour, where D is small, and their corresponding ordinates are summed up and divided by two, the resulting hydrograph will be a D-hour UH. Finally, the DRHs are computed by convoluting the rainfall-excess with UH.

6.5 DATA PREPARATION AND ANALYSIS

The hydrologic data of storm rainfall-runoff for eight isolated single peaked storms separately for Gagas and Chaukhutia watersheds were obtained from the Divisional Forest Office, Ranikhet, Uttarakhand, India, and used in this study. For computation of geomorphological parameters, the DEMs were obtained from SRTM data having fineness of 3-arc second spatial resolution, downloaded from Global Land Cover Facility (GLCF, 2008). A PC-based GIS and Remote Sensing software: Integrated Land and Water Information System (ILWIS) 3.31 have been used to delineate watershed boundary and extraction of geomorphological parameters of the study watersheds. It is worth emphasizing here that a slight distortion in DEM data can lead to dramatic difference in the resulting hydrological features and hence in the modeled results. Therefore, due care has been taken to make SRTM derived DEMs free from undefined pixels.

6.5.1 Extraction of Drainage Network

In order to delineate the consistent drainage network of the Gagas and Chaukhutia watersheds, the SRTM mosaic were passed through subsequent processes like fill sinks, flow direction, flow accumulation, drainage network extraction, drainage network ordering, catchment extraction, and finally, catchment merge according to the location of outlet of the watershed. All these modules are well embedded in the ILWIS under "DEM Hydro-Processing" operation. However, to schematize and parameterize more realistic drainage network, an adequate value of stream threshold (minimum number of pixels that should drain into a pixel examined to add this pixel to the output drainage map) and minimum drainage length is provided which fully depends on the user's familiarity with the study area. For this study, to examine the most appropriate stream threshold, the Melton (1958) number approach is employed. The Melton number is defined as the stream frequency (stream number per unit area) divided by the square of the drainage density (stream length per unit area). This constant, in fact, relates all the planimetric characteristics of river network structure and universally, it can be assumed to have a value of about 0.694 irrespective of the basin scale (Melton, 1958). An approximation to

the Melton number was also given by Elsheikh and Gurceio (1997) in terms of Horton ratios as equal to $(R_B-R_L)/(R_B-1)$.

To obtain the realistic drainage maps of the study areas from the raster DEM, the drainage network was extracted for different stream thresholds (ranging from 1 to 300 pixels) by following the procedure described earlier using ILWIS 3.31 version and the corresponding Horton ratios R_B, R_L, and R_A were computed graphically by plotting total number of streams, mean stream length, mean stream area versus the order of the channel and finding the slope of the lines. Melton numbers were computed using Horton's ratios for different stream thresholds ranging from 1 pixel to 300 pixels size. Fortunately, at threshold value of 60, the Melton number was found most close to the aforementioned value for both watersheds and its values were 0.662 and 0.676 for Gagas and Chaukhutia watershed, respectively. A good agreement was seen (Figs. 6.1&6.2) when the extracted drainage network (at 60 stream threshold from SRTM DEM) was overlaid on the actual drain map (extracted from toposheets) of the study watersheds. A stream threshold of 60 produced the best results for both the study watersheds. The geomorphological parameters corresponding to this threshold derived from drainage network are given in Table 6.1. It can be observed from Table 6.1 that the values of R_B, R_L, and R_A are 4.81, 2.29, and 5.45, respectively, for Gagas watershed. These values are very close to the corresponding values, i.e., $R_B = 4.82$, $R_L = 2.39$ and $R_A = 5.37$ derived from toposheets and as reported by Kumar and Kumar (2008). Following the same procedure for Chaukhutia watershed as per Melton number, the suitable stream threshold was again 60. At this threshold, the values of R_B, R_L, and R_A were 4.74, 2.21, and 5.49, respectively, for Chaukhutia watersheds. Theses values are also close to the values obtained from toposheets (Table 6.1). Notably, for both the study watersheds, it can be inferred from Table 6.1 that the values of Horton ratios, viz., R_B, R_L and R_A are within the range as suggested by Rodriguez-Iturbe and Valdes (1979) as: $2.5 \leq R_B \leq 5.0$, $3.0 \leq R_A \leq 6.0$, and $1.5 \leq R_L \leq 4.0$.

6.5.2 Sensitivity of Horton Ratios to Stream Threshold

As observed from the aforementioned discussion, the selection of stream threshold has direct implication on Horton ratios and hence it would be rational to perform the sensitivity analysis of these two important parameters. The sensitivity of Horton ratios to the stream threshold is shown in Figs. 6.3 & 6.4 for Gagas and Chaukhutia watersheds, respectively. It is evident from Figs. 6.3 & 6.4 that the three ratios, viz., R_B, R_L, and R_A

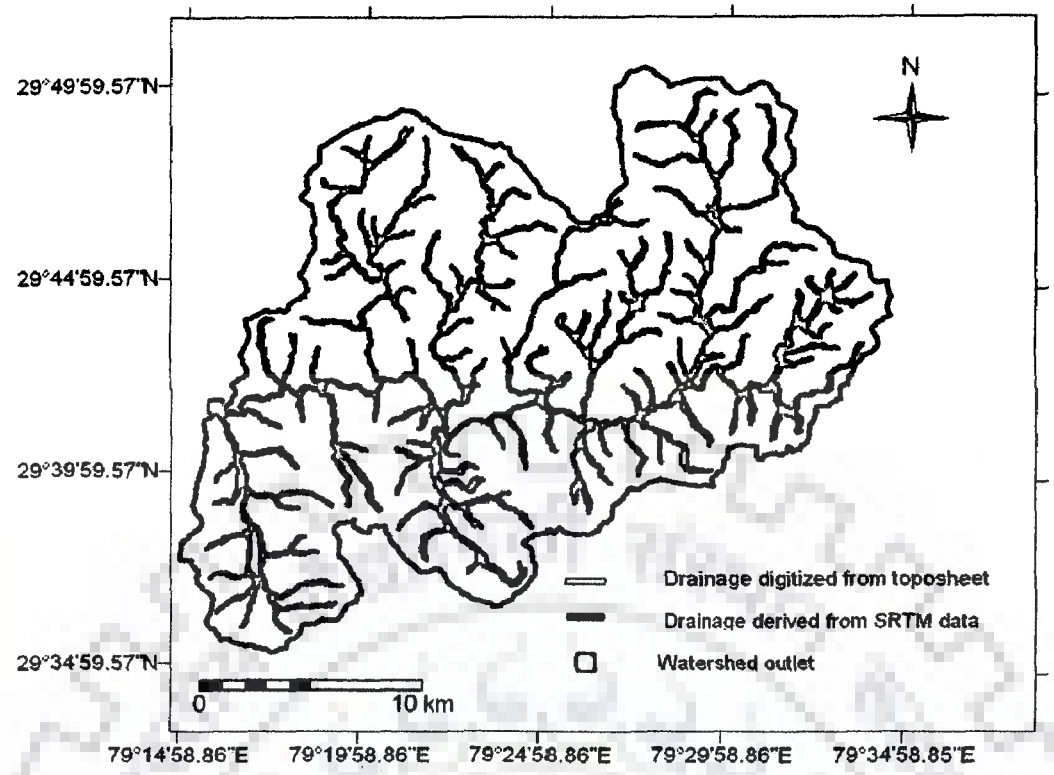

Fig. 6.1: Map showing close agreement of drainage networks extracted from SRTM DEM and toposheets of Gagas watershed.

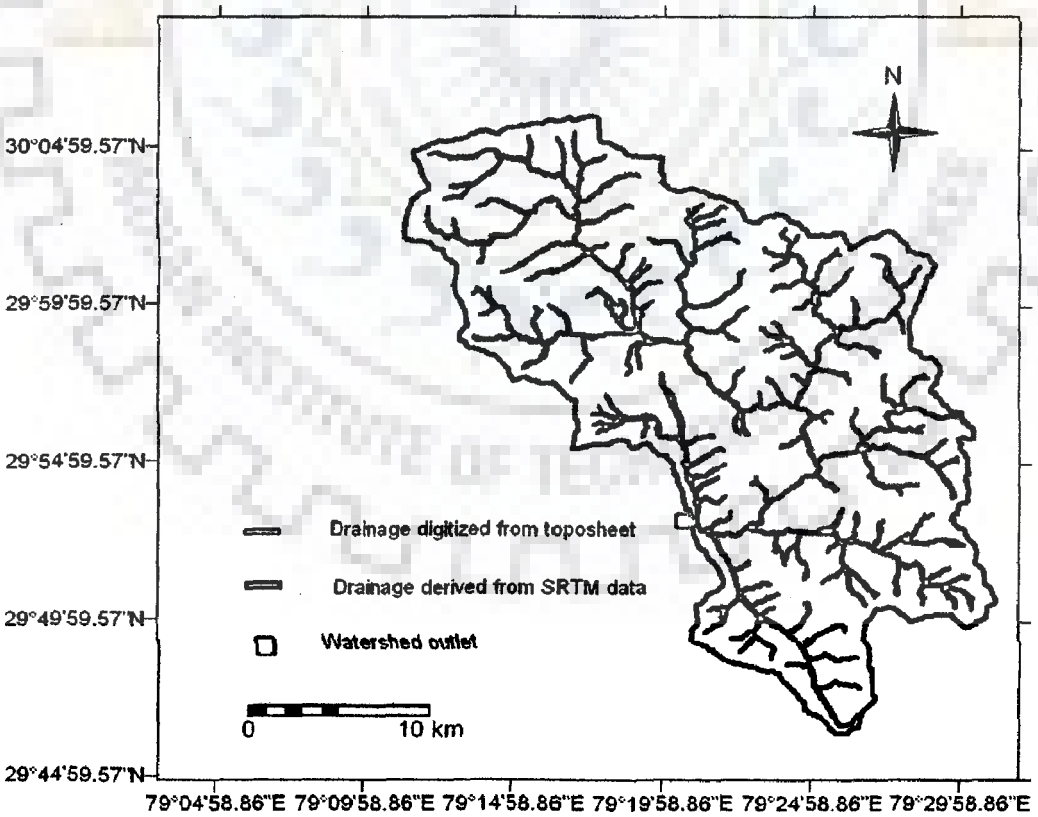

Fig. 6.2: Map showing close agreement of drainage networks extracted from SRTM DEM and toposheets of Chaukhutia watershed.

Table 6.1: Geomorphological characteristics of Gagas and Chaukhutia watersheds extracted from SRTM DEM using ILWIS3.31

Stream Order	Total Number of streams	Mean stream length (km)	Mean stream area (km^2)	Bifurcation ratio (R_B)	Stream length ratio (R_L)	Stream Area ratio (R_A)
			Gagas watershed			
1	123	2.19	2.8			
2	25	3.66	17.45	4.81	2.29 (2.39)	5.45 (5.37)
3	7	5.92	68.76	(4.82)		
4	1	29.42	506			
			Chaukhutia watershed			
1	122	2.14	2.99			
2	22	3.95	21.52	4.74	2.21(2.47)	5.49 (5.73)
3	7	6.89	76.19	(5.04)		
4	1	25.23	571.79			

Note: the values in parenthesis represent corresponding values extracted from toposheets

increases/decreases linearly in similar manner when the drainage network extracted with new value of stream threshold. Further, a break in the continuity of the lines indicates changing of the basin order. It can be observed from Figs. 6.3 & 6.4 that the stream order of Chaukhutia watershed is changing more rapidly than Gagas watershed for same range (1-300 pixels) of stream threshold. This may be attributed to more rapid variations in slope range of Chaukhutia (slope ranges from 0% to 160.1%) than that of Gagas (slope ranges from 0% to 125.5%) watershed which encourages rapid formulations of new drain lines with a change in stream threshold. The values of R_B, R_A, and R_L varied from 4.26 to 6.25, 3.64 to 5.43, and 1.97 to 2.5, respectively, for Gagas watershed and 4.37 to 8.7, 3.88 to 6.93, and 1.75 to 3.59, respectively, for Chaukhutia watershed in the entire range of stream threshold (i.e. 1 pixel to 300 pixels) used in this study. Such kind of wide variation in Horton's ratio shows that stream threshold plays a vital role in extraction of drainage network from SRTM derived DEM. In this context, Melton number would be helpful in deciding the appropriate threshold value.

6.5.3 Lag Time Estimation

Following lag time computation approach as discussed above, the distribution graphs were plotted for Gagas and Chakhutia watersheds and depicted in Fig. 6.5. Consequently, the time value corresponding to 50% runoff ordinate (Fig. 6.5) was 2 hour for Gagas, and 2.2 hour for Chaukhutia watershed, and theses are assigned as lag time or basin lag for respective watersheds. It is worth noting that, in the present study, lag time

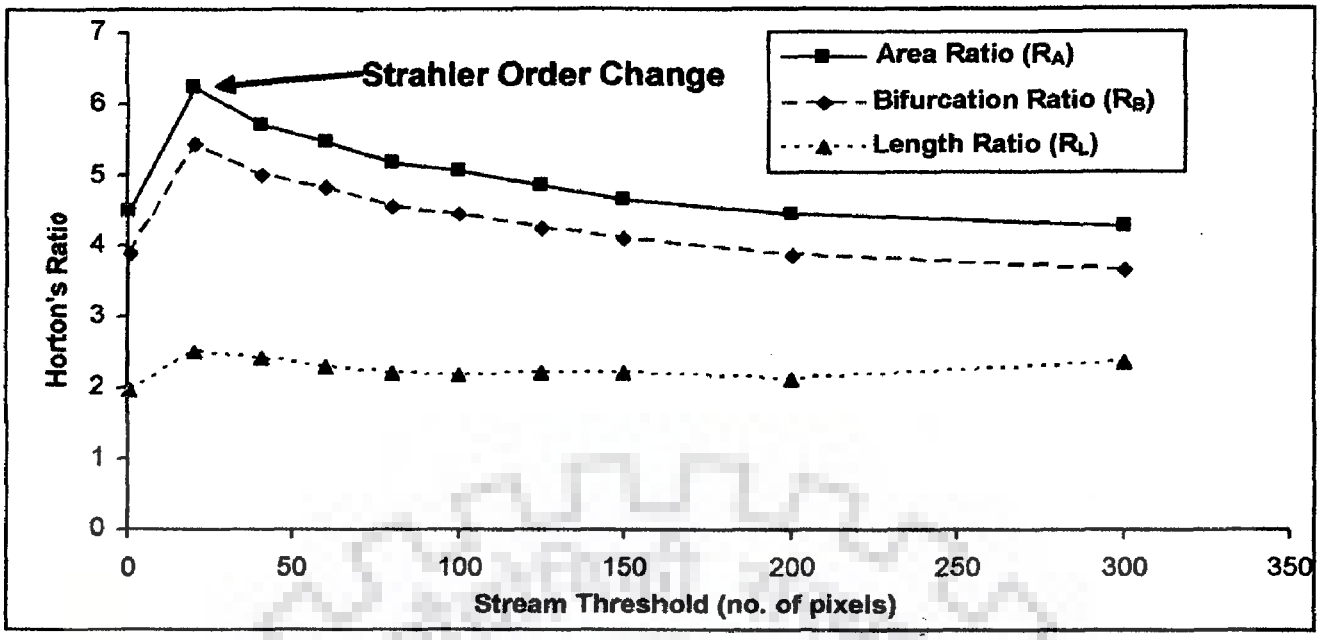

Fig. 6.3: Variation in bifurcation ratio, area ratio, and length ratio with stream threshold for Gagas watershed.

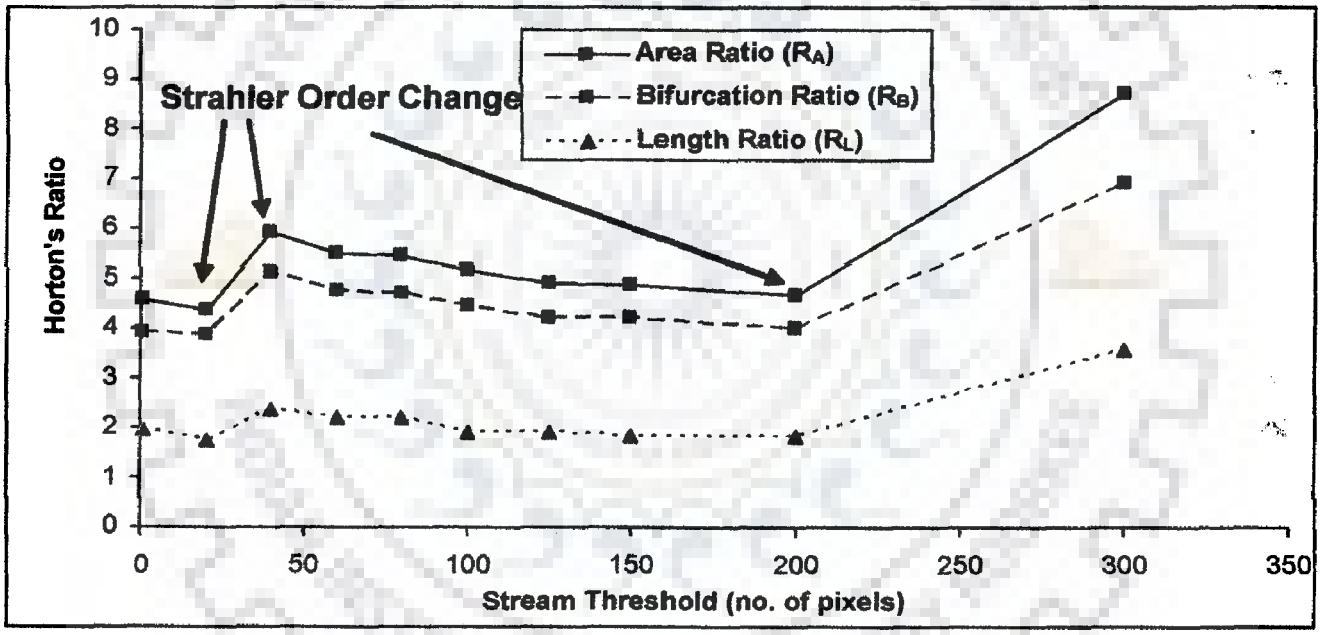

Fig. 6.4: Variation in bifurcation ratio, area ratio, and length ratio with stream threshold for Chaukhutia watershed

was taken as constant considering that peak flow of appreciable magnitude is characterized by a relatively small variability of lag time (Rossi, 1974; Boyd, 1982).

6.6 MODEL PERFORMANCE

The performance of the model is evaluated for two cases: In the first case, the model is applied to the published data of the Gagas watershed, and secondly, the model is further tested for its application to the data of Chaukhutia watershed as discussed below.

6.6.1 Statistical Indices

Four types of statistical indices such as root mean absolute error (RMAE), root mean square error (RMSE), relative error in peak (REP), and Nash-Sutcliffe coefficient of efficiency (NSE) have been used to assess the accuracy of the model for two mountainous watersheds. RMSE, REP, and NSE have been discussed in Chapter 5. However RMAE is discussed as below:

Root Mean Absolute Error (RMAE): It is described as:

$$\text{RMAE} = \frac{\frac{1}{N}\sum_{1}^{N}[U_{oi} - U_{ci}]}{U_{opi}} \tag{6.24}$$

where U_{oi} is the i^{th} ordinate of observed hydrograph, U_{ci} is the i^{th} ordinate of the computed hydrograph, U_{opi} is the peak of observed hydrograph, and N is the total number of hydrograph ordinates.

The results for the above four goodness-of-fit criteria are given in Table 6.2 & 6.3 for Gagas and Chaukhutia watersheds, respectively.

6.6.2 Case 1: Application to Gagas Watershed

Using Eqs. (6.17) & (6.20), the parameters 'n' and 'k' were computed and substituted in Eq. (6.1) to get the complete shape of GIUH. As an illustration, using Eq. (6.23), the corresponding one-hour UH is obtained. Finally, convoluting the unit hydrograph with the rainfall-excess of different eight storm events, the corresponding DRHs were predicted as shown in Figs. 6.6a-h.

From Figs. 6.6a-h, there appears to be a good match between observed and predicted DRHs for all events, specially for time to peak, time base, peak discharge rate and overall shape. The peak discharge is closely predicted by the proposed lag time (LT) method. Different statistical errors, as described above, of the proposed lag time-based GIUH method have been given in Table 6.2. The proposed approach was compared with the GIUH approach based on kinematic-wave (KW) theory and geomorphologic parameters which was applied by Kumar & Kumar (2008) for the same events of Gagas watershed and results are summarized in Table 6.2. It can be seen from this table that both the methods produce almost the same average NSE, RMSE, and RMAE values. However, average peak error in case of the proposed method is 5.5% while it is significantly high, i.e. 14.9% in case of kinematic wave-based method. Furthermore, a sudden jump has been reported in the rising limb which yields high values of RMSE by both the methods.

However, recession limb is closely matching the observed in application of both the methods and it is slightly better due to kinematic wave-based method. Overall, peak discharge and time to peak are two important characteristics of the unit hydrograph theory, and by this way, the simple lag time based method was superior in this study. The prediction accuracy of kinetic wave-based GIUH model depends on the degree of accuracy in adoption of Manning's roughness coefficient for overland and channel flows. Notably, these parameters are very sensitive to peak discharge rate and time to peak of IUH, and therefore, any error in adoption of Manning coefficient directly alters the peak discharge and time to peak, and hence, the complete shape of GIUH and the resulting DRH. High value of NSE (82.9%) and lower values of REP (5.5%) support the suitability and efficacy of the proposed GIUH model for DRH prediction.

6.6.3 Case 2: Application to Chaukhutia Watershed

The model is also applied to eight single peaked isolated storm events of peak discharge ranging from 55 m^3/s to 226 m^3/s of hilly watershed Chaukhutia, a sub-watershed of Ramganga river basin. Similar to the procedure followed for the Gagas watershed, 1 hour-UH was derived for the Chaukhutia watershed, and DRHs computed for all the eight storm events by convoluting 1 hr UH form corresponding rainfall-excess, as shown in Figs. 6.7 a-h. A visual comparison between the observed and predicted DRHs shows that the salient points such as time to peak, peak discharge as well as the complete shape match reasonably well. Further, the goodness-of-fit was evaluated and the results are given in Table 6.3. It can be observed that significantly low values are seen for RMAE varying from 0.067 to 0.091 with an average of 0.084, REP varies from 1.2% to 9.4% with an average of 6%, and RMSE varies from 8.85 to 36.82 with an average value of 16.33. However, the coefficient of efficiency varies from 68.3% to 84.2% with an average of 74.9%.

The results described as above for different storm events from two mountainous watersheds indicated the suitability and efficacy of the proposed simple lag time-based GIUH approach for DRH prediction.

6.7 UTILITY OF THE PROPOSED CONCEPT FOR UNGAUGED WATERSHED

The unit hydrograph derived from lag-time concept is a reflection of integrated effects of all factors responsible for translation of a rainfall hyetograph into hydrograph. Some equations compute the lag time as a constant parameter of the watershed, such as

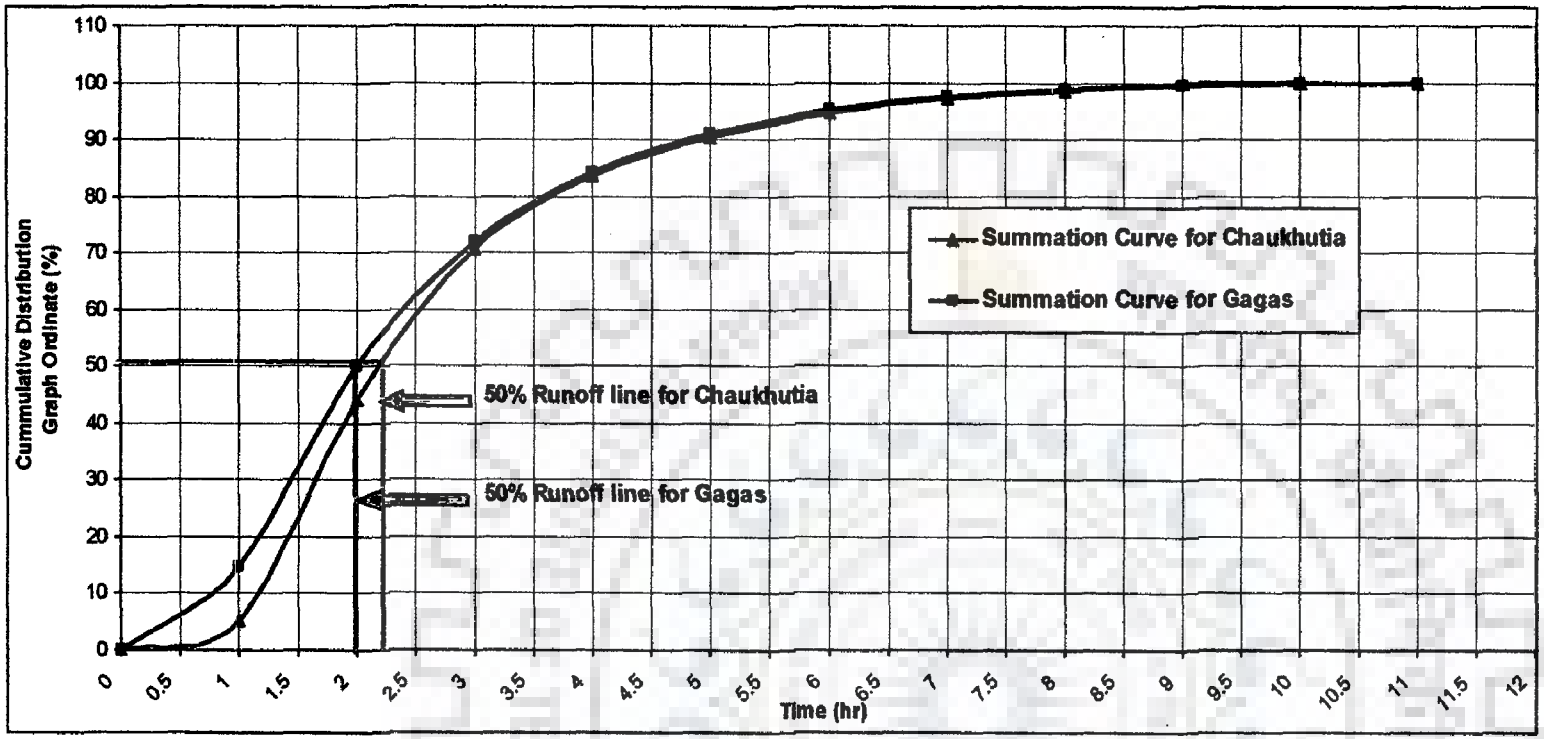

Fig 6.5: Cumulative distributed hydrograph for Gagas and Chaukhutia Watersheds for estimation of lag time.

Table 6.2: Storm-wise statistical measures for prediction of DRHs using proposed Lag Time (LT) and Kinematic Wave-based (KW)(Kumar & Kumar, 2008) GIUH approaches for Gagas watershed.

Storm Date	Rainfall Excess (cm/hr)	RMAE		RMSE (m^3/s)		REP (%)		NSE (%)	
		LT	KW	LT	KW	LT	KW	LT	KW
June 4, 1977	0.208	0.054	0.063	11.364	13.215	1.2	17.3	88.4	84.4
June 25, 1978	0.257	0.076	0.065	14.882	14.875	11.7	8.7	85.6	85.6
June 20, 1981	0.136	0.067	0.065	7.079	7.606	0.3	18.5	89.1	87.4
July 31, 1982	0.111	0.068	0.069	6.631	7.239	0.6	18.8	86.3	83.7
August 11, 1983	0.127	0.068	0.072	7.900	8.718	4.2	21.7	86.2	83.1
August 30, 1984	0.168	0.103	0.083	12.486	11.686	11.3	9.4	72.5	76.0
August 10, 1985	0.178	0.106	0.075	13.289	11.793	10.4	9.8	69.1	75.6
August 15, 1985	0.169	0.073	0.057	10.054	9.886	4.2	14.9	83.7	84.3
Average		**0.069**	**0.077**	**10.627**	**10.461**	**5.5**	**14.9**	**82.6**	**82.5**

Table 6.3: Storm-wise statistical measures for prediction of DRHs using proposed Lag Time (LT) based GIUH approach for Chaukhutia watershed.

Storm Date	Rainfall Excess (cm/hr)	RMAE	RMSE (m^3/s)	REP (%)	NSE (%)
23-Aug-76	0.116	0.085	8.857	5.8	74.5
21-Jun-79	0.146	0.082	11.015	9.4	74.5
31-Aug-80	0.213	0.080	12.652	6.7	84.2
2-Aug-81	0.264	0.086	19.685	4.9	72.8
23-Jul-82	0.165	0.067	10.021	7.9	82.8
5-Sep-83	0.188	0.091	14.279	1.2	68.3
25-Jun-84	0.219	0.089	17.349	7.7	70.3
22-23 Aug, 84	0.484	0.088	36.827	4.3	72.3
Average		**0.084**	**16.336**	**6.0**	**74.9**

the main stream length, and the main stream slope, whereas the other method link the lag time to rainfall intensity as well.

A method for computation of lag time proposed by SCS is described as:

$$t_l = \frac{L^{0.8}(2540 - 22.86 * CN)^{0.7}}{14104 * CN^{0.7} * H^{0.5}} \quad (6.25)$$

where t_l is the watershed lag in hours, L is the hydraulic length measured along the main channel form the outlet to the divide in meters, CN is the runoff curve number, and H is the average watershed slope in meter per meter. The parameters of Eq. 6.25 such as hydraulic length and average slope can be easily computed from SRTM derived DEM. However, CN can be derived from land use map (extracted from LANDSET or IRS satellite images) and soil map easily available throughout the globe.

In Eq. (6.25), all parameters except CN are fixed, and lag time inversely relates with CN. In the present study, lag time was taken as a fix value. However, Eq. (6.25) indicates different values of lag time due to variation in CN for the same watershed. Moreover, at least three values of CN (corresponding to three AMC conditions, if land use and other parameters are assumed unchanged for short duration) can be possible. It is well known that CN is minimum for AMC-I (dry condition) and maximum for AMC-III (wet condition). For AMC-III, CN will be high and hence low lag time (from Eq. 6.25). Consequently, low value of k (Eq. 6.20) and finally results in higher peak discharge (Eq. 6.1). In nutshell, the storm during rainy season (generally AMC-III condition prevailing) exhibit higher peak due to lower value of time lag than those due to non-monsoon storms.

In fact, lag time is a fingerprint of the drainage basin, reflecting the storage and velocity of water in its travel over the basin and down channel. It is clear that the disturbance of the basin surface and its channels will alter lag time. Urbanization tends to speed water downstream by eliminating channel and surface storage and increasing mean velocity in channels. Similarly, forest cutting, overgrazing, channelization, or other basic alterations decrease lag time for the same reasons. Aforestation or soil conservation measures increase lag time. Furthermore, UHs derived from variable lag time concept would be helpful to quantify the effect of urbanization and land use changes on water resources.

6.8 SUMMARY

In this chapter, direct runoff hydrographs of two Himalayan watersheds were derived with high degree of accuracy by redefining the gamma IUH parameters 'n' and 'k' in terms of geomorphological parameters and lag time of watershed. The approach proposed for estimation of parameters is more conceivable than the older one due to elimination of dynamic velocity 'v', which involves greater subjectivity in its estimation in routine applications. The suggested methodology can be used in completely ungauged catchments. A PC-based GIS and Remote Sensing software "Integrated Land and Water Information System (ILWIS)" has been used for extraction of geomorphological parameters from SRTM data with 3-arc second spatial resolution for extraction of DEM, drainage network and geomorphological parameters. Melton number concept was used for extraction of drainage network using "DEM Hydro-processing" module of ILWIS GIS-based software. It is also helpful in drainage network extraction when the toposheets of the study area are not available. To test the applicability of the proposed approach, different isolated rainfall-runoff events belonging to two mountainous watersheds, namely Gagas and Chaukhutia from western Himalayan region of India were considered. Firstly, the approach was applied to eight isolated runoff events of Gagas watershed and results were compared with the observed data as well as the kinematic wave-based GIUH approach. The proposed approach showed better correlation between predicted and observed DRHs than that due to kinetic wave-based GIUH approach for Gagas watershed. Secondly, the approach was applied for estimation of runoff hydrographs for eight storm events of Chaukhutia watershed and found to be in close agreement with the observed. Since geomorphological parameters used in the study were

extracted from the SRTM derived DEM in GIS environment, the model is easy-to-use for any catchment.

Apart from event based modelling, accurate long term simulation of runoff has equal importance in hydrology. The next chapter is dedicated to long-term simulation of runoff from three mountainous watersheds. A radial basis artificial neural network (RBFANN) model is proposed to model the rainfall-runoff process using k-means clustering algorithm.

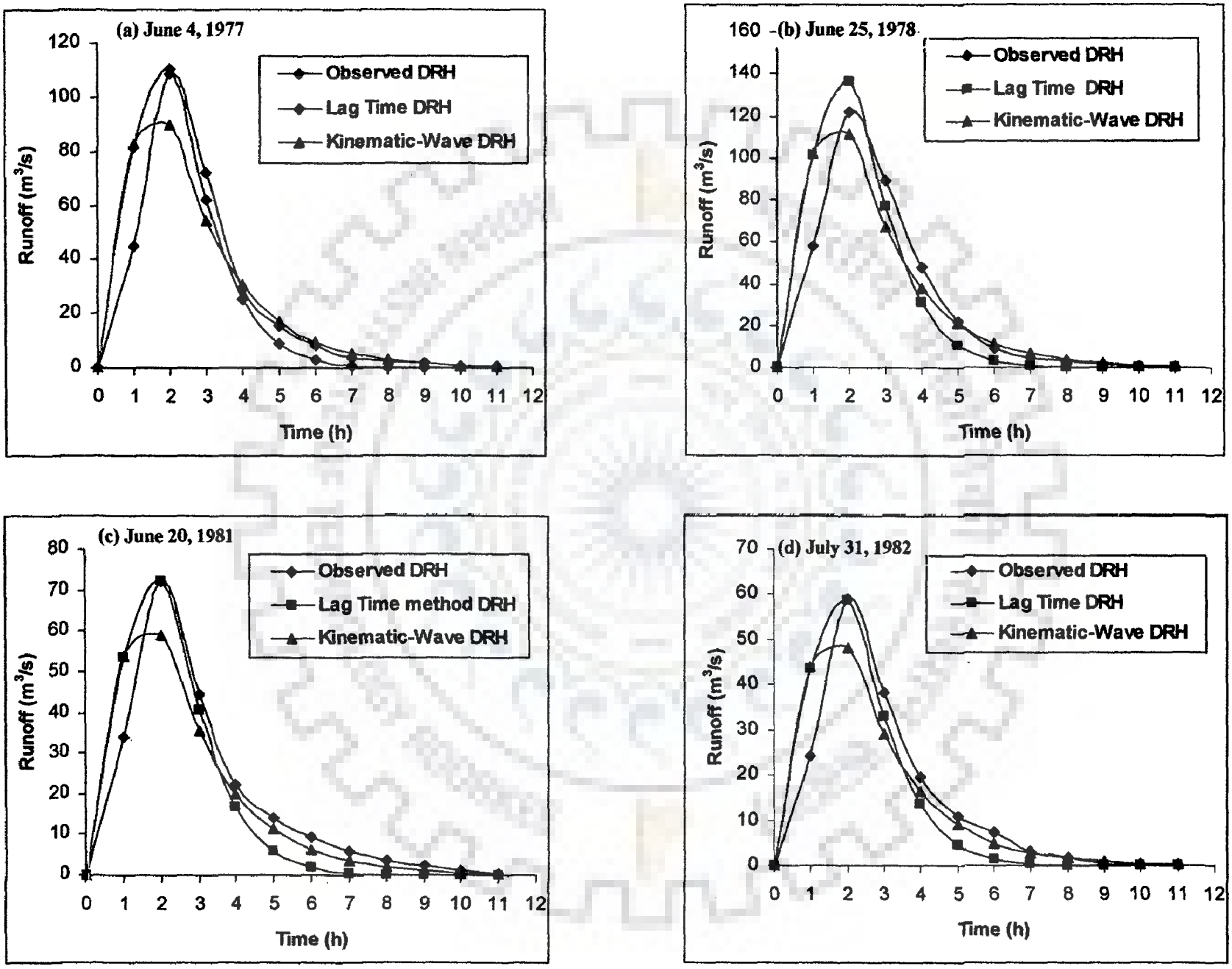

Figs. 6.6a,b,c&d: Comparison of observed and predicted DRHs for Gagas watershed for different storms.

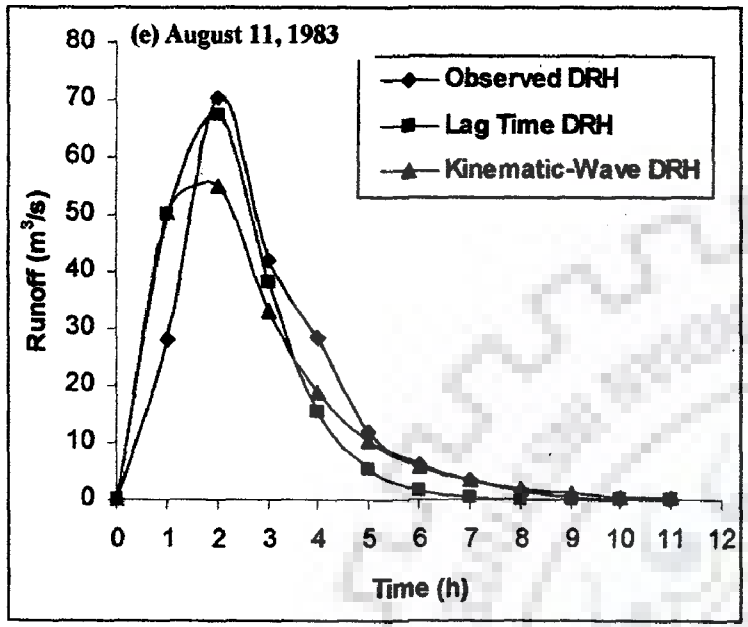

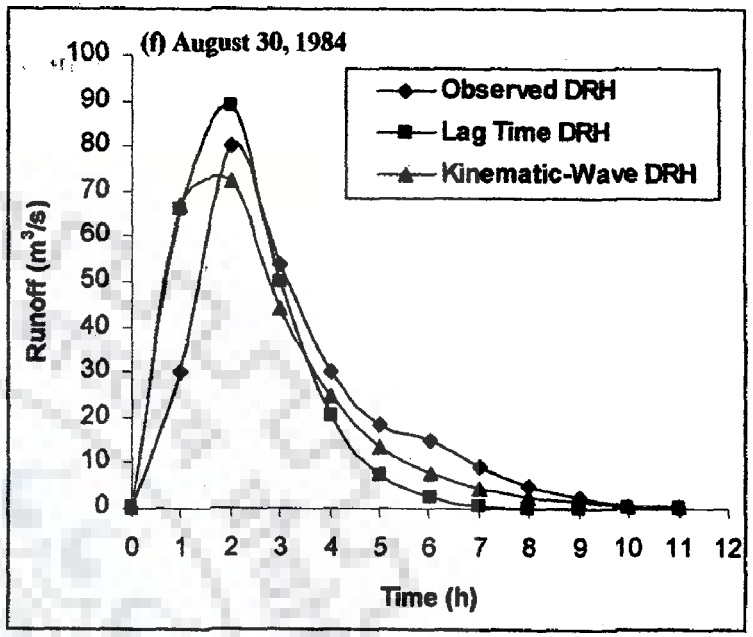

(e) August 11, 1983

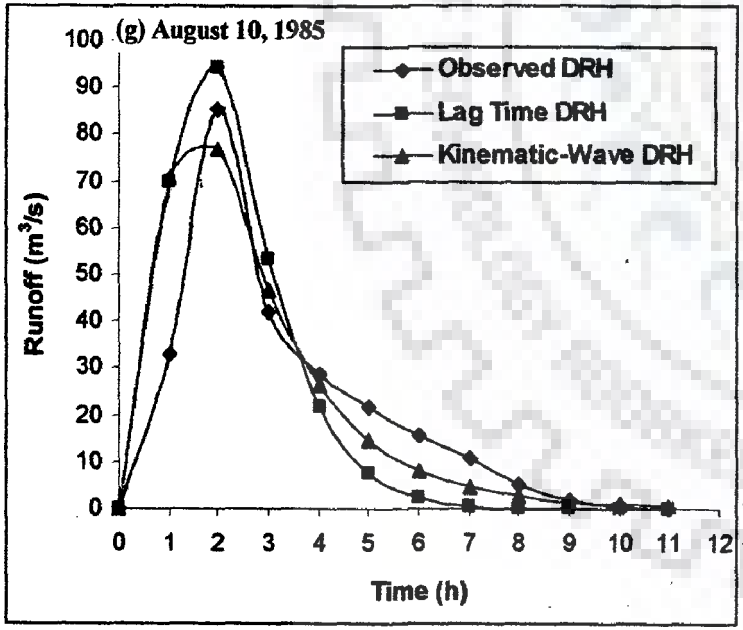

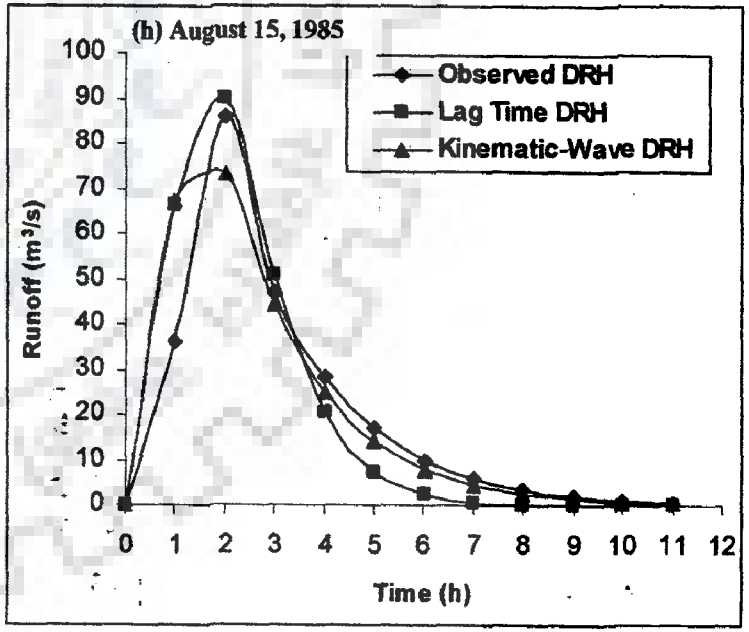

Figs. 6.6e,f,g&h: Comparison of observed and predicted DRHs for Gagas watershed for different storms.

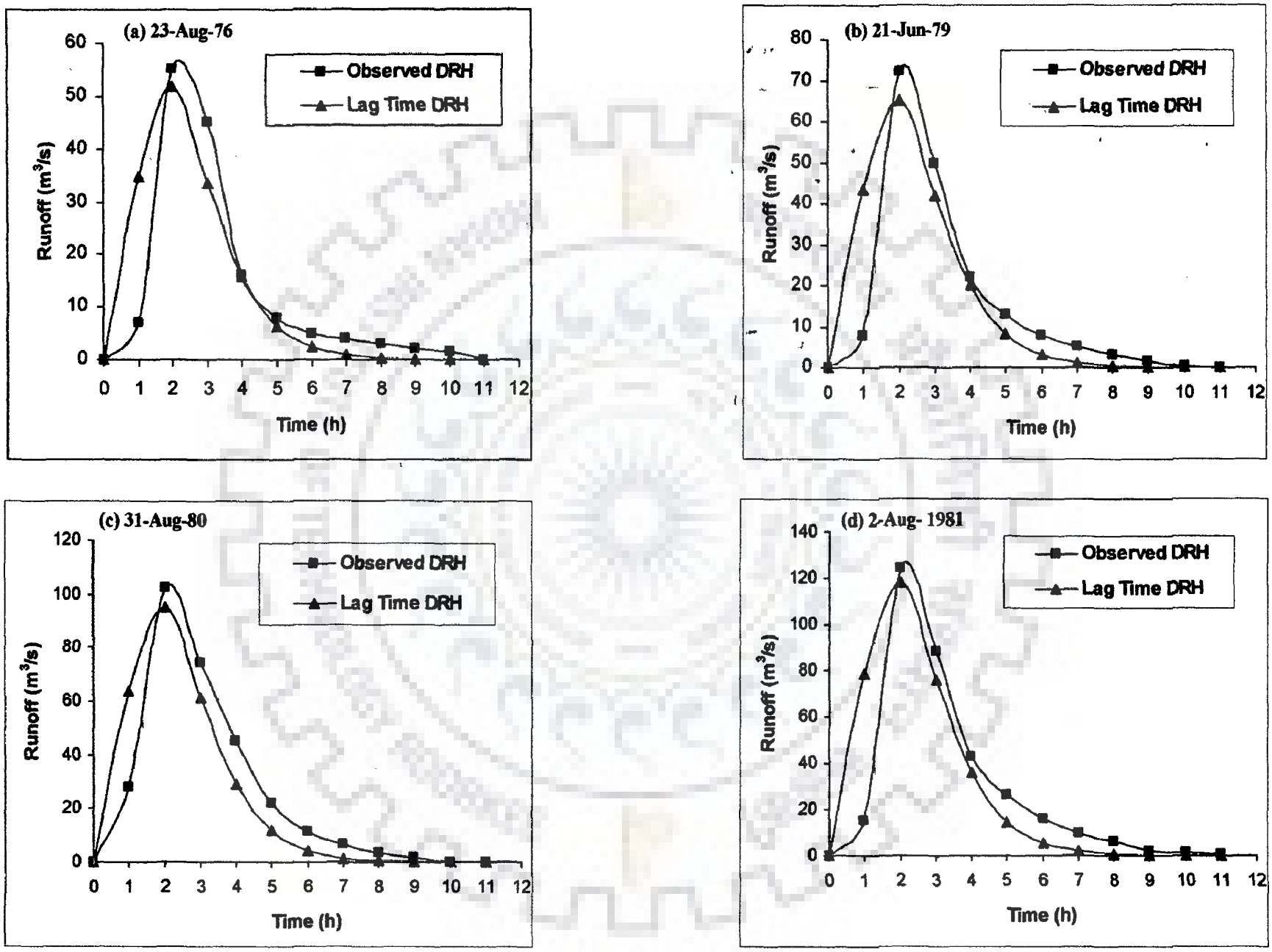

Figs. 6.7a,b,c&d: Comparison of observed and predicted DRHs for Chaukhutia watershed for different storms.

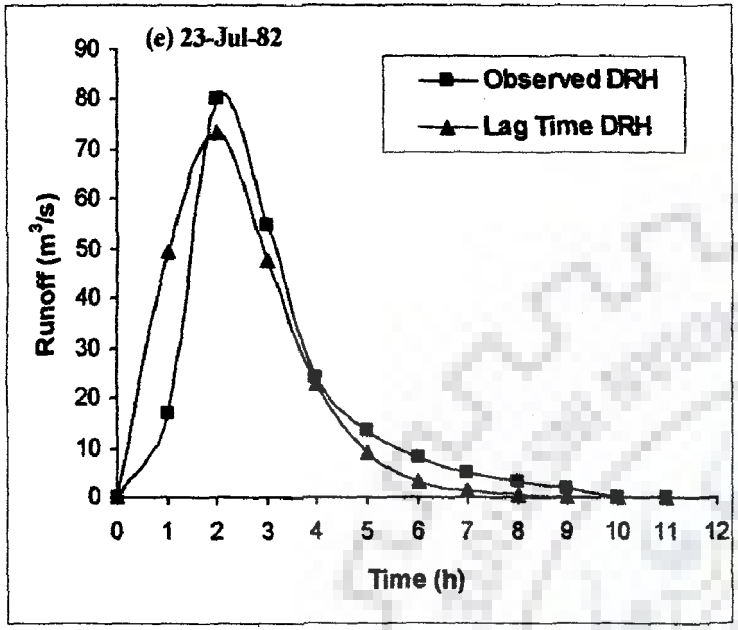

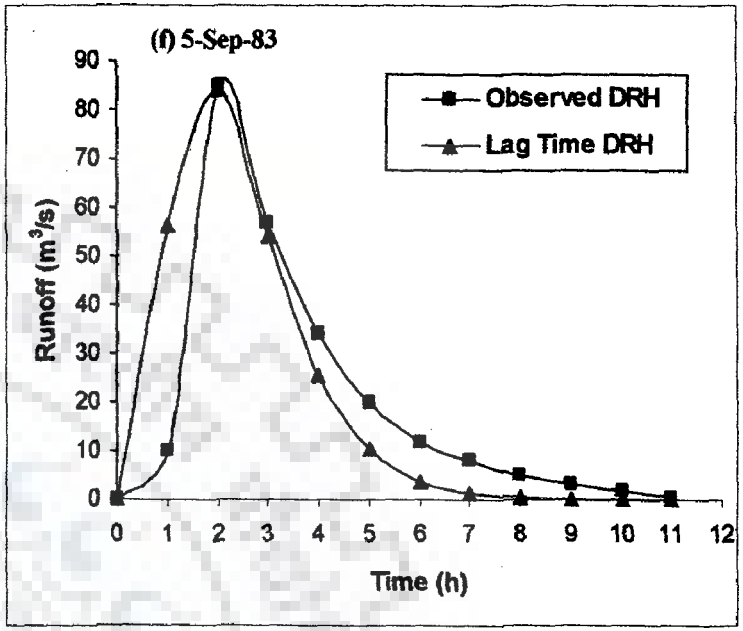

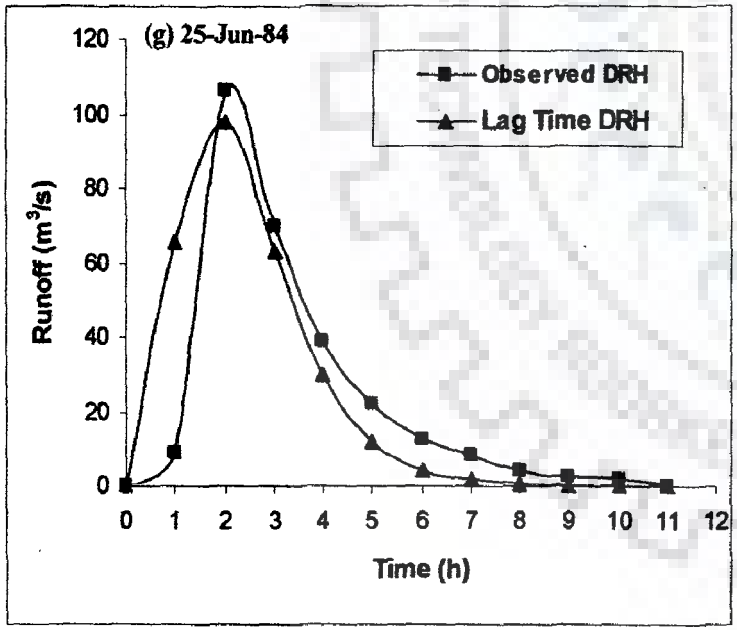

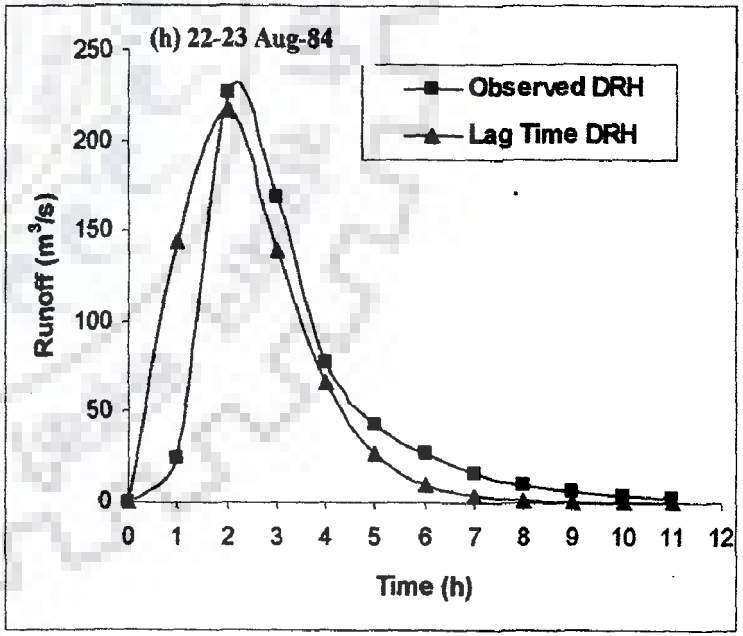

Figs. 6.7e,f,g&h: Comparison of observed and predicted DRHs for Chaukhutia watershed for different storms.

CHAPTER 7
ANN-BASED LONG-TERM RAINFALL-RUNOFF MODELLING

7.1 INTRODUCTION

Artificial Neural Network (ANN) is a black box model that has been applied in several diverse hydrological problems and the results has been encouraging. ANNs are capable to handle nonlinearity of the complex systems to be modeled with flexible mathematical structure along with the activation function. The important characteristics of ANNs include their adaptive nature and learning by examples (Deco and Obradovic, 1996; Haykin, 1999). ANN can find useful relationships between different inputs and outputs without even attempting to understand the nature of the phenomena. ANNs have been applied in hydrological study for rainfall-runoff modelling (French et al., 1992; Shamseldin, 1997; Anwala et al., 2000; Agarwal and Singh, 2004; Chiang et al., 2004; Lin and Chen, 2004; de Vos and Rientjes, 2005); flood forecasting (Fernando and Jayawardena, 1998); ground water modelling (Yang et al., 1997; Krishna et al., 2008); reservoir inflow forecasting (Coulibaly et al., 1998; Jain et al., 1999; Chaves and Kojiri, 2007), suspended sediment estimation (Agarwal et al., 2005; Raghuwanshi et al., 2006); evapotranspiration modelling (Kumar et al., 2002; Sudheer et al., 2003; Jain et al., 2008); and aquifer parameters determination (Rashid and Wong, 1992). The nonlinear nature of the relationship, universal function approximation, robustness, ability to learn, and the complexity of physically based models are some of the factors that have suggested the use of ANN in rainfall-runoff modelling (ASCE, 2000a&b).

Mason et al. (1996) and, Fernando and Jayawardena (1998) found Radial Basis Function ANN (RBFANN) networks to be more effective than the conventional Back Propagation ANN (BPANN) due to less time consuming and faster convergence. Lin and Chen (2004) simulated the rainfall-runoff process in the Fei-Tsui reservoir watershed in northern Taiwan using RBFANN with supervised learning and hybrid-learning, for setting up the number of hidden layer neurons. The fully supervised learning algorithm provided better training and accuracy than the network trained using the hybrid-learning algorithm. Comparatively, the RBFANN network required more hidden neurons but trained faster than the BPANN network. Kumar et al. (2005) fixed the structure of RBFANN networks using an appropriate training algorithm while simulating the rainfall-generated runoff, whereas BPANN networks required a long trial-and-error procedure to

fix the optimal number of hidden nodes. In brief, ANN models have its unique application in water resources and they have been applied in different ways in hydrologic literature.

In this chapter, an RBFANN model was developed using k-means clustering algorithm to model the rainfall-runoff process of three watersheds of Ramganga river basin located in Himalayan region of Uttarakhand State of India. The computer program code was written in FORTRAN environment. The best input combination was decided by cross-correlation matrix method and it consists of rainfall and discharge values. The model has been evaluated for performance through the normally adopted statistical and hydrological performance evaluation criteria, viz., Root Mean Square Error (RMSE), Correlation Coefficient (CC), Coefficient of Efficiency (NSE), and Volumetric Error (EV). In the present study, dynamic approach has been applied for calculation of spread value in radial basis function artificial neural network. The performance of the model is improved by proper selection of suitable learning rates and optimized number of iterations to train the network. The results of the model are compared with the observed runoff values.

7.2 METHODOLOGY

The Radial Basis Function ANN (RBFANN) network has gained popularity and momentum in hydrological science in recent years (Fernando and Jayawardena, 1998; Dawson et al., 2002; Moradkhani et al., 2004). These networks were introduced into the ANN literature by Broomhead and Lowe (1988). Since then several studies indicate the superiority of RBFANN over the BPANN and it is well outlined in the review of literature. Following are the steps involved in the development of RBFANN model.

7.2.1 Network Topology

An RBFANN having input, function, and output layers of nodes with j, i, and k are shown in Fig. 7.1. The structure of RBFANN shows jj-dimensional input pattern (x) being mapped to kk-dimensional output (O). The values j and k are problem-dependent, the value i is to be determined by the network designer. In RBFANN operation, input of nth pattern with each pattern made up of jj variables represents a point in the jj - dimensional input space. It enters the network at the input layer such that one variable is fed into one node. The input layer does not transform the pattern, but it transfers a copy of variables to each node in the function layer. The nodes in each function layer are specified by a transfer function f (d), which radically transforms the incoming

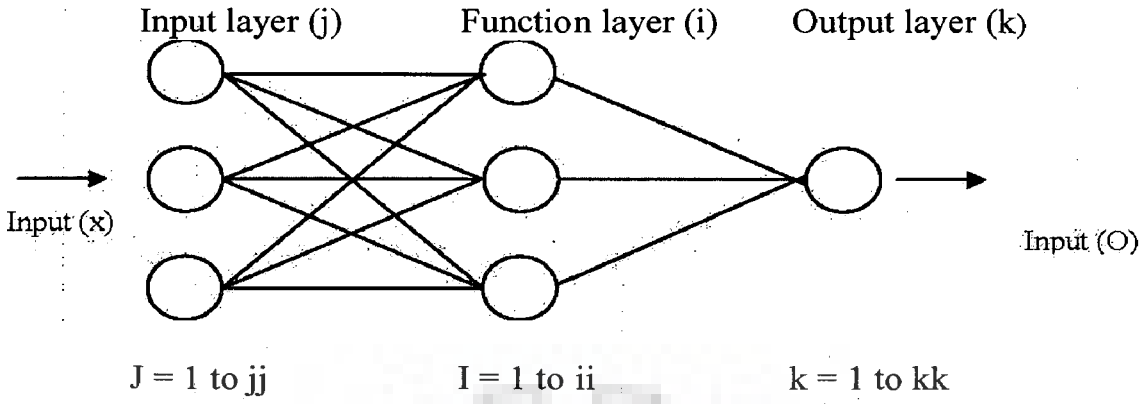

Fig. 7.1: Structure of RBFANN

information. For n input patterns x having jj dimensionality (x^n_{jj}), the response of O_i of function layer, through radial transformation, can be expressed in mathematical terms as:

$$Q_i = f(d) \tag{7.1}$$

where Q_i is the output of function layer and f(d) is a nonlinear function.

7.2.2 Concept of Model Development

For a discrete lumped hydrological system, the rainfall-runoff relationship can be generally expressed as (Hsu et al., 1995).

$$Q_t = f\left[R(t), R(t-\Delta t).....R(t-n_x\Delta t), Q(t-\Delta t).....Q(t-n_y\Delta t)\right] \tag{7.2}$$

where R represents rainfall, Q represents runoff at the outlet of the watershed, f is any kind of model structure (linear or nonlinear), Δt is the data sampling interval, n_x and n_y are positive integer numbers reflecting the memory length of the watershed. ANN architecture clearly shows the network topology with the input determination and the activation function used (Fig. 7.2).

7.2.3 Activation Function

Normally, BPANN uses sigmoid function as an activation function in its hidden layer. But it belongs to the set of monotonic basis and the unit step functions have a slowly decaying behavior in a large area of its arguments. Because of this consequence of using sigmoid function, one needs locally restricted basis functions, such as a Gaussian function, bell-shaped function, wavelets or the B-spline functions. In this study, the Gaussian activation function is selected as activation function (Fig. 7.3). The mathematical structure of this function can be given as:

$$f(d) = e^{-(d^2/\sigma^2)} \quad (7.3)$$

when d = 0, then f(d) = 1, d = ∞ then f(d) = 0. Here, d = eculidean distance and σ = spread. In general, the RBF nodes are locally tuned, i.e. to be active only for a delimited region of the input space. The selected Gaussian function is radially-symmetric with a single maximum at the origin, dropping off rapidly to zero for large distances. Locally tuned receptive fields are widely found in biology, even though they are not single cell properties, but usually emerge from groups of cells.

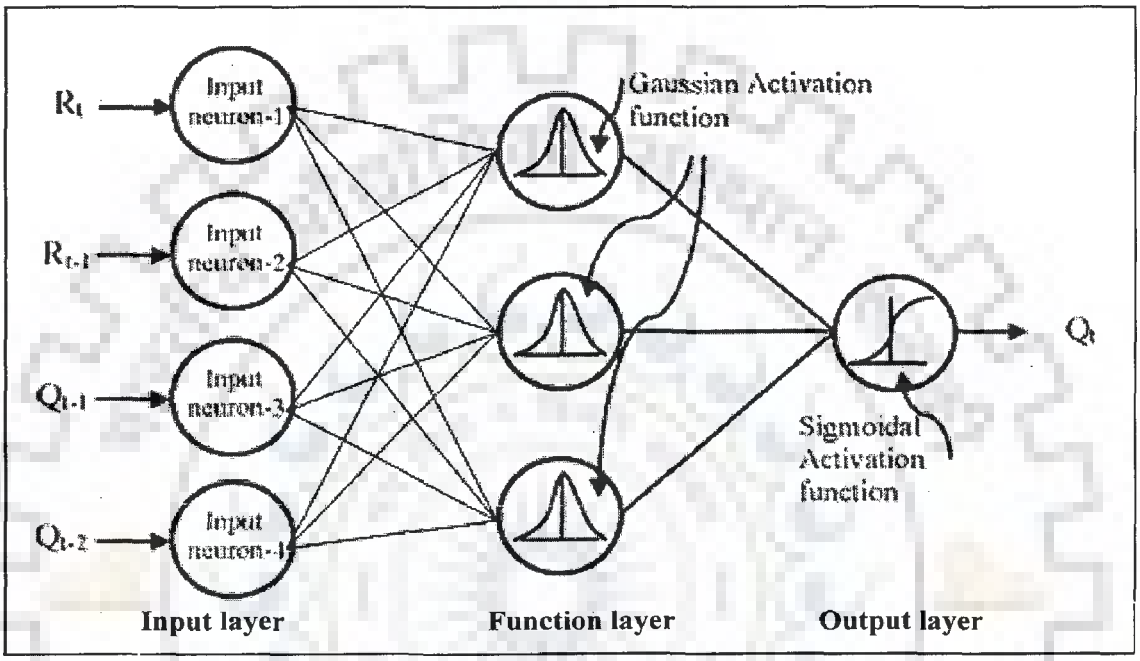

Fig. 7.2: Configuration of an RBFANN with model input.

7.2.4 Euclidean Distance

The euclidean distance 'd' is calculated between the set of inputs and respective center of variable is given as:

$$d_{ij} = \| x_j - c_i \| \quad (7.4)$$

The main objective of the transfer function is to minimize the Euclidean distance to produce the maximum function output.

7.2.5 Determination of RBF Center

Performance of the radial basis function network critically depends on the chosen center. The selection of center could be through an arbitrary selection from the data points of the subset or the mean of data points of the subset or ordinary least square of subset or orthogonal least square of subset. If less data is available, there exists no option to position the centers of radial basis functions at the data points. However, such problems may be ill-posed and lead to poor generalization. If more training data presented, several

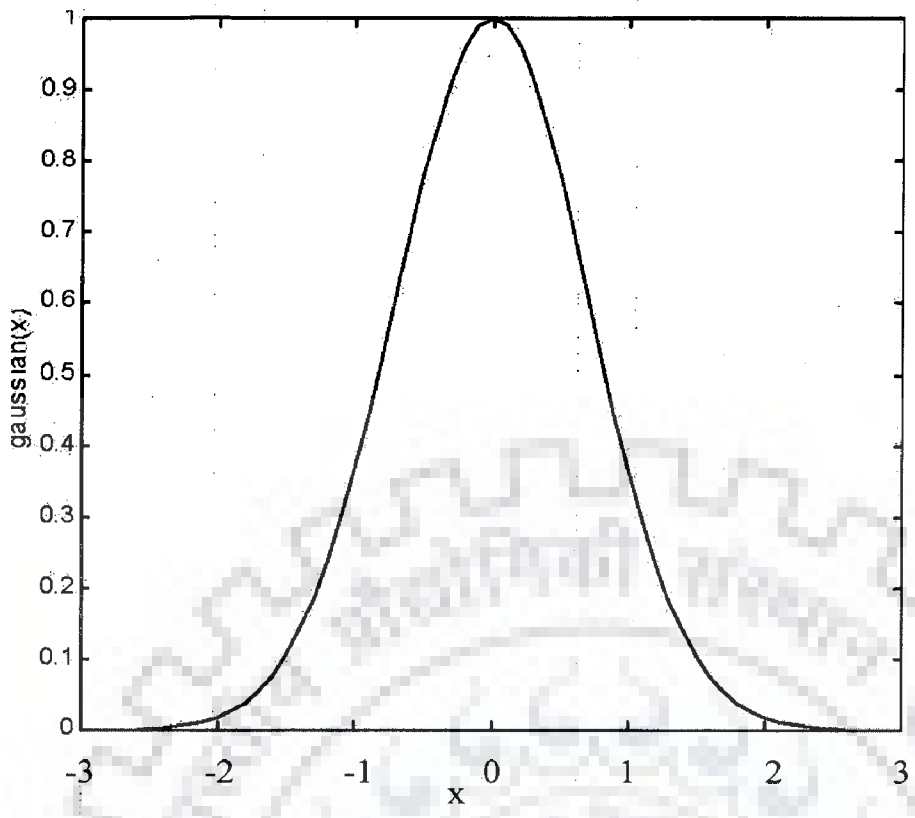

Fig. 7.3: Gaussian activation function.

solutions are possible:

- Randomly select the centers of basis functions from the available training data.
- Following the k-means rule, allocate each point to a particular radial basis function such that the greatest component of the hidden layer's activation comes from a particular neuron.

7.2.6 Estimation of Spread

The function spread around the center determines the ratio of the function decay with its distance from the centre. Based on the spread value used in Eq. (7.3), the model has been separated into two types, static and dynamic. As far as concerned to the spread, the dynamic type of model is more efficient than the static type model. Hence in this study, only dynamic type of spread is being discussed.

In dynamic model, the spread value is calculated from the input pattern. The value changes from pattern to pattern and in successive iterations as well. This model has good flexibility to adapt complex nature of the environment. Based on the data distribution and cluster formation, the model has a choice to activate the cluster which is nearest to the particular instance. In general, hydrological processes are complex and the output from these processes is also complex. The distribution of data is very large and it does not have

a definite boundary. The measure of spread (σ) is commonly described as the average distance between the cluster and training instances (number of input variables) in that cluster.

$$\sigma_i^2 = \frac{1}{M} \sum_{j=1}^{jj} x_j w_{ij} - c_i \qquad (7.5)$$

where M is the number of training instances in that cluster.

Finally, the transformation of information is the response of each function unit and is scaled by its connecting weights to the output units and then summed to produce the overall network output. The overall response of network is calculated by the following equation:

$$O_k = \sum w_{jk} f(d) \qquad (7.6)$$

where w_{jk} is the weight coefficient between $(j)^{th}$ hidden unit and $(k)^{th}$ output unit.

7.2.7 Training Algorithm

Finding the RBF weights is called network training. Using the known input and output dataset (called training set), the optimization of the network parameters fits the network outputs to the given inputs. The fit is evaluated by statistical means such as root mean square error (RMSE), correlation coefficient (CC), and coefficient of efficiency (NSE). In general, two types of learning methods are adopted i.e., supervised learning and unsupervised learning.

In supervised learning, a standard gradient descent procedure can be used. This involves the minimization of an objective function with respect to the actual output. However, such procedures are liable to be trapped in local minimum of the parameter space. In unsupervised learning, k- means clustering algorithm is used. The algorithm k-means (MacQueen, 1967) is one of the simplest unsupervised learning algorithms that solve the well known clustering problem. The procedure follows a simple and easy way to classify a given dataset through a certain number of clusters. The main idea is to define k-centroids, one for each cluster. These centroids should be placed in such a way that different locations yield different results. Therefore, a better choice is to place them as much far away from each other as possible. The next step is to take each point belonging to a given dataset and associate it to the nearest centroid. After grouping all points with nearest centroids, the recalculation of k-new centroid from the previous centroids value is

calculated by initializing suitable weights. All connecting weights adjacent to the winner node are adjusted by making a weight movement proportional to a Mexican hat function (Ralph, 2008). The construction of the Mexican hat function is a second derivative of the Gaussian function (exp-($d^2/2$)).

$$f^{!!}(d) = (d_{ij}^2 - 1) * \exp(d_{ij}^2/2) \tag{7.7}$$

The proportional movement related to the Mexican hat function may be explained with the third derivative of the Gaussian function.

$$f^{!!!}(d) = \Delta w_{ij} = (3d_{ij}^2 - d_{ij}^3) * \exp(d_{ij}^2/2) \tag{7.8}$$

The Mexican hat function has the effect in moving near neighbors close or no movement while neurons slightly away moved closer and the neurons still further away will have their weights moved away from the input space. Based on the change in weight from the Mexican hat function, the move is calculated as follows:

$$move_{ij} = (x_j - w_{ij}) * \Delta w_{ij} * \alpha \tag{7.9}$$

where Δw_{ij} = change in weight and α= learning rate. The new updated weight for the next iteration is

$$w_{ij}(t) = w_{ij}(t-1) = move_{ij} \tag{7.10}$$

As a result of this, the k-centroids change their location step by step until no more changes are done. In other words centroids do not move any more. The influence of activation function decreases according to the euclidean distance from the center. This means that data samples located at a large euclidean distance from the RBF center will fail to activate that basis function. The maximum activation is achieved when the data sample coincides with the mean vector. Finally, this algorithm aims to attain the minimum euclidean distance between the set of inputs and respective center of variable.

Training of weights between the function and the output layer nodes are weighted according to their strengths. The response of the function layer neurons are summed up according to these output layer weights by the nodes in the output layer.

Learning in radial basis network can be divided into two stages. For any iteration, first the learning is carried out in function layer that is followed by learning in output layer. The learning in function layer is performed using unsupervised method, such as the k-means clustering algorithm. While learning in the output layer used supervised methods, such as the initial solution is obtained by this approach, a supervised learning

algorithm (back propagation) could be applied in both the layers to fine-tune the weights of the network as an optional strategy.

7.2.8 Outline of Algorithm (Dynamic Model)

The algorithm of dynamic model can be outlined as follows:

1. Initialize the weights to small random values and take the average of weights for the calculation of center.
2. Select an input pattern (x) from the training set and present it to the network.
3. Calculate the spread value based on the input, weight vector, and cluster center.
4. Find the best matching or "winning" node whose weight vector w_{ij} is closest to the current input vector x using the vector distance (i.e. euclidean distance).
5. Find the network response for the winning node by Gaussian activation function.
6. Update the weight values using Mexican hat function.
7. Repeat steps 1-6 with a number increase in iterations until weights are stabilized.

7.2.9 Normalization of Input Data

Data were normalized (between 0-1) before the start of model training using following equation:

$$x_n = \frac{x_0}{x_{max}} \qquad (7.11)$$

where x_n and x_o represent the normalized and original data, respectively; and x_{max} is the maximum value of the selected variable. After training the network, the de-normalization is performed at the output nodes.

7.3 MODEL EVALUATION

The output from the model was evaluated statistically as well as hydrologically, as follows:

7.3.1 Statistical Evaluation Criteria

The network is trained on the training dataset and its performance is evaluated both in verification and in cross-validation periods following the different standard statistical error criteria. The statistical performance evaluation criteria include root mean square error (RMSE), correlation coefficient (CC), Nash-coefficient of efficiency (NSE). All have been described in Chapter 5.

7.3.2 Hydrological Evaluation Criteria

(a) Volumetric error (EV)

This is also called as absolute prediction error (Kachroo and Natale, 1992) and is estimated as:

$$EV = \left\{ \frac{\sum_{i=1}^{n} (\bar{y}_i - y_i)^2}{\sum_{j=1}^{n} y_i} \right\} x100 \qquad (7.12)$$

where y_i is the observed runoff in m^3/s , $\bar{y}$ is the mean observed runoff in m^3/s, $\hat{y}$ is the estimated runoff in m^3/s, and y is the mean of estimated runoff in m^3/s. This is mainly used to represent error in peak observation, error in low observation, and error in time to peak.

7.4. RESULTS AND DISCUSSION

The proposed model was applied to the data of three watersheds of Ramganga river basin. The fourteen years daily rainfall-runoff data of monsoon period (June to September) for the years 1974-1988 (except 1984), 1974-1987, and 1979-1992, were used for rainfall-runoff modelling of Naula, Chaukhutia, and Ramganga, watersheds, respectively. The data from 1974 to 1979 were used for calibration whereas the data from 1980 to 1983 and 1985 to 1988 were used for cross-validation and verification, respectively, for Naula watershed. However, the data from 1974 to 1979 for calibration and the data from 1980 to 1983 and 1984 to 1987 were used for the cross-validation and verification, respectively, for Chaukhutia watershed. In case of Ramganga watershed, data from 1979 to 1984 were used for model calibration whereas the data from 1985 to 1988 and 1989 to 1992 were used for cross-validation and verification, respectively.

7.4.1 Proposed Model

The RBFANN model is trained by both k-means clustering algorithm and gradient descent algorithm employing the best trained input to the network which consists of daily rainfall and discharge values. Considering different inputs, the following model is finalized using correlation matrix method, maintaining the parsimony of the model for all three study watersheds:

$$Q_t = f[R_t, R_{t-1}, Q_{t-1}, Q_{t-2}] \qquad (7.13)$$

where Q_t represents the runoff at time (t) and R_t represents rainfall at time (t). In this study, the dynamic RBFANN model is developed based on the criteria to estimate spread. The spread value is described as the average distance between the cluster center and training instances (number of input variables) in that cluster. In dynamic model, the value of spread is estimated using Eq. (7.5).

Learning rate for models is selected in such a way that it should increase the convergence ability of the network. The learning rate cannot be negative because this would cause the change of weight vector to move away from ideal weight vector position. If the learning rate is zero, no learning takes place and hence the learning must be positive. In this study, the learning rate in the function layer (ALR) and learning rate in output layer (ALRG) has been selected according to network behavior. The program code was developed in FORTRAN environment for the dynamic RBFANN model. The program code was developed with the objective that a user can alter the program for different conditions and can see the network behavior. This is the major advantage of this model. However, in already developed MATLAB RBFANN models, such a change is difficult.

7.4.2 Application

In the proposed dynamic RBFANN model, the spread value changes in successive iteration, and therefore, not required to be fixed; and two different values of learning rate have been used as ALR in unsupervised part and ALRG in supervised part. To optimize learning rate and the number of iterations, first ALRG and number of iterations were kept fixed and varied the ALR value. Based on experience and from literature, initially the value of ALRG and number of iterations were taken as 0.5 and 1000, respectively (Agarwal, 2002). After getting the best ALR value, ALRG was optimized for fixed ALR and the number of iterations. After optimizing the ALR and ALRG, the number of iterations were evaluated to get the best performance of the model. To ensure the proper selection of ALR, ALRG, and the number of iterations from lower network to higher network, three network structures (4-4-1, 4-16-1, and 4-32-1) are selected. In this study, particular values of ALR, ALRG, and the number of iterations have been optimized through the network behavior for three selected study watersheds.

(a) Naula watershed

The model performance for different ALR values and three different networks for fixed ALRG (= 0.5) and iterations (= 1000) was evaluated. The results are presented in

Table 7.1. The model performance improves rapidly when ALR increases from 0.5 to 20 in calibration, cross-validation, and verification for network (4-4-1). The volumetric error increases as ALR deviates from 20 either higher side or lower side. Thus, ALR = 20 is suitable for network (4-4-1). From Table 7.1, it can be seen that the values of CC and NSE decrease and RMSE increases as ALR increases beyond 20 in calibration and cross-validation for network (4-16-1). The volumetric errors are quite low when ALR = 20 rather than ALR value differs from 20, and hence the model performed best at ALR = 20. For network (4-32-1), NSE tends to decrease as ALR other than 20 in calibration, cross-validation, and verification. Low value of volumetric error in calibration and cross-validation suggests that the most suitable value of ALR is 20.

After fixing ALR at 20, learning rate in the output layer (ALRG) was assigned. To this end, different values of ALRG varying from 0.5 to 10 were tried and the results are given in Table 7.2 for all three networks. As seen from the table, the model performance does not improve significantly when ALRG ranges from 0.5 to 10. The error in volume however slightly fluctuates with ALRG. A lower value of ALRG may be selected (i.e. 0.5) for lower network (i.e. 4-4-1). Selection of a higher value does not justify if similar model performance can be achieved using a lower value. Therefore, ALRG = 0.5 is suitable for network 4-4-1. Similarly, RMSE, CC, and NSE do not change significantly with ALRG varying from 0.5 to 10 for network (4-16-1) (Table 7.2). The resulting EV however fluctuates with ALRG variation and it considerably increases specially in cross-validation when ALRG is varied from 2 to 10. Therefore, ALRG should lie in the range of 0.5 to 2. It is seen from Table 7.2 that RMSE, CC, and NSE values are almost the same for different ALRG values ranging from 0.5 to 10 for network 4-32-1. But at the same time, error in volume gradually increases with increase in ALRG form 0.5 to 10. It follows that ALRG equal to 0.5 is most suitable for network 4-32-1. The value of ALRG = 0.5 is also supported by the literature (Agarwal, 2002) to run the model in the range of all networks selected for the study.

Fixing ALR = 20 and ALRG = 0.5, the initial selection of the number of iterations is rechecked. To fix the optimum value, the number of iterations in different runs for three networks (4-4-1, 4-16-1, and 4-32-1) were varied from minimum (100) to maximum (10000), and the results are given in Table 7.3. It is evident from Table 7.3 that CC, and NSE values are considerably increases while RMSE decreases up to 1000 number of iterations for network (4-4-1) during calibration, cross-validation, and verification. However, the results are inconclusive as EV fluctuates with increase in number of

iterations beyond 500. Therefore, RMSE, CC, and NSE suggest 1000 no. of iterations to be suitable for network (4-4-1). However EV slightly increases in calibration and verification, and decreases in cross validation after 500 iterations. The model efficiency due to network (4-16-1) significantly increases up to first 500 iterations, gradually increases up to 1000 iterations, and finally becomes almost stable after 1000 iterations (Table 7.3). The minimum volumetric error occured around 500 iterations in calibration and cross-validation. In other words, the model performed best around 500 iterations. Furthermore, the performance of network (4-32-1) improves up to 500 iterations, and no further improvement is seen with increasing iterations. EV reduces up to 500 iterations and thereafter it slightly vibrates.

Thus, the number of iterations required for optimal results for network 4-4-1 is about 1000, and the number for networks 4-16-1 and 4-32-1 is about 500. It can be inferred that, in general, the number of iterations decreases as the network changes to 4-16-1 or 4-32-1 from 4-4-1. Moreover, there is no need to go beyond 1000 iteration for all networks.

Overall, ALR = 20 found suitable for all RBFANN structures. The lower network structure is independent of the ALRG variation from 0.5 to 10. Notably, the higher values of ALRG with higher network resulted in higher volumetric error, and therefore, not suitable for good results. Thus, the value of ALRG is fixed to 0.5 in order to suite all network structures. The maximum number of iterations required for lower networks (4-4-1) is 1000, and it reduces to 500 with increase in network structure. Moreover, the efficiency of RBFANN model was around 85% in prediction of daily 14 years monsoon runoff patterns of Naula watershed. The observed and estimated values of runoff in calibration, cross-validation, and verification for networks (4-4-1), (4-16-1), and (4-32-1) with ALR = 20 and ALRG = 0.5 are shown in Figs. 7.4, 7.5, and 7.6, respectively. It is evident from theses figures that the daily runoff pattern predicted by proposed RBFANNs model is well matched with observed in calibration, cross-validation and verification.

(b) Chaukhutia watershed

Following the similar procedure adopted for Naula watershed, different parameters of RBFANNs networks such as ALR, ALRG, and the number of iterations were optimized for Cahukhuita watershed. Taking initial values of ALRG as 0.5 and number of iteration as 1000, the model was run for different values of ALR, and based on the statistical criteria, the most suitable value of ALR was 15.

Table 7.1: Performance of (4-4-1), (4-16-1), and (4-32-1) dynamic RBFANN models. ALRG = 0.5, number of iterations = 1000, ALR = 0.5 to 25 for Naula watershed.

Period	RMSE			CC			NSE			EV		
	4-4-1	4-16-1	4-32-1	4-4-1	4-16-1	4-32-1	4-4-1	4-16-1	4-32-1	4-4-1	4-16-1	4-32-1
						ALR = 0.5						
Calibration	156.57	154.12	153.06	56.27	57.08	57.44	-558.8	-538.4	-529.6	182.3	175.4	172.7
Cross-validation	162.57	159.88	158.82	61.08	61.97	62.28	-1168	-1126.3	-1110.1	236.7	227.8	224.1
Verification	154.18	151.46	150.37	56.21	56.95	57.21	-793.6	-762.3	-750	215.4	206.5	202.7
						ALR = 5						
Calibration	51.28	50.87	50.95	78.56	78.55	78.73	29.32	30.44	30.22	-8.52	-10.85	-10.27
Cross-validation	44.86	44.45	44.58	79.83	79.57	79.78	3.44	5.23	4.66	-13.19	-15.76	-15.31
Verification	44.06	43.89	43.87	81.3	81.17	81.42	27.04	27.58	27.65	-20.7	-22.79	-22.43
						ALR = 10						
Calibration	38.39	30.86	27.29	83.36	86.35	89.07	60.39	74.4	79.24	-1.23	3.92	2.81
Cross-validation	31.08	21.18	20.25	85.19	89.67	90.62	53.66	78.47	80.34	-1.65	8.76	7.47
Verification	31.96	22.34	21.08	86.21	90.38	91.39	61.61	81.24	83.29	-6.74	5.66	4.09
						ALR = 15						
Calibration	30.99	27.74	23.61	87.24	89.11	92.25	74.19	79.31	85.02	-0.94	2.95	2.47
Cross-validation	23.52	19.96	18.58	89.04	90.91	91.99	73.47	80.89	83.44	0.08	7.02	6.27
Verification	24.44	20.95	19.76	90.13	91.6	92.76	77.55	83.49	85.32	-3.43	4.18	5.97
						ALR = 20						
Calibration	29.5	25.77	22.59	87.99	90.77	92.92	76.61	82.16	86.28	-0.31	-0.68	1.61
Cross-validation	21.83	19.37	17.74	89.52	91.79	92.44	77.14	81.99	84.91	1.33	2.61	5.18
Verification	22.92	20.92	18.73	90.67	91.82	93.5	80.25	83.55	86.81	-1.06	-1.29	6.35
						ALR = 25						
Calibration	29.07	26.29	23.01	88.03	90.35	92.66	77.29	81.43	85.77	3.83	3.98	2.52
Cross-validation	20.92	20.05	18.92	89.98	91.3	91.94	78.99	80.72	82.83	7.83	8.11	5.54
Verification	21.83	19.89	19.29	91.04	93.03	93.63	82.09	85.2	86.08	5.65	5.3	5.31

Table 7.2: Performance of (4-4-1), (4-16-1), and (4-32-1) dynamic RBFANN models. ALR = 20, number of iterations = 1000, and ALRG = 0.5 to 10 for Naula watershed.

Period	RMSE			CC			NSE			EV		
	4-4-1	4-16-1	4-32-1	4-4-1	4-16-1	4-32-1	4-4-1	4-16-1	4-32-1	4-4-1	4-16-1	4-32-1
						ALRG = 0.5						
Calibration	29.5	25.77	22.59	87.99	90.77	92.93	76.61	82.16	86.28	-0.31	-0.68	1.61
Cross-validation	21.83	19.37	17.74	89.52	91.79	92.44	77.14	81.99	84.91	1.33	2.61	5.18
Verification	22.92	20.92	18.73	90.67	91.82	93.5	80.25	83.55	86.81	-1.06	-1.29	6.35
						ALRG = 1						
Calibration	29.21	25.37	22.51	88.22	91.11	92.98	77.06	82.69	86.38	-0.56	-1.04	2.02
Cross-validation	21.59	19.35	17.73	89.71	91.95	92.51	77.65	82.04	84.92	0.83	2.11	5.61
Verification	22.52	20.67	18.72	90.47	92.15	93.54	80.94	83.94	86.83	-1.44	-1.63	6.65
						ALRG = 2						
Calibration	29.16	25.17	22.37	88.31	91.3	93.08	77.24	82.97	86.55	-0.63	-1.01	2.4
Cross-validation	21.5	19.48	17.68	89.78	91.95	92.63	77.82	81.79	85	0.68	2.04	6.09
Verification	22.34	20.62	18.65	91.11	92.29	93.63	81.24	84.01	86.93	-1.54	-1.53	6.9
						ALRG = 5						
Calibration	28.95	24.82	22.15	88.43	91.56	93.25	77.47	83.44	86.81	-0.16	0.25	2.72
Cross-validation	21.38	19.58	17.17	89.91	91.95	92.91	78.07	81.6	85.86	1.32	3.27	6.82
Verification	22.16	20.62	18.04	91.24	92.36	93.88	81.54	84.02	87.77	-0.92	0	6.2
						ALRG = 10						
Calibration	28.86	24.25	22.51	88.52	91.98	93.26	77.61	84.19	86.38	0.6	2.2	-1.95
Cross-validation	21.33	19.63	16.62	90.04	91.97	93.2	78.17	81.52	86.74	2.27	5.29	6.89
Verification	22.04	20.61	17.33	91.34	92.4	94.23	81.74	84.03	88.71	0	2.46	6

Table 7.3 Performance of (4-4-1), (4-16-1), and (4-32-1) dynamic RBFANN models. ALR = 20, ALRG = 0.5, and number of iterations = 100 to 10000 for Naula watershed.

Period	RMSE			CC			NSE			EV		
	4-4-1	4-16-1	4-32-1	4-4-1	4-16-1	4-32-1	4-4-1	4-16-1	4-32-1	4-4-1	4-16-1	4-32-1
ITERATION = 100												
Calibration	31.83	29.06	23.89	85.79	88.11	92.14	72.77	77.3	84.66	5.06	1.49	3.38
Cross-validation	23.65	20.97	18.43	88.18	90.14	91.98	73.17	78.91	83.7	9.86	5.06	7.75
Verification	24.64	22.62	19.67	88.99	90.31	92.81	77.19	80.76	85.45	6.36	1.42	8.07
ITERATION = 500												
Calibration	30.03	26.44	22.7	87.6	90.24	92.87	75.77	81.21	86.15	-0.21	0.08	1.8
Cross-validation	22.32	19.67	17.85	89.12	91.44	92.34	76.09	81.43	84.72	1.63	3.48	5.41
Verification	23.58	21.37	18.86	90.19	91.38	93.4	79.1	82.84	86.62	-0.87	-0.44	6.62
ITERATION = 1000												
Calibration	29.5	25.77	22.59	87.99	90.77	92.93	76.61	82.16	86.28	-0.31	-0.68	1.61
Cross-validation	21.83	19.37	17.74	89.52	91.79	92.44	77.14	81.99	84.91	1.33	2.61	5.18
Verification	22.92	20.92	18.73	90.67	91.82	93.5	80.25	83.55	86.81	-1.06	-1.29	6.35
ITERATION = 2000												
Calibration	29.22	25.38	22.48	88.2	91.1	93	77.05	82.68	86.42	-0.65	-1.2	1.55
Cross-validation	21.57	19.34	17.64	89.71	91.94	92.53	77.67	82.06	85.07	0.75	1.94	5.1
Verification	22.51	20.68	18.65	90.97	92.13	93.53	80.96	83.92	86.92	-1.53	-1.82	6.15
ITERATION = 5000												
Calibration	29.07	25.13	22.26	88.31	91.32	93.14	77.29	83.03	86.68	-0.88	-1.41	1.49
Cross-validation	21.45	19.47	17.49	89.79	91.91	92.67	77.93	81.81	85.32	0.46	1.58	5.01
Verification	22.28	20.64	18.55	91.12	92.26	93.59	81.34	83.98	87.07	-1.78	-1.97	5.81
ITERATION = 7500												
Calibration	29	24.98	22.14	88.35	91.42	93.22	77.39	83.23	86.83	-0.87	-1.25	1.44
Cross-validation	21.38	19.46	17.42	89.83	91.9	92.74	78.06	81.83	85.45	0.54	1.7	4.96
Verification	22.2	20.63	18.48	91.17	92.26	93.63	81.48	84	87.17	-1.71	-1.73	5.63
ITERATION = 10000												
Calibration	28.95	24.82	22.04	88.39	91.52	93.28	77.47	83.44	86.95	-0.85	-1.04	1.41
Cross-validation	21.33	19.43	17.36	89.87	91.89	92.79	78.17	81.89	85.54	0.62	1.89	4.91
Verification	28.45	20.61	18.41	88.39	92.26	93.67	77.47	84	87.25	-0.85	-1.44	5.5

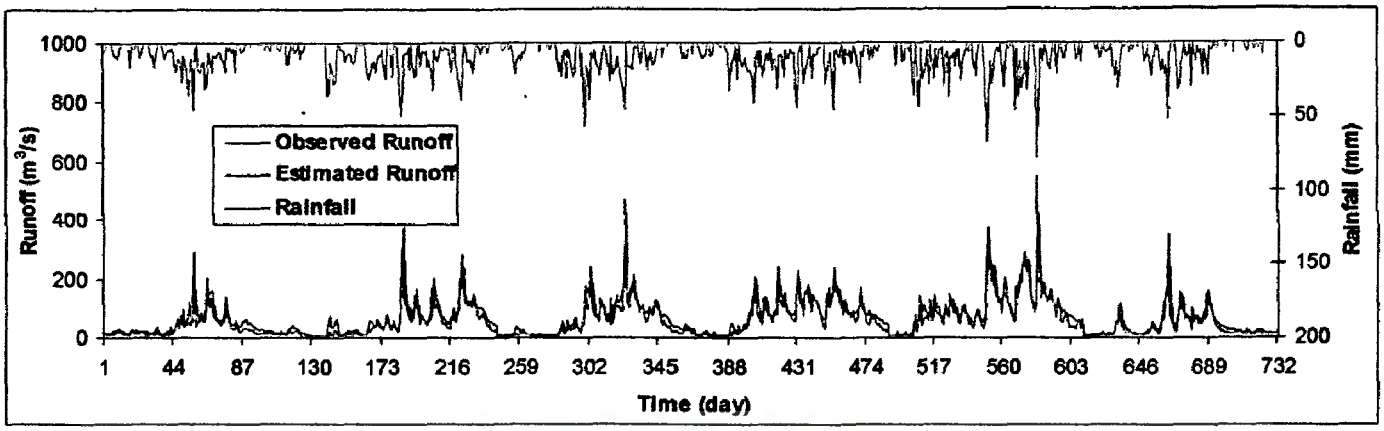

(a) Calibration

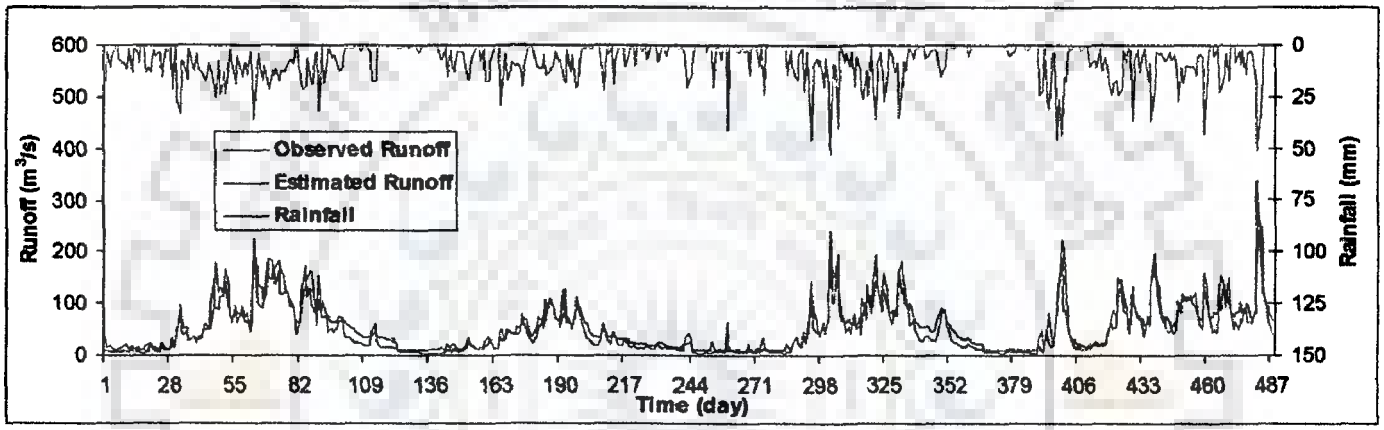

(b) Cross-validation

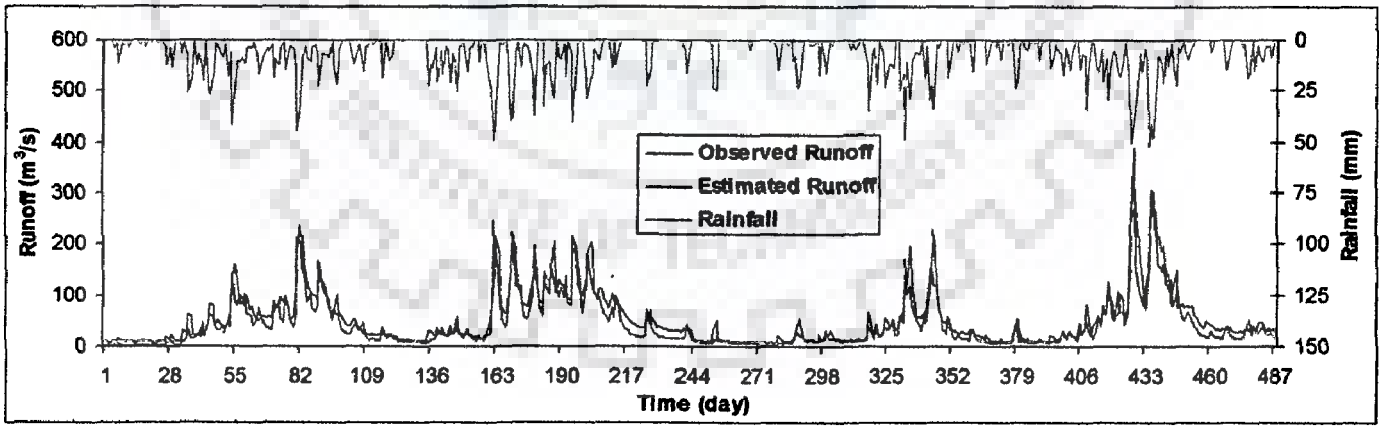

(c) Verification

Fig. 7.4: Observed and estimated runoff by dynamic RBFANN model having (4-4-1) network with ALR as 20 and ALRG as 0.5 for Naula watershed in (a) Calibration; (b) Cross-validation; and (c) Verification period.

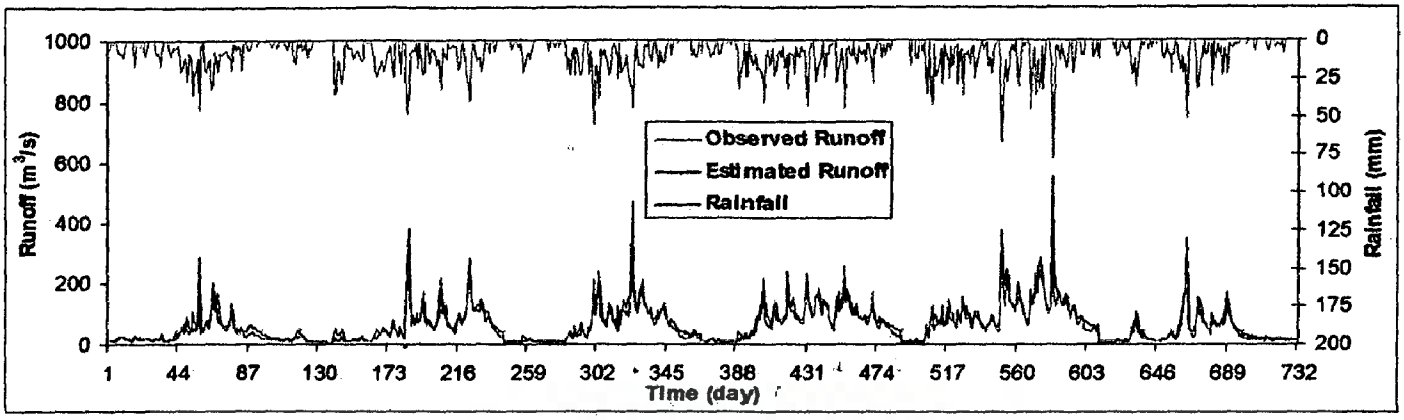

(a) Calibration

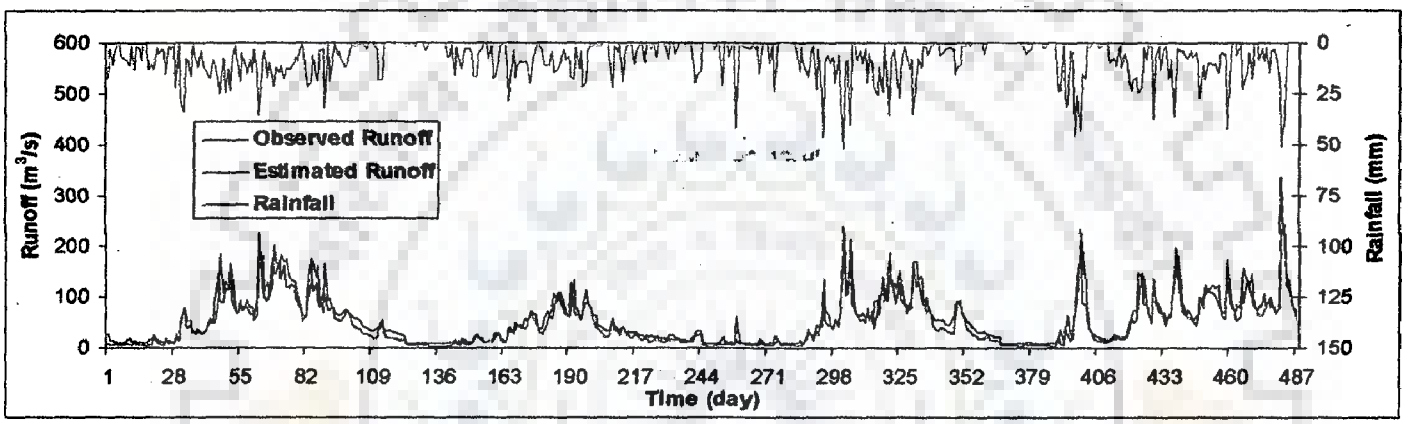

(b) Cross-validation

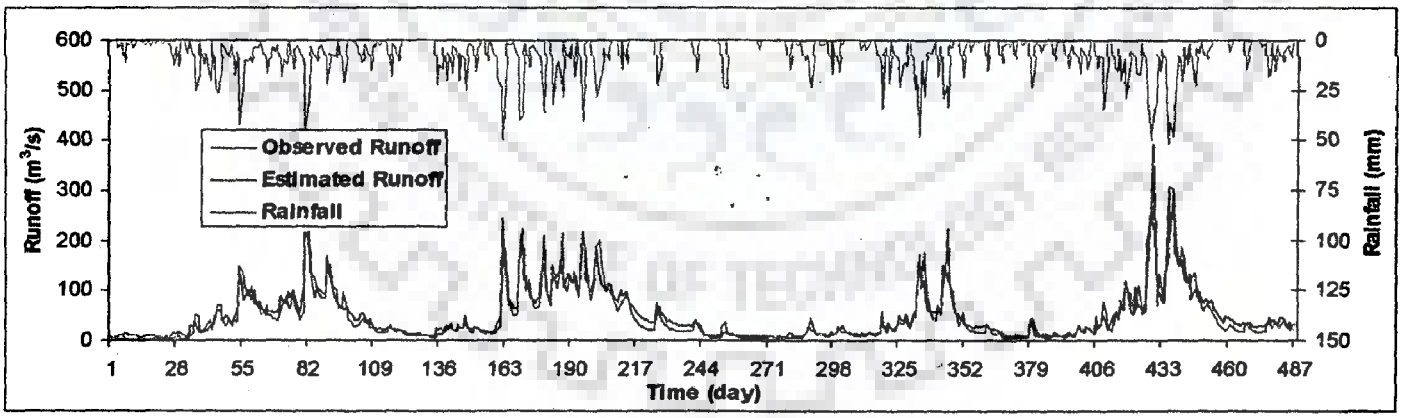

(c) Verification

Fig. 7.5: Observed and estimated runoff by dynamic RBFANN model having (4-16-1) network with ALR as 20 and ALRG as 0.5 for Naula watershed in (a) Calibration; (b) Cross-validation; and (c) Verification period

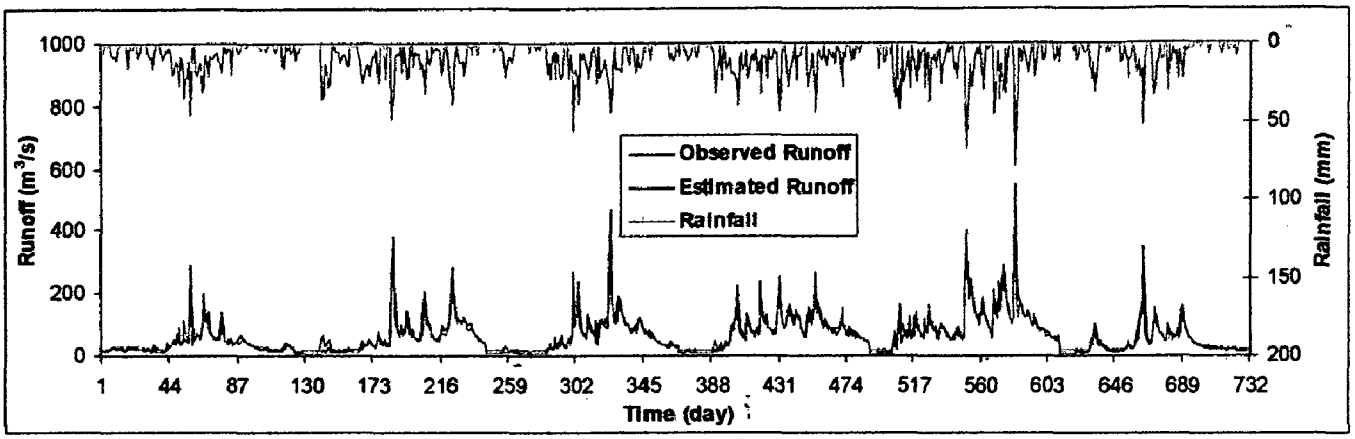

(a) Calibration

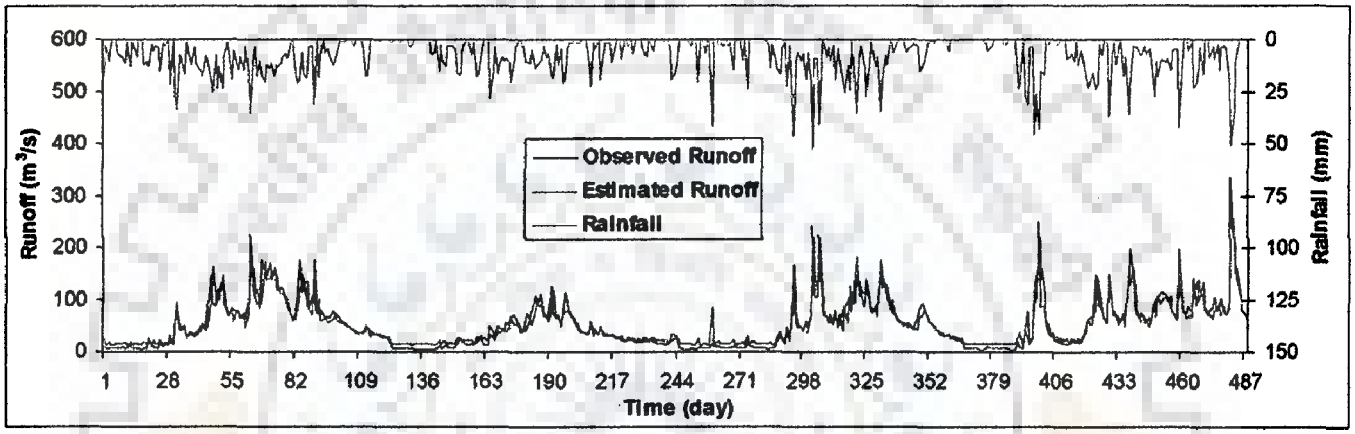

(b) Cross-validation

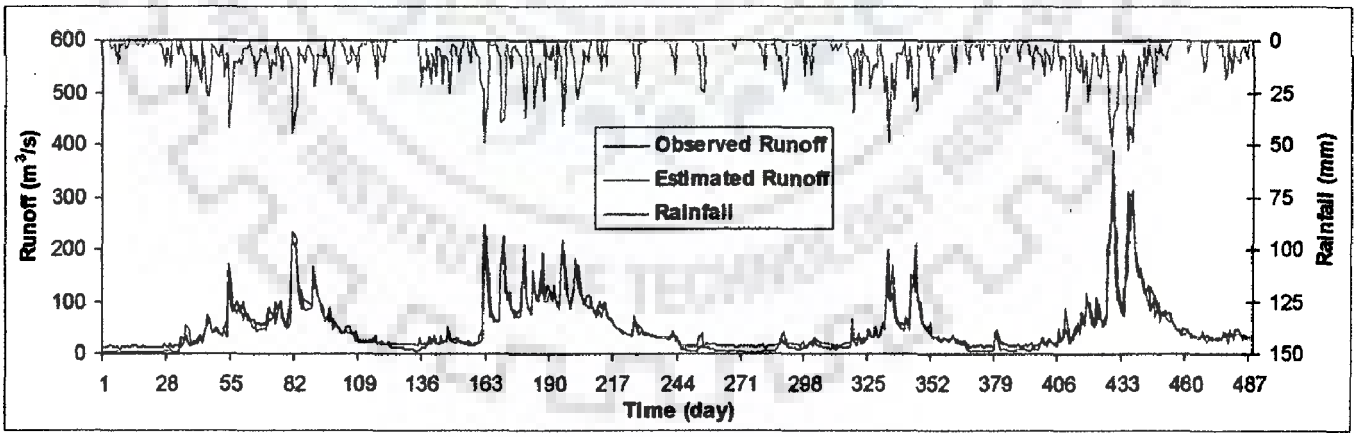

(c) Verification

Fig. 7.6: Observed and estimated runoff by dynamic RBFANN model having (4-32-1) network with ALR as 20 and ALRG as 0.5 for Naula watershed in (a) Calibration; (b) Cross-validation; and (c) Verification period.

The model performance for different ALR values (ranging from 0.5 to 20) is described in Appendix C (Table C1). After fixing ALR, the model was performed for the different values of ALRG ranging from 0.5 to 10, and presented in Appendix C (Table C2). It was observed that the lower network structure (4-4-1) is independent of ALRG values ranging from 0.5 to 10. However, with increase in network (4-16-1 or 4-32-1) structure, ALRG sticks to 0.5 or maximum 1.0. Notably, the higher values of ALRG in a higher network resulted in higher volumetric error (Table C2 of Appendix C). Overall the value of ALRG as 0.5 was suit for all networks and durations. Consequently, taking ALR = 15 and ALRG = 0.5, the model was performed for all three networks (4-4-1, 4-16-1, and 4-32-1) for iterations ranging from 100 to 10000 and depicted in Appendix C (Table C3). Based on the statistical error used in the study, model gives best results around 5000 iterations for network (4-4-1), around 1000 iterations for (4-16-1), and around 500 iterations for network (4-32-1). This indicated that the lower network required higher number of iterations, while higher network required less number of iteration for best performance of the model. The observed and estimated daily values of runoff for the calibration, cross-validation, and verification of networks 4-4-1, 4-16-1, and 4-32-1 with ALR = 15 and ALRG = 0.5 are plotted in Appendix D (Figs. D1, D2, and D3) and found good agreement between observed and predicted daily runoff values. Moreover, the efficiencies of the RBFANNs model (network 4-32-1) were found 77.48%, 84.76%, and 84.59% during calibration, cross-validation, and verification, respectively, for Chaukhutia watershed.

(c) *Ramganga watershed*

Similar to Naula watershed, the suitable ALR value for Ramganga watershed was 20 for all periods and networks by following the statistical criteria as above. The effect of different ALR values on model performance can be seen from Appendix E (Table E1). After fixing the ALR value as 20, the emphasis has been focused towards the selection of learning rate in output layer (ALRG). To identify proper value of ALRG, different values varying from 0.5 to 10 have been tried and the results are presented in Appendix E (Table E2). Considering RMSE, CC, NSE, and EV, a value of 0.5 of ALRG was selected for RBFANN model (Table E2 of Appendix E). After fixing the values of ALR as 20 and ALRG as 0.5, the initial selection of number of iteration is rechecked. To fix the optimum number of iteration, the system is run from minimum to maximum number of iterations for all three different

networks, and presented in Appendix E (Table E3). The model performed best with around 1000 iterations for 4-4-1 network. However, for networks (4-16-1) and (4-32-1), 500 iterations are sufficient. The observed and estimated daily values of runoff for the calibration, cross-validation, and verification of networks 4-4-1, 4-16-1, and 4-32-1 with ALR = 15 and ALRG = 0.5 are plotted in Appendix F (Figs. F1, F2, & F3) and found to be in good agreement between observed and predicted daily runoff values. The maximum coefficient of efficiency (NSE) was obtained as 76%, 77.68%, and 68.25% in calibration, cross-validation, and verification, respectively, for the network 4-32-1.

7.5 SUMMARY

A Radial Basis Function Artificial Neural Network (RBFANN) model was proposed based on k-means clustering algorithm to model the daily rainfall-runoff process for three Himalayan watersheds of India. For improved model performance, different parameters of the model like learning rate in function layer (ALR), learning rate in the output layer (ALRG), and the number of iterations were optimized for three different network structures. Available fourteen years rainfall-runoff dataset of three watersheds were divided into three periods, calibration, cross-validation, and verification. Following the standard statistical criteria such as Root Mean Square Error (RMSE), Correlation Coefficient (NSE), Coefficient of Efficiency (NSE), and Volumetric Error (EV), the model performance was evaluated. The performance of RBFANNs is excellent and consistent in all three periods in case of Naula watershed and it was 86.28%, 84.91%, and 86.81%, in calibration, cross-validation, and verification, respectively. However, the efficiency of the model was found excellent and consistent in cross-validation and verification (84.76% and 84.59%) and good in calibration (77.48%) for Chaukhutia watershed. In case of Ramganga watershed, the model performed well in both calibration and cross-validation (76% and 77.68%). However, it was reasonable (68.25%) in verification. Overall, RBFANN model performed very well on the data of all the three watersheds. Furthermore, the efficiency of model to converge the error was excellent with 1000 number of iterations. However, the higher networks mostly achieved their best performance within 500 iterations. The model was very sensitive to the learning rate in function layer (ALR). However, there is no significant variation seen with variation in learning rate in output layer (ALRG).

It is well known that the soil erosion, especially in hilly area, is one of major consequence of rainfall-runoff process. On-site soil erosion causes the removal of top fertile soil layer; however off-site erosion is resulted in reduction of capacity of costly reservoir. In this continuation, a spatially distributed sediment yield model has been developed for a typical hilly watershed and presented in the next chapter.

CHAPTER 8

GIS-SUPPORTED SPATIALLY DISTRIBUTED SEDIMENT YIELD MODEL

8.1 INTRODUCTION

The processes of sediment generation, transport, and deposition have been well described elsewhere (Rose, 1993; Haan et al., 1994; Govindaraju and Kavvas, 1991). On the basis of the experiment conducted on 10000 plots of USA, Wischmeier and Smith (1965) first proposed an equation popularly known as USLE to estimate the soil erosion. Subsequently, the equation was modified by the researcher as Modified Universal Soil Loss Equation (MUSLE) (Williams, 1975) or Revised Universal Soil Loss Equation (RUSLE) (Renard et al., 1991), and frequently used for estimation of surface erosion (Williams and Berndt, 1972; Griffin et al., 1988; Ferro et al., 1998; Jain and Kothyari, 2000; Jain and Goel, 2002; Kothyari et al., 2002; Mishra et al., 2006). It is well known that all the soil eroded at a place does not reach at the outlet of the catchment. In reality, it depends on several parameters responsible for the soil detachment and the transport capacity of the path followed by the sediment to reach the outlet. However, the linking on-site soil erosion rate within a basin to the sediment yield at the basin outlet is often problematic because of the lack of detailed input data at a river catchment scale (100-100000 km^2) (Van Rompaey et al., 2001). To this end several researchers (Roehl, 1962; Vanoni, 1975; Walling, 1983; Ferro and Minacapilli, 1995; Klaghofer et al., 1992; Bazoffi et al., 1996) used a sediment delivery ratio (SDR) approach to link the soil erosion within a basin to the sediment yield at outlet. However, the SDR-based sediment yield estimation approach is empirical lumped approach (Walling, 1983; Atkinson, 1995; Bazoffi et al., 1996; Verstraeten and Poesen, 2001) and hence performs well on the data of catchment belonging to inherent region.

Nevertheless, the sediment control management policy should not only concentrate to those areas which directly contribute the sediment to river channels, however more emphasis should be on the areas which are major contributor of the sediment (Verstraeten et al., 2007). In this context, the lumped SDR based approach is not helpful in prioritization of watershed management/treatment activities within a river basin/catchment. Prosser and Rustomji (2000) found the problem in defining the spatial pattern of sediment in hilly catchments due to lack of hydrological model for hillslope.

Despite the development of a range of physically based soil erosion and sediment transport models, sediment yield predictions at a watershed or regional scale are at present achieved mainly through simple empirical models such as USLE and its derivatives. However, the popular soil erosion model USLE, MUSLE, RUSLE and its derivative are generally developed for plot size area and hence do not perform very well when applied to a large area or catchment. It has been observed that USLE over-predicts combined length-slope value (LS) at higher slope and longer slope-lengths. In reality, the term λ used in estimation of LS factor in USLE is only applicable to 2-D non-converging and non-diverging hill slope. Therefore, the equation can not be extended for real 3-D landscape. Furthermore, both of these quantities, viz., the surface erosion and sediment yield are found to have large spatial variability in a catchment due to the spatial variation of rainfall and catchment heterogeneity. The technique of Geographical Information System (GIS) is well suited for quantification of heterogeneity (not only in space but also in time) in the topographic, cover type, and drainage features of a watershed by partitioning the watershed into small homogenous grids (Jain and Kothyari, 2000; Gosain and Sandhya, 2004; Jain et al., 2004, 2005; Onyando et al., 2005; Wu et al., 2005; Eldho et al., 2006; Naik et al., 2009).

Keeping all the above discussion in view, a simple distributed sediment yield model has been proposed in the present study which is parsimonious in terms of data, time, and funds. The accuracy of the developed model has been verified by the historical sediment data of a hilly watershed belonging to Himalayan region of India, i.e. Naula. Furthermore, the spatial capability of the proposed distributed sediment model has been cross-checked with the observed sediment yield data at three different upstream locations of the study watershed. Most of the model parameters are extracted from the geospatial data which is most update, easily available, and probably free of cost throughout the globe.

8.2 MODEL DEVELOPMENT

The proposed model comprises of three major components (1) the assessment of seasonal gross soil erosion for each grid cell; (2) the assessment of seasonal transport capacity for each grid cell; and (3) a transport limited accumulation algorithm for routing sediment from each of the discretized grid cell to the outlet of the catchment by taking into account the local transport capacity of each grid cell.

8.2.1 Estimation of Gross Soil Erosion

Universal Soil Loss Equation (USLE) has been found to produce realistic estimates of surface erosion over small size areas (Wischmeier and Smith, 1978; Ferro et al., 1998; Jain and Kothyari, 2000; Kothyari et al., 2002; Jain and Goel, 2002; Lee, 2004; Onyando et al., 2005; Pandey et al., 2007, Jain et al., 2009). Although USLE is a lumped empirical model, this equation has been a part of several spatially distributed process-based models. This is possible due to the discretization of heterogeneous catchment into small homogeneous unit/cell. In the present study, USLE is used to estimate gross soil erosion from each of the discretized cells. The USLE for estimation of gross soil erosion within a cell is expressed as:

$$GSE_i = RK_iLS_iC_iP_i \quad (8.1)$$

where GSE_i = gross amount of soil erosion in cell *i* (MT ha^{-1} $year^{-1}$); R = rainfall erosivity factor (MJ mm ha^{-1} h^{-1} $year^{-1}$); K_i = soil erodibility factor in cell *i* (MT ha h ha^{-1} MJ^{-1} mm^{-1}); LS_i = slope steepness and length factor for cell *i* (dimensionless); C_i = cover management factor (dimensionless) and P_i = supporting practice factor for cell *i* (dimensionless).

8.2.2 Sediment Transport and Outflow

Use of Eq. (8.1) produces the estimate of gross soil erosion in each of the discretized cell of the catchment. Gross amount of soil erosion for each cell area during a season can be generated by multiplying the term KLSCP with the R-factor for the corresponding season. The eroded sediment from each cell follows a defined drainage path as shown in Fig. 8.1 for a particular cell to the catchment outlet. The rate of sediment transport from each of the discretized cell depends on the transport capacity of the flowing water (Meyer and Wischmier, 1969).

The sediment outflow from an area is equal to soil erosion in the cell plus contribution from upstream cells if transport capacity is greater than this sum. However, if transport capacity is less then the amount of sediment available, sediment load equal to transport capacity is discharged to the next downstream cell and amount of sediment excess of transport capacity gets deposited (Wischmeier and Smith, 1969).

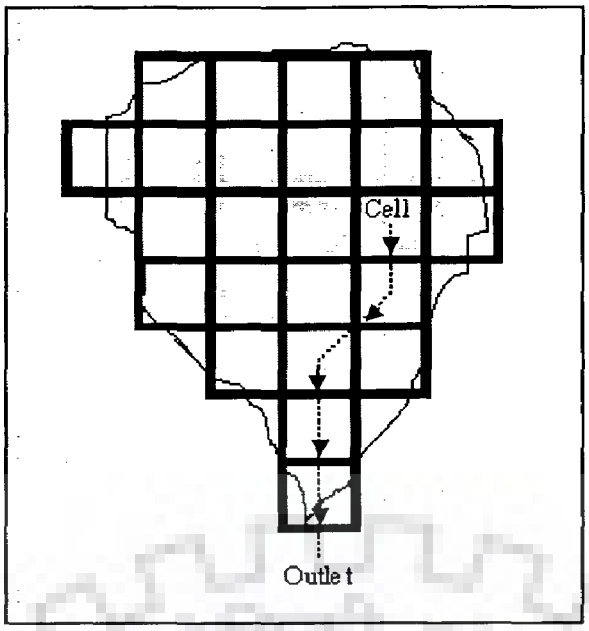

Fig. 8.1: Schematic diagram showing a drainage path.

(a) Mean annual sediment transport capacity

Desmet and Govers (1995) and Van Oost *et al.* (2000) considered the mean annual transport capacity to be directly proportional to the potential rill (and ephemeral gully) erosion:

$$TC = K_{TC}E_{PR} \tag{8.2}$$

where TC is the transport capacity (kg m^{-2} $year^{-1}$); K_{TC} is the transport capacity coefficient; and E_{PR} is the potential for rill erosion (kg m^{-2} $year^{-1}$). Van Rompaey et al. (2001) estimated E_{PR} in terms of potential inter-rill erosion (E_{PIR}) and potential total erosion E_{PT} as follows:

$$E_{PR} = E_{PT} - E_{PIR} \tag{8.3}$$

E_{PT} can be estimated from USLE by assuming the erosion from completely barren land without any conservation measures. However, E_{PIR} can be estimated by the equation proposed by McCool et al. (1989) as follows:

$$E_{PIR} = aRK_{IR}S_{IR} \tag{8.4}$$

where 'a' is a coefficient, K_{IR} is the inter-rill soil erodibility factor (kg h MJ^{-1} mm^{-1}) and S_{IR} is the inter-rill slope gradient factor. Due to non-availability of data, Van Rompaey et al. (2001) assumed K_{IR}=K and arrived at the expression of transport capacity as follows:

$$TC = K_{TC}RK(LS - aS_{IR}) \tag{8.5}$$

From Eq. 8.5, it is clear that transport capacity does depend on the same topological variable as gross soil erosion depends (Eq. 8.1). Van Rompaey et al. (2005) found poor performance (R=0.25, for mountainous part) when the model was applied to the Italian catchments following the stratified calibration procedure whereby a distinction was made

between mountainous and non-mountainous parts of the catchment. In reality, the topography of hilly areas is such that flow converges at some points, generally at the junction of the steep slope and valley floor (or toe of the slope). Theses points are generally the end point of the steep slope or where sudden flattened in the slope is observed. However, these points represent high flow accumulation values. Theoretically, the smaller transport capacity of such points due to low slope gradient (according to Eq. 8.5) is not capable to transport the huge amount of sediment that comes from the steep slopes or upland areas resulting in large amount of sediment deposition in theses areas and hence model underestimate the sediment yield at the outlet of the watershed. To overcome this problem an upslope contributing area factor is incorporated which represents the actual flow accumulation of any cell and the equation for transport capacity for i^{th} cell can be written as:

$$TC_i = K_{TC} RK_i S_i^{\beta} A_{si}^{\gamma} \quad (8.6)$$

where A_{si} is the upslope contributing area for cell *i*. The major advantage of this equation is to solve the problem of deposition of huge amount of sediment at the flow convergent point (normally at the toe of the slope) which frequently occurred in the hilly catchment. Using Eq. (8.6), transport capacity of such points will be sufficiently high, even having low slope gradient to carry the sediment coming from the steep slopes. However, similar equation has been used by Verstraeten (2007) for the computation of sediment transport capacity for an Australian catchment named Murrumbidgee basin. The value of exponent of upslope area (γ) and slope gradient (β) is taken as 1.4 for both exponent (Prosser and Rustomji, 2000).

(b) Transport limited accumulation

Eroded sediment from each cell follows a definite path defined by direction of flowing water. The amount of sediment outflow from one cell to its downstream cell depends on local sediment transport capacity for a cell. If the local TC is smaller than the sediment flux, then sediment deposition is modeled. This approach assumes that sediment transport is not necessarily restricted to a transport limited system. If the TC is higher than the sediment flux, then sediment transport will be supply limited. Thus, by introducing the K_{TC}, transport capacity coefficient, a more realistic representation of overland flow sediment transport can be simulated. The model produces different maps of erosion, sediment transport, and sediment deposition rates. For cell-based discretization system transport limited accumulation can be computed as:

$$T_{out_i} = \min(GSE_i + \sum T_{in_i}, TC_i) \quad (8.7)$$

$$D_i = GSE_i + \sum T_{in_i} - T_{out_i} \quad (8.8)$$

where GSE_i = annual gross soil erosion of cell *i*, TC_i = transport capacity, T_{in_i} = sediment inflow from upstream cells, T_{out_i} = sediment outflow from the cell *i*. D*i* = deposition in cell *i*. The flow chart of the proposed model is shown schematically in Fig. 8.2.

8.3 FORMATION OF INPUT DATABASE

As discussed in Chapter 3, eight years seasonal (June-September) rainfall-sediment yield data belonging to a Himalayan watershed i.e. Naula were used for modelling of sediment. However, the other input parameters were extracted from different maps prepared in GIS environment. It is worth emphasizing here that the result of a spatially distributed model greatly depends on the spatial and temporal quality of the input dataset. Therefore, proper care should be taken in preparation of error free digital elevation model (DEM), appropriate classification of land use and soil map, realistic schematization of drainage network of the watershed, and finally, more important is to provide adequate value of different input parameters for each cell. In the following text, the input data required for the above developed model are being described in detail.

8.3.1 Extraction of Drainage Network and Watershed from DEM

In this study SRTM derived DEM (Fig. 8.3) is used to generate different maps such as slope, gradient, length-slope factor, drainage network, and finally delineation of watershed boundary. Drainage and catchments are extracted from SRTM DEM using ARC HYDRO module (ARC/INFO Window; version 9 2005). In this sequence, the first step is to FILL SINKS of raster DEM which are the pixel of no data value or local depression. The physical significance of this step is to avoid the discontinuation of drainage line or local drainage. Using FLOW DIRECTION tool, we determine in which neighboring pixel, the water from any central pixel will flow naturally. Then the FLOW ACCUMULATION in each pixel is determined, which represents a cumulative count of the number of pixels that are contributing at any pixel. The stream generation threshold or channel initiation threshold is a numerical value, pixels having flow accumulation value less than channel initiation threshold are termed as overland flow pixels and those having higher flow accumulation value than channel initiation threshold are termed as channel/stream pixels (ESRI, 1994).

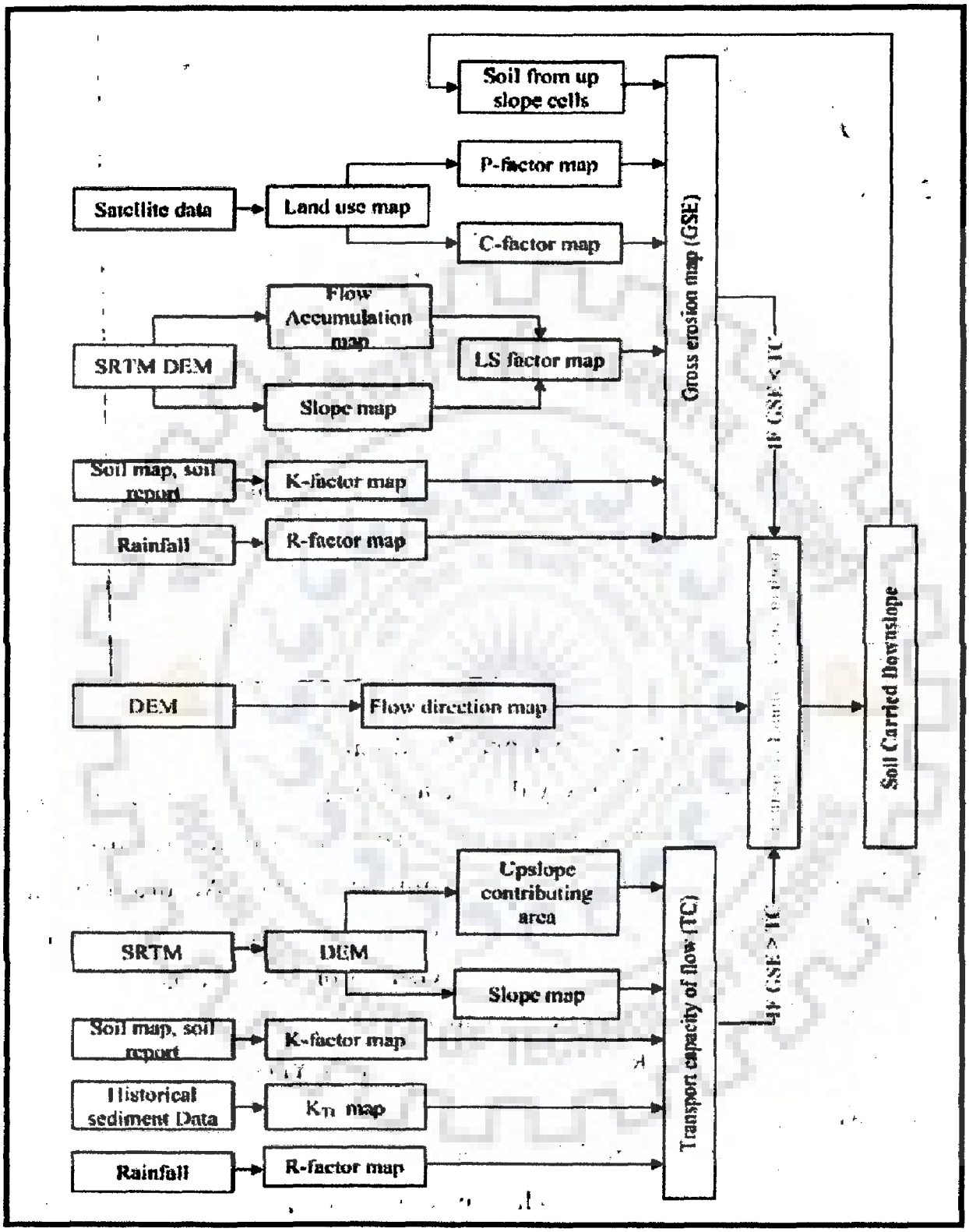

Fig. 8.2: Flow chart of the proposed sediment yield model.

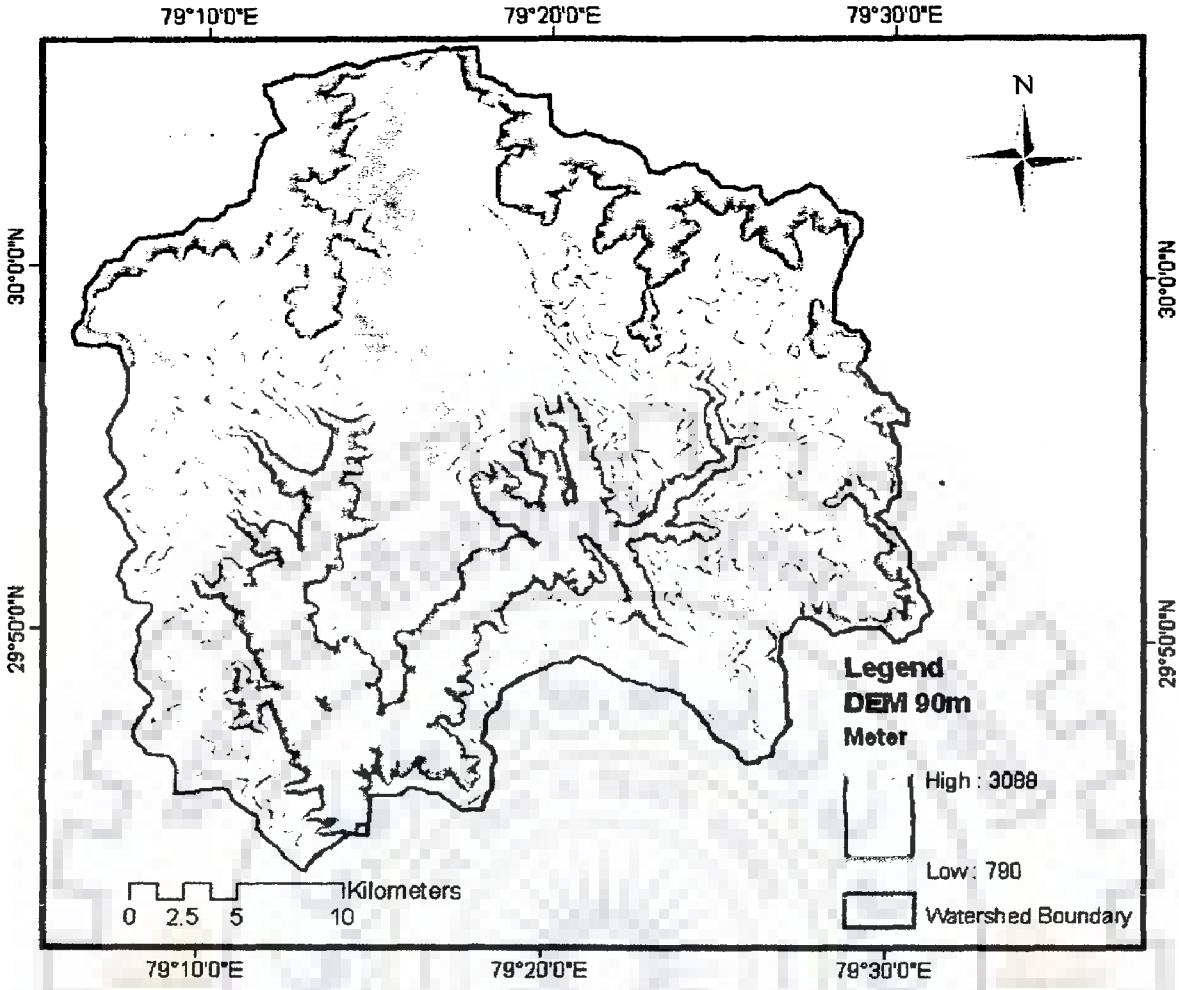

Fig. 8.3: Extracted DEM of the study area from SRTM data.

The threshold has to be chosen in such a way that the total stream length generated using threshold and channel network seen in satellite data and SOI Toposheet (digitized in vector form) should be equivalent (Jain and Kothyari, 2000). Accordingly, a channel initiation threshold value of 0.486 km^2 is adjudged appropriate to define channel cells. The extracted drainage of the Naula watershed from SRTM data is depicted in Fig. 8.4. Finally, the watershed boundary is extracted by supplying the location of outlet of the watershed in the WATERSHED option of the ARCHYDRO module.

8.3.2 Rainfall Erosivity (R)

The R-factor expresses the erosivity of rainfall at a particular location. An increase in the intensity and amount of rainfall results in an increase in the value of R. Realistic estimation of monthly or annual rainfall erosivity values requires long-term pluviographic data at 15 minutes intervals or less (Wischmeier and Smith, 1978). In many parts of the world, especially in developing countries, spatial coverage of pluviographic

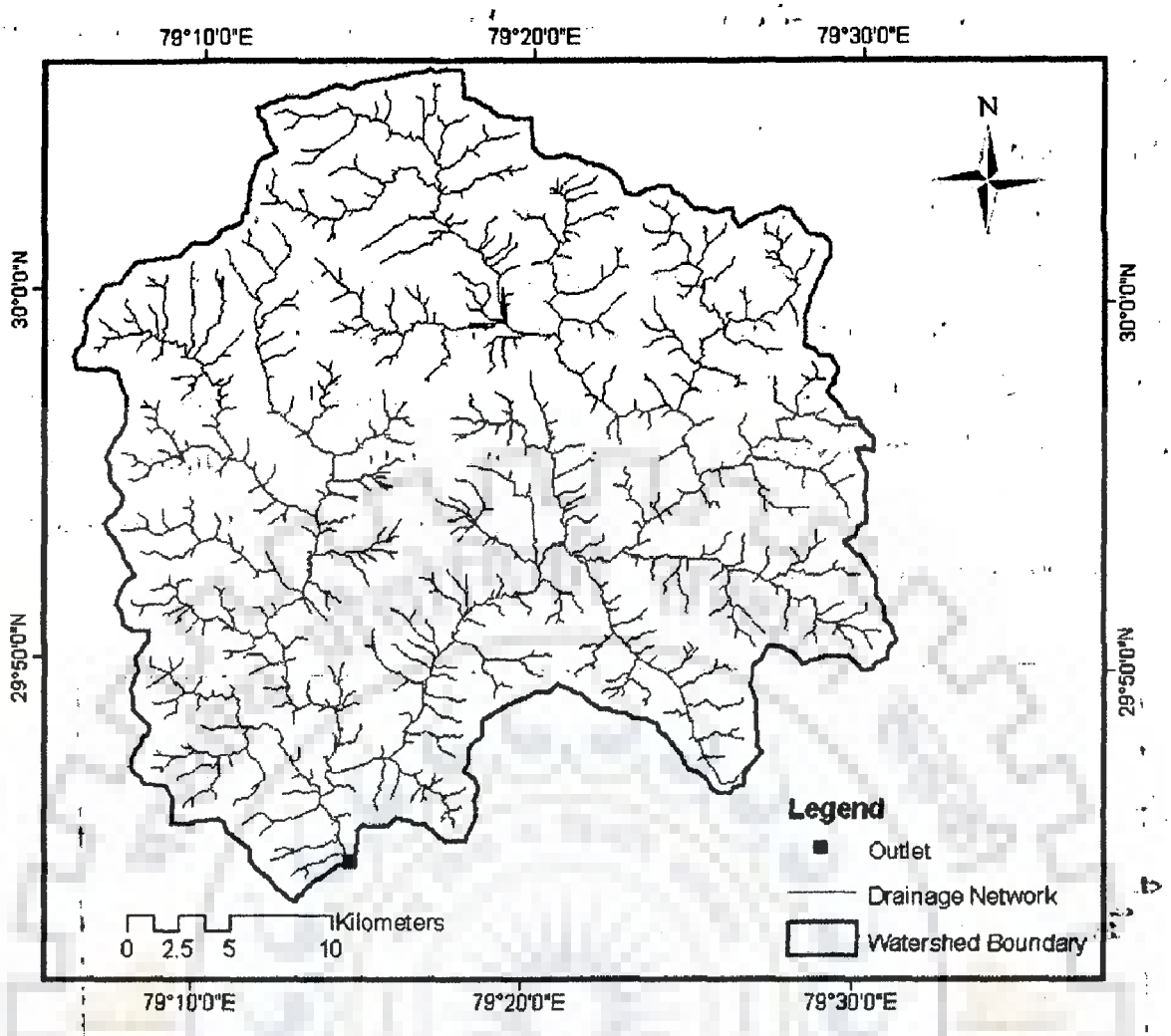

Fig 8.4: Extracted drainage network of the Naula watershed from SRTM data.

data are often difficult to obtain (Yu et al., 2001; Cohen et al., 2005; Shamshad et al., 2008). Wischmeier (1959) found that the product of kinetic energy of the storm and the 30 minutes intensity (EI_{30}) is the most reliable single estimate of rainfall erosion potential. Rainfall erosivity estimation using rainfall data with long time intervals have been attempted by several researchers for different regions (for example, Morgan, 1995; Millward and Mersey, 1999; Mati et al., 2000; Grimm et al., 2003; Natalia, 2005; Shamshad et al., 2008). Using the data for storms from several raingauge stations located in different zones, linear relationships were derived between average annual/seasonal rainfall and computed EI_{30} values for different zones of India, and iso-erodent maps were drawn for annual/seasonal EI_{30} values (Babu et al., 2004). In this study, rainfall erosivity was calculated by the relationship developed by Babu et al. (2004) for this particular zone and presented as:

$$R = 71.9 + 0.361\,P \quad (r = 0.91, \text{ for } 293 \leq P \leq 3190) \tag{8.9}$$

where P is the average seasonal rainfall in mm. In the present study, Eq. 8.9 is used to

compute seasonal values of R-factor by replacing P with observed seasonal rainfall of a particular year.

8.3.3 Soil Erodibility (K)

The soil erodibility factor K expresses inherent erodibility of the soil or surface material. The value of "K" depends on the particle-size distribution, organic-matter content, structure, and permeability of the soil or surface material. To this end, soil map of the watershed was digitized from soil survey report prepared by National Bureau of Soil & Landuse Planning (NBSS&LUP, 2004) using ArcGIS®. The digitized polygon map of Naula watershed is then rasterized at 90 m grid cells by using GIS Arc Vector to Raster tool and the same is depicted in Fig. 8.5.

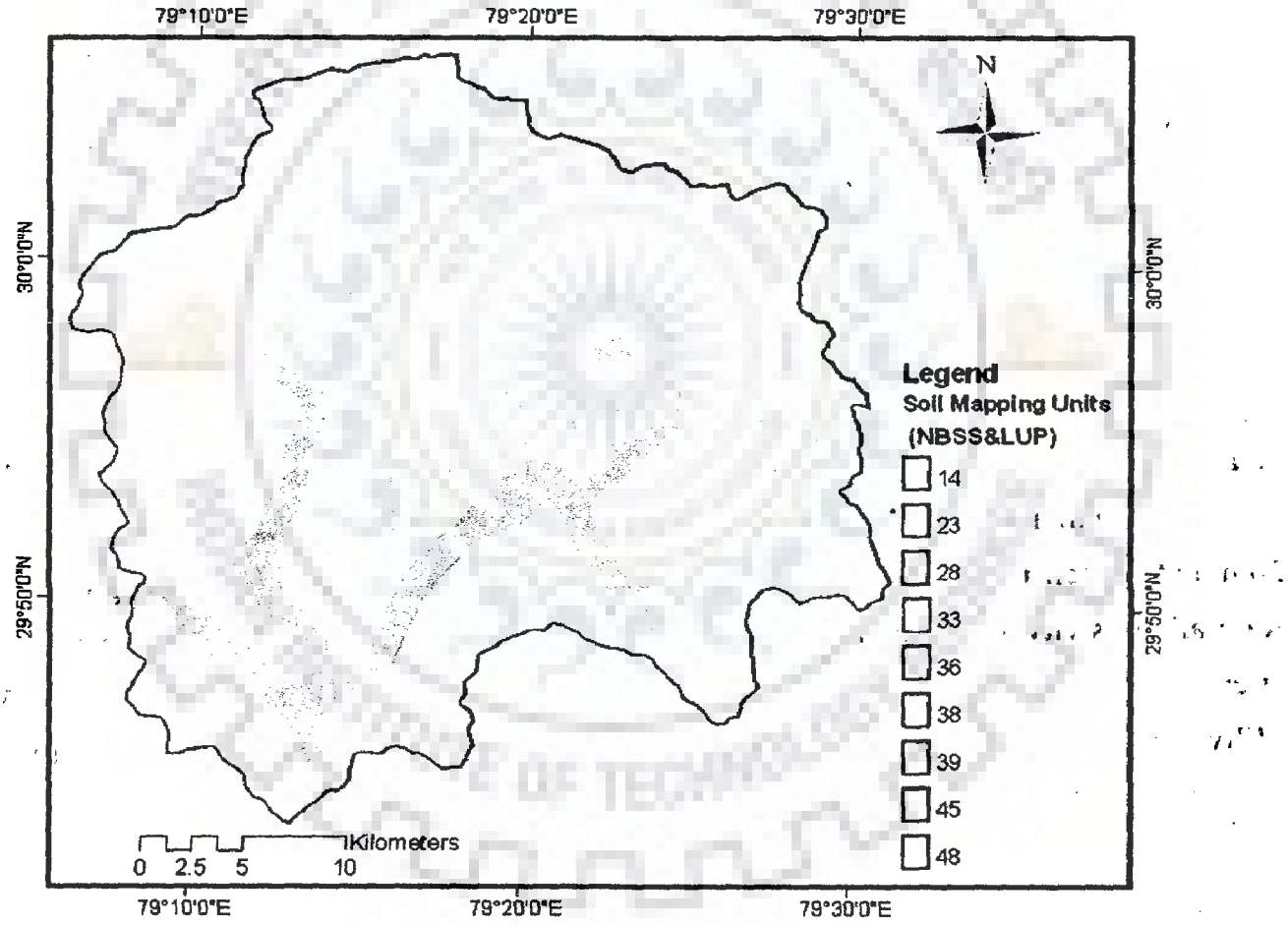

Fig. 8.5: Soil map of Naula watershed.

Details such as fraction of sand, silt, clay and organic matter and other related parameters information for different mapping units are taken from NBSS&LUP (2004) for Naula watershed. K-values for mapped soil categories are then calculated for each ofthe mapping units using Haan et al. (1994) procedure, and the results are given in Table 8.1.

Table 8.1: Soil characteristics of Naula watershed.

Soil Map Unit	Texture	Depth	Erosion	Slope	Surface	Drainage	Soil Erodibility (K)
14	Thermic fine loamy to loamy skeletal soils	Moderately shallow	Moderate	Moderate	Loamy	Excessively drained	0.020
23	Thermic to coarse loamy soils	Shallow to moderately shallow	Severe to moderate	Steep	Loamy to sandy	Excessively drained	0.032
28	Thermic skeletal to coarse loamy soils	Moderately deep to moderate shallow	Moderate	Moderate steep to steep	Loamy	Excessively drained	0.057
33	Thermic loamy skeletal soil	Moderately shallow	Moderate	Steep	Loamy	Excessively drained	0.030
36	Thermic coarse to fine loamy soils	Moderately deep	Moderate to slight	Moderate steep	Loamy	Excessively drained	0.049
38	Thermic loamy skeletal to fine loamy soils	Moderately shallow deep to moderate deep	Moderate to slight	Steep to moderate steep	Loamy	Excessively drained	0.023
39	Thermic Fine loamy soil	Deep	Slight	Moderate ly steep	loamy	Excessively drained	0.022
45	Thermic coarse to fine loamy soils	Moderately deep to deep	Moderate to slight	Moderate	Loamy	Well drained	0.049
48	Thermic sandy skeletal soil	Very shallow	Very severe	Very steep	Sandy	Excessively drained	0.042

8.3.4 Length-Slope Factor (LS)

The LS factor expresses the effect of topography, specifically hillslope length and steepness, on soil erosion. An increase in hillslope length and steepness results in an increase in the LS factor. It is well known that the combined length-slope (LS) factor in the Universal Soil Loss Equation (USLE) is a measure of the sediment transport capacity of overland flow and can also be derived from the DEM of the study area. There are many relationships available for estimation of the LS factor (Wischmeier and Smith, 1978; Moore and Burch, 1986a, b; McCool et al., 1989; Moore and Wilson, 1992; Desmet and Govers, 1996). Among these, the one that is best suited for integration with the GIS is the theoretical relationship proposed by Moore and Burch (1986a, b) and Moore and Wilson (1992) based on unit stream power theory, given as:

$$LS_i = \left[\frac{A_{si}}{22.13}\right]^n \left[\frac{\sin\theta_i}{0.0896}\right]^m \tag{8.10}$$

where A_{si} is the specific area at cell i defined as the upslope contributing area for overland grid (A_{up}) per unit width normal to flow direction; θ_i is the slope gradient in degrees for cell i. It has been shown that the values of $n = 0.6$, $m = 1.3$ give results consistent with the RUSLE LS factor for slope lengths <100 m and slope angles <14 degrees (Moore and Wilson, 1992). Exponent n and m can also be obtained through calibration if data are available for a specific prevailing type of flow and soil conditions.

In original equation of LS factor, the slope length (λ) is defined as the distance from the point of the origin of overland flow to the point where either the slope gradient decreases enough that deposition begins or runoff water enters a well-defined channel (Wischmeier and Smith, 1978). In the present study the slope length (L) is replaced by the unit upslope contributed area at which formation of channel is started and taken as channel/stream threshold (Jain and Kothyari, 2000). The main aim of the replacement of slope length by upslope contributing area is to incorporate the effect of converging and diverging terrain on soil erosion and hydrological aspect of the watershed. Consequently, a new theme has been prepared which represent the grids as a channel whose flow accumulation is greater than threshold value for channel initiation. However, the grids having the flow accumulation values less than or equal to channel initiation still remain in overland region. The LS factor for a cell area is computed with Eq. 8.10 in ArcGIS® using upslope contributing area and slope gradient computed from DEM of the study watershed. Fig. 8.6 represents the LS map for the entire watershed.

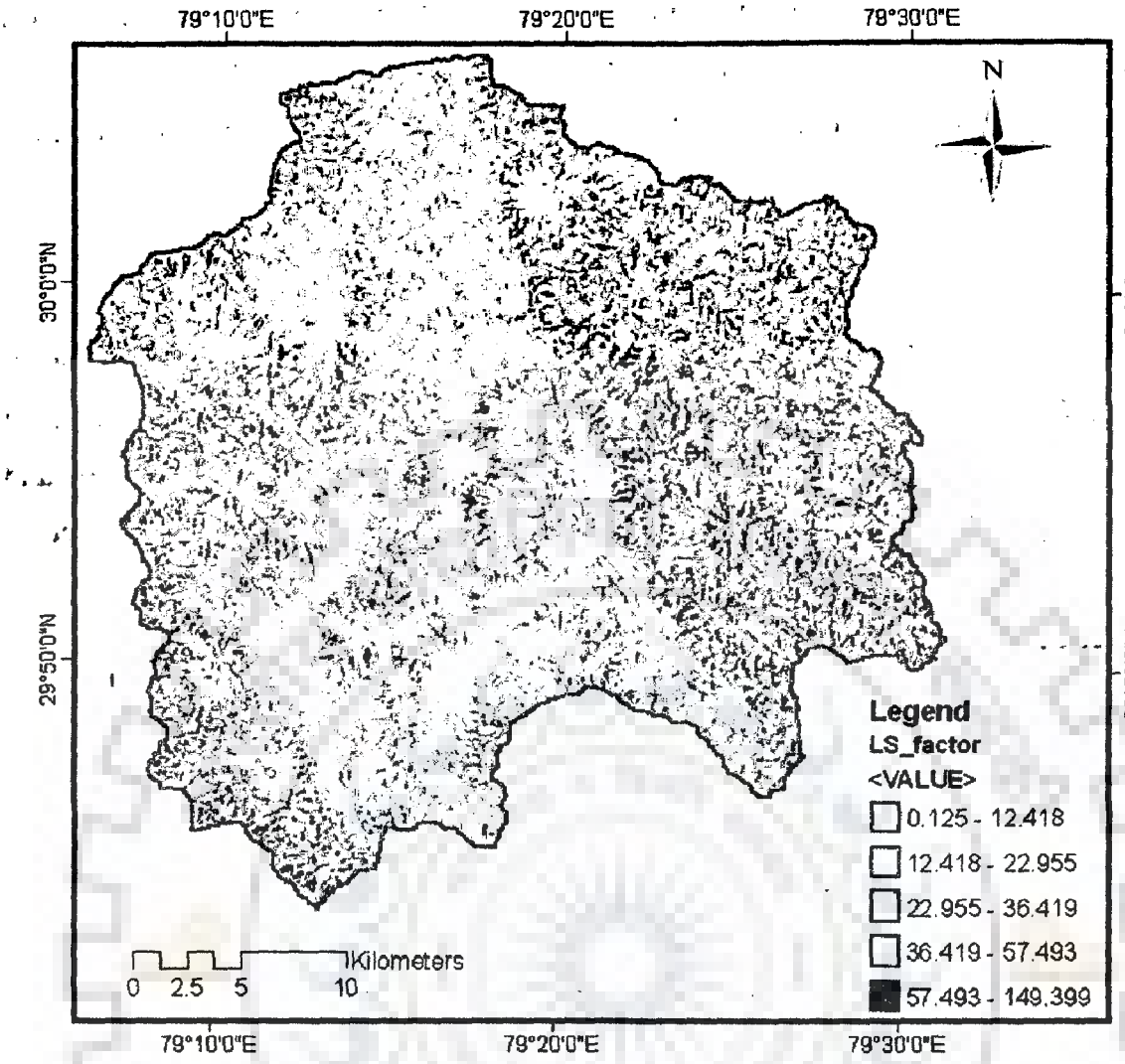

Fig. 8.6: Length-Slope factor map of Naula watershed.

8.3.5 Crop Management Factor (C)

The crop management factor is used to express the effect of plants and soil cover. Plants can reduce the rainfall erosivity and runoff velocity and protect surface pores. The C-factor measures the combined effect of all interrelated cover and management variables, and it is the factor that is most readily changed by human activities. Vegetation cover and cropping systems have a large influence on runoff and erosion rates. Soil erosion can be controlled with proper management of vegetation, plant residue and tillage. The crop management factor can be determined with the use of land cover data. A lower C value represents a cover type that is more effective at defending against soil erosion. C factor map of the study area is prepared using land use map. Hence land use/land cover map is prepared first using the LANDSAT TM satellite data corresponding to November 1st, 1992 (path 140 to 141 and Row 43 to 44) downloaded from GLCF site. The geometrically corrected image is analyzed using image processing software ERDAS

Imagine™ (ERDAS 2005). To discriminate the vegetation from other surface cover types, the Tassel Cap transformations (TCT), Vegetation Index (VI), Water Index (WI) are performed in ERDAS. Then a stratified supervised classification using Maximum Likelihood Method is carried out to generate the land use/land cover map for the watershed. The classified image is further verified for locations and extensions of various lands cover classes using limited ground truth information, Google Earth image and Survey of India topographic maps. Finally, a land use map of desired classes, viz., forest, agriculture, river bed, pasture, water is generated. However, one more class i.e. settlement is incorporated in the map by digitizing the urban area with the help of Toposheet and Google Earth images. Generated land use/land cover map of the watershed is depicted in Fig 8.7

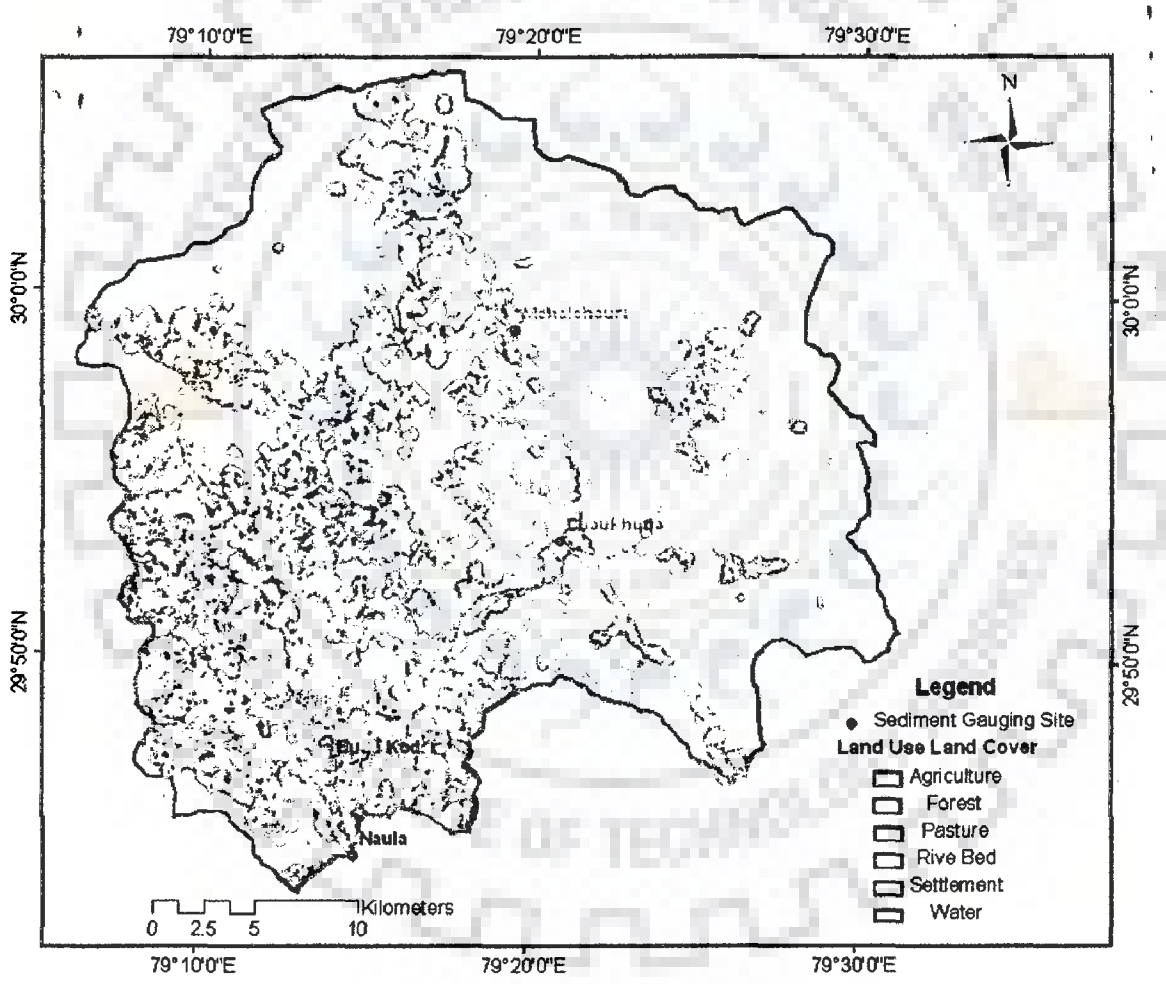

Fig. 8.7: Land use/land cover map for Naula watershed.

Based on the land cover categories, the attribute values for the C-factor are assigned to individual cells from the tabulated values suggested by Wischmeier and Smith (1978), Singh et al. (1981, 1992), Haan et al. (1994). Table 8.2 summarizes the land cover statistics and *C*-factor used for the Naula watershed.

Table 8.2: Land use pattern and their corresponding crop management factor values for Naula and its sub-watersheds.

Landuse	% of watershed area				Crop management factor (C)
	Naula	Chaukhutia	Kedar	Mehalchauri	
Forest	46.44	59.29	33.93	50.64	0.003
Agriculture	23.07	14.65	33.53	20.64	0.34
River bed	6.37	5.57	7.06	3.15	0.65
Pasture	22.91	19.51	24.05	24.18	0.20
Water	0.20	0.11	0.19	0.04	0.13
Settlement	1.01	0.86	1.23	1.35	0.13

8.3.6 Management Practice Factor (P)

The P-factor is the support practice factor. It expresses the effects of supporting conservation practices, such as contouring, buffer strips of close-growing vegetation, and terracing on soil loss at a particular site. A good conservation practice may result in reduced runoff volume, velocity, and less soil erosion. The management practice factor, P by definition is the ratio of soil loss from any conservation support practice to that with up and down slope tillage. It is used to evaluate the effects of contour tillage, strip cropping, terracing, subsurface drainage, and dry land farm surface roughening. A bare fallow land surface causes maximum soil erosion especially when it is cultivated up and down the slope or in other words, cultivated across the contours of the land surface. When a sloping land is put under cultivation, it needs to be protected by practices that will attenuate the runoff velocity, so that much less amount of soil is carried away by the runoff water. P is always ≤ 1.0. Based on experimental investigations, values for P-factor have been tabulated for many management conditions (Haan et al., 1994). The P-factor was taken equal to 0.9 for agricultural lands as mostly contour cultivation is followed on agricultural lands, and unity for other land use/land cover types. P-factor values are added in the attribute field of land use Map, and depicted in Fig. 8.8.

8.3.7 Generation of Erosion Potential Maps

The land use, soil, slope steepness and management practices are the main factors governing soil erosion potential at particular location to the erosive power of rainfall. Assessment of gross soil erosion (GSE) of Naula watershed has been done using ArcGIS Raster Calculator. The layers of topographic factor (LS), crop management factor C, soil erodibility factor K, and support practice factor P were overlaid. Then evaluated values of

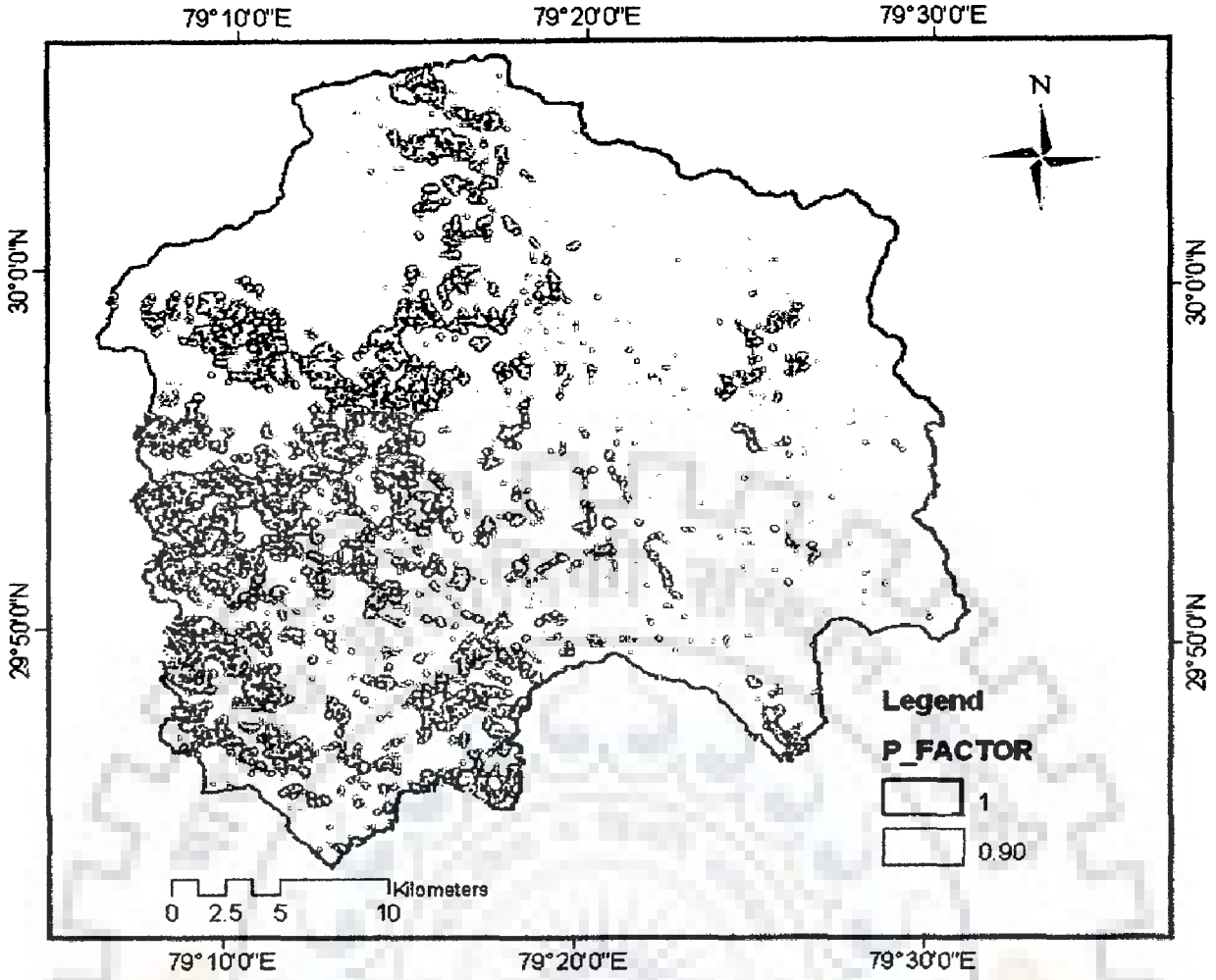

Fig. 8.8: Management practice (P) factor map of Naula watershed.

LS, K, C and P maps are multiplied by values of R, rainfall erosivity factor, and presented in Table 8.3 from years 1979 to 1987, respectively, to estimate the gross soil erosion in tons per annum/season for the watershed. Multiplication of R-factor into KLSCP factor map resulted in maps of gross erosion for different years (season). Fig. 8.9 presents gross soil erosion for the year of 1987.

8.4 MODEL APPLICATION AND DISCUSSION

8.4.1 Sediment Routing

Gross soil erosion and transport capacity of each pixel/Grid is estimated using raster calculator tool of ArcGIS, but as on today there is no ready to use tool available in GIS, which estimates the sediment transport from one pixel to next (sediment routing). The basic principle of overland flow routing is applied to generate a tool for sediment routing. The programme for this is developed in Interactive Data Language (IDL), a general purpose scientific computing package, sold by ITT Visual Information Systems,

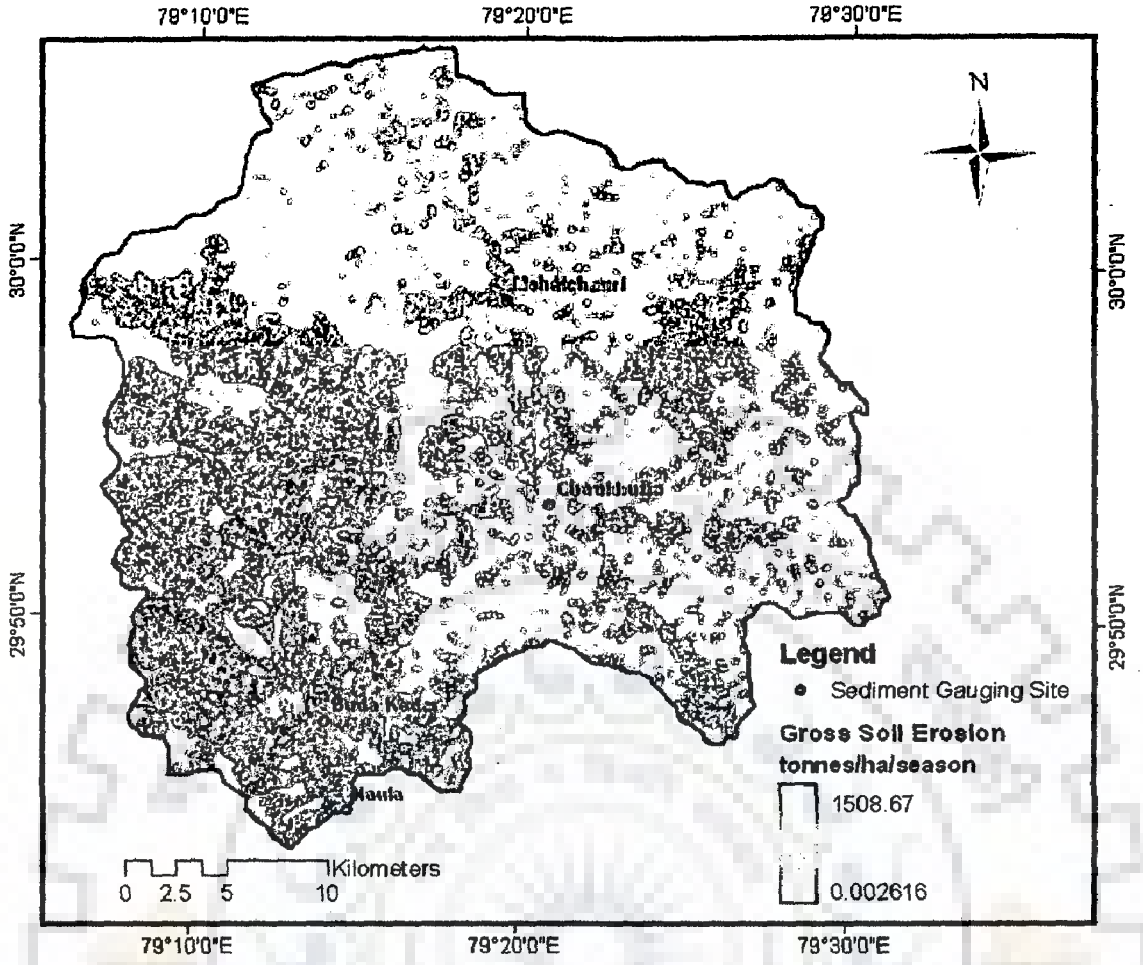

Fig. 8.9: Gross soil erosion map of Naula watershed for year 1987.

which provides a suite of mathematical functions, data analysis tools, as well as some scientific visualization and animation tools. The developed tools/programme estimate the sediment transport for each pixel using flow direction, flow accumulation, gross soil erosion, and transport capacity maps. The generation of all these maps is discussed in previous section, but care was taken to have same spatial reference, extent, and pixel size in all the maps. The programme starts the estimation of sediment transport from ridge pixels (i.e. Flow Accumulation = 0). The tool compares the gross soil erosion (total soil ready to move out of a particular pixel) and transport capacity of the flow in that pixel, if transport capacity is equal or greater than gross soil erosion then entire eroded soil will be transported into the next pixel. The destination of this transported soil/sediment is determined using flow direction map. In overland flow pixels the total soil ready to move out of particular pixel is summation of gross soil erosion of that pixel and sediment inflow from upstream area. If the transport capacity of any pixel is less than total soil ready to move out of particular pixel, the tool will assign the difference between transport capacity and the total soil ready to move out, as amount of sediment deposited in that

pixel. Batch processing option is given in programme to process temporal data and to save time in repeated operations/process. The tool provides the output maps of total sediment yield at any pixel in tons, deposition per pixel in tons, and net erosion from each pixel in raster format (Geo TIFF). The spatial reference, extent and pixel size of the output map is kept as same as input maps.

8.4.2 Generation of Transport Capacity Maps

Transport capacity of overland flow is calculated for each season and each pixel from the relationship stated in Eq. (8.6) by multiplying the R factor of each year in ArcGIS. The parameter K_{TC} appearing in Eq. (8.6) is taken as unity at the beginning and then its value is calibrated by minimizing error between observed and computed values of five years sediment data (1979-83) by varying K_{TC} values. To find the optimum value of K_{TC} for Naula watershed two statistical criteria, viz., Model Efficiency (ME), (Nash and Sutcliffe 1970) and Relative Root Mean Square Error (RRMSE) are used in calibration. Model efficiency (ME) can be calculated as follows:

$$ME = 1 - \frac{\sum(Y_{obs} - Y_{pred})^2}{\sum(Y_{obs} - Y_{mean})^2} \tag{8.11}$$

where Y_{obs} observed seasonal sediment (tons), Y_{pred} is predicted seasonal sediment (tons), Y_{mean} is mean of the observed sediment (tons). Value of ME ranges from $-\infty$ to 1, the value close to 1 indicated that model performed very well. However the negative value of ME implies the inefficiency of the model in prediction. Relative Root Mean Square Error is estimated by the following formula:

$$RRMSE = \frac{\sqrt{\frac{1}{n}\sum_{i=1}^{n}(Y_{obs} - Y_{pred})^2}}{\frac{1}{n}\sum_{i=1}^{n} Y_{obs}} \tag{8.12}$$

where Y_{obs} and Y_{pred} are the same as above and n is the number of data points. It is evident from Fig 8.10 that at K_{TC} value of $3x10^{-5}$, ME is the highest (0.74) and RRMSE is at the lowest (0.29). Changing the K_{TC} value from $3x10^{-5}$, RRMSE and ME increased and decreased, respectively. It is worth noting that final calibrated K_{TC}-value in this case is somewhat in between K_{TC} obtained by Verstraeten (2007) for good to moderate vegetation. Notably, about 46% area of the study watershed is covered by the forest (Table 8.2). Low value of RRMSE represents that 66% prediction of the proposed sediment yield model having error less than 29% (at 1σ). Transport capacity maps are

generated using calibrated K_{TC} value for all years (1979-87). Transport capacity map for year 1987 is presented in Fig. 8.11 as illustration. It is evident from this figure that the ridges and the flattened area near the channel, generally cultivated (viz., south-west

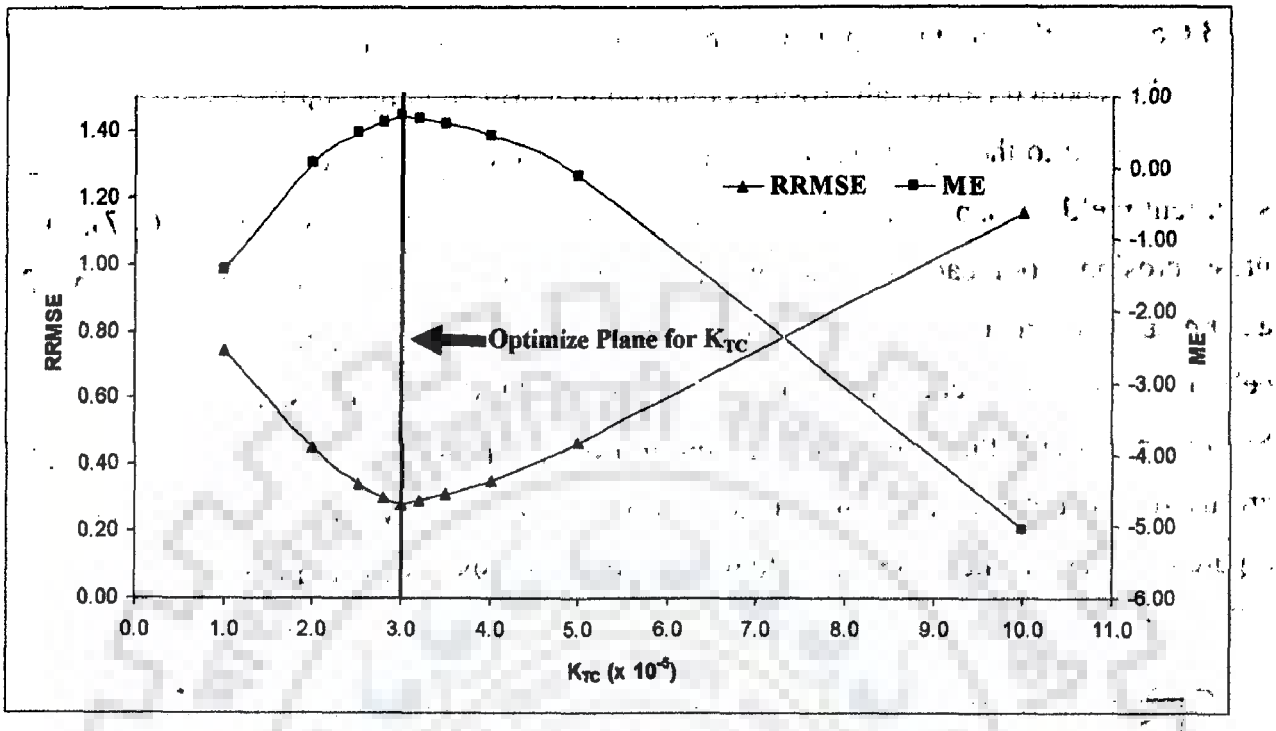

Fig. 8.10: Calibration of K_{TC} for Naula watershed using five years (1979-83) seasonal rainfall-sediment yield data.

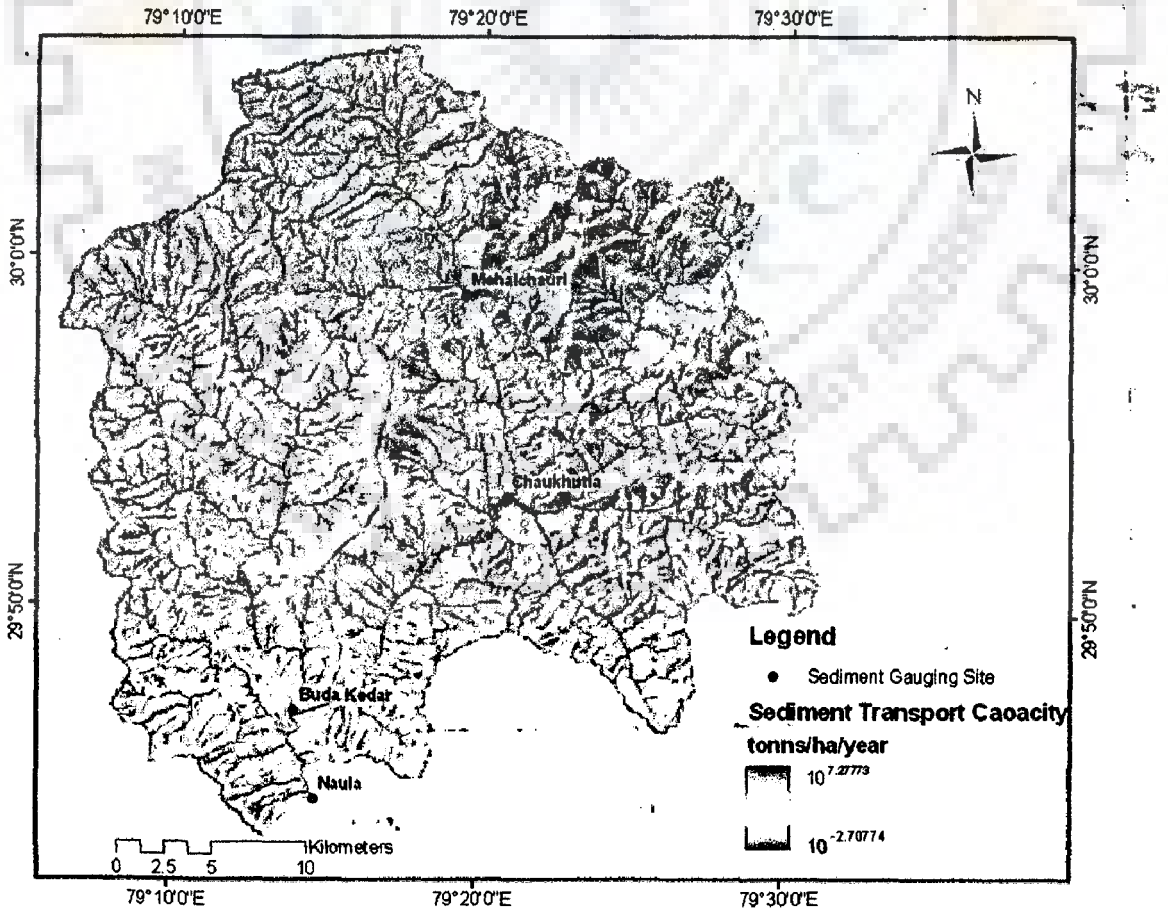

Fig. 8.11: Transport capacity map of Naula watershed for year 1987.

direction of Chaukhutia gauging site) are the areas possessing low transport capacity. However, transport capacity is high in channel areas and the steep head water areas especially where the slope plane curvature is convex in nature.

8.4.3 Computation of Transport Limited Sediment Accumulation and Outflow

As reported earlier, all erosion produced in a grid cell does not find opportunity to get transported to the outlet. Therefore, to convert gross erosion into spatially distributed sediment yield, transport limited accumulation concept is applied. Using Eq. (8.7), the gross erosion from each cell is routed following drainage path to generate map of accumulated sediment yield and deposition by considering the transport capacity of each cell. This process is repeated for all eight years (1979-87) of data used in the analysis. Such maps provide the amount of sediment transported from the system at every cell and are useful for determination of sediment flowing out of the watershed at any location. Figure 8.12 depicts the sediment yield map for the year 1987 as illustration.

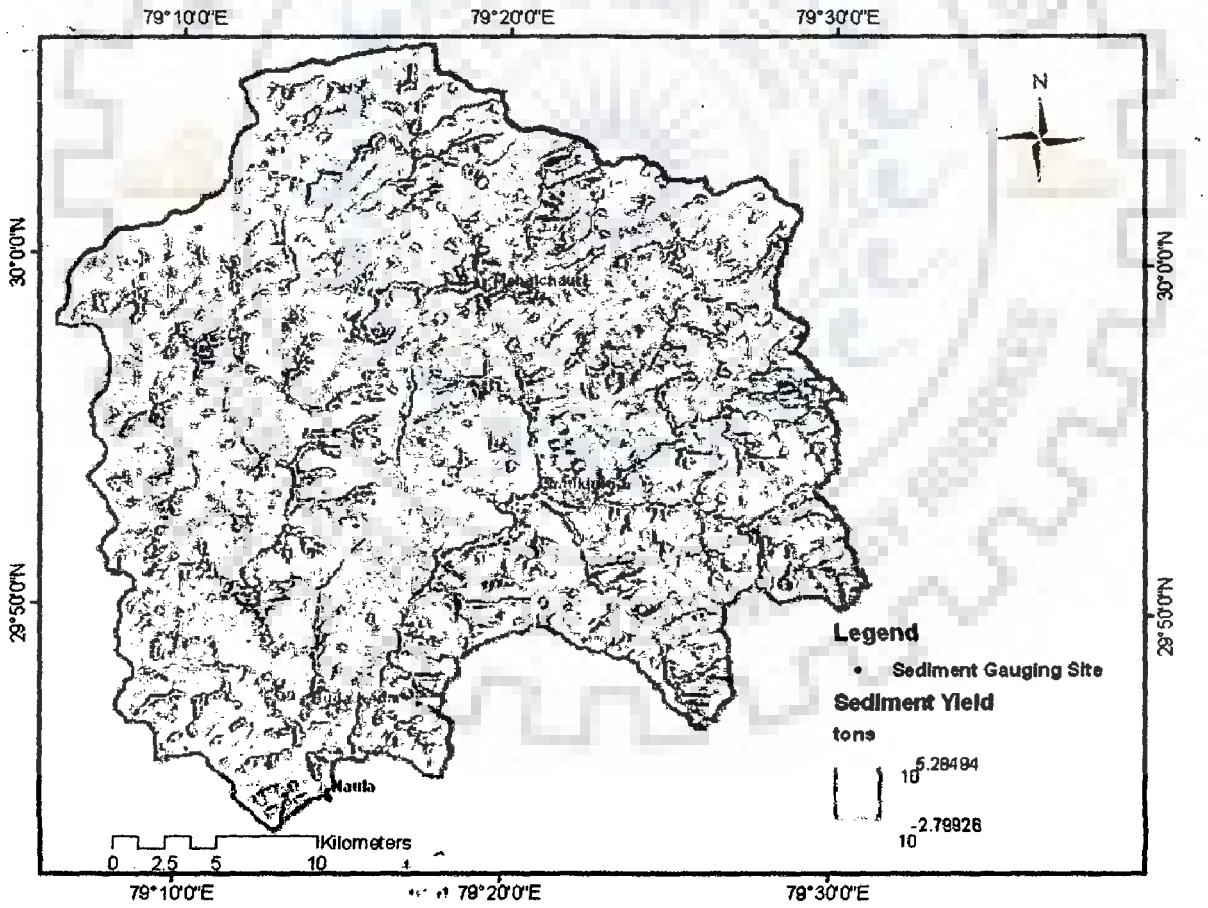

Fig. 8.12: Sediment outflow map of Naula watershed for year 1987.

The pixel value of the sediment outflow map denotes the amount of sediment leaving the current cell to the next downstream cell. Comparison of predicted sediment yield with the observed sediment yield for all years from 1979 to 1987 is shown in Table 8.3. As discussed earlier, the years 1979 to 1983 are used for calibration, and the rest three year data (1985-87) for validation. It is evident from Table 8.3 that the errors in validation period are very low, viz., 26.1%, 9.0%, and 0.2% for 1985, 86, and 87, respectively. Furthermore, model closely simulated the sediment yield in calibration period (1979-83) (Table 8.3). Such low errors in calibration and validation periods indicated that the model performed very well on Naula watershed. Sediment yields maps for years 1979-1986 are presented in Appendix G (Figs. G1&G2).

8.4.4 Investigation of Spatial Distribution Prediction Ability of Model

Takken et al., (1999) found that the validation of spatially distributed models is not sufficient only at outlet due to their highly complex nature. Therefore, to investigate the spatial distribution capability of the proposed model, the data of three gauging sites (Mehalchauri, Budakedar, and Chaukhutia) located an upstream of the Naula site are used in the study. These three gauging sites define sub-watersheds of the study watershed. Mehalchauri (drainage area 162 km^2) and Chaukhutia (drainage area 572 km^2) are located in the main Ramganga catchment while Budakedar (Bino sub-watershed, drainage area 295 km^2) is located at Bino river, a tributary of Ramganga, and just before the confluence of Bino and Ramganga. Sediment yield values of a particular year of these three gauging sites are the numerical values of corresponding pixel from sediment yield map of Naula of the same year. All theses sediment yields with their percent error in prediction for different years are given in Table 8.3. It can be seen from the table that in most of the years, model predicted the sediment yield very well. However, in few years only, the model either over-predicted or under-predicted the sediment yields. In reality, the large errors may be attributed to probable uncertainties in observations and/or model formulation. It can be seen from Table 8.3 that the large errors are mostly negative (over-prediction of model) specially in 1979 for all gauging sites, which is probably attributed to large temporal variability in sediment yield that influenced the observation of sediment data at outlet greatly. Nevertheless, the spatial and temporal variability in rainfall, dynamic nature of vegetation which influence greatly transport capacity and crop management factor for overland regions may be other reason of large error and can be studied in future.

Table 8.3: Year wise comparison between observed and predicted sediment yield at different gauging sites.

Name of Gauging Station	Year	Seasonal Rainfall (mm)	Seasonal Rainfall Erosivity (R)	Observed Sediment Yield (tons)	Predicted Sediment Yield (tons)	Error (%)	
Naula	1979	513.9	257.4	129870.5	181989.5	-40.1	
	1980	808.5	363.8	364101.9	316950.1	13.0	
	1981	449.0	234.0	85613.4	74671.0	12.8	
	1982	615.0	293.9	216658.3	207821.1	4.1	
	1983	674.6	315.4	282875.3	299899.1	-6.0	
	1985	639.6	302.8	289680.6	214088.6	26.1	
	1986	678.7	316.9	246159.0	224057.6	9.0	
	1987	556.0	272.6	192337.1	192727.1	-0.2	
Kedar	1979			94838.2	57333.3	39.5	
	1980			159331.5	81033.0	49.1	
	1981			57955.8	52112.6	10.1	
	1982			71411.9	65469.7	8.3	
	1983			70683.6	70252.3	0.6	
	1985			66718.5	67445.8	-1.1	
	1986			63724.5	70586.4	-10.8	
Chaukhutia	1979	608.9	291.7	67107.0	94790.6	-41.3	(-69.7)
	1980	957.5	417.6	204844.5	133973.8	34.6	(20.4)
	1981	522.5	260.5	52479.0	37600.0	28.4	(15.7)
	1982	729.9	335.4	159862.5	108244.8	32.3	(18.1)
	1983	750.3	342.8	134064.0	116148.8	13.4	(0.2)
	1985	806.9	363.2	129889.8	111509.8	14.2	(-9.2)
Mehalchauri	1979	840.3	375.2	9157.4	12395.2	-35.4	(-69.6)
	1980	943.3	412.4	29729.0	24905.2	16.2	(5.0)
	1981	602.1	289.3	7942.2	11266.9	-41.9	(-64.2)
	1982	985.2	427.6	36282.4	20121.1	44.5	(19.3)
	1983	910.1	400.5	37118.1	21591.8	41.8	(26.1)
	1985	886.3	391.9	50452.5	20729.3	58.9	(46.8)

Furthermore, it is noticed from Table 8.3, the average error gradually increases in the sequence of Budakedar, Chaukhutia, and Mehalchauri. Actually, the rainfall erosivity values used for computation of sediment yields are derived from the weighted rainfall of the Naula. Since the gauging site Budakedar is close to Naula (about 4.8 km aerial distance), no significant difference in weighted rainfall and hence, an attribute of less error recognized. However, Chaukhutia and Mehalchauri having aerial distance of about 18.9 km and 27.8 km, respectively far away from Naula, and hence, using the weighted rainfall of Naula for computation of sediment at these sites may introduce errors. To avoid such circumstances, the sediment yield at Chaukhutia and Mehalchauri is recomputed using new value of rainfall erosivity (R). The values in parenthesis in error column of Table 8.3 represented the error, using the individual value of R in prediction of sediment yield at Chaukhutia and Mehalchauri. It can be seen from the table that in most of the cases (except 3 data points out of 12 data points of Chaukhutia and Mehalchauri), previous error has reduced by approximately 15%. Maximum 25% reduction in error is seen in case of Mehalchauri for year 1982. This suggests the use of spatially distributed rainfall erosivity thiessen map in input domain of the model so that the spatial distribution capability of the model can be improved. Moreover, considering all data points, the accuracy obtained is considered good because even the more elaborate process-based soil erosion models are found to produce results with still larger errors (ASCE, 1975; Foster, 1982; Hadley et al., 1985; Wu et al., 1993; Wicks and Bathurst, 1996).

8.4.5 Generation of Net Erosion/Deposition Maps

Using Eq. (8.8), maps for deposition of sediment can be obtained. When sediment deposition map superimposed over gross erosion map, a net soil erosion/deposition map is produced. Such maps are helpful in identifying areas vulnerable to silt deposition and sediment erosion in the watershed area. Fig. 8.13 depicts net soil erosion/sediment deposition map for year 1987 as illustration. As can be seen from Fig. 8.13 that deposition of sediment resulted at side of some of the stream reaches where transport capacity is low. It is possible to identify the critical areas delivering most of the sediment to the river system. Notably, these areas are not necessarily the same as those producing most erosion, as most of the eroded sediment is deposited within the catchment, before reaching the river system. The net erosion estimated on a cell basis for the watershed is grouped into the following scales of priority: Slight (0 to 5 t ha^{-1} $year^{-1}$), Moderate (5 to 10 t ha^{-1} $year^{-1}$), High (10 to 20 t ha^{-1} $year^{-1}$), Very High (20 to 40 t ha^{-1} $year^{-1}$), Severe

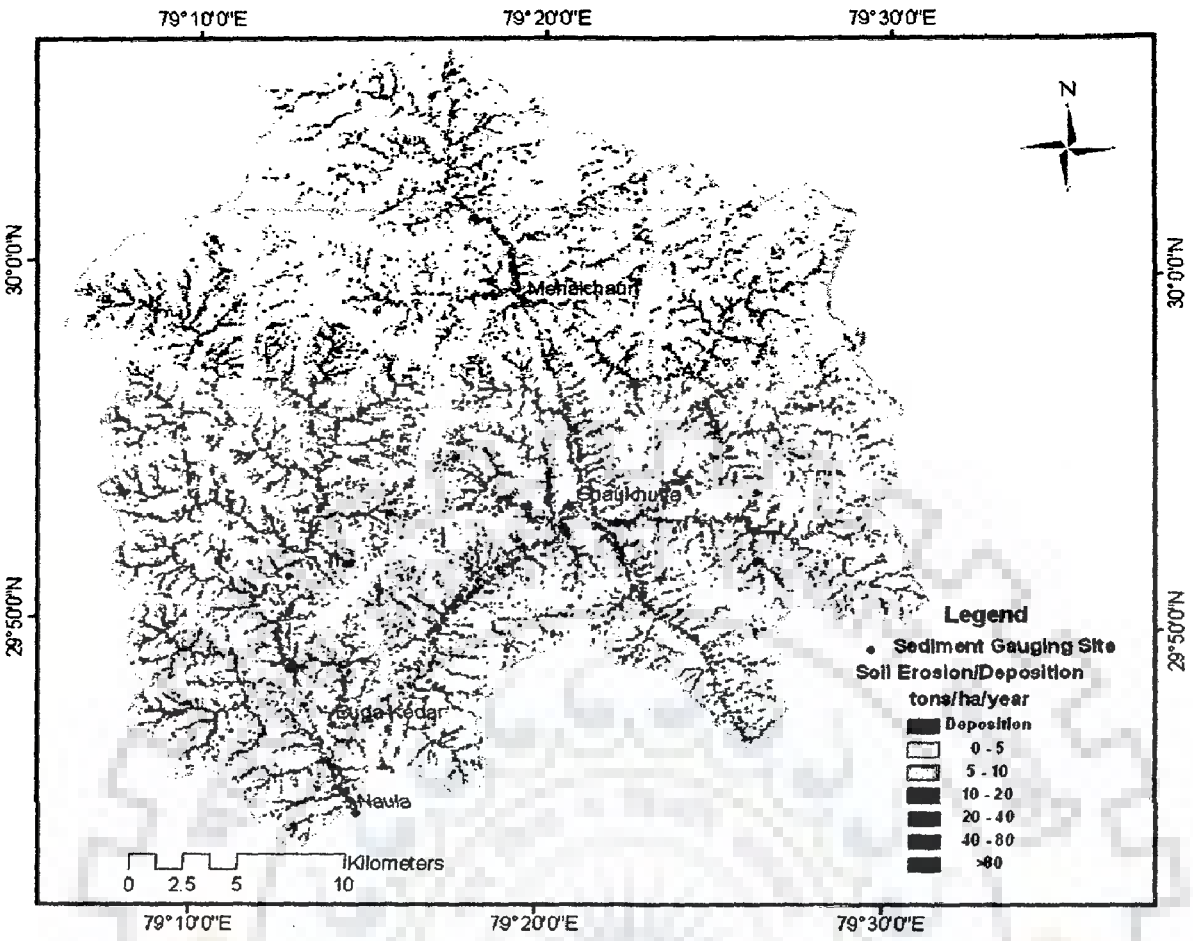

Fig. 8.13: Net erosion/deposition map for year 1987 of Naula watershed.

(40 to 80 t ha^{-1} $year^{-1}$) and Very Severe (> 80 t ha^{-1} $year^{-1}$) erosion classes as per the guidelines suggested by Singh et al. (1992) for Indian conditions. Such a categorization of net soil erosion as illustrated in Fig. 8.13 and it can be of immense significance in deciding the priority levels for implementation of the suitable measures (biological or engineering) for watershed treatment. The net erosion/deposition maps for years 1979-1986 are presented in Appendix H (Figs. H1&H2).

8.5 SUMMARY

A simple model involving only elementary processes of soil erosion/sediment deposition is used to predict the sediment delivery by surface runoff from hill slopes to watershed outlet. Model application is in principle not restricted by the size of the watershed on condition that digital elevation data and land use data are available. Various thematic layers representing different factors of USLE are generated and overlaid to compute spatially distributed gross soil erosion maps for watershed using recorded rainfall for 8 years of the Himalayan watershed. A concept of transport limited accumulation is formulated and used in ArcGIS for generating maps for transport

capacity. Gross soil erosion is routed to the catchment outlet using hydrological drainage paths resulting in generation of transport capacity limited sediment outflow maps. Transport capacity coefficient is calibrated using five year observed rainfall-sediment yield data, a low value of K_{TC} ($3x10^{-5}$) is found. Very low calibrated value of parameter K_{TC} indicates good vegetation cover which reduces transport capacity. Low yearly errors of 26.1%, 9.0%, and 0.2% in prediction of sediment yield are observed when model was applied for three-year data of validation period of the same watershed. Further, the spatial distributed capabilities of model is checked at three different upstream gauging sites of the watershed and found good except for a few points. The errors in estimation further reduced when data on rainfall erosivity values derived from individual weighted rainfall of gauging sites are used. Superimposition of sediment deposition map over gross erosion map resulted in identification of areas vulnerable to soil erosion and deposition. According to recommended range of net soil erosion for Indian conditions, the entire watershed is categorized. The values of net soil erosion/deposition (upto a small unit i.e. a pixel) are described through maps for their use in field for implementation of suitable protection measures.

CHAPTER 9
SUMMARY AND CONCLUSIONS

Rainfall-runoff-sediment yield modelling is basic to design of a wide variety of hydraulic structures, environmental impact assessment, evaluation of the impact of climatic change, irrigation scheduling, flood forecasting, planning of tactical military operation, augmentation of runoff records, pollution abatement, watershed management and so on. To this end, several rainfall-runoff-sediment yield models were developed to mimic the process from plot to catchment scale, however research is still ongoing largely by linearizing different components of rainfall-runoff-sediment yield process.

In developing country like India, where rural population is often more than 65%, assessment of erosion focuses mainly towards on-site effects of erosion. On site erosion strongly affects crop yield, undermines the long term sustainability of farming system, and repeat a major threat to the livelihood of the farmers and rural communities. In the present era of industrialization, more attention is being paid to the society at large, viz., in flood prevention, water reservoir preservation, and water pollution control (Garen et al., 1999). Whether the main concern of soil and water conservation planning is towards prevention of onsite or off-site effects of erosion, there is a growing need for tools that enable to define the spatial distribution of erosion within a catchment i.e to identify sources of sediment erosion. Indeed the location of sediment sources and sinks is more important than the quantification of soil losses, as it is more cost effective than over-dimensioned erosion control measures. Therefore, modelling should be focused on spatial distribution of sediment within the watershed as well sediment yield at the outlet of the watershed.

The main objective of the present research work was to model different major components of rainfall-runoff-sediment yield process in such a manner that the resulted models were simple in structure, easy to use, even by a field worker, and simultaneously parsimonious in data, time, and funds. A summary of the research work and the conclusions arrived at are presented below in sequence of development of models.

9.1 CN-PET RELATIOSHIP

Evapotranspiration plays a vital role in rainfall-runoff process especially in long term hydrological modelling. Several empirical, semi-empirical, physically based methods have been developed over the last 50 years in different parts of the world but no

one can be recommended as the best for any area or any season in terms of its accuracy, profitability and versatility. The following conclusions can be drawn from the study:

1. Different durations PET values for seven watersheds belonging to different agro-climatic zones of India were derived using nine temperature; radiation; and combination-based commonly used methods. Significant variation (upto 42%) among different PET values from different methods was found. Thus, due care should be taken in selection of an appropriate PET estimation method.
2. Following the recommendation of FAO 56, the Penman-Monteith method was used as a standard method for comparing the results due to remaining eight PET method used in this study. Following statistical criteria, Hargreaves-Samani method was found to be the closest to standard method with least RMSE values for all three watersheds of Narmada river basin located in Central India. However, Businger-van-Bavel method yielded the highest RMSE for all three study watersheds, indicating the results being farthest of standard method.
3. The duration-dependent curve numbers derived from rainfall-runoff data of seven different agro-climatic river basins in India exhibit a strong correlation (of power form) with PET of same duration derived from standard Penman-Monteith method. High R^2-values ranging from 0.96 to 0.99 support the general applicability of the proposed concept. Such a relationship invokes to describe the SCS-CN parameter S (or CN) in terms of the maximum possible evaporable depth and to determine PET from the available NEH-4 CN values when corrected for duration, and thus very useful for field engineers.
4. The proposed methodology may be a substitute of the complex PET estimation methods especially in developing countries where establishment of new meteorological stations is difficult due to their high installation and operation costs.

9.2 PDF-BASED SUH DERIVATION

9.2.1 Two-Parameter Inverse Gamma Distribution (2PIGD)

The use of probability distribution function as synthetic unit hydrograph (SUH) has a long successful history in surface water hydrology. The similarity between pdf of a distribution with area under the pdf curve to be unity and a conventional unit hydrograph are considered to be the important features of a pdf for derivation of SUH. In the present study, potential of the two-parameter inverse gamma distribution (2PIGD) was explored

for SUH derivation under limited data availability condition. A simple analytical procedure was proposed for estimation of the 2PIGD distribution parameters, the calculations for which can be performed on simple spread-sheet calculator. For limited data conditions, i.e. one UH parameters, either peak discharge or time-to-peak was known, the other parameter is obtained using Horton ratios (Rodriguez-Iturbe and Valdes, 1979). The distribution parameters of 2PIGD were determined using dimensionless term β and following the developed analytical procedure. Using 2PIGD and geomorphological parameters of Ramganga watershed, simple regression models for peak flow rate and time to peak flow for known value of dynamic flow velocity were proposed. Following conclusions were drawn from this study:

1. For describing the shape of the SUH in limited data condition, the proposed 2PIGD approach gives better results for all storm events than the most flexible and accurate 2PWD, and conventional 2PNGM. However, both 2PWD and 2PNGM performed satisfactory.
2. High value of coefficient of efficiencies, 95% and 89%, and low values of REP, 7.5% and 4.7%, for two Himalayan watersheds namely Gagas and Myantdu-Leska, respectively, support the suitability of 2PIGD in SUH derivation especially for hilly watershed.
3. SRTM data with 3-arc second spatial resolution, most updated, and easily available GIS data are sufficient to extract the realistic drainage network of a river catchment.
4. The proposed simple regression models for peak flow rate and time to peak flow with known value of dynamic flow velocity will be helpful for the field engineers for regional flood prediction and warning systems as well as hydraulic engineers for design of hydraulic structures particularly for Ramganga watershed.
5. Considering data accessibility, time, and funds, major constraints in developing countries, the combination of PDF-SRTM-GIS can play a vital role in the development of more accurate regional methodologies.

9.2.2 Lag Time-Based GIUH Approach

Direct runoff hydrographs of two Himalayan watersheds were estimated with high degree of accuracy by redefining the gamma IUH parameters n and k in terms of geomorphological parameters and lag time of watershed. Melton number concept coupled with "DEM hydro-processing" module of ILWIS GIS software was used for extraction of

drainage network of study watersheds. The workability of revised GIUH approach was checked using different isolated rainfall-runoff events of Gagas and Chaukhutia watersheds. The following conclusions can be drawn from this study:

1. Direct runoff from mountainous watersheds can be estimated with high degree of accuracy by redefining the gamma IUH parameters n and k in terms of geomorphological parameters and lag time of the watershed.
2. The approach Proposed for estimation of parameters is more conceivable than the older one due to elimination of dynamic velocity in which a great subjectivity is involved in its estimation.
3. A PC-based GIS and Remote Sensing software, Integrated Land and Water Information System (ILWIS) was used for extraction of geomorphological parameters from SRTM data with 3-arc second spatial resolution for extraction of DEM, drainage network, and geomorphological parameters. It was found that Melton number concept can be used for extraction of realistic drainage network especially when toposheets of study area are not available.
4. Stream threshold plays a vital role in extraction of drainage network and geomorphological parameters. Selection of wrong stream threshold may lead to errors even change the Strahler stream order of the watershed.

9.3 LONG-TERM RAINFALL-RUNOFF MODELLING

The Artificial Neural Network (ANN) models have been applied to several diverse hydrological problems and the results in each case have been found very encouraging. ANNs are capable to handle nonlinearity of the complex systems to be modelled with flexible mathematical structure. Hence in this study, a radial basis function ANN (RBFANN) was developed to model rainfall generated runoff for Ramganga basin and its Chaukhutia and Naula sub-watersheds. In this study, a computer program was developed using k-means clustering algorithm for the RBF neural network to carry out rainfall-runoff modelling of the Upper Ramganga river basin. The best input combination was decided by cross-correlation matrix method, which consists of rainfall and discharge values. The model performance is improved by proper selection of suitable learning rates and optimized number of iterations to train the network. The following conclusions can be drawn from this study:

- Radial Basis Function can be a better solution for rainfall-runoff modelling as physically based models with partial differential equations of mass and energy are

difficult to employ due to lack of data. The selection of learning rate, especially in function layer (ALR) as well as the number of iterations required is very important in optimization. The proposed program has flexibility to change the input and output variables and fix the radial basis nodes.

- The proposed model performed very well in calibration, cross-validation, and verification for Naula (efficiency as 86.28%, 84.91%, and 86.81%) and Chaukhutia (efficiency as 77.48%, 84.76%, and 84.59%) watersheds. However, in case of Ramganga watershed the model performed very well in calibration (76%) and cross-validation (77.68%) whereas it performed satisfactorily in verification (68.25%).
- The proposed model simulates the long-term daily runoff reasonably well in all the considered watersheds, and therefore, its applicability can be generalized for all the sub-watersheds of the Ramganga river basin.

9.4 SPATIALLY DISTRIBUTED SEDIMENT YIELD MODEL

Gross soil erosion and transport capacity for Naula watershed were calculated by overlaying the different thematic layers prepared in GIS environment, and depicted in the forms of maps for easy use. Considering the transport capacity of each pixel, the concept of transport limited accumulation was formulated and used in ArcGIS for generating sediment outflow from each cell and finally up to the outlet. To this end, a programme in Interactive Data Language (IDL) was prepared using the basic principle of overland flow routing. The workability of model was checked by comparing the results with the historical observed sediment yield data at the outlet of the study watershed. Spatial distribution capability of the model was further checked by the observed sediment data at three different gauging sites located within the study watershed. The following conclusions can be drawn from the study:

1. Very low value of calibrated transport capacity coefficient K_{TC} indicates good vegetation in the study area (about 46% of the study area covered by forest), and hence, the transport capacity is an important factor for routing the sediment up to the outlet.
2. The proposed GIS-based spatially distributed model estimates the sediment yield with high accuracy, accompanying a very low error in validation period. Since SRTM data, satellite images, and soil map (input of the proposed model) are easily available throughout the globe, the model can be easy to apply to hilly watersheds.

3. Variable rainfall erosivity (R) map derived from the individual rainfall of available raingauge station is easy to use in the input domain of the model to achieve high degree of spatial distribution of sediment within the watershed.
4. Deposition of sediment resulted at the sides of some stream reaches in valley due to low transport capacity. Such sites are not suitable for the hydro-based multipurpose projects due to high degree of sedimentation, which may result in rapid reduction in reservoir capacity.

9.5 MAJOR RESEARCH CONTRIBUTIONS OF THE STUDY

The major components of rainfall-runoff-sediment yield process were critically reviewed for their behavior, structure, and realm of application, and the inconsistencies identified. Consequently, the study attempted to propose more improved/modified versions of the rainfall-runoff-sediment yield models based on more practical utility, simplicity of structure, and easy to use in data scarcity situation even in ungauged watersheds. The major research contributions of the present study are summarized as follows:

1. An attempt has been made to extend the concept of SCS-CN methodology for, yet to be explored, estimation of duration-dependent long term mean PET. Knowing one parameter, CN, for a duration, PET of the same duration can be estimated using the PET-CN empirical relation proposed for several hydro-meteorologically different watersheds.
2. 2PIGD is explored for its suitability to SUH derivation using geomorphological parameters under limited data availability conditions. An analytical but simple procedure is developed for parameters estimation of 2PIGD. The performance of 2PIGD was superior to two-parameter Weibull distribution (2PWD) and conventional two-parameter Nash gamma model (2PNGM). Melton number concept was coupled with GIS for extraction of a drainage network
3. Conventional GIUH model is revised using time lag concept. Its introduction to the conventional GIUH approach completely omits the necessity of velocity parameter, which is difficult to estimate in field.
4. A more accurate RBFANN model based on k-means clustering algorithm is proposed for long term prediction of runoff.
5. A simple spatially distributed sediment yield model based on the concept of erosion-deposition process is proposed. It is more rational, and pragmatic than the

lumped Sediment Delivery Ratio (SDR) approach. The proposed cell-based Transport Limited Accumulation (TLA) approach is used to route the sediment up to the outlet by considering the transport capacity of each pixel.

9.6 SCOPE FOR FUTURE RESEARCH

1. In the present study, the proposed PET-CN relation derived for assessment of a long-term mean potential evapotranspiration is not time/duration/season specific. Hence, a particular monthly/seasonal relationship can be developed and different CN-values derived. Furthermore, the ratio of actual retention and potential retention i.e., F/S can be coupled with the ratio of actual evapotranspiration to Potential evapotranspiration i.e., AET/PET. In addition, since parameter λ is a regional parameter that depends on geological and climatic factors and hence most sensitive parameter in PET estimation. The results can be made more promising with the use of adequate value of λ other than the standard value of 0.2. The PET-CN relations proposed may be useful in hydro-meteorologically similar regions and the aspect needs further exploration.
2. In the present study, a constant value of lag time was used, which may however vary with time or season. Therefore, using UHs derived from variable lag time may be a scope for future study to quantify the effect of urbanization and land use changes on water resources.
3. Several probability distributions functions (pdfs) are still remaining for their exploration for SUH derivation.
4. The present study deals with the spatial distribution of soil erosion/sediment deposition with the assumption that land use/land cover and other parameters remain constant with time. However, several parameters change with time/season. Therefore, incorporation of variability of these parameters with time/season in GIS environment may form to be a scope for future study.

REFERENCES

1. Abramowitz, M., and Stegun, D.I. (1964). Handbook of Mathematical Function. Dover, New York.
2. Adam, P., Rowinski P.M., and Napiórkowski J.J. (2006). Assessment of longitudinal dispersion coefficient by means of different neural networks. 7th International Conference on Hydroinformatics HIC.
3. Agarwal, A. (2002). Artificial neural networks and their application for simulation and prediction of runoff and sediment yield. Unpublished PhD thesis thesis, G. B. Pant University of Agriculture and Technology, Pantnagar, U P., India.
4. Agarwal, A., and Singh, R.D. (2004). Runoff modelling through back propagation artificial neural network with variable rainfall-runoff data. Water resources management, **18**(3), 285-300.
5. Agarwal, A., Singh R.D., Mishra, S.K., and Bhunya, P.K., (2005). ANN-based sediment yield models for Vamsadhara river basin (India). Journal of Biosystems Engineering, **31**(1), 95-100.
6. Aksoy, H., and Kavvas, M.L., (2005). A review of hillslope and watershed scale erosion and sediment transport models. Catena, **64**, 247– 271.
7. Allen, R. Pereira, L.S. Raes, D., and Smith M. (1998). Crop evapotranspiration: guidelines for computing crop water requirements. Irrigation and Drainage Paper, **56**, FAO, Rome, Italy
8. Allen, R.G., Jensen, M.E., Wright J.L, and Burman, R.D. (1989). Operational estimates of reference evapotranspiration. Agron. J, **81**, 650–662.
9. Allen, R.G., Smith, M., Pereira, L.S., and Perrier, A. (1994). An update for the calculation of reference evapotranspiration. ICID Bulletin, **43**(2), 35-92.
10. Amatya, D.M., R.W. Skaggs, and Gregory. J.D. (1995). Comparison of Methods for Estimating REF-ET. Journal of Irrigation and Drainage Engineering, **121**, 427-435.
11. American Society of Civil Engineers (ASCE). (1975). Sedimentation Engineering. American Society of Civil Engineering, New York: NY.
12. Andersson, L., and Harding, R.J. (1991). Soil-moisture deficit simulation with models of varying complexity for forest and grassland sites in Sweden and the UK. Water resources Management, **5**, 25-46.
13. Andreassian, V., Perrin, C., and Michel, C. (2004). Impact of imperfect potential evapotranspiration knowledge on the efficiency and parameters of watershed models. Journal of Hydrology, **286**(1- 4), 19–35.
14. Anmala, J.; Zhang, B. and Govindaraju, R.S. (2000). Comparison of ANNS and empirical approaches for predicting watershed runoff. Journal of Water Resources Planning and Management, **126**(3), 156-166.
15. ARC/INFO (2005). ESRI Inc., Redlands, Calif. Window version **9**.
16. Arnold, J.G., Engel, B.A., and Srinivasan, R. (1993). Continuous-time, grid cell watershed model. In: Proceedings of the Conference, Spokane, WA, June 18–19, 267–278.

17. Aron, G., and White, E. L. (1982). Fitting a gamma distribution over a synthetic unit hydrograph. Water Resour. Bull, **18**(1), 95–98.

18. Aron, G., Miller, A. C., J. and Lakatos, D. F. (1977). Infiltration formula based on SCS curve number. J. Irrig. Drain. Div., ASCE, **103** (IR4), 419–427.

19. ASCE, (2000a). Task committee on application of artificial neural networks in hydrology. Artificial neural networks in hydrology. 1: Preliminary concepts. Journal of Hydrologic Engineering, **5**(2), 115-123.

20. ASCE, (2000b). Task committee on application of artificial neural networks in hydrology. Artificial neural networks in hydrology. 11: Hydrology applications. Journal of Hydrologic Engineering, **5**(2), 124-137.

21. Atkinson, E. (1995). Methods for assessing sediment delivery in river systems. Hydrological Sciences, **40**(2), 273–280.

22. Auerswald, K., and Haider J. (1996). Runoff curve numbers for small grain under German cropping conditions. Journal of Environmental Management, Academic Press Ltd. **47**, 223-228.

23. Babu, R., Dhyani, B.L., and Kumar, N. (2004). Assessment of erodibility status and refined Iso- Erodent Map of India. Indian J Soil Conserv., **32**(2), 171–177

24. Banasik, K., and Walling, D.E. (1996). Predicting sedimentgarphs for a small agricultural catchment. Nordic Hydrology, **27** (4), 275–294.

25. Bazoffi, P., Baldasarre, G., and Vasca, S. (1996). Validation of the PISA2 model for the automatic assessment of reservoir sedimentation. In Proceedings of the International Conference on Reservoir Sedimentation, Albertson M (ed.). Colorado State University: Colorado, 519–528.

26. Beasley, D.B., Huggins, L.F., and Monke, E.J. (1980). ANSWERS: a model for watershed planning. Transactions of the ASAE, **23**, 938– 944.

27. Bernard, M. (1935). An approach to determinate stream flow. Trans. ASCE **100**, 347–362.

28. Berod, D.D., Singh, V.P., Devred, D., and Musy, A. (1995). A geomorphologic non-linear cascade (GNC) model for estimation of floods from small alpine watersheds. J. Hydrology, **166**, 147–170.

29. Beven, K.J. (2001). Rainfall–runoff modelling: the primer. Wiley, New York. 360.

30. Bhaskar, N.R., Parida, B. P. and Nayak, A.K. (1997). Flood estimation for ungauged catchments using the GIUH. J. Water Resource Plan. Manage. ASCE, **123**(4), 228–238.

31. Bhunya, P. K., Berndtsson, R., Ojha, C. S. P., and Mishra, S. K. (2007). Suitability of gamma, chi-square, Weibull and beta distributions as synthetic unit hydrographs. J. Hydrology, **334**, 28–38.

32. Bhunya, P.K., Berndtsson, R., Singh, P.K. and Hubert, P. (2008). Comparison between Weibull and gamma distributions to derive synthetic unit hydrograph using Horton ratios. Water Resour. Res. **44**, W04421. doi:10.1029/2007WR006031.

33. Bhunya, P.K., Ghosh, N.C., Mishra, S.K., Ojha, C.S.P. and Berndtsson, R. (2005). Hybrid model for derivation of synthetic unit hydrograph. J. Hydrol. Engg., ASCE, **10**(6), 458-467.

34. Bhunya, P.K., Mishra, S.K., and Berndtsson, R. (2003). Simplified two parameters Gamma distribution for derivation of synthetic unit hydrograph. J. Hydrol. Eng. ASCE, **8**(4), 226–230.

35. Bhunya, P.K., Mishra, S.K., Ojha, C.S.P., and Berndtsson, R. (2004). Parameter estimation of Beta-distribution for unit hydrograph derivation. J. Hydrol. Engg., ASCE, **9**(4), 325–332.

36. Bhunya, P.K., Singh, P.K. and Mishra, S.K. (2009). Fréchet and chi-square parametric expressions combined with Horton ratios to derive a synthetic unit hydrograph. Hydrological Science, **54**(2), 274-286.

37. Biesemans, J. Meirvenne, M.V., and Gabriels, D. (2000). Extending the RUSLE with the Monte Carlo error propagation technique to predict long-term average oV-site sediment accumulation. Journal of Soil and Water Conservation, **55**, 35–42.

38. Blaney, H.F., and Criddle, W.D. (1950). Determining water requirements in irrigated areas from climatological and irrigation data. Technical Paper no. **96**, US Department of Agriculture, Soil Conservation Service, Washington, DC.

39. Bonta, J.V. (1997). Determination of watershed curve number using derived distributions. Journal of Irrigation and Drainage Engineering, ASCE, **123**(1), 234-238.

40. Boszany, M. (1989). Generalization of SCS curve number method. J. Irrig. Drain. Engg., ASCE, **115**(1), 139–144.

41. Boyd, M.J. (1982). A linear branched network model for storm rainfall and runoff. In Rainfall–Runoff Relationship, Singh VP (ed.), Water Resources Publications, Littleton, Colorado, 111–124.

42. Boyd, M.J., Pilgrim, D.H. and Cordery, I. (1979). A storage routing model based on catchment geomorphology. J. Hydrology, **42**, 209-230.

43. Brakensiek, D.L., and Rawls, W.J. (1988). Effects of agricultural and rangeland management systems on infiltration, in proceedings of the American socity of Agricultural engineers Symposium on Modelling Agricultural Forest and Rangeland Hydrology, American socity of Agricultural engineers, St. Joseph, Mich.

44. Broomhead, D., and Lowe, D. (1988). Multivariable functional interpolation and adaptive networks. Complex System, **2**, 321–355.

45. Brutsaert, W. (1982). Evaporation into the Atmosphere: Theory, History, and applications. Reidel, Higham, MA, 229.

46. Brutsaert, W. (1986). Catchment-scale evaporation and the atmospheric boundary layer. Water Resour. Res., **22**(9), 39s-45s.

47. Burman, R.D., Laramie, W.Y., Nixon, P.R., Wright, J.L., and Pruitt, W.O. (1983). Water Requirements. In: Jensen, M.E. (ed.), Design and Operation of Farm Irrigation Systems, Chapter 6, ASAE, Monograph No. **3**. USA.

48. Burnash, R.J.C. (1995). In: Singh, V.P. (Ed.), The NWS river forecast system catchment modeling Computer Models of Watershed Hydrology. Water Resources Publications, Highlands ranch, Co., 311–366.

49. Calder, I.R. (1983). An objective assessment of soil-moisture deficit models. Journal of Hydrology, **60**, 329–355.

50. Chang, F.J., and Chen, Y.C. (2003). Estuary water-stage forecasting by using radial basis function neural network. Journal of Hydrology, **270**, 158–166.

51. Chang, M. (2005). Forest Hydrology: An Introduction to Water and Forests. Boca Raton: Taylor and Francis group.

52. Chang, M., Ting, J.C., and Wong, K.L. (1983). Soil moisture regimes as affected by silvicultural treatments in humid East Texas, in Hydrology of Humid Tropical Regions with Particular References to the Hydrological Effects of Agricltural and Foresty Practices, IAHS Publ,. No. **137**, 175-186.

53. Chaves, P. and Kojiri, T. (2007). Deriving reservoir operational strategies considering water quantity and quality objectives by stochastic fuzzy neural networks. Adv. Water Resour., **30**, 1329-1341

54. Chen, C.L. (1982). An evaluation of the mathematics and physical significance of the soil conservation service curve number procedure for estimating runoff volume. In Rainfall–Runoff Relationship, by Singh VP (ed.). Water Resources Publications: Littleton, CO.

55. Chen, V.J. and Kuo, C.Y. (1986). A Study on Synthetic Sedimentgraphs for Ungaged Watersheds. J. Hydrol., **84**, 35-54.

56. Chiang, Y. M., Chang, L.C., and Chang, F.J (2004). Comparison of staticfeedforward and dynamic-feedback neural networks for rainfall–runoff modeling. Journal of Hydrology, **290**, 297–311.

57. Choisnel, E., de Villele O., and Lacroze, F. (1992). Une approche uniformisee du calcul de lÕevapotranspiration potentielle pour lÕensamble des pays de la Communaute Europeenne (A common procedure to calculate potential evapotranspiration in all nations of the European Community).Centre Commun de Recherche, Commission des Communautes Europeennes, , *L 2920* Luxembourg.

58. Chow, V.T. (1964). Handbook of Applied Hydrology. McGraw-Hill, New York, NY.

59. Christiansen, J.E. (1968). Pan evaporation and evapotranspiration from climatic data. J. Irrig. Drain., **94,** 243–265

60. Christiansen, J.E. and Hargreaves, G.H.. (1969). Irrigation requirements from evaporation. Transactions of the International Commission on Irrigation and Drainage, **23**(3), 569-596.

61. Chutha, I. and Dooge, J.C.I. (1990). The shape parameters of the geomorphologic unit hydrograph. J. Hydrol., **117**(4), 81–97.

62. Clark C.O. (1945). Storage and the unit hydrograph. Transactions of the American Society of Civil Engineers 110, 1419–1446.

63. Cleugh, H.A., Leuning, R. Mu, Q.Z., and Running S.W. (2007). Regional evaporation estimates from flux tower and MODIS satellite data. Remote Sensing of Environment, **106**(3), 285-304.

64. Cohen, M.J., Shepherd, K.D., and Walsh, M.G. (2005). Empirical formulation of the universal soil loss equation for erosion risk assessment in a tropical watershed. Geoderma **124**, 235–252.

65. Coulibaly, P., Anctil, F., and Bobe´e, B. (1998). Real time neural network based forecasting system for hydropower reservoirs. In: Miresco, E.T. (Ed.), Proceedings

of the First International Conference on New Information Technologies for Decision Making in Civil Engineering, University of Quebec, Montreal, Canada, 1001–1011.

66. Croley, T.E. II. (1980). Gamma synthetic hydrographs. J. Hydrol., **47**, 41–52.

67. Cudennec, C., Fouad, Y., Gatot, I. S. and Duchesne, J. (2004). A geomorphological explanation of the unit hydrograph concept. Hydrol. Processes, **18**(4), 603–621.

68. CWC, (1983). Flood Estimation Report for Upper Narmada and Tapi Subzone (Subzone 3C), Directorate of CWC, New Delhi.

69. Dawson, C.W., Harpham, C., Wilby, R L., and Chen, Y. (2002). Evaluation of artificial neural network techniques for flow forecasting in the River Yangtze, China Hydrol. Earth Syst. Sci., **6**(4), 619-626.

70. De Roo, A.P.J., and Jetten, V.G. (1999). Calibrating and validating the LISEM model for two data sets from the Netherlands and South Africa. Catena, **37**(3-4), 477–493.

71. De Roo, A.P.J., Wesseling, C.G., and Ritsema, C.J., 1996. LISEM: a single-event physically based hydrological and soil erosion model for drainage basins: I. Theory, input and output. Hydrological Processes, **10**, 1107– 1117.

72. de Vos, N.J., and Rientjes, T.H.M. (2005). Constraints of artificial neural networks for rainfall-runoff modeling: Trade-offs in hydrological state representation and model evaluation. Hydrol. Earth Syst. Sci., **9**, 111 –126.

73. Deco, G., and Obradovic, D. (1996). An information theory based learning paradigm for linear feature extraction, Neurocomputing, **12**, 203-221.

74. Desmet, P.J., and Govers, G. (1995). GIS-based simulation of erosion and deposition patterns in agricultural landscape: a comparison of model results with soil map information. Catena, **25**, 389–401

75. Desmet, P.J., and Govers, G. (1996). A GIS-procedure for the automated calculation of the USLE LS-factor on topographically complex landscape units. Journal of Soil and Water Conservation **51**, 427–433.

76. Dillaha, T.A., Wolfe, M.L., Shirmohammadi, A., and Byne, F.W. (2001). ANSWERS-2000. In: Parsons, J.E., Thomas, D.L., Huffman, R.L. (Eds.), Non-Point Source Water Quality Models: Their Use and Application. Final Report of USDA-CSREES Southern Region Research Project S-273, Development and Application of Comprehensive Agricultural Ecosystems Models, 200 pp.

77. Doorenbos, J., and Pruitt, W.O. (1977). Crop Water Requirements. Irrigation and Drainage Paper 24, Food and Agriculture Organization of the United Nations: Rome, Italy; 144.

78. Edson, C.G. (1951). Parameters for relating unit hydrograph to watershed characteristics. Trans. Am. Geophys. Union, **32**(4), 591–596.

79. Eldho, T.I., Jha, A. and Singh, A.K. (2006). Integrated Watershed Modelling using a Finite Element Method and a GIS Approach. International Journal of River Basin Management, IAHR, Vol. **4** (1), 1-9.

80. Eldho, T.I., Jha, A. Singh, A.K. and Jana, R. (2007). A GIS and SCS-CN based integrated model for rainfall-runoff simulation of ungauged watershed. Water and Energy International Journal, CBIP, Vol. **64**(4), 30-39 .

81. Elsheikh, S., and Gurceio, R. (1997). GIS topographic analysis applied to unit hydrograph models: sensitivity to DEM resolution and threshold area. Remote sensing and geographic information system for design and operation of water resources system. Rabat symposium S3, IAHS publication no 242.

82. Elwell, H.A. (1978). Modelling soil losses in southern Africa. Journal of Agricultural Engineering Research, **23**: 117–127.

83. Entekhabi, D., Rodriguez-Iturbe, I. and Castelli, F. (1996). Mutual interaction of soil moisture and atmospheric processes. J. Hydrol., **184,** 3–17.

84. ERDAS (Earth Resources Data Analysis System). 2005. ERDAS Imagine 8.6, Users Manual. ERDAS Inc.: Atlanta, GA.

85. Espey, W.H.J., and Winslow, D.E. (1974). Urban flood frequency characteristics, J. Hydraul. Div., **100**(2), 279–293.

86. ESRI (Environmental Systems Research Institute) (1994). Cell based modeling with GRID. Environmental Systems Research Institute Inc., Redlands, California, USA.

87. Federer, C.A., Vörösmarty, C., and Fekete, B. (1996). Inter-comparison of Methods for Calculating Potential Evaporation in Regional and Global Water Balance Models, Water Resources Research, **32,** 2315-2321

88. Fernando, D.A.K., and Jayawardena, A.W. (1998). Runoff forecasting using RBF networks with OLS algorithm. J.Hydrol. Engg., ASCE, **3**(3), 203-209.

89. Ferro, V., and Minacapilli, M. (1995). Sediment delivery processes at basin scale. Hydrol. Sci. J., **40**(5), 703-717.

90. Ferro, V., and Porto, P. (2000). A sediment delivery distributed (SEDD) model. J. Hydrol Engng ASCE, **5**(4), 411-422.

91. Ferro, V., Porto, P., and Tusa, G. (1998). Testing a distributed approach for modelling sediment delivery. Hydrological Sciences Journal, **43,** 425– 442.

92. Fleurant, C., Kartiwa, B. and Roland, B. (2006). Analytical model for a geomorphological instantaneous unit hydrograph. Hydrological Processes, **20**, 3879-3895.

93. Foster, G.R. (1982). Modelling the erosion processes. In Hydrological Modelling of Small Watersheds, Haan CT, Johnson H, Brakensiek DL (eds). ASAE Monograph No. 5, American Society of Agricultural Engineers, St. Joseph, MI; 297–380.

94. Foster, G.R., and Meyer, L.D. (1972). A closed form soil erosion equation for upland erosion. In: Shen, H.W. (Ed.), Sedimentation. Colorado State University, Ft Collins, Colorado, 12.

95. Foster, G.R., Lane, L.J., Nowlin, J.D., Laflen, J.M., and Young, R.A. (1981). Estimating erosion and sediment yield on field-sized areas. Transactions of the ASAE, 1253– 1262.

96. Fowler, A. (2002). Assessment of the validity of using mean potential evaporation in computations of the long-term soil water balance. Journal of Hydrology, **256**(3–4), 248–263.

97. French, M.N., Krajeswski, W.F., and Cuykendall, R.R. (1992). Rainfall forecasting in space and time using a neural network. Journal of Hydrology, **137**, 1-31.

98. Frere, M. and Popov., G.F. (1979). Agrometeorological crop monitoring and forcasting. FAO plant production and protaction paper 17, FAO, United Nations, Rome, 36-43.

99. Fujimaki, H., Shimano, T., Inoue, M., and Nakane, K., (2006). Effect of salt crust on evaporation from a bare saline soil. Vadose Zone Journal, Soil Science Society of America, **5,** 1246-1256.

100. Garen, G., Woodward, D., and Geter, F. (1999). A user agency's view of hydrologic, soil erosion and water quality modelling. Catena, **37,** 277-289.

101. Gaur, M. L. (1999). Modeling of surface runoff from natural watersheds with varied roughness. Unpublished PhD Thesis, Department of Hydrology, Indian Institute of Technology, Roorkee, India, 1–270.

102. Gaur, M. L. (2001). Influence of physiographic factors on watershed response in KW modeling-A case study. Hydrol. J., **24**(1), 15–25.

103. Gaur, M. L., and Mathur, B. S. (2003). Modeling event based temporal variability of flow resistance coefficient. J. Hydrol. Engg., ASCE, **8**(5), 266–276.

104. Geeta, K., Mishra, S.K., Eldho, T.I., Rastogi, A.K., and Pandey, R.P. (2008). SCS-CN-based continuous simulation model for hydrologic forecasting. Water Res. Manage., **22**,165-190.

105. Geetha, K., Mishra, S.K., Eldho, T.I., Rastogi, A.K. and Pandey, R.P. (2007) Modifications to SCS-CN method for long-term hydrologic simulation. J. Irrig. Drain. Eng., **133**(5), 475–486.

106. Georgakakos, K.P., Bae, D.-H. and Cayan, D. R., (1995). Hydroclimatology of continantel watershed, temporal analysis. Water Resour. Res., **31**(3), 655-675

107. George, B. A., Reddy, B.R.S., Raghuwanshi, N.S., and Wallender, W. W. (2002). Decision Support System for estimating reference crop evapotranspiration J. of Irrigation and Drainage. Div. ASCE, **128**(1) 1-10

108. Gidrometeoizdat. (1967). The Water resources and Water Balance of the Territory of the Soviet Union. Leningrad, 199 p.

109. GLCF. (2008). Earth science data interface.<http://glcfapp.umiacs.umd.edu:8080/esdi/index.jsp> (January 2008).

110. Gosain, A. K., and Sandhya, R. (2004). GIS-based Technologies for Watershed Management, Current Science, Vol. **87**(7).

111. Govers, G., and Loch, R., (1993). Effects of initial water content and soil mechanical strength on the runoff erosion resistance of clay soils. Australian Journal of Soil Research, **31**, 549–566.

112. Govindaraju, R.S. (2000). Artificial neural networks in hydrology. I: Preliminary concepts. Journal of Hydrologic Engineering, **5**, 115-123.

113. Govindaraju, R.S., and Kavvas, M.L., (1991). Modeling the erosion process over steep slopes: approximate analytical solutions. J. Hydrol., **127**, 279–305.

114. Graf, W.H. (1971). Hydraulic of Sediment Transport.. McGraw-Hill Book Company, Inc, New York.

115. Gray, D. M. (1961). Synthetic hydrographs for small drainage areas. Proc. Am. Soc. Civil Engrs., **87**(HY4), 33–54.

116. Griffin, M.L., Beasley, D.B., Fletcher, J.J., and Foster, G.R. (1988). Estimating soil loss on topographically non-uniform field and farm units. Journal of Soil Water Conservation **43**, 326–331.

117. Grimm, M., Jones, R.J.A., Rusco, E., and Montanarella, L. (2003). Soil erosion risk in Italy: A revised USLE approach. European Soil Bureau Research Report No. **11**, EUR 19022 EN.

118. Gupta, V.K., Waymire, E., and Wang, C. T. (1980). A representation of an instantaneous unit hydrograph from geomorphology. Water Resour. Res., **16**(5), 863–870.

119. Haan, C.T., Barfield, B.J., and Hayes, J. C. (1994). Design Hydrology and Sedimentology for Small Catchments. Academic Press, New York.

120. Haase, D., and Frotscher, K. (2005). Topography data harmonisation and uncertainties for large and transboundary river basins applying SRTM, laser scanner and cartographic elevation models. Advances in Geosciences 5, 65-73.

121. Hadley, R.F., Lal, R., Onstad, C.A., Walling, D. E. and Yair, A. (1985). Recent developments in Erosion and Sediment Yield Studies. UNESCO (IHP) Publication, Paris, France.

122. Haktanir, T., and Sezen, N. (1990). Suitability of two-parameter Gamma distribution and three-parameter Beta distribution as synthetic hydrographs in Anatolia. Hydrol. Sci. J., **35**(2), 167–184.

123. Hall, M.J. (1984). Urban Hydrology. Elsevier applied science publisher, London, UK.

124. Hargreaves, G.H., and Samani, Z.A. (1982). Estimating potential evapotranspiration. Technical note. Journal of Irrigation and Drainage Engineering, **108**(3), 225–230.

125. Hargreaves, G.H., and Samani, Z.A.. (1985). Reference crop evapotranspiration from temperature. Applied Engineering in Agriculture **1**(2), 96-99

126. Hawkins, R.H. (1978). Runoff curve numbers with varying site moisture. Journal of Irrigation and Drainage Division, ASCE, **104**, 389–398.

127. Hawkins, R.H. (1979). Runoff curve numbers from partial area watersheds. J. Irrig. Drain. Div. ASCE, **105**(IR4), 375–389.

128. Hawkins, R.H. (1993). Asymptotic determination of runoff curve numbers from data, J. Irrig. and Drain. Engrg., ASCE, **119(2)**, 334-345.

129. Hawkins, R.H., Woodward, D.E., and Jiang, R. (2001). Investigation of the runoff curve number abstraction ratio, Paper presented at USDA-NRCS Hydraulic Engineering Workshop, Tucson, Arizona.

130. Haykin, S. (1999). Neural networks: a comprehensive foundation. New Jersey: Prentice Hall.

131. Hengl, T., Maathuis, B.H.P and Wang, L. (2006). Chapter 3: Terrain parameterization in ILWIS. In: European Commission Joint Research Centre (Editor), New terrain parameterization text book. 29-48.

132. Hillel, D. (1971). Soil and Water: Physical Principles and Processes. Academic Press, New York.

133. Hillel, D. (1980). Fundamentals of Soil Physics. Academic Press, New York.

134. Hillel, D. (1982). Introduction to soil physics. Academic Press, New York.

135. Hjelmfelt, A.T.J. (1980). Empirical investigation of curve number technique. J. Hydraul. Div. ASCE **106** (9), 1471–1477.

136. Hjelmfelt, A.T.J. (1991). Investigation of curve number procedure. J. Hydraul. Eng., **117** (6), 725–737.

137. Horton, R.E. (1945). Erosional development of streams and their drainage basins: Hydrophysical approach to quantitative morphology, Bull. Geol. Soc. Amer. **56**, 275–370.

138. Hsu, K. L., Gupta, H.V. and Sorooshian, S. (1995). Artificial neural network modeling of the rainfall–runoff process. Water Resources Research, **31**, 2517-2530.

139. Huang, J., Van den Dool, H.M. and Georgakakos, K.P. (1996). Analysis of model-calculated soil moisture over the United States (1931–1993) and applications to long-range temperature forecasts. J. Climate, **9**, 1350–1362.

140. ILWIS 3.3 (2007). Integrated Land and Water Information System. ILWIS User Guide, ITC, Enschede, The Netherlands.

141. Jain, M. K. and Kothyari, U. C. (2000). Estimation of soil erosion and sediment yield using GIS, Hydrological Sciences Journal, **45**(5), 771-786.

142. Jain, M. K., and Das, D. (2009). Estimation of sediment yield and areas of soil erosion and deposition for watershed prioritization using GIS and remote sensing. Water Resour Manage, DOI 10.1007/s11269-009-9540-0.

143. Jain, M.K., Kothyari, U.C., and Ranga Raju, K.G. (2005). Geographic information system based distributed model for soil erosion and rate of sediment outflow from catchments. Journal of Hydraulic Engineering, ASCE, **131**, 755–769.

144. Jain, M.K., Kothyari, U.C., and Ranga Raju, K.G. (2004). A GIS based distributed rainfall runoff model. Journal of Hydrology, **299**, 107–135.

145. Jain, M.K., Mishra, S.K., Babu, S., and Singh, V.P. (2006). Enhanced runoff curve number model incorporating storm duration and a nonlinear Ia–S relation. J. Hydrol. Eng., **11** (6), 631–635.

146. Jain, S.K. and Goel, M.K. (2002). Assessing the vulnerability to soil erosion of the Ukai Dam catchments using remote sensing and GIS, Hydrol. Sciences, **47**(1), February 2002, 31-40.

147. Jain, S.K., Agarwal, P.K., and Singh, V.P. (2007). Hydrology and Water Resources of India, Published by Springer, The Netherlands.

148. Jain, S.K., Das, D., and Srivastava, D.K. (1999). Application of ANN for reservoir inflow prediction and operation. J. Water Resour. Planning Mgmt, ASCE, **125**(5), 263–271.

149. Jain, S.K., Nayak, P.C., and Sudheer, K.P. (2008). Models for estimating evapotranspiration using artificial neural networks and their physical interpretation. Hydrol. Process, **22**, 2225–2234.

150. Jain, S.K., Singh, R.D., and Seth, S.M. (2000). Design flood estimation using GIS supported GIUH approach. Water Res. Manage, **14**, 369–376.

151. Jain, V., and Sinha, R. (2003). Derivation of unit hydrograph from GIUH analysis for the Himalayan river. Water Resour. Manage, **17**, 355–375.

152. Jensen, M.E., and Haise, H.R. (1963). Estimation of evapotranspiration from solar radiation. Journal of Irrigation and Drainage Division, Proceedings of the American Society of Civil Engineers, **89,** 15-41

153. Jensen, M.E., Burman, R.D., and Allen, R.G. (1990). Evapotranspiration and water requirements, ASCE Manual 70, New York, USA 1990. 332 pp.

154. Johnson, Y.W. (1943). Distribution graphs of suspended- matter concentration. Trans.of ASCE, **108**, 941-964.

155. Kachroo, R.K., and Natale, L. (1992). Non-linear modeling of the rainfall-runoff transromation. Journal of Hydrology, **135**, 341-369.

156. Kalin, L., Govindaraju, R.S., and Hantush, M.M. (2004). Development and application of a methodology sediment source identification. 1: Modified unit sedimentograph approach. Journal of Hydrologic Engineering, ASCE **9**(3), 184–193.

157. Karl, T.R., (1986). The relationship of soil moisture parameterizations to subsequent seasonal and monthly mean temperature in the United States. Mon. Weather Rev., **114**, 675-686.

158. Kashyap, P.S. and Panda, R.K. (2001). Evaluation of evapotranspiration estimation methods and development of crop coefficient fro potato crop in a sub-humid region, Agricultural water management. **50**(1), 9-25

159. Kasko, B., (1992). Neural networks and fuzzy systems. Prentice-Hall Inc., Englewood Cliffs, New Zealand.

160. Kirshen, D.M., and Bras, R.L. (1983). The linear channel and its effect on geomorphological IUH. J of Hydrology, 653, 175-208.

161. Klaghofer, E., Summer, W., and Villeneuve, J.P. (1992). Some remarks on the determination of the sediment delivery ratio. IAHS Publication, **209,** 113–118.

162. Knisel, W.G., (1980). CREAMS: a field-scale model for chemical, runoff and erosion from agricultural management systems. Conservation Research Report No. 26, South East Area, US Department of Agriculture, Washington, DC.

163. Kothyari, U.C., Jain, M.K., Ranga Raju, K.G., (2002). Estimation of temporal variation of sediment yield using GIS, Hydrological Sciences, **47**(5) April 2002, 693-705.

164. Kottegoda, N.T., Natale, L., and Raiteri, E., (2000). Statistical modelling of daily streamflows using input and curve number technique. Journal of Hydrology **234,** 170–186.

165. Koutsoyiannis, D., and Xanthopoulos, T. (1989). On the parametric approach of unit hydrograph identification, Water Resour. Manage. J., **3**, 107– 128.

166. Krishna, B., Satyaji, R.YR., and Vijaya, T. (2008). Modelling groundwater levels in an urban coastal aquifer using artificial neural networks. Hydrlogical processes, **22**, 1180-1188.

167. Kumar, A., and Kumar, D. (2008). Predicting direct runoff from hilly watershed using geomorphology and stream-order-law ratos: case study, Journal of Hydrologic Engineering, **13**(7), 2008, 570-576.

168. Kumar, A.P.S., Sudheer, K.P., Jain, S.K., and Agarwal, P.K. (2005). Rainfall-runoff modeling using artificial neural networks: comparison of network types. Hydrological Processes, **19**, 1277–1291.

169. Kumar, M., Raghuwanshi, N.S., Singh, R., Wallender, W.W., and Pruitt, W.O. (2002). Estimating evapotranspiration using artificial neural network. Journal of Irrigation and Drainage Engineering, **128**(4), 224-233.

170. Kumar, R., Chatterjee, C., Lohani, A.K., Kumar, S., and Singh, R.D. (2002). Sensitivity analysis of the GIUH based Clark model for a catchment. Water Resources Management, **16**, 263–278.

171. Kumar, R., Chatterjee, C., Singh, R. D., Lohani, A. K., and Kumar, S. (2007). Runoff estimation for an ungauged catchment using geomorphological instantaneous unit hydrograph (GIUH) model. Hydrol. Process., **21**, 1829-1840.

172. Kumar, S., and Rastogi, R.A. (1987). Conceptual catchment model for estimation of suspended sediment flow. J. Hydrol., **95**, 155–163.

173. Kusre, B. C. (1995). Development and Validation of Weekly Runoff and Sediment Yield Models for a Himalayan Catchment. M Tech Thesis, Department of Soil and Water Conservation Engineering, G B Pant University of Agricultural and Technology, Pantnagar.

174. Kustas, W.P. (1990). Estimates of evapotranspiration with a one- and two-layer model of heat transfer over partial canopy cover. J. Appl. Meteorol., **29,** 704-715.

175. L´opez-Urrea, R., Santa Olalla, F., Fabeiro, C., and Moratalla, A. (2006). Testing evapotranspiration equations using lysimeter observations in a semiarid climate. Agr.Water Manage., **85**(1–2), 15–26,

176. Lane, L.J., Renard, K.G., Foster, G.R., Laflen, J.M. (1992). Development and application of modern soil erosion prediction technology— the USDA experience. Australian Journal of Soil Research **30,** 893–912.

177. Lee, S. (2004). Soil erosion assessment and its verification using the universal soil loss equation and geographic information system: a case study at Boun, Korea. Environ Geol **45**(3), 457–465

178. Lin, G. F., and Chen, L.H. (2004). A non-linear rainfall–runoff model using radial basis function network. Journal of Hydrology, **289**, 1–8.

179. Lu, J., Sun, G., McNulty, S.G., and Amatya, D.M. (2005). A comparison of six potential evapotranspiration methods for regional use in the southeastern United States. Journal of the American Water Resources Association (JAWRA), **41**(3), 621-633.

180. Maathuis, B., and Sijmons, K. (2005). DEM from Active Sensors – Shuttle Radar Topographic Mission (SRTM), International Institute for Geo-Information Science and Earth Observation.

181. MacQueen, J.B. (1967). Some Methods for classification and Analysis of Multivariate Observations. Proceedings of 5-th Berkeley Symposium on

Mathematical Statistics and Probability, Berkeley, University of California Press, **1**, 281-297.

182. Makkink, G.F. (1957). Testing the Penman formula by means of lysimeters. Journal of the Institution of Water Engineers, **11**, 277-288.

183. Mani, P., and Panigrahy, N. (1998). Geomorphological study of Myntdu- Leska river basin. Tech. Rep. CS/AR 7/97-98, Natl. Inst. of Hydrol., Roorkee, India.

184. Markus, M., and Baker, D. (1994). The Fraser River: Streamflow forecasting and simulation computer package. Tech. Rep., Northern Colorado Water Conservancy District, Loveland, Colo.

185. Martinez-Cob, A., and Tejero-Juste, M. (2004). A Wind-Based Qualitative Calibration of the Hargreaves ET_0 Estimation Equation in Semiarid Regions. Agricultural Water Management, **64**, 251-264.

186. Mason, J.C., Price, R.K., and Temme, A. (1996). A neural network model of rainfall-runoff using radial basis functions. Journal of Hydraulic Research, **34**(4), 537-548.

187. Mati, B.M., Morgan, R.P.C., Gichuki, F.N., Quinton, J.N., Brewer, T.R., and Liniger, H.P. (2000). Assessment of erosion hazard with the USLE and GIS: A case study of the Upper Ewaso Ng'iro North basin of Kenya. JAG 2, 78–86.

188. McCarthy, G.T. (1938). The unit hydrograph and flood routing. Unpublished manuscript presented at a conference of the North Atlantic Division, 24 June 1938, US Army Corps of Engineers.

189. McCool, D.K., Foster, G.R., Mutchler, C.K., and Meyer, L.D. (1989). Revised slope length factor for the Universal Soil Loss Equation. Trans. ASAE, **32**, 1571-1 576.

190. McCuen, R.H. (1982). Hydrologic Analysis and Design. Prentice Hall Inc., Englewood Cliffs, New Jersey07632, USA.

191. McCuen, R.H. (2002). Approach to confidence interval estimation for curve numbers. J. Hydrol. Eng., 7(1), 43–48.

192. McCuen, R.H. Snyder, M.W. (1986). Hydrologic modeling: Statistical methods and applications. Prentice-Hall, Englewood Cliffs.

193. Melton, M.A. (1958). Geometric properties of mature drainage systems and their representation in an E_4 phase space. J. Geol., **66**, 35-54.

194. Meyer, L.D., Wischmeier, W.H. (1969). Mathematical simulation of the processes of soil erosion by water. Transactions of American Society of Agricultural Engineers, **12**, 754–759.

195. Michel, C., Andre´assian, V., Perrin, C. (2005). Soil Conservation Service Curve Number method: how to mend a wrong soil moisture accounting procedure?. Water Resour. Res., 41,W02011, DOI 10.1029/2004WR003191.

196. Millward, A., and Mersey, J.E. 1999. Adapting the RUSLE to model soil erosion in a mountainous tropical watershed. Catena 38, 109–129.

197. Minns, A.W., and Hall, M.J. (1996). Artificial neural networks as rainfall runoff models. Hydrol. Sci. J., **41**(3), 399-417.

198. Mintz, Y., and Walker, G.K. (1993). Global fields of soil moisture and land surface evapotranspiration derived from observed precipitation and surface air temperature. Journal of Applied Meteorology, **32**, 1305-1334.

199. Mishra, S.K, Sansalone, J.J., and Singh, V.P. (2004). Partitioning analog for metal elements in urban rainfall-runoff overland flow using the soil conservation service curve number concept. Journal of Environmental Engineering, ASCE, **130**(2), 145-154.

200. Mishra, S.K., and Singh, V.P. (1999a). Another look at the SCS-CN method. Journal of Hydrologic. Engrg., ASCE, **4**(3), 257-264.

201. Mishra, S.K., and Singh, V.P. (1999b). Behaviour of SCS-CN method in C-I_a^*-λ spectrum,' Submitted to Int. Conf. Water, Environment, Ecology, Socio-economics, and Health Engineering, Oct. 18-21, Korea.

202. Mishra, S.K., and Singh, V.P. (2002a). SCS-CN method: Part-I: Derivation of SCS-CN based models. Acta Geophysica Polonica, **50**(3), 457-477.

203. Mishra, S.K., and Singh, V.P. (2002b). SCS-CN based hydrologic simulation package. In Mathematical Models in Small Watershed Hydrology (ed. V. P. Singh & D. K. Frevert), pp. 391–464. Water Resources Publication, Littleton, CO.

204. Mishra, S.K., and Singh, V.P. (2003a). Soil conservation Service Curve Number (SCS-CN) Methodology, Kluwer Academic Publishers, P. O. Box 17, 3300 AA Dordrecht, The Netherlands.

205. Mishra, S.K., and Singh, V.P. (2003b). SCS-CN method Part-II: Analytical treatment, Acta Geophysica Polonica, **51**(1), 107-123.

206. Mishra, S.K., and Singh, V.P. (2004a). Long-term hydrologic simulation based on the Soil Conservation Service curve number. Hydrological Processes **18**, 1291-1313.

207. Mishra, S.K., and Singh, V.P. (2004b). Validity and extension of the SCS-CN method for computing infiltration and rainfall-excess rates. Hydrological Processes, **18**(17), 3323-3345.

208. Mishra, S.K., Pandey, R.P., Jain, M.K., and Singh, V.P. (2008). A rain duration and modified AMC-dependent SCS-CN procedure for long rainfall-runoff events. Water Resources Management **22**, 861-876.

209. Mishra, S.K., Tyagi, J.V., Singh, and V.P., Singh, R. (2006). SCS-CN-based modeling of sediment yield. Journal of Hydrology, **324**, 301-322.

210. Miyoung, S., and Cheehang, P. (2000). A radial basis function approach to pattern recognition and its application. ETRI Journal, **22**(2).

211. Mockus, V. (1949). Estimation of total (peak rates of) surface runoff for individual storms. Exhibit A of Appendix B, Interim Survey Report Grand (Neosho) River Watershed, USDA, Dec. 1.

212. Moglen, G.E. (2000). Effect of orientation of spatially distributed curve numbers in runoff calculations. Journal of the American Water Resources Association **36**(6), 1391–1400.

213. Monteith, J.L. (1965). Evaporation and Environment. 19th Symposia of the Society for Experimental Biology, University Press: Cambridge, **19,** 205-234.

214. Moore, I., and G. Burch, (1986b). Modeling erosion and deposition: topographic effects. Trans. of ASAE, **29**(6), 1624-1630, 1640.

215. Moore, I., and G. Burch. (1986a). Physical basis of the length-slope factor in the universal soil loss equation. Soil Science Society of America Journal, **50,** 1294-1298.

216. Moore, I., and Wilson, J.P. (1992). Length slope factor for the Revised Universal Soil Loss Equation: simplified method of solution. J. Soil Wat. Consrv., **47**(5), 423-428.

217. Moore, R.J. (1983). The Probability-Distributed Approach to Spatial Conceptual Rainfall–Runoff Modeling. Report to Flood Protection Commission, Ministry of Agriculture, Fisheries and Food, Institute of Hydrology, Wallingford.

218. Moore, R.J. (1985). The probability-distributed principle and runoff production at point and basin scales. J. Hydrol. Sci., **30**(2), 273–297.

219. Moore, R.J., and Clarke, R.T. (1981). A distribution function approach to rainfall-runoff modeling. Water Resour. Res., **17** (5), 1367–1382.

220. Moradkhani, H., Hsu, K.L., Gupta, H.V., and Sorooshian, S. (2004). Improved streamflow forecasting using self organizing radial basis function artificial neural networks. Journal of Hydrology, **295**, 246–262

221. Moran, M.S., Peters-Lidard, C.D., Watts, J.M., and McElroy, S. (2004), Estimating soil moisture at the watershed scale with satellite-based radar and land surface models, Can. J. Remote Sens., **30**(5), 805– 826.

222. Morgan, R.P.C. (1995). Soil Erosion and Conservation (2nd edn). Longman Group: Harlow.

223. Morgan, R.P.C. (2001). A simple approach to soil loss prediction: a Revised Morgan-Morgan-Finney model. Catena, **44**, 305-322.

224. Morgan, R.P.C., Morgan, D.D.V., and Finney, H.J. (1984). A predictive model for the assessment of erosion risk. Journal of Agricultural Engineering Research, **30**, 245–253

225. Morgan, R.P.C., Quinton, J.N., Smith, R.E., Govers, G., Poesen, J.W.A., Auerswald, K., Chisci, G., Torri, D., and Styczen, M.E. (1998). The European Soil Erosion Model (EUROSEM): a dynamic approach for predicting sediment transport from fields and small catchments. Earth Surface Processes and Landforms **23**(6), 527–544.

226. Morton, F.I. (1994). Evaporation research—a critical review and its lessons for the environmental sciences. Critical Reviews in Environmental Science and Technology **24** (3), 237–280.

227. Moughamian, M.S., McLaughlin, D.B. and Bras, R.L., (1987). Estimation of Flood Frequency: An Evaluation of Two Derived Distribution Procedures', Water Resources Research, **23**(7), 1309-1319.

228. Musgrave, G.W. (1947). The Quantitative Evaluation of Factors in Water Erosion-A First Approximation. Journal Soil Conservation, 321-327, UK.

229. Nadarajah, S. (2007). Probability models for unit hydrograph derivation. J Hydrol **344**, 185–189.

230. Nagler, P.L., Clerverly, J., Glenn, E., Lampkin, D., Huete, A., and Wan, Z. (2005). Predicting riparian evapotranspiration from MODIS vegetation indices and meteorological data. Remote Sensing of Environment, **94**, 17-30.

231. Naik, G.M., Rao, E.P., and Eldho T. I. (2009), Finite Element Method and GIS Based Distributed Model for Soil Erosion and Sediment Yield in a Watershed, Journal of Water Resources Management, 23, 553-579.

232. Nandakumar, N., Mein, R.G. (1997). Uncertainty in rainfall–runoff model simulations and the implications for predicting the hydrologic effects of land-use change. Journal of Hydrology **192**, 211–232.

233. Nash, J.E. (1957). The form of instantaneous unit hydrograph. International Association of Sciences and Hydrological Publications, **45**(3), 114–121.

234. Nash, J.E. (1959). Synthetic determination of unit hydrograph parameters. J. Geophys. Res. 64(1), 111–115.

235. Nash, J.E. (1960). A unit hydrograph study with particular reference to British catchnets. Proc., Inst. Civ. Eng., London, **17**, 249–282.

236. Nash, J.E., and Sutcliffe, J.V. (1970). River flow forecasting through conceptual models. Part I. A discussion of principles. J Hydrol., **10**, 282–290.

237. Nasri, S., Cudennec, C., Albergel, J. and Berndtsson, R. (2004). Use of geomorphological transfer function to model design floods in small hill side catchments in semi arid Tunisia. J. Hydrol., **287**, 197–213.

238. Natalia, H. (2005). Spatial modeling of soil erosion potential in a tropical watershed of the Colombian Andes. Catena, **63**, 85–108.

239. NBSS&LUP. (2004). Soils of Uttar Pradesh for Optimizing Land Use: Executive Summary. National Bureau of Soil Survey and Land Use Planning: ICAR, Publication No., 68, Nagpur, India.

240. Nearing, M.A., Foster, G.R., Lane, L.J., and Finkner, S.C. (1989). A process-based soil erosion model for USDA-water erosion prediction project technology. Transactions of the ASAE, **32**(5), 1587– 1593.

241. Norman, S.E. (1989). An evaluation of ANSWERS, a distributed parameter watershed model. Thesis submitted in partial satisfaction of the requirements for the degree of master of science in Water Science in the Graduate Division of the University of California, Davis, California.

242. Onyando, J.O., Kisoyan, P., and Chemelil, M.C. (2005). Estimation of potential soil erosion for river perkerra catchment in Kenya. Water Resources Management, **19,** 133–143.

243. Pandey, A., Chowdary, V.M., and Mal, B.C. (2007). Identification of critical erosion prone areas in the small agricultural watershed using USLE, GIS and remote sensing. Water Resources Management, Springer, **21**, 729–746.

244. Pandit, A., and Gopalakrishnan, G. (1996). Estimation of annual storm runoff coefficients by continuous simulation. J. Irrig. Drain.Eng., ASCE, **122**(40), 211–220.

245. Panuska, J.C., Moore, I.D., and Kramer, L.A. (1991). Terrain analysis: integration into the agricultural nonpoint source (AGNPS) pollution model. J Soil Water Cons **46**(1), 59–64

246. Parmele, L.H. (1972). Errors in output of hydrologic models due to errors in input of potential evapotranspiration. Water Resour. Res., **8**, 348-359.

247. Parmele, L.H., and McGuinness, J.L. (1974). Comparision of measured and estimated daily potential evapotranspiration in a humid region. J. Hydrol., **22,** 239-251.

248. Paturel, J.E., Servat, E., and Vassiliadis, A. (1995). Sensitivity of conceptual rainfall–runoff algorithms to errors in input data—case of the GR2M model. Journal of Hydrology, **168**, 111–125.

249. Penman, H.L. (1948). Natural evaporation from open water, bare soil and grass. Proceedings of Royal Society London, **193**, 120–145.

250. Penman, H.L. (1961). Weather, plant and soil factors in hydrology. Weather, **16**, 207-219

251. Penman, H.L. (1963). Vegetation and Hydrology. Tech. Comm. No., **53**, Commonwealth Bureau of Soils, Harpenden, England

252. Philip, B.B., and Huber, W.C. (2002). Hydrology and floodplain analysis (3rd edition). Prentice Hall, Upper Saddle River, NJ 07458.

253. Ponce, V.M. (1989). Engineering Hydrology: Principles and practices. Prentice Hall Inc., Englewood Cliffs, New Jersey 07632, USA.

254. Ponce, V.M., and Hawkins, R.H. (1996). Runoff curve number: Has it reached maturity?. Journal of Hydrolog. Eng., ASCE, **1**(1), 11-19.

255. Prescott, A.J. (1986a). Irrigation Scheduling by Evaporation Pan. Zimbabwe Agric. Journal, **83**(2), 67-72.

256. Priestley, C.H.B., and Taylor, R.J. (1972). On the assessment of surface heat flux and and evaporation using large scale parameters. Mon. Wealth. Rev, **100,** 81-92.

257. Prosser, I.P., and Rustomji, P., (2000). Sediment transport capacity relations for overland flow. Progress in Physical Geography, **24**(2), 179– 193.

258. Pyasi, S.K., and Singh, J.K. (2004). Prediction of Sediment Yield on Integrated Time Scale basis for a Himalayan Catchment. Institute of Engineers (India) Journal, **85**(5), 8-12

259. Qudin, L., Hervieu, F., Michel, C., Perrin, C., Andreassian, V., Anctil, F., and Loumagne, C. (2005). Which potential evapotranspiration input for a lumped rainfall-runoff model? Part 2-Towards a simple and efficient potential evapotranspiration model for rainfall-runoff modeling. Journal of Hydrology, **303**, 290-306.

260. Raghuwanshi, N.S. (1986). Mathematical watershed models for runoff and sediment flow from Chaukhutia catchment of Ramganga river. ME thesis, G. B. Pant University of Agriculture and Technology, Pantnagar, U P., India.

261. Raghuwanshi, N.S., Rastogi, R.A., and Kumar, S., (1994). Instantaneous unit sediment graph. ASCE J. Hydraul. Eng., **120**(4), 495–503.

262. Raghuwanshi, N.S., Singh, R., and Reddy L.S. (2006). Runoff and sediment yield modelling using artificial neural network. Hydrologic Engineering, ASCE, **11**(1), 71-79

263. Rai, R.K., Sarkar, S., and Singh, V.P. (2008). Evaluation of the adequacy of statistical distribution functions for deriving unit hydrograph. Water Resour. Manage., **23**, 899–929.

264. Rallison, R.E. (1980). Origin and evaluation of the SCS runoff equation. Proc. Symp. Watershed Management, ASCE, Idaho, July, 912–924

265. Ralph, B. (2008). On the convergence of derivatives of B-splines to derivatives of the Gaussian function. Computational and Applied mathematics, **27**(1), 79-92.

266. Ramasastry, K.S., and Seth, S.M. (1985). Rainfall-runoff Relationships. Rep. RN-20, National Institute of Hydrology, Roorkee, India.

267. Rashid, A.A., Aziz, K.F., and Wong; A (1992). Neural Network Approach to the Determination of Aquifer Parameters, Ground Water, **30**(2), 164-166.

268. Rawls, W.J and Brakensiek, D.L. (1983). A procedure to predict Green and Ampt infiltration parameters, in proceedings of the American socity of Agricultural engineers Conference on Advances in infiltration, pp. 102-112, American socity of Agricultural engineers, St. Joseph, Mich.

269. Raymo, M.E., and Ruddiman, W.F. (1992). Tectonic forcing of late Cenozoic climate. Nature (London), **359**, 117-122.

270. Renard, K.G., Foster, G.R., Weesies, G.A., and Porter, J.P., (1991). RUSLE: revised universal soil loss equation. Journal of Soil and Water Conservation, 30–33 (January–February).

271. Rendon-Herrero, O. (1978). Unit sediment graph. Water Resourc. Res., **14**(5), 889-901.

272. Rinaldo, A., and Rodriguez-Iturbe, I. (1996). Geomorphological theory of the hydrological response. Hydrol. Processes, **10**(6), 803–829.

273. Rodriguez-Iturbe, I., and Rinaldo, A. (1997). Fractal River Basins: Chance and Self-organization, Cambridge University Press, Cambridge.

274. Rodriguez-Iturbe, I., and Valdés, J.B. (1979). The geomorphologic structure of the hydrologic response, Water Resour. Res., **15**(6), 1409– 1420.

275. Rodriguez-Iturbe, I., Gonzalez-Sanabria, M., and Bras, R.L. (1982). The geomorphoclimatic theory of the instantaneous unit hydrograph, Water Resour. Res., **18**(4), 877–886.

276. Roehl, J.W. (1962). Sediment source areas, delivery ratios and influencing morphology factors. In: Symposium of Bari (1-8 October 1962), 202-213. IAHS Publ. no. 59.

277. Rose, C.W. (1993). Erosion and Sedimentation. Chapter 14 in Hydrology and Water Management in the Humid Tropics (M. Bonell, M. N. Hufschmidt and J. S. Gladwell, eds.). Cambridge University Press, Cambridge, UK, pp. 301 - 343.

278. Rossi, F. (1974). Criteri di similitudine idrologica per le stime della portata al colmo di piena corrispondente ad un assegnato tempo di ritorno. Atti XXV Convegno di Idraulica e Costruzioni Idrauliche. University of Naples: Naples; Vol. **2**, 235–261.

279. Rosso, R. (1984). Nash model relation to Horton order ratios, Water Resour. Res., **20**(7), 914– 920.

280. Rovey, E.W., Woolhiser, D.A., and Smith, R.E., (1977). A distributed kinematic model of upland watersheds. Hydrology Papers, vol. 93. Colorado State University, Fort Collins, CO.

281. Rumelhart, D. E., Hinton, G.E. Williams, R.J. (1986). Learning internal representation by back- ropagating errors. In Parallel Distributed Processing: Explorations in the Microstructure of Cognition Press, Rumelhart, D.E., McCleland, J.L. and the PDP Research Group, eds. MA: MIT.

282. Rumelhart, D.E., Widrow, B., and Letr, M.A. (1994). The basic ideas in neural networks. Communications of the ACM, 37(43), 87-92.

283. Sahoo, B., Chatterjee, C., Raghuwanshi, N.S., Singh, R., and Kumar, R. (2006). Flood estimation by GIUH-based Clark and Nash models. J. Hydrologic Engrg., **11**(6), 515-525.

284. Schneider, K., Ketzer, B., Breuer L., Vache, K.B., Berunhofer, C., and Frede, H. G. (2007). Evaluation of evapotranspiration methods for model validation in a semiarid watershed in north China. Adv. Geosci., **11**, 37-42.

285. Schneider, L. E., and McCuen, R.H. (2005). Statistical guidelines for curve number generation. J. Irrigat. Drain. Eng. ASCE **131**(3), 282–290.

286. SCS. (1956). Hydrology. National Engineering Handbook, Supplement A, Section 4, Chapter 10, Soil Conservation Service, USDA, Washington, D.C.

287. SCS. (1971). Hydrology. National Engineering Handbook. USDA, Washington, D.C.

288. SCS. (1972) Hydrology. National Engineering Handbook. USDA, Washington, D.C.

289. SCS. (1985). Hydrology. National Engineering Handbook. USDA, Washington, D.C.

290. Shamseldin, A.Y. (1997). Application of a neural network technique to rainfall–runoff modeling. J. of Hydrology, **199**, 272–294.

291. Shamshad, A., Azhari, M.N., Isa, M.H., Wan Hussin, W.M.A., and Parida, B.P. (2008). Development of an appropriate procedure for estimation of RUSLE EI30 index and preparation of erosivity maps for Pulau Penang in Peninsular Malaysia. Catena, **72**, 423–432.

292. Sharda, V.N., Juyal, G.P., and Singh, P.N. (2002). Hydrologic and sedimentologic behavior of a conservation bench terrace system in a sub-humid climate. Trans. ASAE **45**(5), 1433–1441.

293. Shaw, E.M. (1988). Hydrology in Practice. Chapman and Hall, London.

294. Sherman, L.K. (1932). Streamflow from Rainfall by the Unit Graph Method. Eng. NewsRec., **108**, 501-505.

295. Shrestha, D.P. (2007). Lecture notes on Soil degradation assessment and modelling. Department of Earth System Analysis, ITC, Enschede.

296. Shuttleworth, W.J. (1993). Evaporation, in: Maidment DR. (Ed.), Handbook of Hydrology. McGraw-Hill, New York.

297. Singh, G., Babu, R., Narain, P., Bhusan, L.S., and Abrol, I.P. (1992). Soil erosion rates in India. Journal of Soil and water Conservation, **47**, 97–99.

298. Singh, G., Chandra, S., and Babu, R. (1981). Soil Loss and Prediction Research in India. Central Soil and Water Conservation Research & Training Institute, India, Bulletin No. T-12/D9.

299. Singh, K.P. (1990). Unit hydrographs for developing design flood hydrographs. Water Resources Bulletin, **26**, 901–911.

300. Singh, P.K., Gaur, M.L., Mishra, S.K., and Rawat, S.S. (2010). An updated hydrological review on recent advancements in soil conservation service-curve number technique. Journal of Water and Climate Change.**01.2**, 118-134

301. Singh, S. K. (2009). Time base as invertible function of the parameters of Gamma unit hydrograph. J. Irrig. Drain. Eng., **136**(6), 802–805.

302. Singh, S.K. (2000). Transmuting synthetic hydrographs into Gamma distribution. J. Hydrol. Eng. ASCE, **5**(4), 380–385.

303. Singh, V.P. (1987). On Application of the Weibull Distribution in Hydrology. Water Resources Management, **1**(1), 33-43.

304. Singh, V.P. (1988). Hydrologic systems, Vol. 1: Rainfall-Runoff Modeling, Prentice Hall, Englewood Cliffs, NJ.

305. Singh, V.P. (1989). Hydrologic systems, Vol. 2: Watershed Modeling, Prentice Hall, Englewood Cliffs, NJ.

306. Singh, V.P., Baniukiwicz, A., and Chen, V.J. (1982). An instantaneous unit sediment graph study for small upland watersheds, in Singh, V. P. (Ed.), Modelling Components of Hydrologic Cycle, Water Resour. Publ., Littleton, Colorado, 539-554.

307. Skaggs, R.W. (1982). Field evaluation of a water management simulation model. Trans. ASAE, **25**(3), 666-674.

308. Smith, M.R., Allen, R.G., Monteith, J.L., Pereira, L.S., and Segeren, A. (1991). Rep. on the Expert Consultation on Procedures for Revision of FAO Guidelines for Predicting Crop Water Requirements. FAO, Land and Water Devel. Div., Food and Agricultural Organization of the United Nations, Rome.

309. Smith, R.E. (1981). A kinematic model for surface mine sediment yield. Transactions of the ASAE, 1508– 1514.

310. Snyder, F.F. (1938). Synthetic unit hydrographs. Trans. Am. Geophys. Union 19, 447–454.

311. Soil Conservation Service (SCS). (1957). Use of storm and watershed characteristics in synthetic hydrograph analysis and application, U.S. Dep. Of Agric., Soil Conserv. Serv., Washington, D. C.

312. Soni, B., and Mishra, G.C. (1985). Soil water accounting using SCS hydrologic soil classification, case study. National Institute of Hydrology, Roorkee (India).

313. Sorman, A.U. (1995). Estimation of peak discharge using GIUH model in Saudi Arbia, Journal of Water Resources Planning and Management. **121**(4), July-August, 1995.

314. Sorooshian, S., (1991). Parameter Estimation, Model Identification, and Model Validation: Conceptual-Type Models. In: Recent Advances in the Modelling of

Hydrologic SystemsI, D.S. Bowles and P.E. O'Connell (eds.). Kluwer Academic Publishers, Netherlands, 443–467

315. Spear, R.C. (1995). Large simulation models: Calibration, uniqueness and goodness of fit. In: International Congress on Modelling and Simulation Proceedings, (Agriculture, Catchment Hydrology and Industry), **1**, 8–15.

316. Steenhuis, T.S., Winchell, M., Rossing, J., Zollweg, J.A., and Walter, M.F. (1995). SCS runoff equation revisited for variable-source runoff areas. Journal of Irrigation and Drainage Engineering, **121**(3), 234-238.

317. Stocking, M. (1981). A working model for the estimation of soil loss suitable for underdeveloped areas, University of East Anglia, Development Studies Occasional Paper, 15.

318. Stoddart, D.R. (1969). World erosion and sedimentation in water. In: Chorley, R.J., (Ed.), Water, Earth, and Man, Methuen, London, 43–64.

319. Strahler, A.N. (1957). Quantitative Analysis of Watershed Geomorphology, Transaction of American Geophysicsical Union **38**(6), 913–920.

320. Subramanya, K. (1984). Enginnering Hydrology. Tata McGraw-Hill, New Delhi.

321. Sudheer, K. P., Srinivasan, K., Neelakantan, T.R., and Srinivas, V.V. (2008). A nonlinear data driven model for synthetic generation of annual streamflows. Hydrol. Process, **22**, 1831–1845.

322. Sudheer, K.P., Gosain, A.K., and Ramasastri, K. S. (2003). Estimating actual evapotranspiration from limited climatic data using artificial neural network technique. Journal of Irrigation and Drainage Engineering, ASCE, **129**(3), 214-218.

323. Takken, I., Beuselinck, B., Nachtergaele, J., Govers, G., Poesen, J., and Degraer, G. (1999). Spatial evaluation of a physically-based distributed erosion model (LISEM). Catena, 37, 431–447.

324. Tarboton, D.G., Bras, R.L., and Rodriguez-Iturbe, I. (1991). On the extraction of channel network fron digital elevation data. Hydrological process, **5**, 81-100.

325. Taylor, A.B. and Schwartz, H.E. (1952). Unit-hydrograph lag and peak flow related to basin characteristics, Transact. Amer. Geophys. Union, **33**, 235–246.

326. Thom, A.S., and Oliver, H.R. (1977). On Penman's equation for estimating regional evapotranspiration. Quarterly J. Royal Meteorological Soc., Bracknell, U.K., **103**, 345–357.

327. Thornthwaite, C.W. (1948). An approach toward a rational classification of climate. Geographical Review, **38**, 55-95.

328. Todini, E. (1988). Rainfall-runoff modeling- past, present, and future. J. Hydrol., **100**, 341 - 352.

329. Tokar, A.S. and Markus, M. (2000). Precipitation-runoff modeling using artificial neural networks and conceptual models. Journal of Hydrologic Engineering, **5**(2), 156-161.

330. Troutman, B.M., and Karlinger, M.R. (1985). Unit hydrograph approximation assuming linear flow through topologically random channel networks. Water Resources Research, **21**(5), 743–754.

331. Turc, L. (1961). Estimation of irrigation water requirements, potential evapotranspiration: a simple climatic formula evolved up to date. Annals of Agronomy **12**, 13-49.

332. Tyagi, J.V., Mishra, S.K., Singh, R. and Singh, V.P. (2008). SCS-CN based time distributed sediment yield model. J. Hydrol., **352**, 388–403.

333. Van Bavel, C.H.M. (1966). Potential evaporation: the combination concept and its experimental verification. Water Resour. Res., **2**, 455-467.

334. Van Oost, K., Govers G., and Desmet, P.J.J. (2000). Evaluating the effects of changes in landscape structure on soil erosion by water and tillage. Landscape Ecology, **15**(6), 579-591.

335. Van Rompaey A., Bazzoffi P., Jones, R.J.A., and Montanarella, L. (2005). Modelling sediment yields in Italian catchments. Geomorphology, **65**, 157–169.

336. Van Rompaey, A., Verstraeten, G., Van Oost, K., Govers, G. and Poesen, J. (2001). Modeling mean annual sediment yield using a distributed approach. Earth Surface Processes and Landforms, **26**(11), 1221-1236.

337. Van-Mullem, J.A. (1989). Runoff and peak discharges using Green- Ampt model. J. Hydraul. Eng. ASCE, **117**(3), 354–370.

338. Vanoni, V.A. (ed) (1975). Sedimentation Engineering. Manuals & Reports on Engineering Practice, no. **54**, ASCE, New York, USA.

339. Venkatesan, P., and Anitha, S. (2006). Application of a radial basis function neural Network for diagnosis of diabetes mellitus. Current science, **91**(9), 1195-1199.

340. Verstraeten, G., and Poesen, J. (2000). Assessment of sediment-fixed nutrient export from small drainage basins in central Belgium using retention ponds. IAHS Publication, **263**, 243–249.

341. Verstraeten, G., Poesen, J. (2001). Factors controlling sediment yields from small intensively cultivated catchments in a temperate humid climate. Geomorphology, 40, 123–144.

342. Verstraeten, G., Prosser, I.P., and Fogarty, P. (2007). Predicting the spatial patterns of hillslope sediment delivery to river channels in the Murrumbidgee catchment, Australia. Journal of Hydrology, **334**, 440–454.

343. Viney, N.R., and Sivapalan, M. (1999). A conceptual model of sediment transport: application to the Avon River Basin in Western Australia. Hydrological Processes, **13**, 727–743.

344. Vinnikov, K.Y., Robock, A., Stouffer, R., Walsh, J.J.E., Perkinson, C.L., Cavalieri, D.J., Mitshell, J.F., Garrett, B.D., and Zakharov, V. F. (1999). Global Warming and Northern Hemisphere Sea ice extent, Science, **286**, 1934– 1937.

345. Vörösmarty, C., Federer, C.A., and Schloss, A.L. (1998). Potential evaporation functions compared on US watersheds: Possible implications for global-scale water balance and terrestrial ecosystem modeling. Journal of Hydrology, **207**, 147-169.

346. Walling, D. E. (1983). The sediment delivery problem. J. Hydrol., Data 65, 209-237.

347. Wei, S.. Zhenghong, G., and Yingtao, Z. (2008). Application of RBF neural network ensemble to aerodynamic optimization. 46th AIAA Aerospace Sciences Meeting and Exhibit, Nevada.

348. Weibull, W. (1939). The phenomenon of ruptures in solids. Ingenjoersvetenskapsakad Handlingar, 153, 17.

349. Wheater, H.S., Jakeman, A.J., and Beven, K.J. (1993). Progress and directions in rainfall-runoff modelling. In: Jakeman, A.J., Beck, M.B., McAleer, M.J. (Eds.), Modelling Change in Environmental Systems, John Wiley and Sons, Chichester, 101–132.

350. White, D. (1988). Grid-based Application of Runoff Curve number, Journal of Water Resources Planning and Management, ASCE, **114**(6), 601-612

351. Whitehead, D. (1986). A review of processes in the water relations of forests. Water Relations & Hydro., 94-124.

352. Wicks, J.M., and Bathurst, J.C. (1996). SHESED: a physically based, distributed erosion and sediment yield component for the SHE hydrological modelling system. J. Hydrology, **175**, 213-238.

353. Williams, J.R. (1975). Sediment routing for agricultural watersheds. Wat. Resources, Bull. **11**, 965-974.

354. Williams, J.R. (1978). A sediment graph model based on an instantaneous unit sediment graph, Water Resour. Res., **14**(4), 659-664.

355. Williams, J.R., and LaSeur, W.V. (1976). Water yield model using SCS curve numbers. J. Hydraulics Division, ASCE, 102, (HY9), Proc. Paper 12377, 1241-1253.

356. Williams, J.R., Dyke, P.T., and Jones, C. A. (1983). EPIC-A modelfor assessing the effects of erosion on soil productivity. pp. 553-572. In W.K. Lauenroth, G.V. Skogerboe, and M. Hug (ed.), Analysis of ecological systems: state-of-the-art in ecological mo-delling. Elsevier Scientific Publishing Co., Amsterdam.

357. Williams, R., and Berndt, H. D. (1972) Sediment yield computed with universal equation. J. Hydraulic Div. ASCE 98 (HY 12), 2087-2098.

358. Wischmeier, W.H. (1959). A rainfall erosion index for a universal soil loss equation. In: Proc. Soil Sci. Soc. Am. 23, 246-249.

359. Wischmeier, W.H., and Smith, D.D. (1965). Predicting rainfall-erosion losses from cropland east of the Rocky Mountains. Agr. Handbook No. 282, U.S. Dept. Agr., Washington, DC.

360. Wischmeier, W.H., and Smith, D.D. (1978). Predicting rainfall erosion losses. Agricultural Handbook no.537, US Dept of Agriculture, Science and Education Administration.

361. Woolhiser, D.A., Smith, R.E., and Goodrich, D.C., (1990). KINEROS, a kinematic runoff and erosion model. Documentation and User Manual, USDA, Agricultural Research Service, ARS-77., 130.

362. Wright, J.L. (1982). New Evapotranspiration Crop Coefficients. Journal of Irrigation and Drainage Division, ASCE, **108**, 57-74.

363. Wright, J.L., and Jensen, E. (1972). Peak water requirements of crops in southern Idaho. Proc. Am. Soc. Civ. Eng., J. Irrig. Drain. Div. 98(IR2), 193-201.

364. Wu, S., Li, J., Huang, G. (2005). An evaluation of grid size uncertainty in empirical soil loss modelling with digital elevation models. Environmental Modeling and Assessment, **10**, 33–42

365. Wu, T.H., Hall, J.A., and Bonta, J.V. (1993). Evaluation of runoff and erosion models. Journal of Irrigation and Drainage Engineering, ASCE **119**, 364–382.

366. Xu, C.Y. and Singh V.P. (2000). Evaluation and generalization of radiation-based methods for calculating evaporation. Hydrological Processes, **14**(2), 339-349

367. Xu, C.Y., and Singh, V.P. (2002). Cross comparison of empirical equations for calculating potential evapotranspiration with data from Switzerland. Water Resources Management **16**(3), 197–219.

368. Xu, C-Y, and Singh, V.P. (2001). Evaluation and generalization of radiation-based methods for calculating evaporation. Hydrological Processes, **15**, 305–319.

369. Yang, C.C., Prasher, S. O., Lacroix, R., Sreekanth, S., Patni, N. K., and Masse, L. (1997). Artificial neural network model for subsurface-drained farmland. J. Irrig. Drain. Eng., **123**, 285–292.

370. Yen, B.C., and Lee, K.T. (1997). Unit hydrograph derivation for ungauged watersheds by stream order laws. Journal of Hydrologic Engineering, ASCE, **2**(1), 1–9.

371. Young, R.A., Onstad, C.A., Bosch, D.D., and Anderson, W.P. (1989). AGNPS: a non-point source pollution model for evaluating agricultural watersheds. Journal of Soil and Water Conservation, 168–173 (March–April).

372. Yu, B. (1998). Theoretical justification of SCS-CN method for runoff estimation. Journal of the Irrigation and Drainage Division, ASCE, **124**(6), 306–310.

373. Yuan, Y., Mitchell, J.K., Hirschi, M.C. and Cooke, R.A.C. (2001). Modified SCS curve number method for predicting sub-surface drainage flow. Trans. of ASAE, **44** (6), 1673–1682.

374. Zhang, X.C., Nearing, M.A., Risse, L.M., and McGregor, K.C. (1996). Evaluation of WEPP runoff and soil loss predictions using natural runoff plot data. Transactions of the ASAE, **39**(3), 855– 863.

375. Zhigang, J., Yajing, L. (2009). The Application of RBF Neural Network on Construction Cost Forecasting. Second International Workshop on Knowledge Discovery and Data Mining.

376. Zhi-Hua, S., Li-Ding, C., Nu-Fang, F., De-Fu, Q. and Chong-Fa, C. (2009). Research on the SCS-CN initial abstraction ratio using rainfall-runoff event analysis in the three Gorges Area, China. Catena, **77**, 1–7.

Appendix A

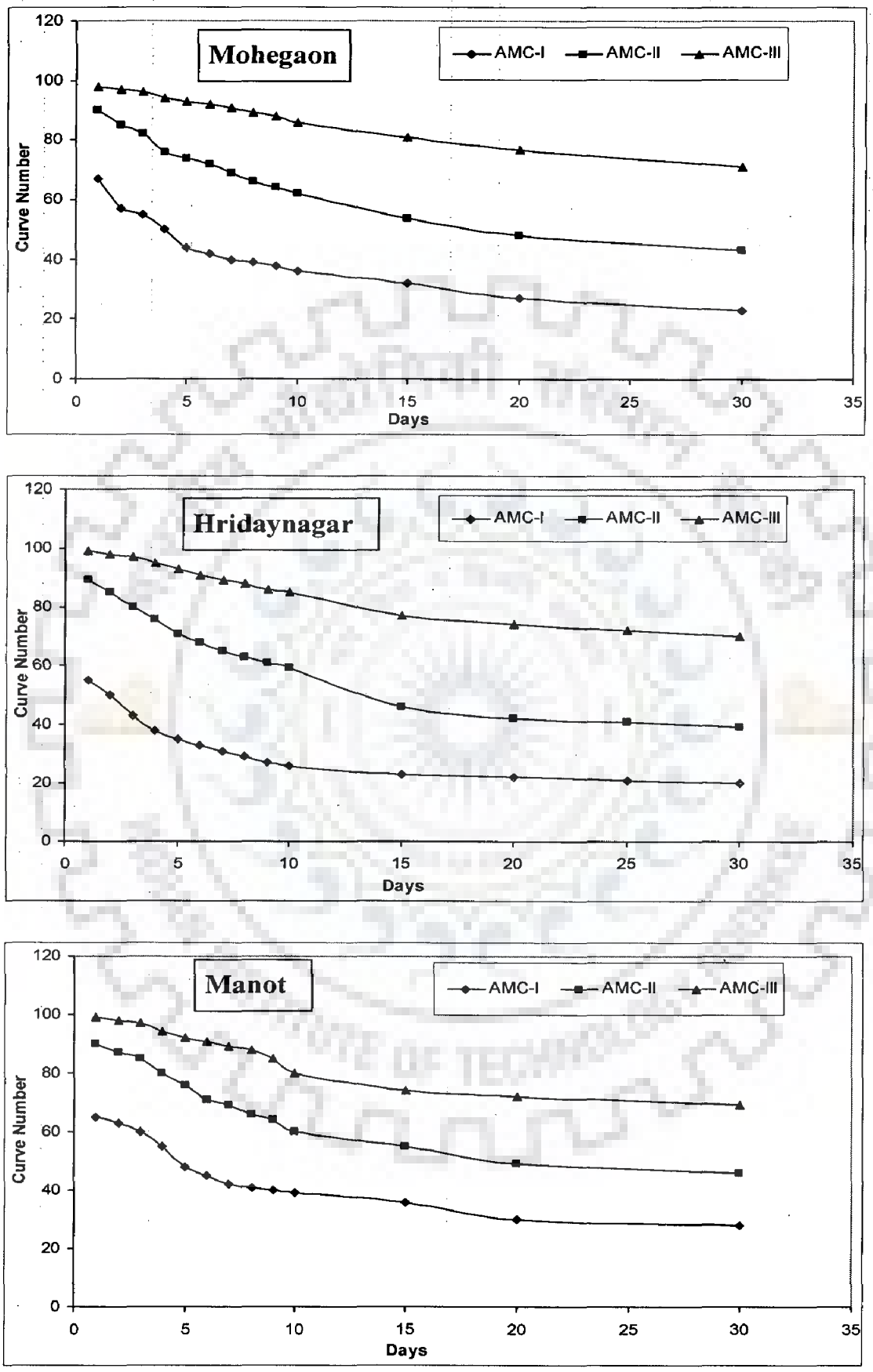

Figure A1: CN Variation with rainfall duration (greater than 1 day) for different catchments.

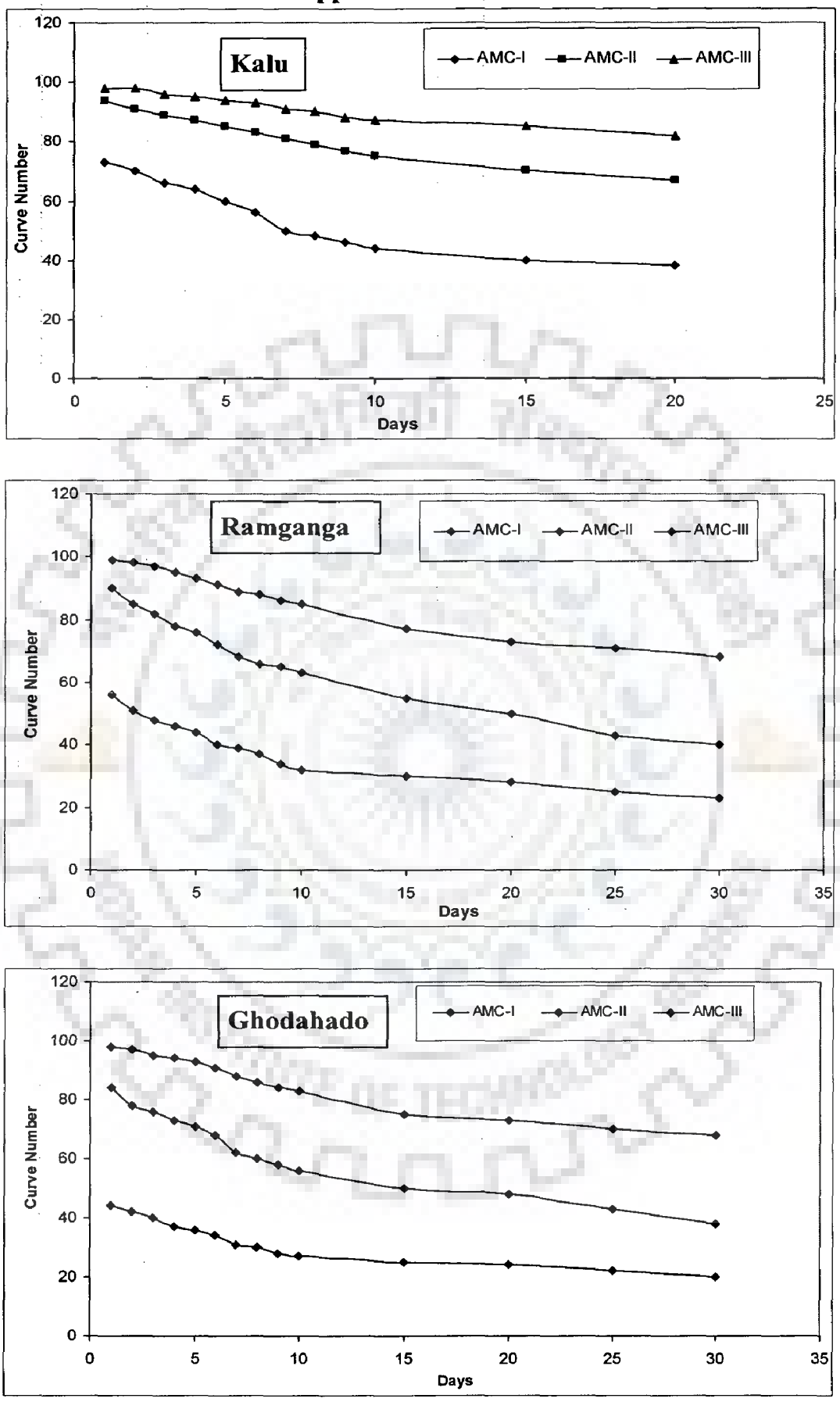

Figure A2: CN Variation with rainfall duration (greater than 1 day) for different watersheds.

APPENDIX B

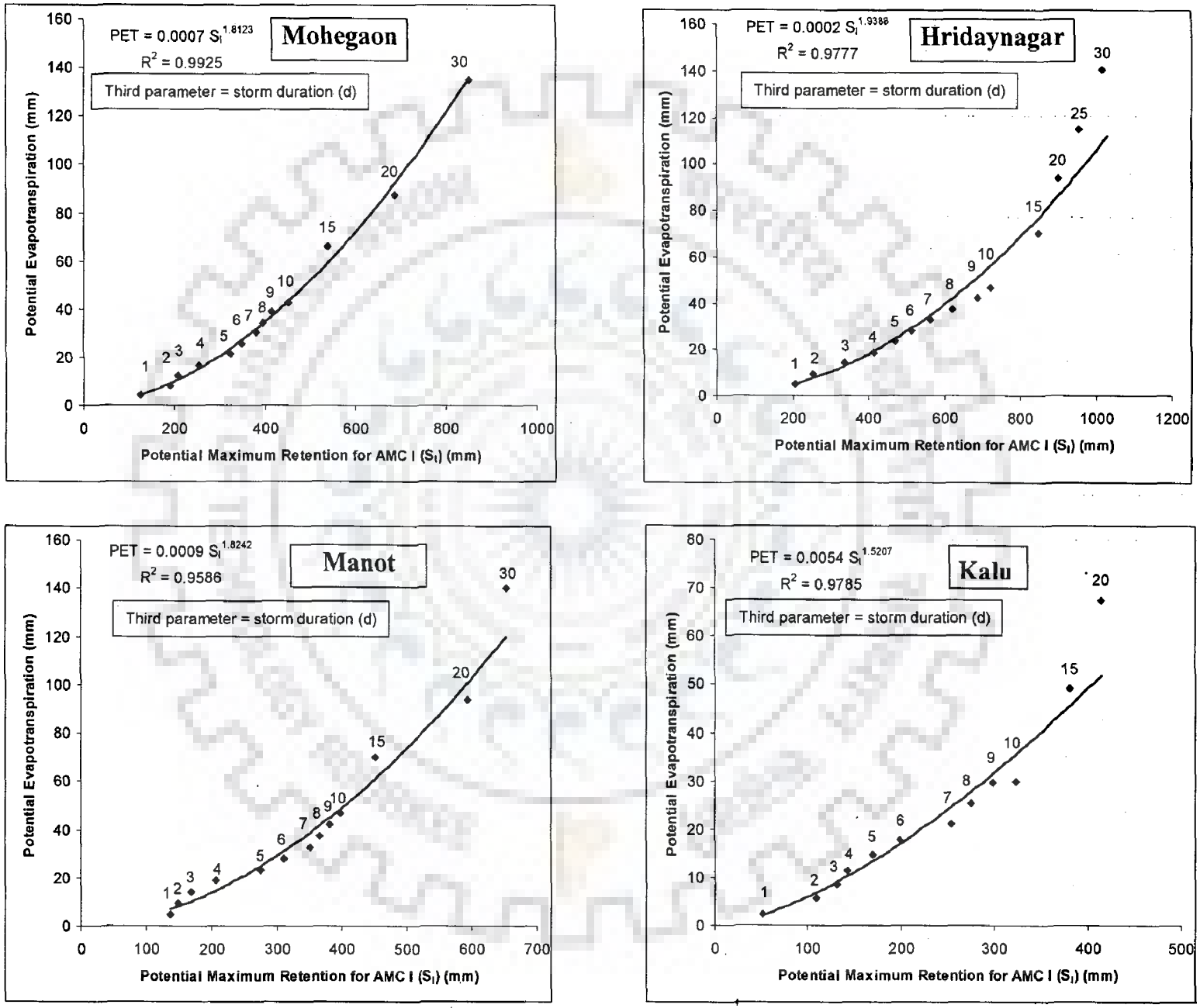

Fig. B1: Penman-Monteith PET and potential maximum retention for AMC I (S_I) relationship for different catchments.

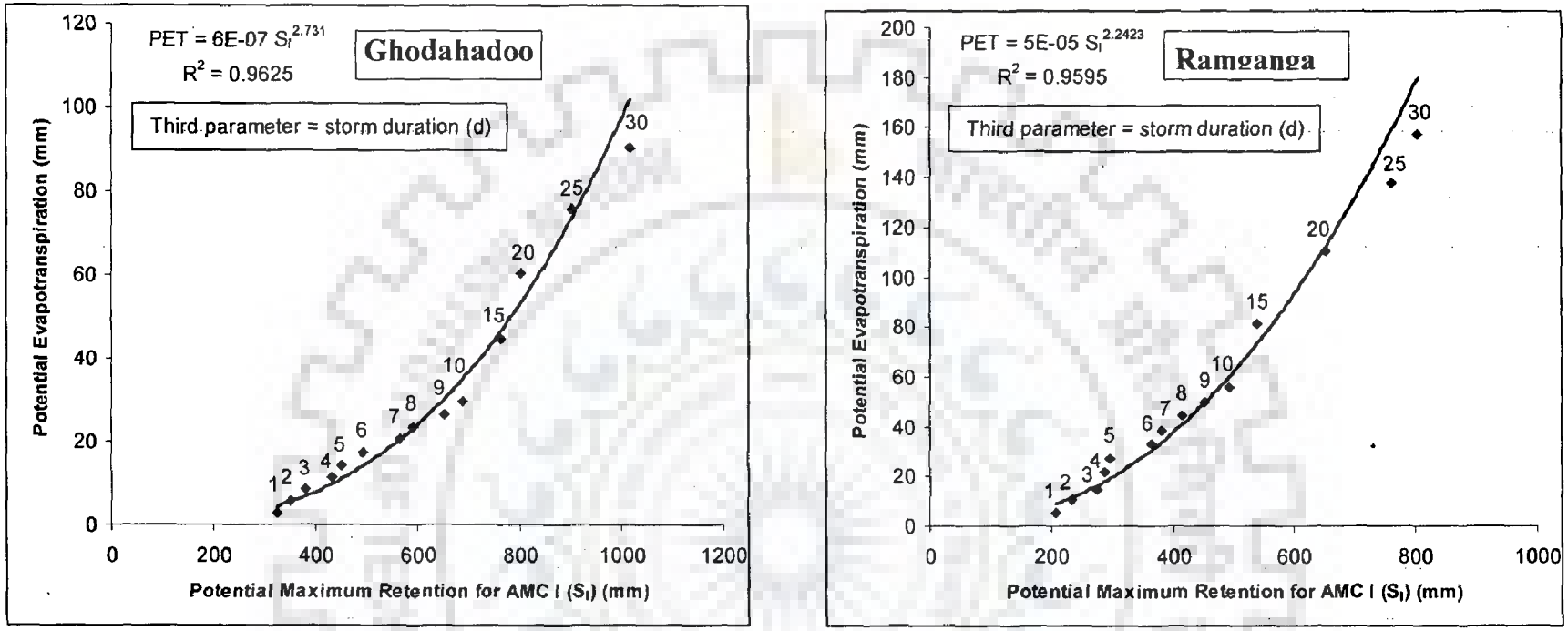

Fig. B2: Penman-Monteith PET and potential maximum retention for AMC I (S_I) relationship for different catchments.

APPENDIX C

Table C1: Performance of (4-4-1), (4-16-1), and (4-32-1) dynamic RBFANN models. ALRG = 0.5, No. of iterations = 1000. ALR = 0.5 to 20 for Chaukhutia watershed.

Period	RMSE			CC			CE			EV		
	4-4-1	4-16-1	4-32-1	4-4-1	4-16-1	4-32-1	4-4-1	4-16-1	4-32-1	4-4-1	4-16-1	4-32-1
						ALR = 0.5						
Calibration	77.52	76.32	75.77	58.7	59.5	59.81	-728.6	-703.1	-691.7	193.7	186.1	182.6
Cross-validation	76.17	75.24	74.76	57.76	58.49	58.85	-503.7	-489.1	-481.5	173.7	169.3	167.1
Verification	75.31	74.38	73.45	56.63	57.08	57.26	-594.3	-577.3	-569.5	188.2	179.1	176.3
						ALR = 5						
Calibration	29.1	28.5	26.36	73.66	72.65	70.45	-16.78	-12.03	4.2	-3.39	-15.89	-9.58
Cross-validation	25.23	24.66	23.86	84.91	84.22	81.4	33.76	36.71	40.75	1.86	-9.71	-3.99
Verification	26.02	25.55	24.51	80.69	80.04	76.42	17.14	20.1	26.44	-5.83	-17.03	-12.36
						ALR = 10						
Calibration	15.31	14.09	13.06	82.29	85.22	87.56	67.68	72.61	76.49	1.53	0.96	0.27
Cross-validation	14.97	13.63	12.49	88.03	90.02	91.98	76.67	80.66	83.76	-0.32	-0.03	-0.48
Verification	14.61	13.03	12.27	86.1	89.1	90.64	73.87	79.23	81.56	1.01	0.39	0.17
						ALR = 15						
Calibration	16.51	13.04	12.78	84.68	87.53	88.15	62.41	76.85	77.48	1.69	0.13	-0.76
Cross-validation	14.16	12.29	12.1	91.65	92.96	92.89	79.13	84.27	84.76	1.06	-1.06	-0.77
Verification	14.28	11.52	11.22	89.78	91.79	92.49	75.04	83.75	84.59	0.12	0.09	-0.39
						ALR = 20						
Calibration	15.22	13.52	12.69	85.76	87.73	88.25	68.07	74.81	77.78	2.18	0.46	-0.61
Cross-validation	13.02	12.38	11.79	91.28	91.79	93.08	82.35	84.06	85.53	4.07	1.71	2.13
Verification	13.01	12.11	11.13	90.64	90.64	92.47	79.29	82.04	84.83	1.15	-0.44	-0.84

Table C2: Performance of (4-4-1), (4-16-1), and (4-32-1) dynamic model. ALR = 20, no. of iterations = 1000, and ALRG = 0.5 to 10 for Chaukhutia watershed.

Period	RMSE			CC			CE			EV		
	4-4-1	4-16-1	4-32-1	4-4-1	4-16-1	4-32-1	4-4-1	4-16-1	4-32-1	4-4-1	4-16-1	4-32-1
						ALRG = 0.5						
Calibration	16.51	13.04	12.78	84.68	87.53	88.15	62.41	76.85	77.48	1.69	0.13	-1.76
Cross-validation	14.16	12.29	12.1	91.65	92.96	92.89	79.13	84.27	84.76	3.96	-1.06	-3.77
Verification	14.28	11.52	11.22	89.78	91.79	92.49	75.04	83.75	84.59	0.12	0.09	-2.39
						ALRG = 1						
Calibration	15.07	12.86	12.63	86.35	87.9	88.56	68.67	77.18	78	3.42	-1.04	-2.61
Cross-validation	13.2	12.16	12.02	92.39	92.42	93.22	81.87	84.61	84.96	5.4	-2.1	-4.65
Verification	12.76	11.31	11.09	91.43	92.09	92.87	80.08	84.33	84.94	2.45	-1	-3.06
						ALRG = 2						
Calibration	13.94	12.74	12.6	87.2	88.17	88.89	73.2	77.61	78.12	3.57	-1.56	-3.69
Cross-validation	12.24	12.02	12.25	92.75	92.71	93.43	84.42	84.98	84.38	5	-2.72	-6.04
Verification	11.5	11.18	11.21	92.36	92.34	93.11	83.81	84.7	84.62	3.45	-1.53	-4.03
						ALRG = 5						
Calibration	13.36	12.76	13.57	87.28	88.3	88.9	75.4	77.54	74.6	2.73	-2.58	-9.8
Cross-validation	11.6	12.16	14.82	92.86	92.99	92.66	85.99	84.61	77.13	3.33	-4.17	-13.71
Verification	10.88	11.26	13.21	92.6	92.58	92.44	85.52	84.47	78.62	3.37	-2.63	-10.69
						ALRG = 10						
Calibration	13.25	13.31	16.13	87.31	88.2	87.09	75.78	75.57	64.14	2.32	-6.93	-19.38
Cross-validation	11.54	13.39	19.78	92.86	93.09	88.22	86.15	81.35	59.3	2.6	-9.34	-25.91
Verification	10.83	12.17	17.53	92.59	92.68	87.82	85.63	81.86	62.4	2.91	-7.28	-22.03

Table C3: Performance of (4-4-1), (4-16-1), and (4-32-1) dynamic RBFANN model. ALR = 20, ALRG = 0.5, and No. of iterations = 100 to 10000 for Chaukhutia watershed.

Period	RMSE			CC			CE			EV		
	4-4-1	4-16-1	4-32-1	4-4-1	4-16-1	4-32-1	4-4-1	4-16-1	4-32-1	4-4-1	4-16-1	4-32-1
						ITERATION = 100						
Calibration	19.3	14.57	13.45	81.17	84.16	86.7	48.65	70.74	75.05	4.09	2.44	-0.07
Cross validation	16.24	13.39	13.03	89.62	91.05	91.39	72.54	81.37	82.34	5.75	0.91	-1.47
Verification	17.16	13.56	12.39	86.11	88.48	90.51	63.98	77.48	81.22	1.87	2.4	-0.32
						ITERATION = 500						
Calibration	17.75	13.38	12.94	82.92	86.86	87.81	56.55	75.32	76.91	-1.13	1.21	-1.54
Cross validation	14.98	12.46	12.35	90.73	92.22	92.54	76.64	83.84	84.12	1.31	-0.1	-3.65
Verification	15.59	11.97	11.49	88.06	91.23	92.06	70.26	82.46	83.83	-2.96	1.21	-2.33
						ITERATION = 1000						
Calibration	16.51	13.04	12.78	84.68	87.53	88.15	62.41	76.55	77.48	1.69	0.13	-1.76
Cross validation	14.16	12.29	12.1	91.65	92.26	92.89	79.13	84.27	84.76	3.96	-1.06	-3.77
Verification	14.28	11.52	11.22	89.78	91.79	92.49	75.04	83.75	84.59	0.12	0.09	-2.39
						ITERATION = 2000						
Calibration	15.08	12.83	12.58	86.34	87.95	88.15	68.64	77.31	78.17	3.4	-0.44	-1.63
Cross validation	13.21	12.12	11.86	92.38	92.42	93.2	81.85	84.7	85.37	5.39	-1.65	-3.45
Verification	12.77	11.26	10.96	91.41	92.12	92.88	80.03	84.47	85.3	2.42	-0.53	-1.95
						ITERATION = 5000						
Calibration	13.69	12.61	12.35	87.3	88.38	89.01	74.16	78.07	78.98	3.45	-0.51	-1.62
Cross validation	11.99	11.85	11.6	92.8	92.8	93.46	85.05	85.38	86	4.63	-1.89	-3.27
Verification	11.25	11.02	10.73	92.46	92.48	93.18	84.51	85.13	85.92	3.55	-0.65	-1.66
						ITERATION = 7500						
Calibration	13.42	12.56	12.27	87.33	88.49	89.15	75.17	78.25	79.24	3.07	-0.55	-1.69
Cross validation	11.69	11.77	11.52	92.85	92.91	93.54	85.79	85.85	86.19	3.84	-1.94	-3.36
Verification	10.97	10.96	10.67	92.56	92.58	93.23	85.28	85.3	86.05	3.54	-0.68	-1.72
						ITERATION = 10000						
Calibration	13.33	12.53	12.22	87.3	88.55	89.25	75.49	78.35	79.42	2.79	-0.58	-1.74
Cross validation	11.6	11.72	11.47	92.85	92.68	93.61	86	85.71	86.31	3.35	-1.96	-3.49
Verification	10.9	10.92	10.65	92.56	92.64	93.26	85.46	85.41	86.11	3.4	-0.69	-1.83

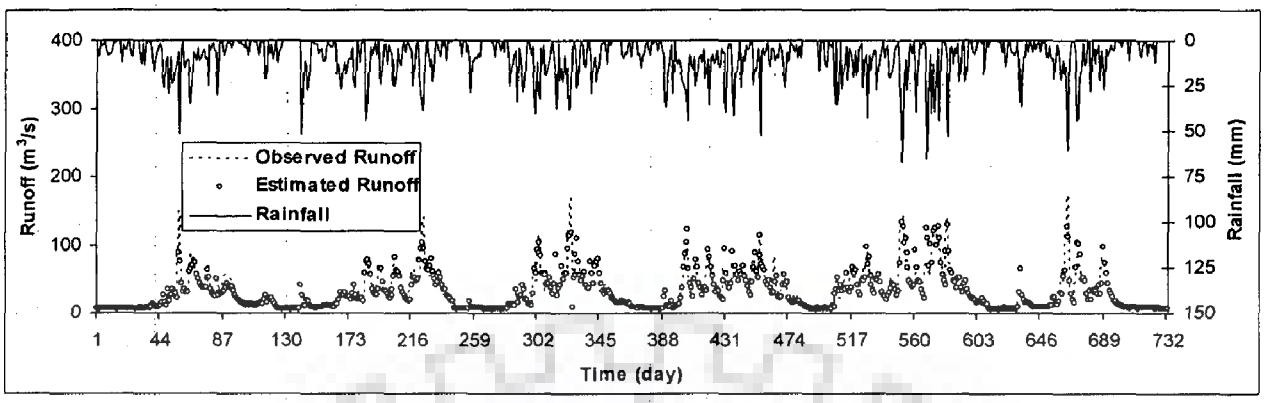

(a) Calibration

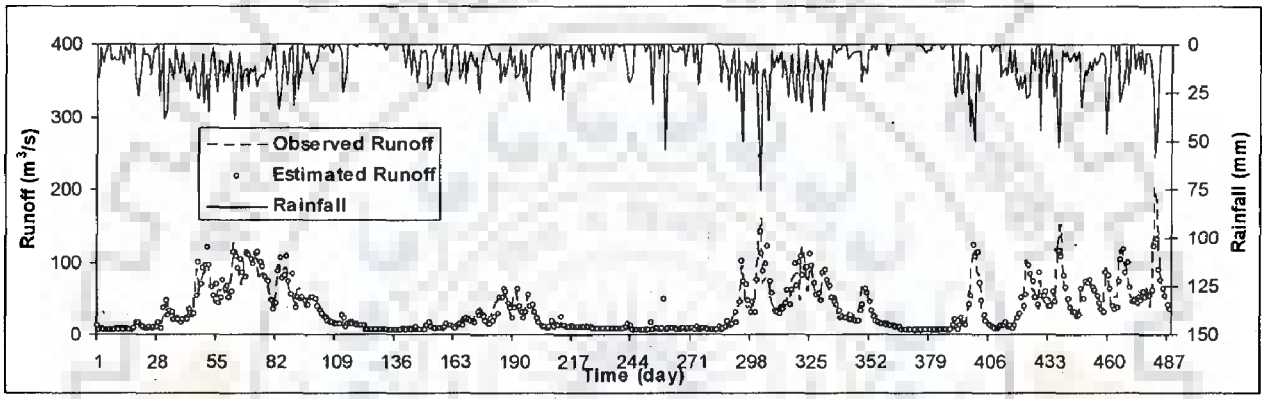

(b) Cross-validation

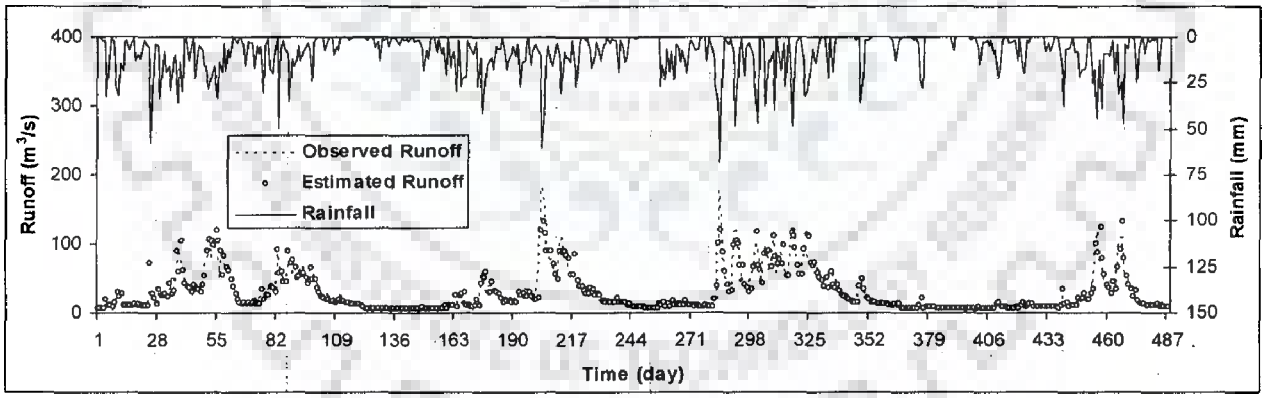

(c) Verification

Fig. D1: Observed and estimated runoff by dynamic RBFANN model having (4-4-1) network with ALR as 20 and ALRG as 0.5 for Naula watershed during (a) Calibration; (b) Cross-validation; and (c) Verification period.

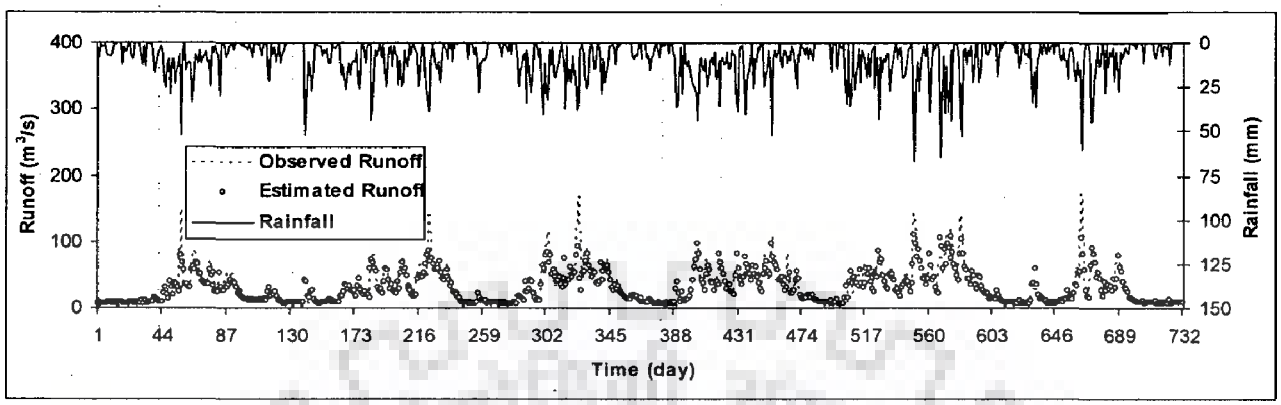

(a) Calibration

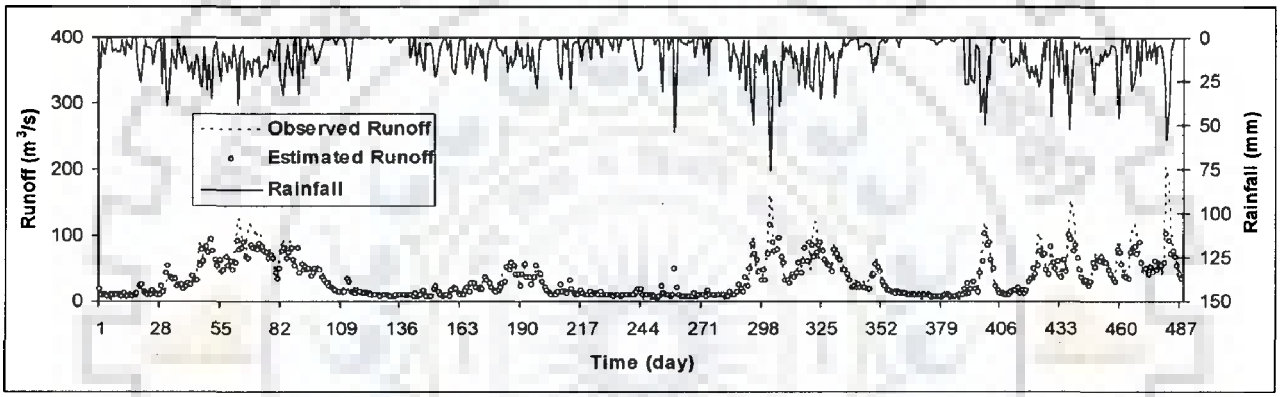

(b) Cross-validation

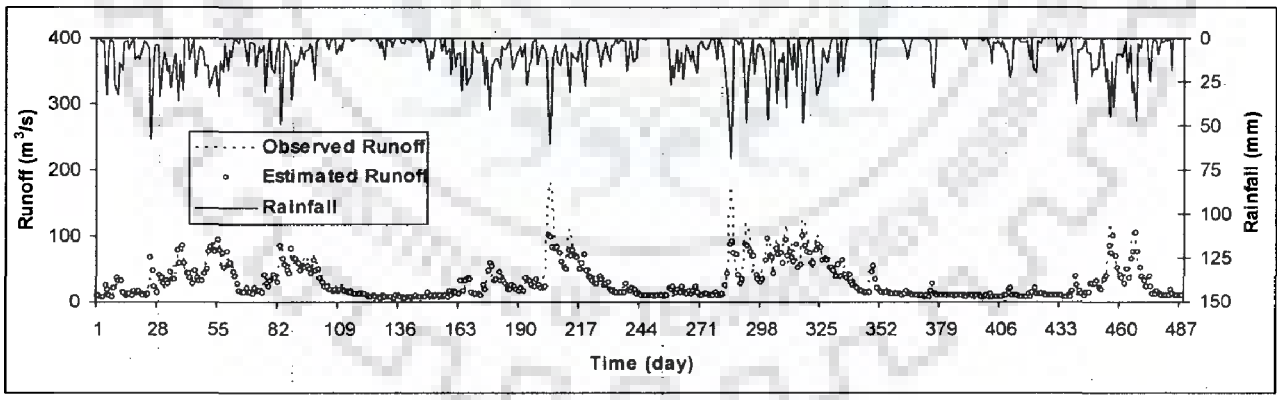

(c) Verification

Fig. D2: Observed and estimated runoff by dynamic RBFANN model having (4-16-1) network with ALR as 20 and ALRG as 0.5 for Naula watershed during (a) Calibration; (b) Cross-validation; and (c) Verification period.

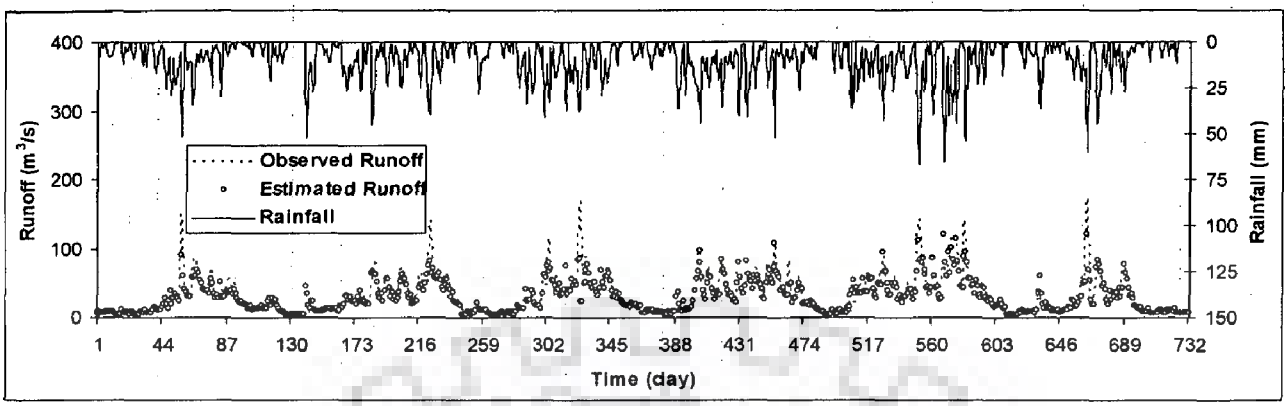

(a) Calibration

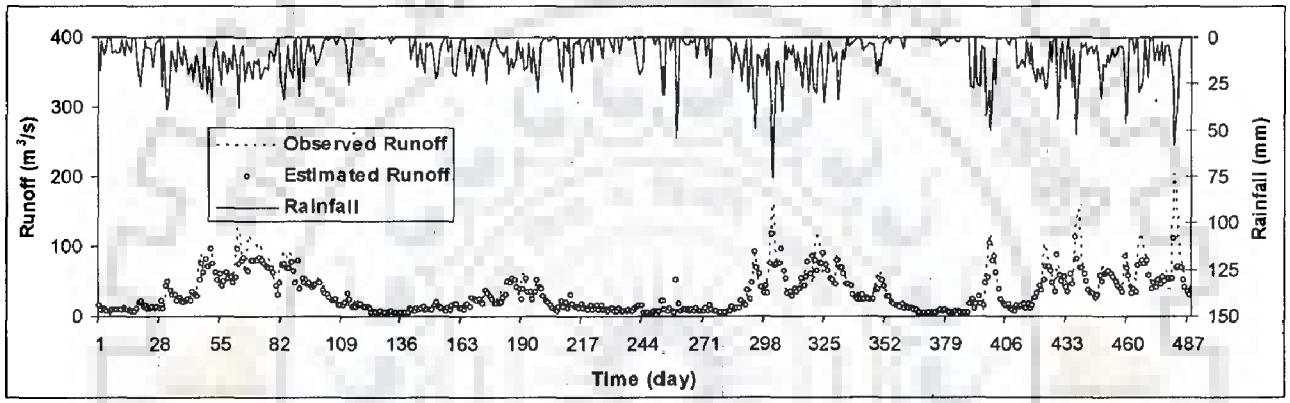

(b) Cross-validation

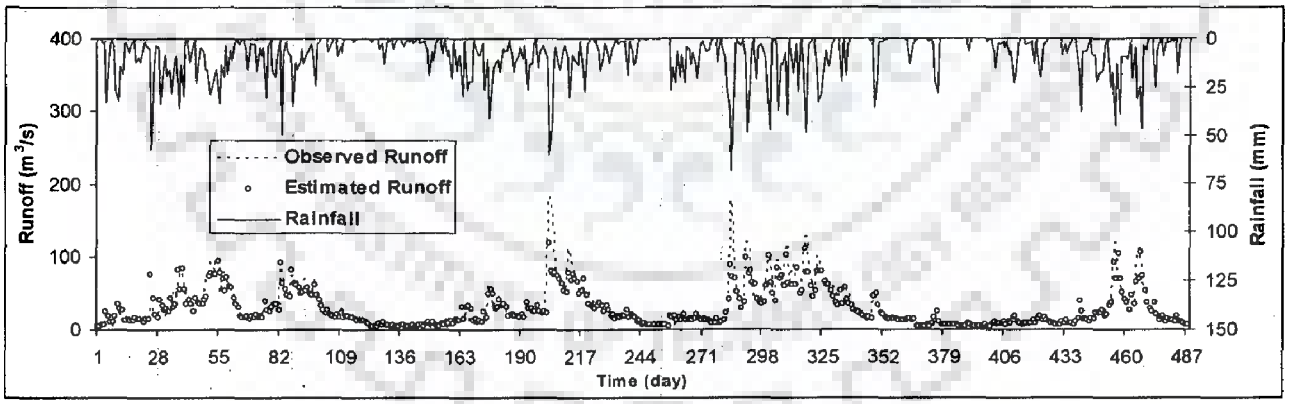

(c) Verification

Fig. D3: Observed and estimated runoff by dynamic RBFANN model having (4-32-1) network with ALR as 20 and ALRG as 0.5 for Naula watershed during (a) Calibration; (b) Cross-validation; and (c) Verification period.

APPENDIX E

Table E1: Performance of (4-4-1), (4-16-1), and (4-32-1) dynamic RBFANN models. ALRG = 0.5, No. of Iterations = 1000, and ALR = 0.5 to 25 for Ramganga watershed.

Period	RMSE			CC			CE			EV		
	4-4-1	4-16-1	4-32-1	4-4-1	4-16-1	4-32-1	4-4-1	4-16-1	4-32-1	4-4-1	4-16-1	4-32-1
						ALR = 0.5						
Calibration	217.7	213.7	211.8	53.74	54.81	55.3	-350.1	-333.8	-326.2	160.52	152.86	149.49
Cross-validation	223.6	219.3	217.4	50.11	51.11	51.52	-244.1	-231.1	-225.2	159.3	151.59	148.06
Verification	235.7	230.6	228.4	45.73	47.04	47.64	-262.4	-247.2	-239.9	168.6	161.13	157.2
						ALR = 5						
Calibration	76.63	75.06	71.31	78.83	79.37	79.03	44.24	46.51	51.72	-7.65	-7.61	-3.23
Cross-validation	80.5	79.07	78.7	79.78	80.31	78.47	55.4	56.98	57.38	-1	-0.71	0.25
Verification	90.13	88.31	91.15	74.29	74.76	71.27	47	48.53	45.79	-3.29	-2.98	-0.25
						ALR = 10						
Calibration	59.14	55.35	54.39	83.37	84.21	84.91	66.79	70.91	71.92	-2.02	-0.15	4.27
Cross-validation	65.07	63.87	62.98	84.37	84.91	85.59	70.86	71.93	72.71	1.18	1.2	5.78
Verification	79.11	77.55	77.05	77.3	77.96	78.45	59.16	60.76	61.26	-0.09	0.14	3.78
						ALR = 15						
Calibration	55.34	53.22	51.5	84.39	85.51	86.54	70.93	73.11	74.81	-0.91	0.01	2.79
Cross-validation	62.82	62.2	59.9	85.44	85.81	87.1	72.84	73.38	75.31	1.15	2.04	5.19
Verification	77.08	75.71	72.4	78.26	79.22	81.42	61.23	62.6	65.8	-0.1	-0.06	2.61
						ALR = 20						
Calibration	54.77	52.44	50.27	84.57	85.96	87.19	71.52	73.89	76	-0.61	0.25	1.31
Cross-validation	62.85	61.51	56.95	85.71	86.18	88.34	72.82	73.97	77.68	1.13	2.81	4.35
Verification	77.06	74.14	69.75	78.42	80.87	82.84	61.25	65.13	68.25	-0.11	0.17	1.27
						ALR = 25						
Calibration	54.76	52.16	50.19	84.5	86.12	87.23	71.52	74.17	76.08	-0.39	0.35	1.15
Cross-validation	63.22	60.94	57.29	85.7	86.43	88.16	72.5	74.44	77.42	1.16	3.29	4.43
Verification	77.47	73.79	69.32	78.34	81.09	83.1	60.84	65.43	68.65	-0.25	0.45	1.25

Table E2: Performance of (4-4-1), (4-16-1), and (4-32-1) dynamic model. ALR = 20, no. of iterations = 1000, and ALRG = 0.5 to 10 for Ramganga watershed.

Period	RMSE			CC			CE			EV		
	4-4-1	4-16-1	4-32-1	4-4-1	4-16-1	4-32-1	4-4-1	4-16-1	4-32-1	4-4-1	4-16-1	4-32-1
						ALRG = 0.5						
Calibration	54.77	52.44	50.27	84.57	85.96	87.19	71.52	73.89	76.1	-0.61	0.25	1.31
Cross-validation	62.85	61.51	56.95	85.71	86.18	88.34	72.82	73.97	77.68	1.13	2.81	4.35
Verification	77.06	74.14	69.75	78.42	80.27	82.84	61.25	64.13	68.25	-0.21	0.17	1.27
						ALRG = 1						
Calibration	54.41	51.31	48.49	84.8	86.62	88.19	71.89	75	77.67	-0.4	0.81	1.98
Cross-validation	62.74	60.16	54.79	85.89	86.85	89.33	72.92	75.1	79.34	0.97	3.74	5.31
Verification	76.95	72.32	67.16	78.58	81.43	84.37	61.37	65.87	70.56	-0.35	0.51	1.44
						ALRG = 2						
Calibration	54.25	50.28	47.36	84.93	87.26	88.42	72.06	76	78.7	-0.24	1.32	2.37
Cross-validation	62.71	58.74	53.72	86.07	87.59	89.77	72.94	76.26	80.15	0.89	4.46	5.86
Verification	76.92	70.82	65.99	78.71	82.43	85.02	61.39	67.27	71.58	-0.45	0.69	1.31
						ALRG = 5						
Calibration	54.22	49.23	46.22	84.99	87.89	89.41	72.09	76.99	79.72	0.01	2.09	3.34
Cross-validation	62.7	56.75	52.82	86.19	88.57	90.13	72.95	77.84	80.8	1.04	5.34	6.63
Verification	76.96	69.19	66.1	78.76	83.42	84.92	61.36	68.77	71.5	-0.35	1.23	1.82
						ALRG = 10						
Calibration	54.23	48.56	45.46	84.99	88.27	89.8	72.08	77.61	80.38	0.39	3.37	4.18
Cross-validation	62.7	55.55	52.28	86.19	89.14	90.35	72.95	78.77	81.19	1.4	6.52	7.32
Verification	76.98	68.66	65.89	78.74	83.6	84.97	61.33	69.23	71.67	0	2.49	2.89

Table E3: Performance of (4-4-1), (4-16-1), and (4-32-1) dynamic RBFANN model. ALR = 20, ALRG = 0.5, and No. of iterations = 100 to 10000 for Ramganga watershed.

Period	RMSE			CC			CE			EV		
	4-4-1	4-16-1	4-32-1	4-4-1	4-16-1	4-32-1	4-4-1	4-16-1	4-32-1	4-4-1	4-16-1	4-32-1
						ITERATION = 100						
Calibration	56.2	56	55.63	83.77	83.8	84.04	70.1	70.23	70.62	-1.76	-1.08	-1.06
Cross-validation	63.77	65.24	65.23	85.07	84.57	84.42	72.1	70.72	70.72	1.78	2.83	1.89
Verification	77.64	70.34	79.52	77.95	76.96	76.76	60.67	58.92	58.74	0.33	0.28	0.24
						ITERATION = 500						
Calibration	55.28	53.49	52.16	84.28	85.35	86.14	70.98	72.84	74.17	-0.9	0.02	0.65
Cross-validation	63.1	62.71	59.65	85.5	85.64	87.07	72.6	72.94	75.51	1.21	2.2	2.39
Verification	77.24	75.96	73.07	78.25	79.13	80.86	61.1	62.35	65.16	-0.18	0.06	0.15
						ITERATION = 1000						
Calibration	54.77	52.44	50.27	84.57	85.96	87.19	71.52	73.89	76.01	-0.61	0.25	1.31
Cross-validation	62.85	61.51	56.95	85.71	86.18	88.34	72.82	73.97	77.68	1.13	2.81	4.35
Verification	77.1	74.15	69.75	78.42	80.27	82.85	61.25	64.13	68.25	-0.21	0.17	1.27
						ITERATION = 2000						
Calibration	54.42	51.33	48.5	84.79	86.26	88.18	71.89	74.99	77.66	-0.44	0.67	1.67
Cross-validation	62.74	60.16	54.77	85.89	86.85	89.33	72.91	78.1	79.36	0.93	3.61	5.01
Verification	76.95	72.35	67.19	78.58	81.42	84.36	61.36	65.85	70.54	-0.38	0.38	1.15
						ITERATION = 5000						
Calibration	54.25	50.03	47.07	84.95	87.42	88.96	72.1	76.24	78.97	-0.34	0.9	1.41
Cross-validation	62.72	58.23	53.38	86.11	87.84	89.86	72.93	76.67	80.39	0.76	4.12	4.95
Verification	76.94	70.43	65.97	78.72	82.7	85.03	61.37	67.63	78.6	-0.59	0.22	0.29
						ITERATION = 7500						
Calibration	54.24	49.59	46.54	84.98	87.69	89.23	72.1	76.65	79.44	-0.33	0.83	1.28
Cross-validation	62.72	57.31	52.93	86.17	88.28	90.02	72.93	77.4	80.72	0.73	4.13	4.77
Verification	76.96	69.69	66.07	78.75	83.16	84.96	61.35	68.31	71.51	-0.64	0.08	-0.01
						ITERATION = 10000						
Calibration	54.24	49.31	46.17	84.98	87.84	89.4	72.1	76.91	79.96	-0.33	0.77	1.19
Cross-validation	62.71	56.69	82.63	86.19	88.57	90.13	72.94	77.88	80.94	0.72	4.11	4.61
Verification	76.97	69.24	66.16	78.75	83.4	84.89	61.34	68.71	71.14	-0.66	0.01	-0.19

APPENDIX F

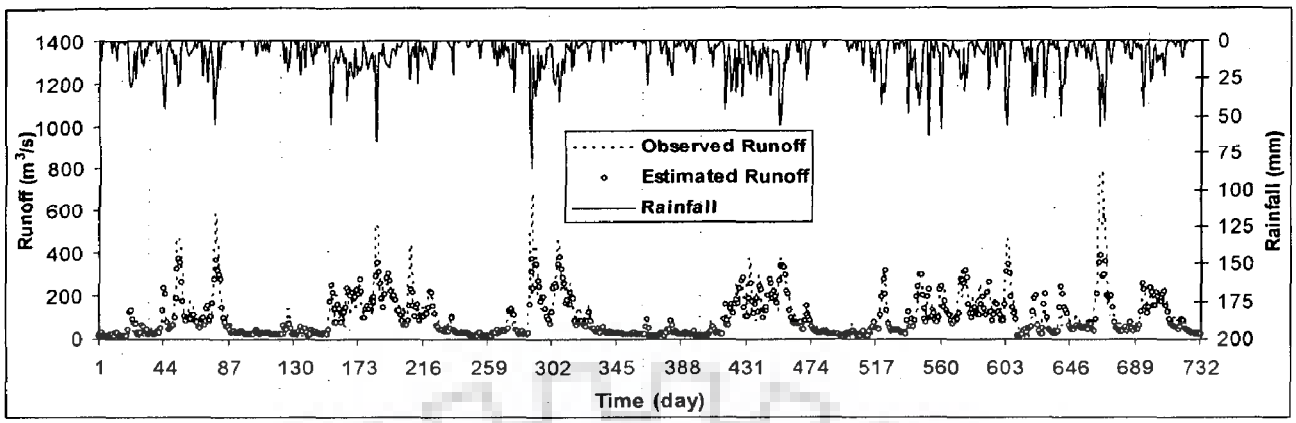

(a) Calibration

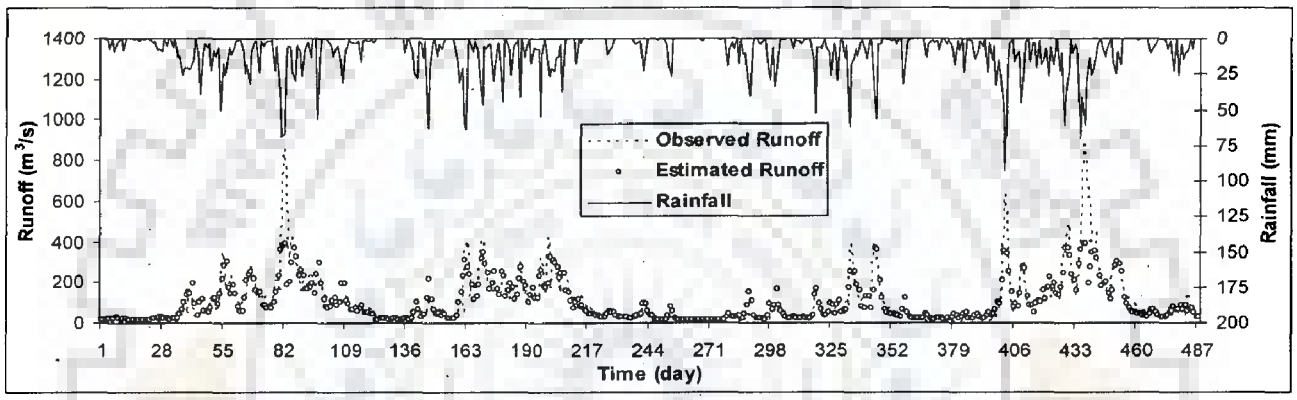

(b) Cross-validation

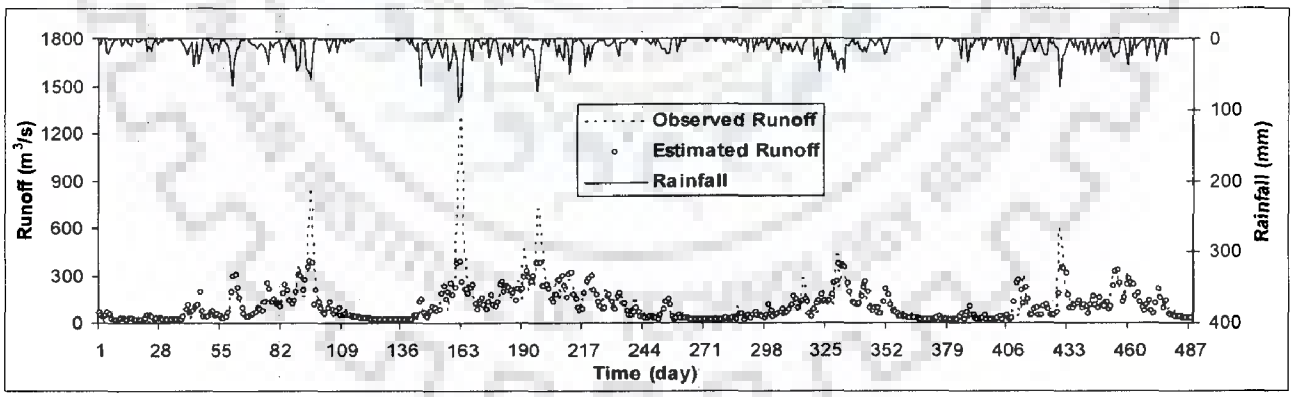

(c) Verification

Fig. F1: Observed and estimated runoff by dynamic RBFANN model having (4-4-1) network with ALR as 20 and ALRG as 0.5 for Ramganga watershed during (a) Calibration; (b) Cross-validation; and (c) Verification period.

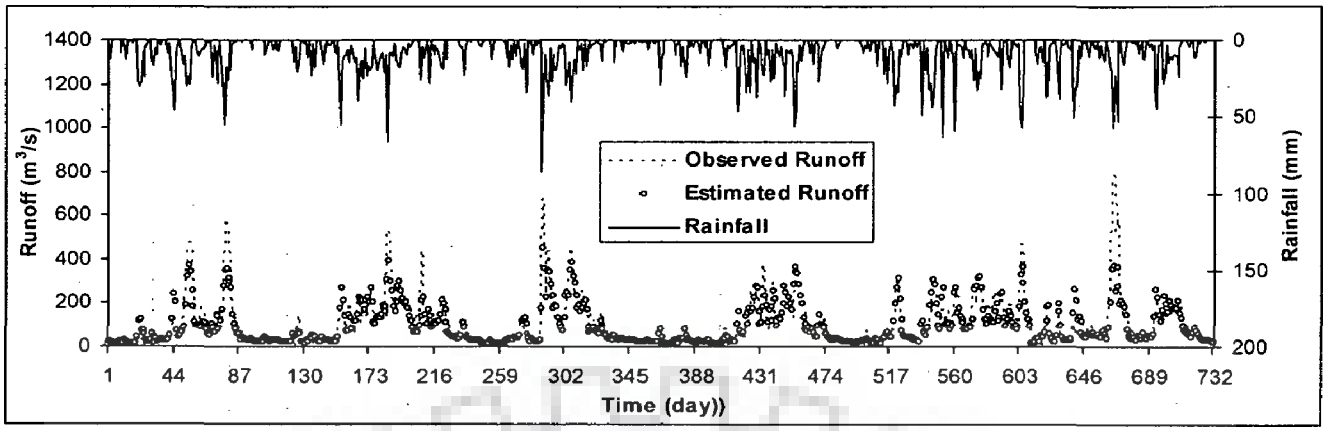

(a) Calibration

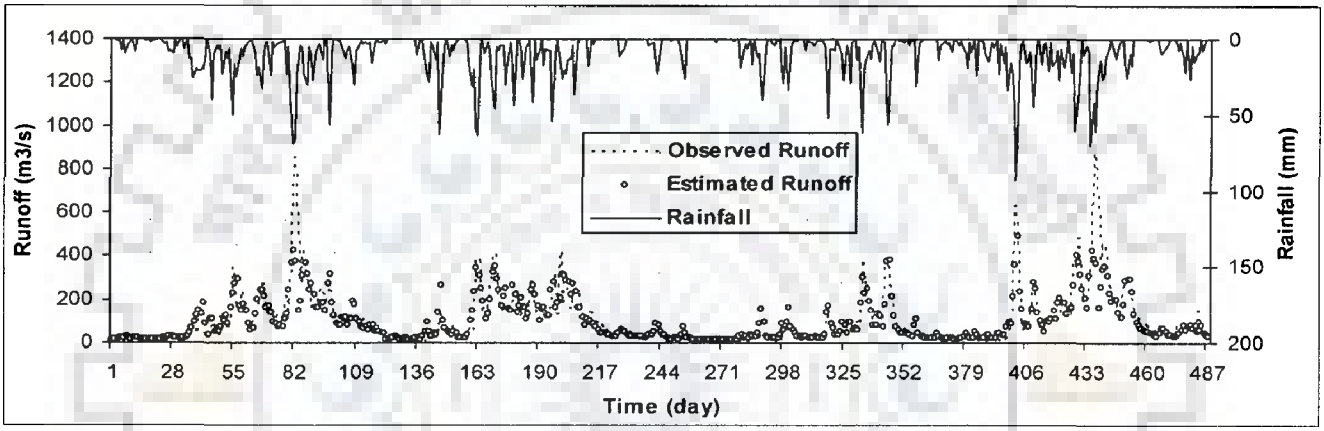

(b) Cross-validation

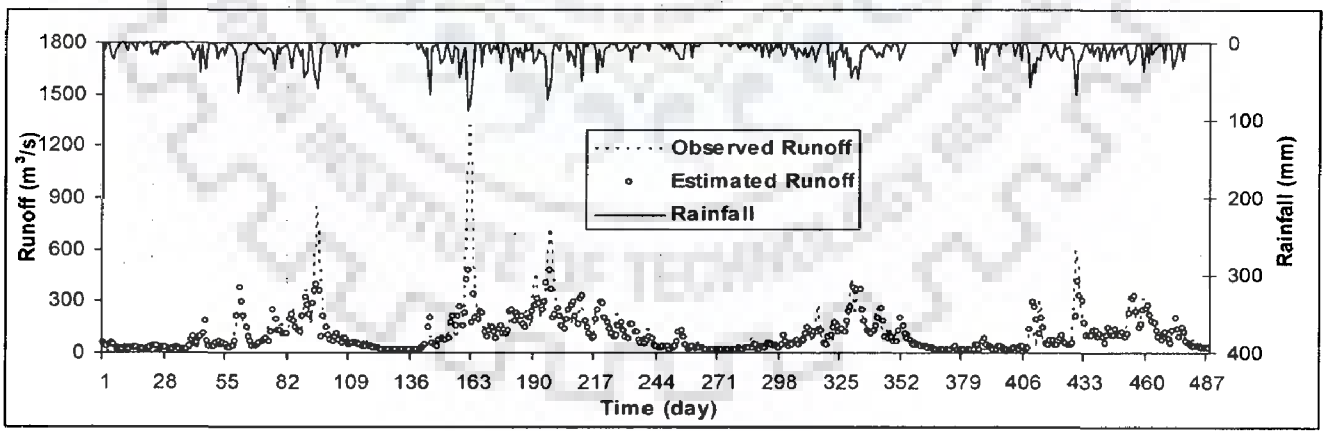

(c) Verification

Fig. F2: Observed and estimated runoff by dynamic RBFANN model having (4-16-1) network with ALR as 20 and ALRG as 0.5 for Ramganga watershed during (a) Calibration; (b) Cross-validation; and (c) Verification period.

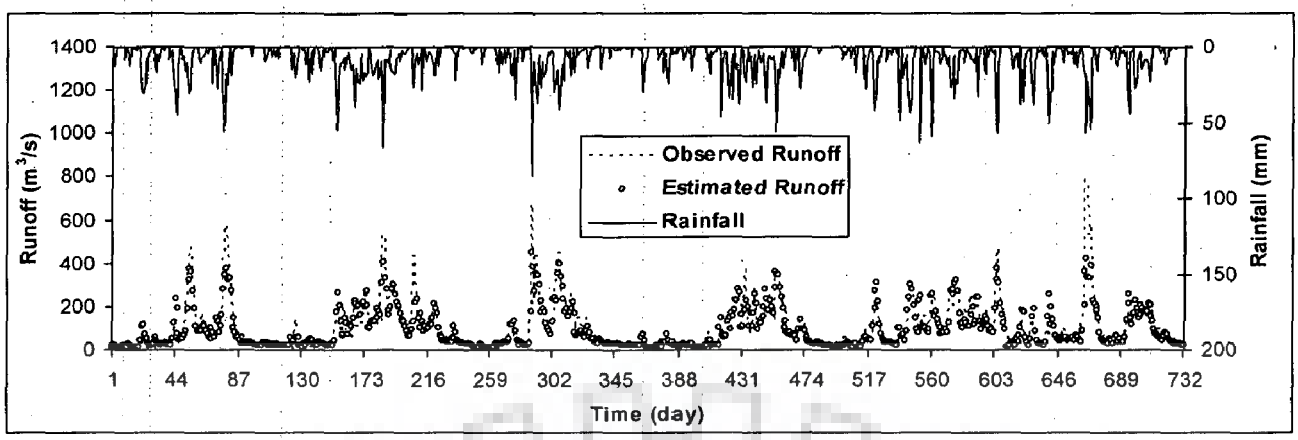

(a) Calibration

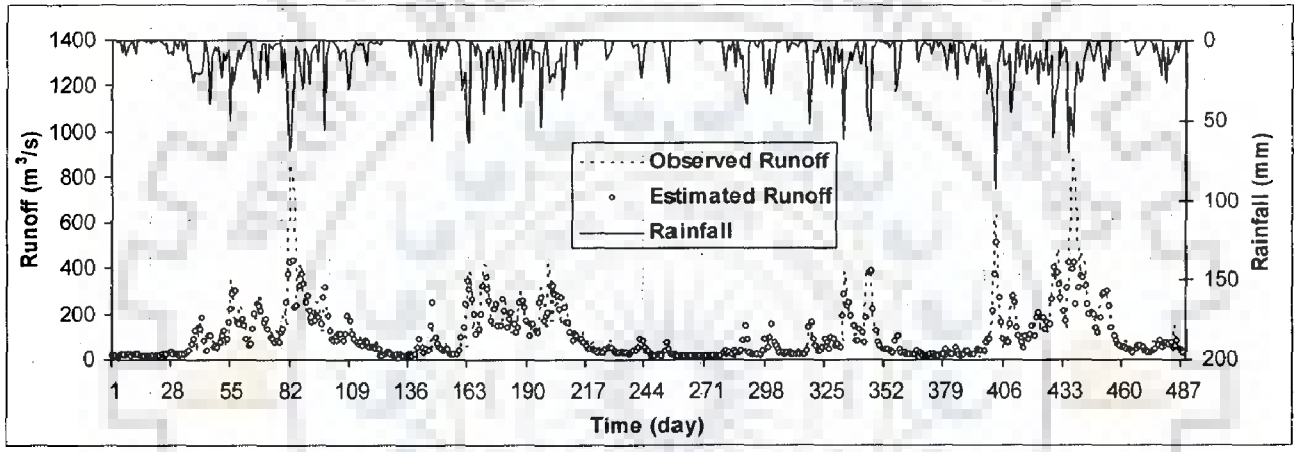

(b) Cross-validation

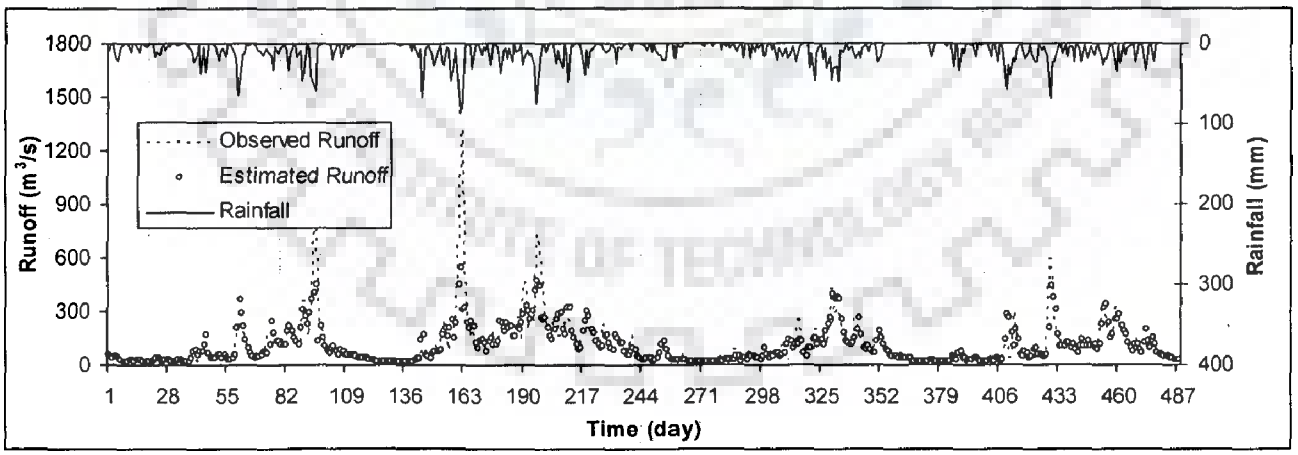

(c) Verification

Fig. F3: Observed and estimated runoff by dynamic RBFANN model having (4-32-1) network with ALR as 20 and ALRG as 0.5 for Ramganga watershed during (a) Calibration; (b) Cross-validation; and (c) Verification period.

APPENDIX G

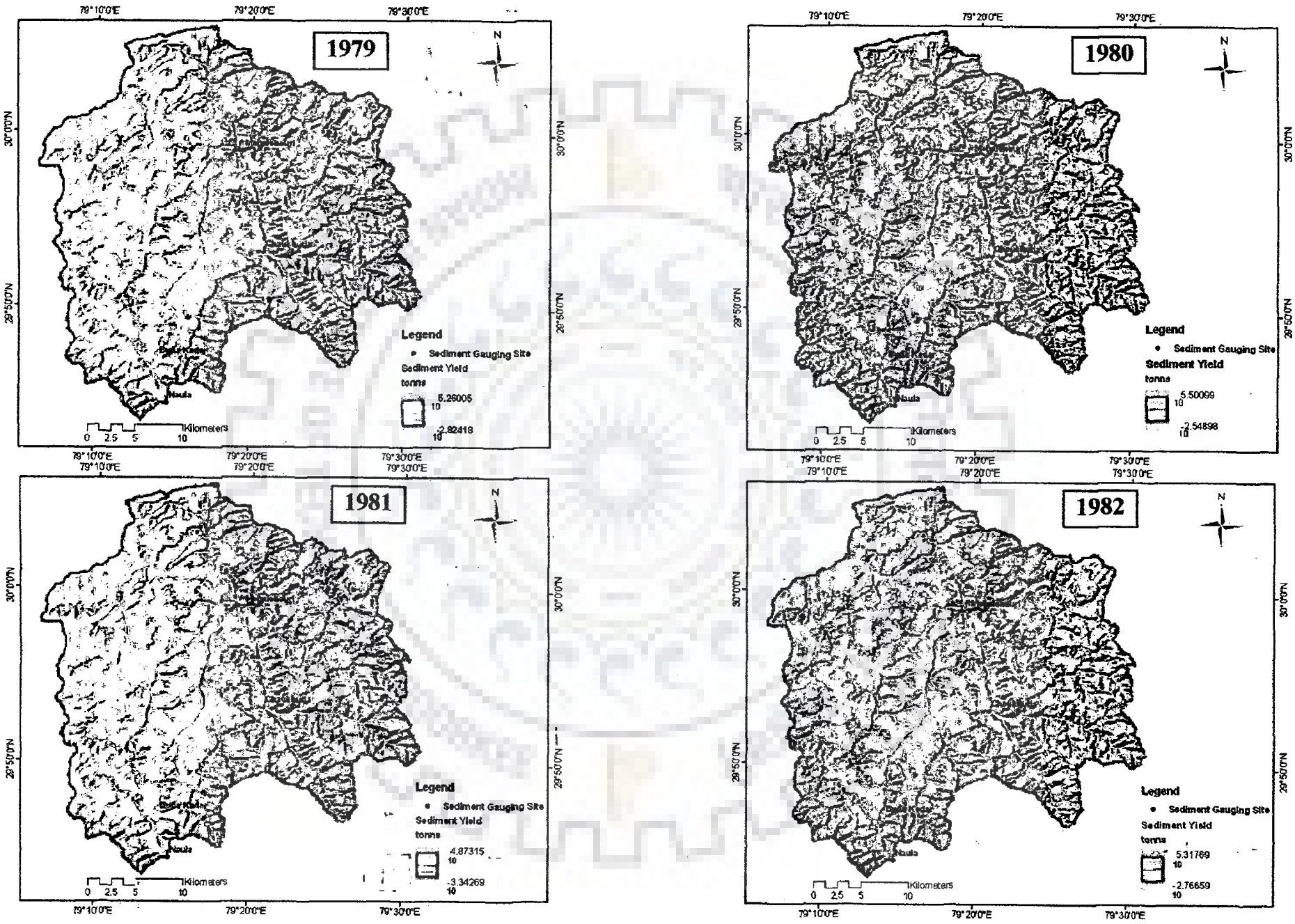

Fig. G1: Sediment outflow maps of Naula watershed for different years.

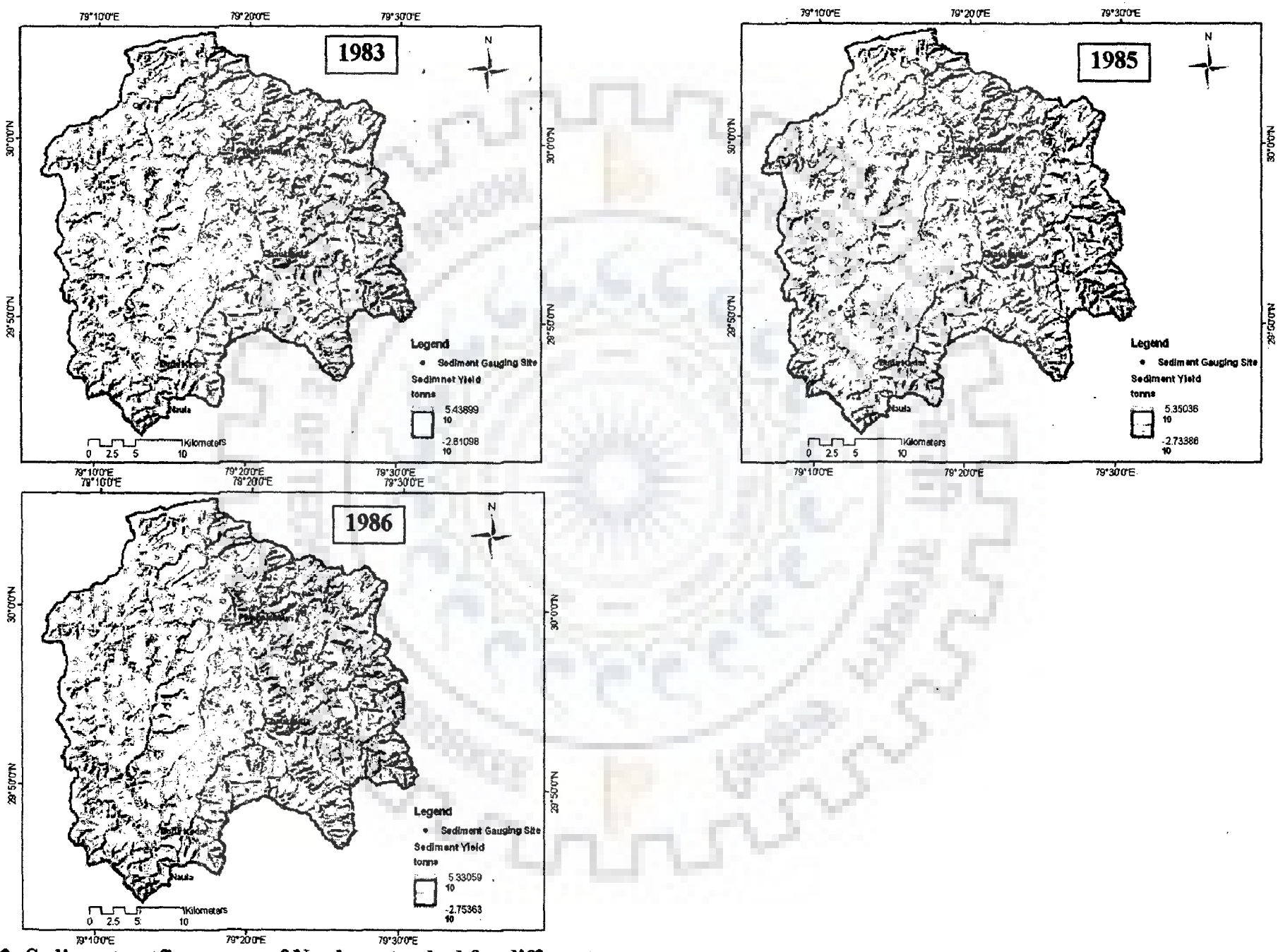

Fig. G2: Sediment outflow maps of Naula watershed for different years.

APPENDIX H

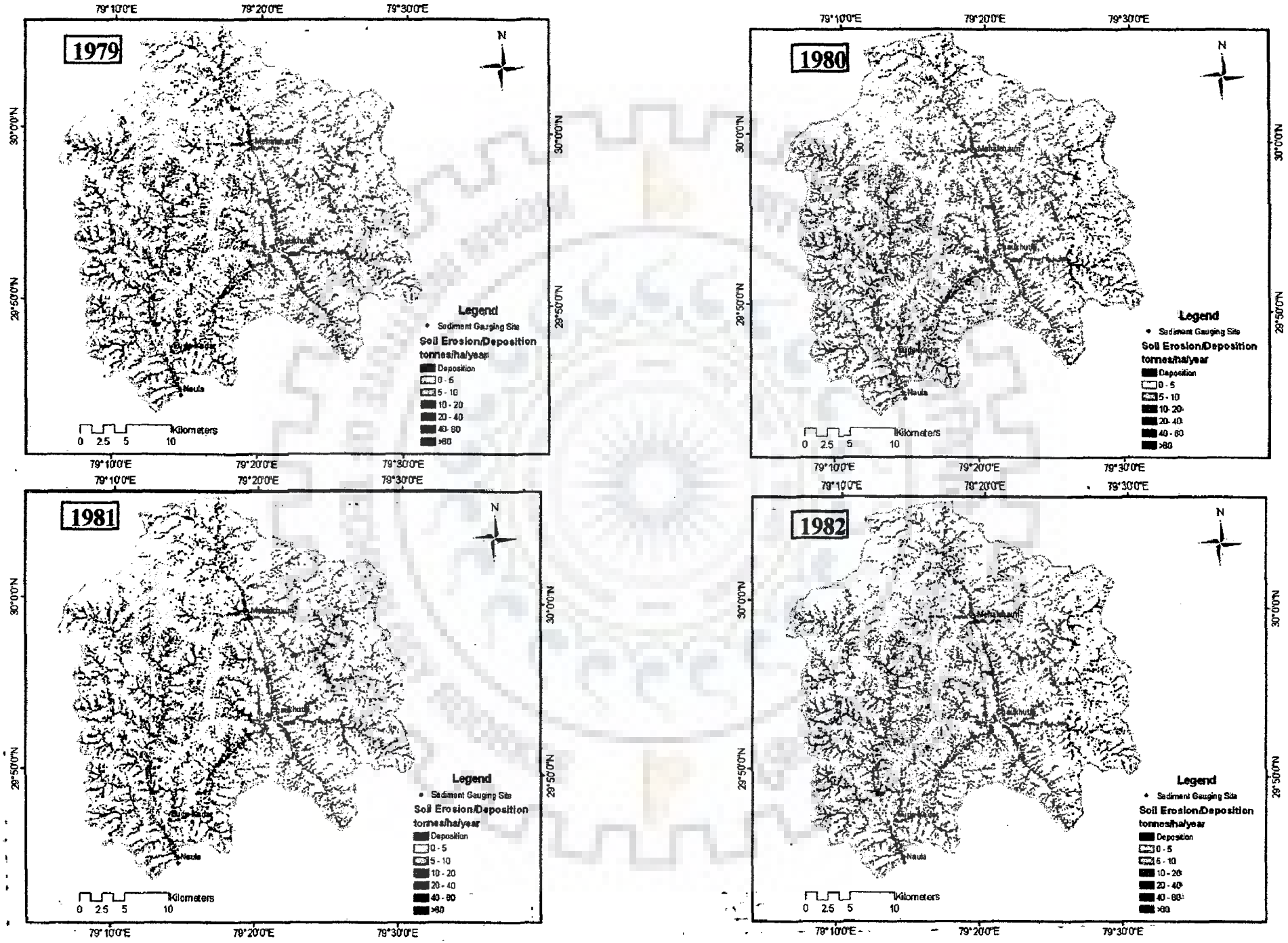

Fig. H1: Net erosion/deposition maps for different years of Naula watershed.

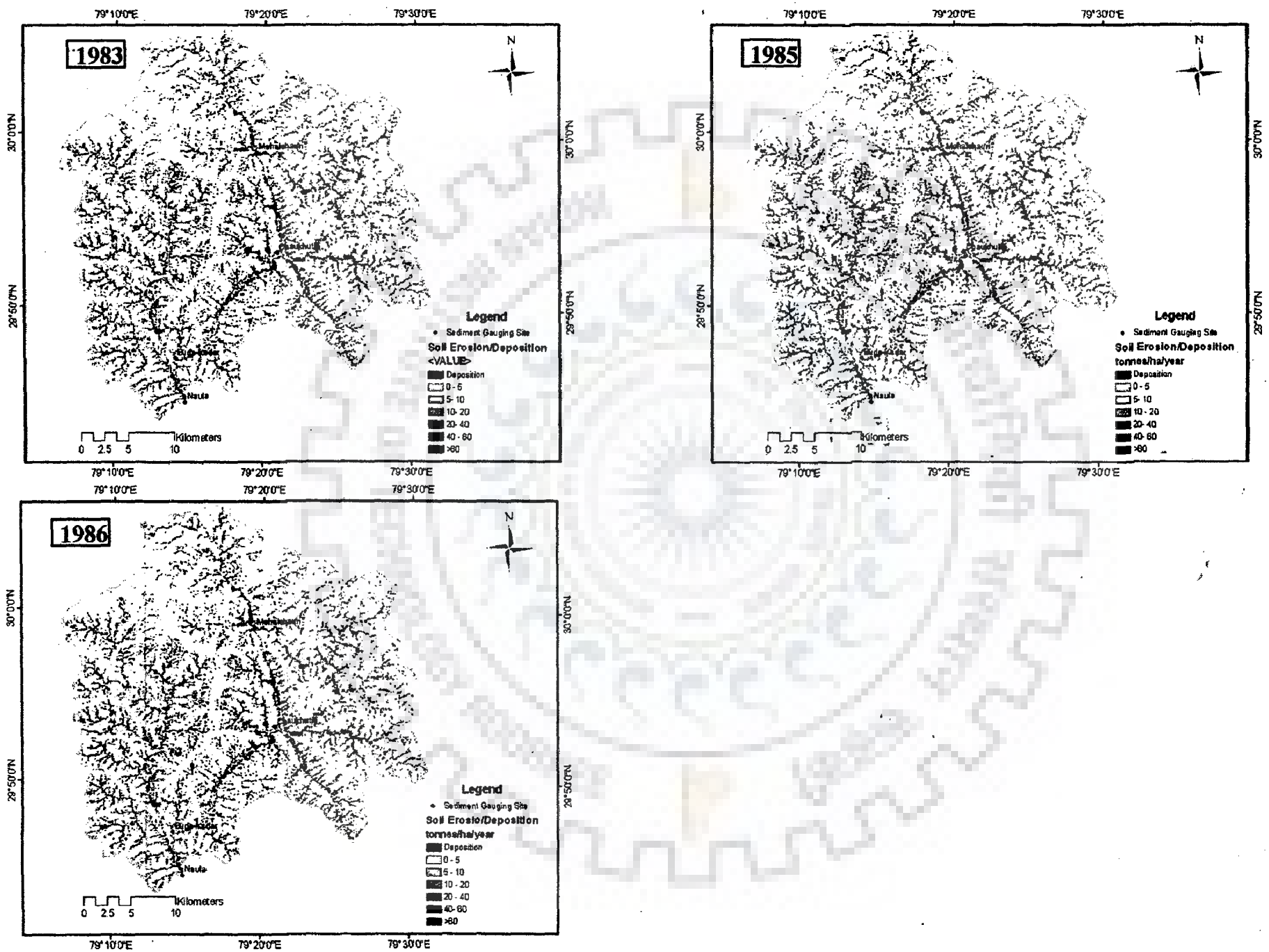

Fig. H2: Net erosion/deposition maps for different years of Naula watershed.